The Journal of Antibiotics (2009) 62, 405

www.nature.com/ja

EDITORIAL

Professor Dr Hans Zähner: an appreciation

The Journal of Antibiotics (2009) **62,** 405; doi:10.1038/ja.2009.58

When Hans Zähner passed away on 18 December 2008 at the age of 79 after a long illness, he left the world a rich scientific legacy. His work has resulted in the discovery of a great number of antibiotics and other natural products from microbial sources, representing most major compound classes. Through studies on their mode of action, particularly in the producing organism, he also contributed greatly to the understanding of physiology and biochemistry, especially of microorganisms. One of the compounds he discovered early on, desferri-ferrioxamine B, became a marketed drug (Desferal) for the treatment of iron-overload diseases. Beyond these discoveries, important both qualitatively and quantitatively, he has shaped his field by training several generations of students who continued his mission and left their mark both in academia and in industry.

In his early work at the ETH Zürich and in his 30 years at the University of Tübingen, he developed an integrated approach to the discovery of microbial natural products, based on novel methods of isolation of producer organisms and new strategies of screening, cultivation and fermentation scale-up. In this way, his students learned real-world skills that served them well in their future careers not only in academia, but particularly in industry. Early on and throughout his career, he also recognized the importance of interdisciplinary collaboration, particularly with natural-products chemists. He developed close collaborations with Professors Walter Keller-Schierlein and Vladimir Prelog at the ETH Zürich and with Professor Axel Zeeck at the University of Göttingen. These interactions were very intense, involving mutual visits at the student level and frequent joint meetings of the groups, endowing students with an interdisciplinary outlook and the ability to communicate and interact across disciplinary lines. In 1972, he tried to recruit me to the University of Tübingen to expand this interdisciplinary approach to include biosynthetic studies. Although in the end I turned down the offer to move to Tübingen, it did result in our studying the biosynthesis of many 'Zähner' antibiotics.

Zähner's thinking profoundly influenced his co-workers and his discipline. He developed a number of important concepts. Contemplating the reasons for the occurrence of so many natural product structures, he developed the concept of the 'evolutionary game room,'[1] in which nature randomly alters and recombines genetic information to constantly create new chemical structures. For any newly invented structures to persist, Zähner postulated that they only should have no negative effects on the essential functions of the producing organism. More current thinking, based on insights from the molecular biology of secondary metabolism, would postulate that for new structures to persist, their formation should represent a selectable advantage to the producer.[2] Zähner also argued that the antibiotic activity of many microbial natural products is an incidental property, unrelated to the reason for their formation. Therefore, he argued that it makes sense to use screening methods unrelated to the traditional antibiotic screens, in the extreme chemical screening, for example, by TLC, to discover new natural products that can then be evaluated in depth for their biological activities.[3] This approach, which he pursued extensively and successfully, may have seemed counterintuitive at the time, but has been amply validated by the more recent successes in discovering non-antibiotic biological activities by screening known natural products and natural product libraries.

Hans Zähner shaped the professional lives of many people, both students and colleagues, through the force of his personality. His impact derived not only from his creativity as a researcher, but also from his charisma, his inquisitiveness and his infectious enthusiasm for science and discovery. He had high expectations of his students and set rigorous standards. Other outstanding traits were his honesty and his strong convictions on many issues, such as the impact of applications of biotechnology on the environment. In his convictions, he was usually rather uncompromising and willing to fight for his beliefs. Although he spent the majority of his academic career in Germany, he was a Swiss at heart. He viewed his countrymen with affectionate wonderment—I remember him telling me with an amused smile that in his youth in many Swiss villages the farmers still braided their manure piles. When it was time to retire, he returned to his native country and spent the rest of his days in Bern.

In many ways, Hans Zähner was a man larger than life, and he is sorely missed.

Heinz G Floss
Department of Chemistry, University of Washington, Seattle, WA, USA
E-mail: floss@chem.washington.edu

1 Zähner, H. What are secondary metabolites? *Folia Microbiol*. **24,** 435–443 (1979).
2 Floss, H. G. Combinatorial biosynthesis—potential and problems. *J. Biotechnol.* **124,** 242–257 (2006).
3 Zähner, H. Some aspects of antibiotics research. *Angew Chem. Int. Ed. Engl.* **16,** 687–694 (1977).

The Journal of Antibiotics (2009) 62, 407–423

www.nature.com/ja

REVIEW ARTICLE

Gem-diamine 1-*N*-iminosugars as versatile glycomimetics: synthesis, biological activity and therapeutic potential

Yoshio Nishimura

Iminosugars, which carry a basic nitrogen in the carbohydrate ring, have attracted increasing interest as new glycomimetics. *Gem*-diamine 1-*N*-iminosugars, a new class of iminosugars, have a nitrogen atom in place of the anomeric carbon. Various kinds of 1-*N*-iminosugars have been synthesized from glyconolactones as a chiral source in a totally stereospecific manner and/or by the convergent strategy from siastatin B, a secondary metabolite of *Streptomyces*. The protonated form of 1-*N*-iminosugar mimics the charge at the anomeric position in the transition state of enzymatic glycosidic hydrolysis, resulting in a strong and specific inhibition of glycosidases and glycosyltransferases. They have been recently recognized as a new source of therapeutic drug candidates in a wide range of diseases associated with the carbohydrate metabolism of glycoconjugates, such as tumor metastasis, influenza virus infection, lysosomal storage disorder and so forth.
The Journal of Antibiotics (2009) **62,** 407–423; doi:10.1038/ja.2009.53; published online 3 July 2009

Keywords: glycosidase inhibitor; heparanase inhibitor; influenza virus infection; lysosomal storage disease; 1-*N*-iminosugar; siastatin B; tumor metastasis

INTRODUCTION

Iminosugars, which are carbohydrate analogs that most frequently carry the nitrogen atom at the position of the endocyclic oxygen, form the most attractive class of glycomimetics reported so far.[1] Several types of iminosugars have been discovered from natural sources[1,2] since nojirimycin[3] was first isolated as an antibiotic from *Streptomyces* culture in 1966. Many more have also been synthesized on the basis of enzymatic glycoside biosynthesis.[1,4] Of late, they have gained remarkable importance not only as molecular tools to unravel the manner in which glycoconjugates regulate various biological functions, but also as new therapeutic agents in a wide range of diseases associated with the metabolism of carbohydrates.

In 1974, siastatin B (**1**), an unusual iminosugar, was isolated as an inhibitor against neuraminidases (NAs) from *Streptomyces* culture.[5] Siastatin B (**1**) also inhibits β-D-glucuronidase and *N*-acetyl-β-D-glucosaminidase. We recognized from biological activity that siastatin B (**1**) structurally resembles D-glucuronic acid (**2**) and *N*-acetyl-D-glucosamine (**3**), as well as *N*-acetylneuraminic acid (**4**) (Figure 1). It is distinct from the known glycosidase inhibitors, such as nojirimycin, that contain a nitrogen atom in place of the ring oxygen. In the course of our study on siastatin B (**1**), we proposed a new class of glycosidase inhibitors, *gem*-diamine 1-*N*-iminosugars[6–8] (*gem*-diamine 1-aza-carbasugar in IUPAC nomenclature,[9] cyclic methanediamine monosaccharide, **5**) in which the anomeric carbon atom is replaced by nitrogen. We hypothesized that the protonated form of *gem*-diamine 1-*N*-iminosugar **6** may mimic the putative glycopyranosyl cation **7** that was formed during enzymatic glycosidic hydrolysis (Figure 2). This turned out to be the case and led to new findings of highly potent and specific inhibitors of glycosidases and glycosyltransferases, as well as potential therapeutics for tumor metastasis and so forth. On the other hand, the synthetic isofagomine (**8**), another type of 1-iminosugar, was developed by Bols and colleagues in 1994.[10] The isofagomine type 1 iminosugars showed a potent inhibition of their corresponding β-glycosidase.[11] These findings suggest that 1-iminosugars might provide another alternative to the development of therapeutic agents based on the inhibitors of metabolism of glycoconjugates different from the common iminosugars, such as Zavesca (*N*-*n*-butyl-1-deoxynojirimycin)[12] used for the treatment of Gaucher's disease.

This review describes our current progress in the chemistry, biochemistry and pharmacology of *gem*-diamine 1-*N*-iminosugars.

SYNTHESIS

Various types of iminosugar inhibitors, such as polyfunctional piperidines and pyrrolidines, have been designed on the basis of a flattened, half-chair oxocarbenium ion-like transition state in the reaction catalyzed by glycosidases.[13–15] They are all carbohydrate mimics in which the ring oxygen is replaced by nitrogen. On the other hand, 1-*N*-iminosugars have a unique structure with a nitrogen atom in place of the anomeric carbon atom. *Gem*-diamine 1-*N*-iminosugars

Bioactive Molecules Research Group, Microbial Chemistry Research Center, Kamiosaki, Shinagawa-ku, Tokyo, Japan
Correspondence: Professor Y Nishimura, Microbial Chemistry Research Center, 3-14-23, Kamiosak, Shinagawa-ku, Tokyo, 141-0021, Japan.
E-mail: nishimuray@bikaken.or.jp
Received 22 May 2009; accepted 22 May 2009; published online 3 July 2009

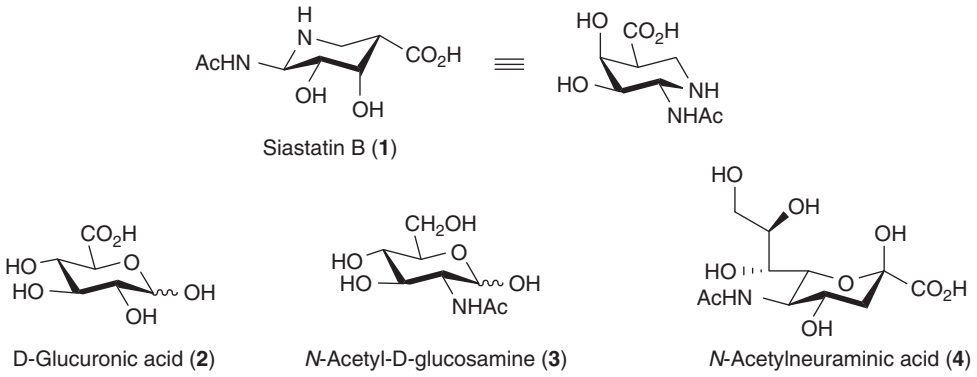

Figure 1 Structural resemblance of siastatin B (**1**) to D-glucuronic acid (**2**), *N*-acetyl-D-glucosamine (**3**) and *N*-acetylneuraminic acid (**4**).

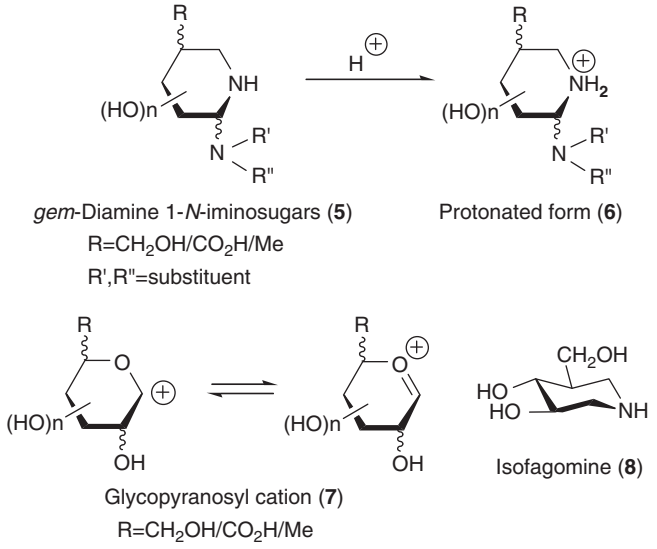

Figure 2 General structures of *gem*-diamine 1-*N*-iminosugars (**5**), its protonated form (**6**), glycopyranosyl cation (**7**), the putative intermediate of enzymatic glycosidic hydrolysis and isofagomine (**8**), another type of 1-iminosugar.

have an especially unusual structure possessing the continuous –CH(OH)–CH(OH)–CH–(NHR)–NH–CH2–CH(CH2OH/COOH)– in a framework. Their multi-functionalized structures with many asymmetric centers in a small molecule and fascinating biological activities have attracted intensive synthetic interest. As the interest in this class of glycomimetics comprised analogs of both D- and L-sugars, we have developed flexible divergent strategies applicable to a wide range of *gem*-diamine 1-*N*-iminosugars using glyconolactones as chiral substrates. Efficient and convenient synthetic methodologies of *gem*-diamine 1-*N*-iminosugars were also developed from natural siastatin B. These convergent strategies using natural siastatin B could be useful and practical for drug development.

Total synthetic route to *gem*-diamine 1-*N*-iminosugars

The chiron strategy using D-ribono-γ-lactone (**9**) was first adapted for the total synthesis of siastatin B (**1**) and its enantiomer.[16,17] D-galacturonic acid-type 2-acetamido-1-*N*-iminosugar was synthesized in a totally stereospecific and enantiospecific manner as shown in Scheme 1.[18] The strategy involves the formation of the cyclic methanediamine using the Mitsunobu reaction[19] on an aminal (**14**→**15**) and the stereospecific introduction of a carboxylic acid group into a ketone (**16**→**21**) as the key steps. The synthesis of the key intermediate, lactam **11**, commenced with L-ribose, which was transformed into azido-L-ribonolactone **10** by the protection of 2,3-diol, azide formation and oxidation. Hydrogenation of the azide group of **10** resulted in crystalline **11** with ring expansion. Stereospecific introduction of the hydroxyl group at the C-2 position was best achieved by hydride reduction of the protected lactam **12** followed by the Swern oxidation to yield aminal **14**. One-step stereospecific transformation of **12** into **14** was also efficiently achieved by the reduction of L-selectride in tetrahydrofuran. The Mitsunobu reaction with phthalimide in dimethylformamide was proved to quantitatively yield the desired cyclic methanediamine **15**. Replacement of the amino substituent, removal of the *tert*-butyldimethylsilyl (TBDMS) group and oxidation to **16** were carried out straightforwardly. Condensation of **16** with nitromethane was found to proceed smoothly to quantitatively yield **17** as a single stereoisomer. The endocyclic nitro olefin **18** was effectively derived from **17** by acetylation followed by base-catalyzed elimination of the acetoxy group. The crucial intermediate, carboxylate **20**, was obtained through α,β-unsaturated aldehyde **19** generated by simply warming in pyridine. Transformation of **20** into siastatin B (**1**) was best achieved by the following three-step sequences: stereoselective reduction to the α,β-saturated hydroxymethyl compound **21**, oxidation and removal of protecting groups. The antipode of **1** was also synthesized from D-ribono-1,4-lactam using the above-mentioned method. Thus, the total synthesis also elucidated the absolute configuration of siastatin B (**1**) as the (3*S*,4*S*,5*R*,6*R*) isomer.

The strategy of total synthesis of siastatin B (**1**) is applicable to a wide range of D-galacturonic acid-type *gem*-diamine 1-*N*-iminosugars (Schemes 2 and 3).[20,21]

Syntheses of D-galacturonic acid-type 2-acetamido- and trifluoroacetamido-1-*N*-iminosugars (**27a** and **27b**) having a hydroxyl group at the C-5 position and their antipodes **27c** and **27d** are achieved in a straightforward manner. The nitromethane condensation of the ketones **23a** and **23b** stereospecifically proceeded to afford adducts **24a** and **24b**. The *S*-configuration at position C-5 was clarified by an X-ray crystallographic analysis of the antipode of **23a**. Successive sequences of catalytic reduction, ninhydrin oxidation of the resultant aminomethyl group, oxidation of the resultant aldehyde with sodium chlorite and removal of the protecting groups afforded the final products. The antipodes **27c** and **27d** were also synthesized starting from D-ribono-1,4-lactone using similar methods that are mentioned above.

An alternative route from the ketone **23b** to D-galacturonic acid-type 2-trifluoroactamido-1-*N*-iminosugar **32** was also developed

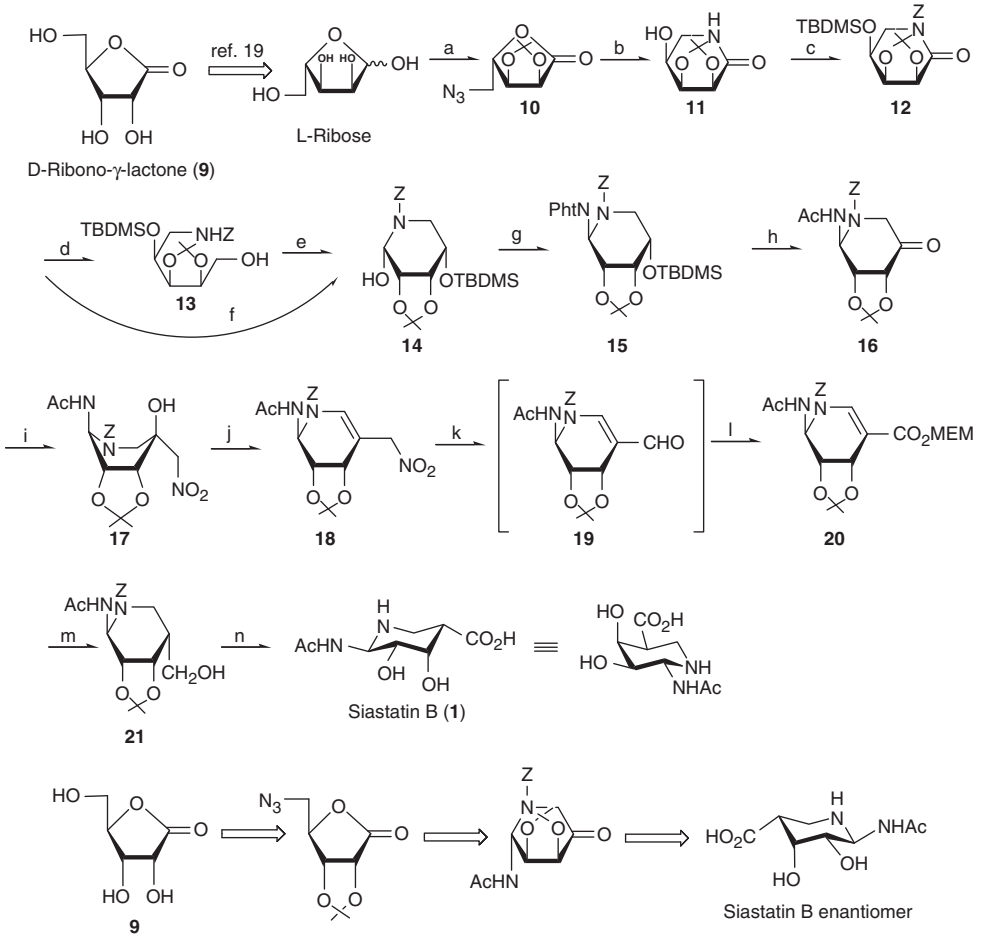

Scheme 1 Reagents and conditions: (a) *p*-TsOH, Me_2CO; MsCl, py; NaN_3, DMSO; CrO_3/py, CH_2Cl_2 (89%); (b) H_2, Raney Ni, MeOH (88%); (c) TBDMSCl, imidazole, DMF; ZCl, NaH, DMF (99%); (d) $NaBH_4$, EtOH (96%); (e) Swern oxidation (88%); (f) L-selectride, THF (88%); (g) phthalimide, Ph_3P, DEAD, DMF (100%); (h) $H_2N{\cdot}NH_2$, MeOH; Ac_2O, py; *n*-Bu_4NF, THF; RuO_4, CH_2Cl_2 (99%); (i) $MeNO_2$, NaH, DME (100%); (j) Ac_2O, *p*-TsOH; K_2CO_3, PhH (100%); (k) py, 38 °C, 1 week (80%); (l) $NaClO_2$–NaH_2PO_4, $CH_3CH{=}CMe_2$, H_2O-*t*-BuOH; MEMCl, *i*-Pr_2NEt, CH_2Cl_2 (55%); (m) $NaBH_4$, THF–CF_3CH_2OH (75%); (n) PDC, DMF; H_2, 10% Pd/C, MeOH; 1 M HCl, then Dowex 50W X_4 (H^+) eluted with 2% NH_4OH (66%).

using the Wacker process oxidation of the enol ethers **28** and **29** as a key step. The Wacker process oxidation stereospecifically proceeded to yield carboxylate **30** as a sole product. The transformation of **30** into **32** was unexceptional.

A flexible synthetic route to four *gem*-diamine 1-*N*-iminosugars of D- and L-uronic acid type (D-glucuronic, D-mannuronic, L-iduronic and L-guluronic acid) from L-galactono-1,4-lactone was also developed in an enantiodivergent manner through a sequence involving as the key steps (1) the formation of *gem*-diamine 1-*N*-iminopyranose ring by the Mitsunobu reaction of an aminal (**44**→**45, 46**) and (2) the flexible introduction of a carboxylic acid group by the Wittig reaction on a ketone, followed by hydroboration and oxidation, as well as the Sharpless oxidation (**45** and **46**→**47**, **48** and **55**, **56**) (Schemes 4 and 5).[22,23] The diastereoselective construction of amino and carboxylic acid substituents at positions C-2 and C-5, respectively, on the versatile aminal **44** led to the formation of four enantiomerically pure stereoisomers (**51**, **54**, **61** and **66**). The Wittig reaction on the ketone **37** derived from L-galactono-1,4-lactone resulted in the methylene derivative **38**, which was converted into the diol **39**. The monoalcohol **40** was successfully obtained by the Luche reduction of the labile aldehyde generated by the periodate oxidation of **39**. Conversion of the hydroxyl group of **40** to the azide group was best achieved from the corresponding sulfonate by one-pot reaction *in situ*. Hydrogenation of the azide group of **41** with sodium hydrogentelluride (NaTeH) was found to proceed preferentially without any effect on the reduction of the methylene group. The pivotal intermediate, aminal **44** was obtained as an epimeric mixture by the removal of a TBDMS group and the Swern oxidation. The Mitsunobu reaction with phthalimide afforded both desired epimers of iminophthalimides **45** and **46** in a 3:1 ratio. The absolute stereochemistry and a boat conformer of **45** were clarified by an X-ray crystallographic analysis. Another epimer **46** was assigned its stereochemistry and boat conformation by the hydrogen-1 nuclear magnetic resonance (^{1}H-NMR) spectrum. Hydroboration of **45** followed by oxidation efficiently yielded the D-*gluco* isomer **47** and the L-*idulo* isomer **48** in a 2:9 ratio. Hydrazinolysis of **47** and conventional trifluoroacetylation furnished the trifluoroacetamide **49**. The ruthenium tetraoxide-catalyzed Sharpless oxidation effectively yielded the carboxylic acid **50**. Removal of the protecting groups of **50** resulted in D-glucuronic acid-type 2-trifluoroacetamido-1-*N*-iminosugar **51**. The same sequences of reactions also successfully resulted in L-iduronic acid-type 2-trifluoroacetamido-1-*N*-iminosugar **54** from **48**. The ^{1}H-NMR spectrum of **51** showed the $^4C_1$-conformation, whereas the ^{1}H-NMR spectrum of **54** indicated the boat conformation. On the other hand, D-mannuronic

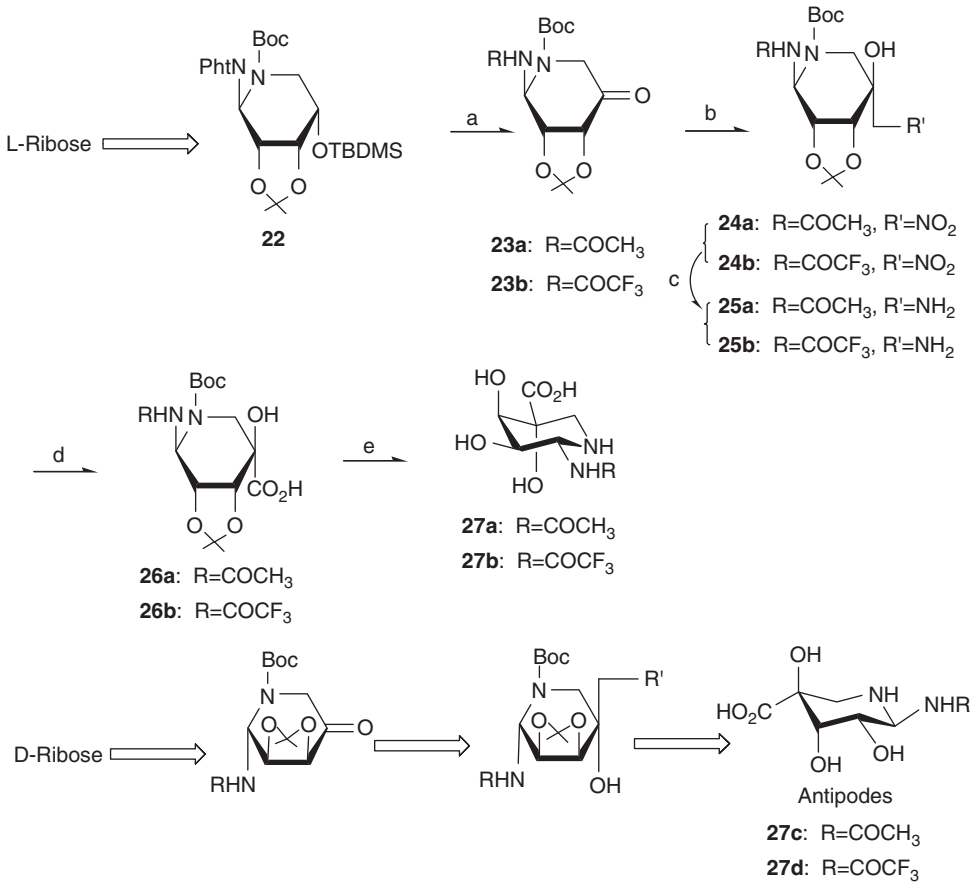

Scheme 2 Reagents and conditions: (a) $H_2N{\cdot}NH_2$, MeOH; Ac_2O, py (or CF_3CO_2Et, *i*-Pr_2NEt, DMF): *n*-Bu_4NF, THF; RuO_4, CH_2Cl_2 (81 and 91%); (b) CH_3NO_2, NaH, DME (69 and 74%); (c) H_2, Raney Ni, MeOH (100 and 98%); (d) ninhydrin, $NaHCO_3$, $MeOH/H_2O$; $NaClO_2$, NaH_2PO_4, $MeCH{=}CMe_2$, *t*-$BuOH/H_2O$ (38 and 43%); (e) 4 M HCl/dioxane (92 and 96%).

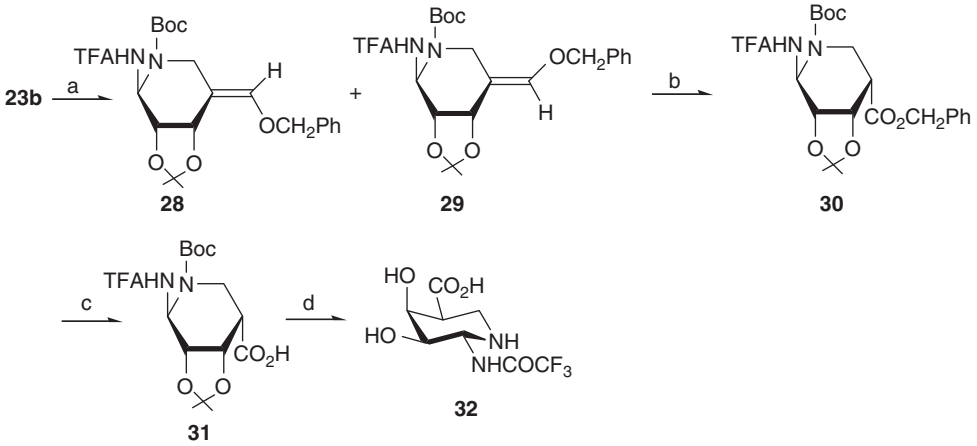

Scheme 3 Reagents and conditions: (a) $PhCH_2OCH_2PPh_3Cl$, PhLi, THF (48%); (b) $PdCl_2$, CuCl, O_2, DMF/H_2O (46%); (c) H_2, Pd/C, EtOAc (92%); (d) 4 M HCl/dioxane (96%).

acid-type and L-guluronic acid-type 1-*N*-iminosugars **61** and **66** were prepared in a straightforward manner by a similar sequence of structure transformation, except for the protection of the hydroxyl groups of **55** and **56** before hydrazinolysis of the phthalimide group for improvement in yield. The ^{1}H-NMR spectra of **61** and **66** showed the boat and $^1C_4$-conformations, respectively.

An enantioselective synthesis of L-fucose-type *gem*-diamine 1-*N*-iminosugars from D-ribono-γ-lactone was developed that used the Mitsunobu reaction on an aminal in the *gem*-diamine 1-*N*-iminopyranose ring formation (**74**→**75**) and a stereospecific reduction of an *exo*-methylene group to form the correct configuration of L-fucose (**75**→**76**) (Scheme 6).[24,25] The synthesis of the pivotal intermediate,

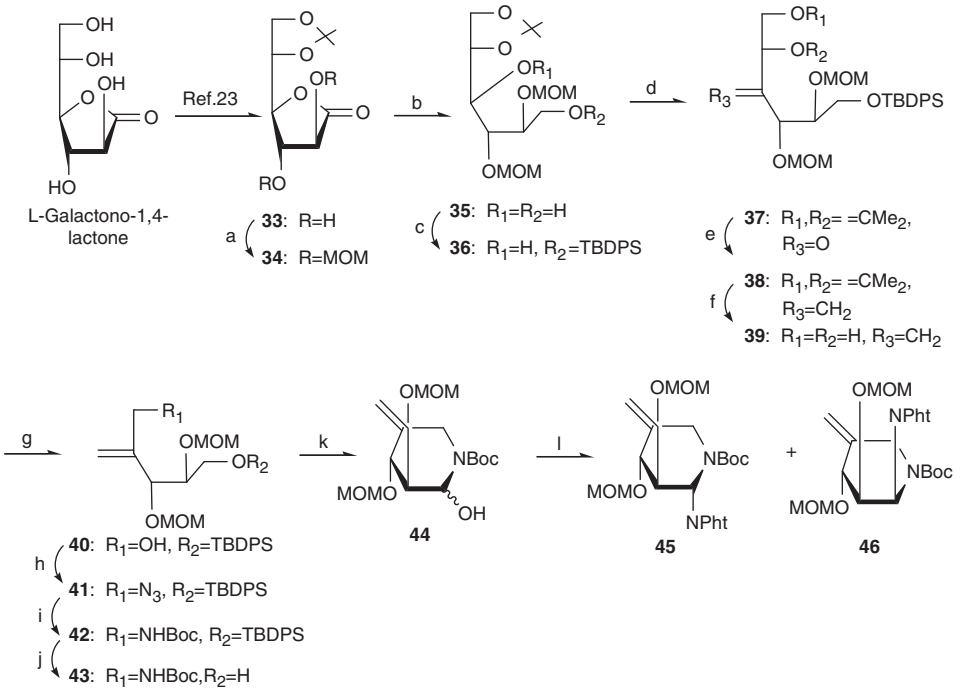

Scheme 4 Reagents and conditions: (a) $MeOCH_2Cl$, *n*-Bu_4NI, *i*-Pr_2NEt, 70 °C, 81%; (b) $LiAlH_4$, THF, 100%; (c) *t*-Bu(Ph_2)SiCl, *i*-Pr_2NEt, DMAP, CH_2Cl_2, 99.7%; (d) Dess–Martin periodinane, CH_2Cl_2, 93%; (e) Ph_3PMeBr, *n*-BuLi, THF, −78 °C, 96%; (f) 80% AcOH, rt, 99%; (g) $NaIO_4$, MeCN/H_2O; $NaBH_4$, $CeCl_3$, MeOH, 88%; (h) MsCl, py; NaN_3, DMF, 88.7%; (i) Te, $NaBH_4$, EtOH; (*t*-BuCO)$_2$O, *i*-Pr_2NEt, DMF, 88%; (j) *n*-Bu_4NF, THF, 100%; (k) $(COCl)_2$, DMSO, CH_2Cl_2, 93%; (l) PPh_3, DEAD, phthalimide, DMF, **45**: 61.4%; **46**: 20%.

aminal **74** began with the known lactam **67**. Transformation of **67** into the diol **70** was unexceptional. The Dess–Martin oxidation of **70** followed by the Wittig reaction with methylenetriphenylphosphorane yielded the *exo*-methylene **72**. Removal of a protecting group of **72** and the Swern oxidation resulted in the desired aminal **74** as a sole product. The Mitsunobu reaction of **74** with phthalimide efficiently afforded the iminophthalimide **75**. The catalytic hydrogenation of **75** yielded the desired product **76**, its epimer **77** and the rearranged derivative **78** in a ratio of 15:1:3. Compound **78** was also successfully converted into the desired **76** on the same hydrogenation. The expected stereochemistry and a boat conformation of **76** were clarified by an X-ray crystallographic analysis. Hydrazinolysis of **76** yielded the amine **79**, which was transformed into the acetamide **80**, the trifluoroacetamide **81** and the trichloroacetamide **82**. Removal of the protecting groups resulted in L-fucose-type 2-acetamido, 2-trifluoroacetamido and 2-trichloroacetamido-1-*N*-iminosugars **83**, **84** and **85**. Other L-fucose-type 1-*N*-iminosugars **86**, **87** and **88** were also obtained from the intermediates **76**, **77** and **75**, respectively, by conventional transformation. The ^{1}H-NMR spectra of **83**, **84**, **85** and **86** showed $^1C_4$-conformations.

Intermediates prepared during the total synthetic route to uronic acid-type *gem*-diamine 1-*N*-iminosugars are also available for the synthesis of various kinds of glycose and glycosamine-type *gem*-diamine 1-*N*-iminoisugars (Scheme 7).[22]

Semi-synthetic route to *gem*-diamine 1-*N*-iminosugars

Natural siastatin B (**1**) can also serve as a starting material in a simple and easy route to D-galacturonic acid-type *gem*-diamine 1-*N*-iminosugars (Scheme 8).[26,27] Transketalization using chlorotrimethylsilane successfully proceeded to yield the ketal **94**. A sequence of esterification, hydride reduction and hydrazinolysis efficiently afforded the amino alcohol **97**, which was converted into the trifluoroacetamide **98**. The ruthenium-catalyzed Sharpless oxidation followed by the removal of the protecting group resulted in the desired product **32**. 2-Trichloroacetamido, guanidino and phthaloyl analogs **106**, **107** and **108** were also prepared using similar methods.

Configurational inversion of the carboxyl group of siastatin B (**1**) leads to *gem*-diamine 1-*N*-iminosugars corresponding to L-sugars.[28,29] The intramolecular Michael addition of *O*-imidate to the α,β-unsaturated ester through *cis* oxiamination[30] (Overman rearrangement, **110**→**111**) as a key step effectively yielded L-uronic acid-type *gem*-diamine 1-*N*-iminosugars (Schemes 9 and 10). The α,β-unsaturated ester **110** readily available from siastatin B (**1**) smoothly underwent *cis* oxiamination through the conjugate addition of the intermediate imidate anion to result in the desired oxazoline **111** in a good yield and a trace amount of its epimer. Hydrolysis of **111** afforded the trichloroacetamides **112** and **113**, which were converted into the amines **114** and **115**, respectively, on reductive cleavage of the trichloroacetamide group. Removal of the protecting groups of **114** and **115** resulted in L-alturonic acid-type and L-mannuronic acid-type 2-acetamido-1-*N*-iminosugars **116** and **117**, respectively. Another type of L-alturonic acid-type 2-acetamido-1-*N*-iminosugar **119** with a guanidine group was also obtained by the conventional method. The ^{1}H-NMR spectra of **116**, **117** and **119** showed $^1C_4$-conformations. 2-Trifluoroactamide analogs **130** and **133** were also prepared by a similar sequence of reactions using the α,β-unsaturated ester **123** readily available from **97**.

Siastatin B (**1**) has the correct configuration corresponding to D-galactose- and D-galactosamine-type gem-diamine 1-*N*-iminosugars. Therefore, the various kinds of D-glycose and D-glycosamine-type *gem*-diamine 1-*N*-iminosugars could be obtainable by a semi-synthetic method starting from **1** (Schemes 11 and 12)[30,31]

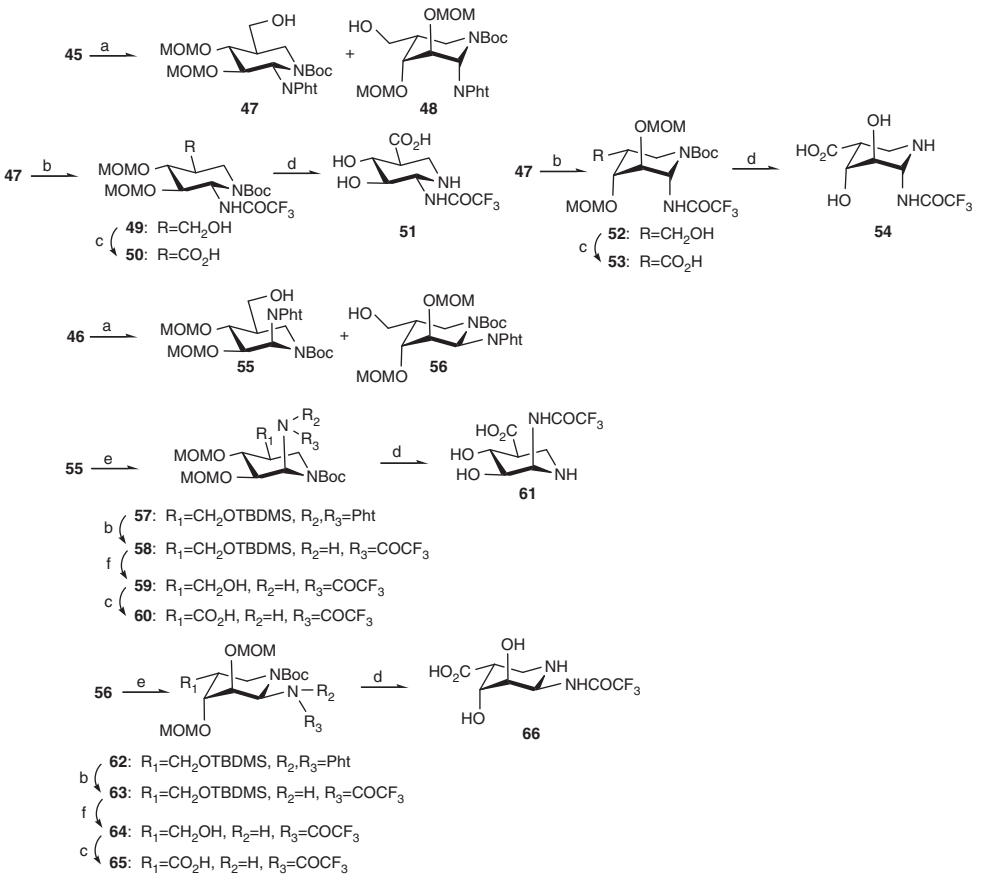

Scheme 5 Reagents and conditions: (a) $BH_3{\cdot}Me_2S$, THF; H_2O_2, 2 M NaOH/H_2O, **47**: 16.6%; **48**: 77.1%; **55**: 50%; **56**: 38%; (b) $H_2NNH_2{\cdot}xH_2O$, MeOH; $(CF_3CO)_2O$, py, CH_2Cl_2, **49**: 90%; **52**: 87%; **58**: 88%; **63**: 79%; (c) RuO_2, $NaIO_4$, CCl_4/MeCN/H_2O, **50**: 91%; **53**: 90%, **60**: 92%; **65**: 87%; (d) 4 M HCl/dioxane, **51**: 99.7%; **54**: 99%; **61**: 99.7%; **66**: 91%; (e) *t*-Bu(Me_2)SiCl, imidazole, DMF, **57**: 91%; **62**: 100%; (f) *n*-Bu_4NF, THF, **59**: 93%; **64**: 100%.

Configurational inversions at the C-4 position of **144** and **145** by two-step reactions led to the facile synthesis of D-glucosamine and glucose-type *gem*-diamine 1-*N*-iminosugars **150** and **151**, respectively (Scheme 13).[32]

BIOLOGICAL ACTIVITY

Glycoconjugates such as glycoprotein, glycolipid and proteoglycan are ubiquitous in nearly all forms of life and are involved in cell-to-cell communication, cell-to-cell recognition, cell adhesion, cell growth regulation, differentiation and transport. Specific inhibitors of glycosidase and glycosyltransferases are useful for unraveling the manner in which glycoconjugates regulate biological function, and also for developing new drugs for a wide range of diseases associated with both the biosynthesis and degradation of glycoconjugates, namely cancer, tumor metastasis, diabetes, lysosomal storage disorders, viral and bacterial infections and so forth. Iminosugars generally show potent and specific inhibition against glycosidases and glycosyltransferases from various organisms.[1,33–35] Of these, *gem*-diamine 1-*N*-iminosugars have been proven to be highly potent and specific inhibitors of glycosidases, glycosyltransferases and sulfotransferases, and also potential therapeutics for tumor metastasis, lysosomal storage disorders and other diseases.[1,6,36–38]

Glycosidase, glycosyltransferase and sulfotransferase inhibitory activity

The inhibitory activities of L-fucose-type *gem*-diamine 1-*N*-iminosugars against glycosidases are summarized in Table 1.[24,25]

The L-fucose-type 2-trifluoroacetamide **84** showed a very strong and specific inhibition against α-L-fucosidase from bovine kidney. Compound **84** was proved to be a competitive inhibitor by the Lineweaver–Burk plot, and the Ki value of **84** was determined as 5×10^{-9} M by the Dixon plot.[25] The 2-trichloroacetamide **85** and 2-phthalimide **86** also strongly affected α-L-fucosidase equivalent to the trifluoroacetamide **84**. Compounds **84**, **85** and **86** have been proven to smoothly undergo the Amadori rearrangement to yield the common intermediates, the hemiaminal **152** and the hydrated ketone **153** at pH 6.3 (Figure 3).[39] The time-course evaluation of inhibitory activities of **84**, **85** and **86** in the medium indicates that the hemiaminal and the hydrated ketone generated in the medium strongly inhibit α-L-fucosidase as the real active form. The ^{1}H-NMR spectra of the hemiaminal **152** and the hydrated ketone **153** also clearly show their $^1C_4$-conformation. Interestingly, the hemiaminal **152** has the same structure as that of synthetic L-fuconoeuromycin.[11,40] L-fuco-noeuromycin shows a potent inhibition against α-L-fucosidase equivalent to compounds **84**, **85** and **86**. On the other hand, the stable acetamide **83** in the medium shows a moderate inhibition against α-L-fucosidase. These results support the hypothesis that the protonated *gem*-diamine 1-*N*-iminosugars may mimic the presumed glycosyl cation **7** in the transition state of the enzymatic reaction as shown in Figure 2. Compounds **87** and **88** show a weak inhibition against α-L-fucosidase. These results also indicate that the 5-methyl group, its stereochemistry and the $^1C_4$-conformation have important roles as major factors for potency and specificity.

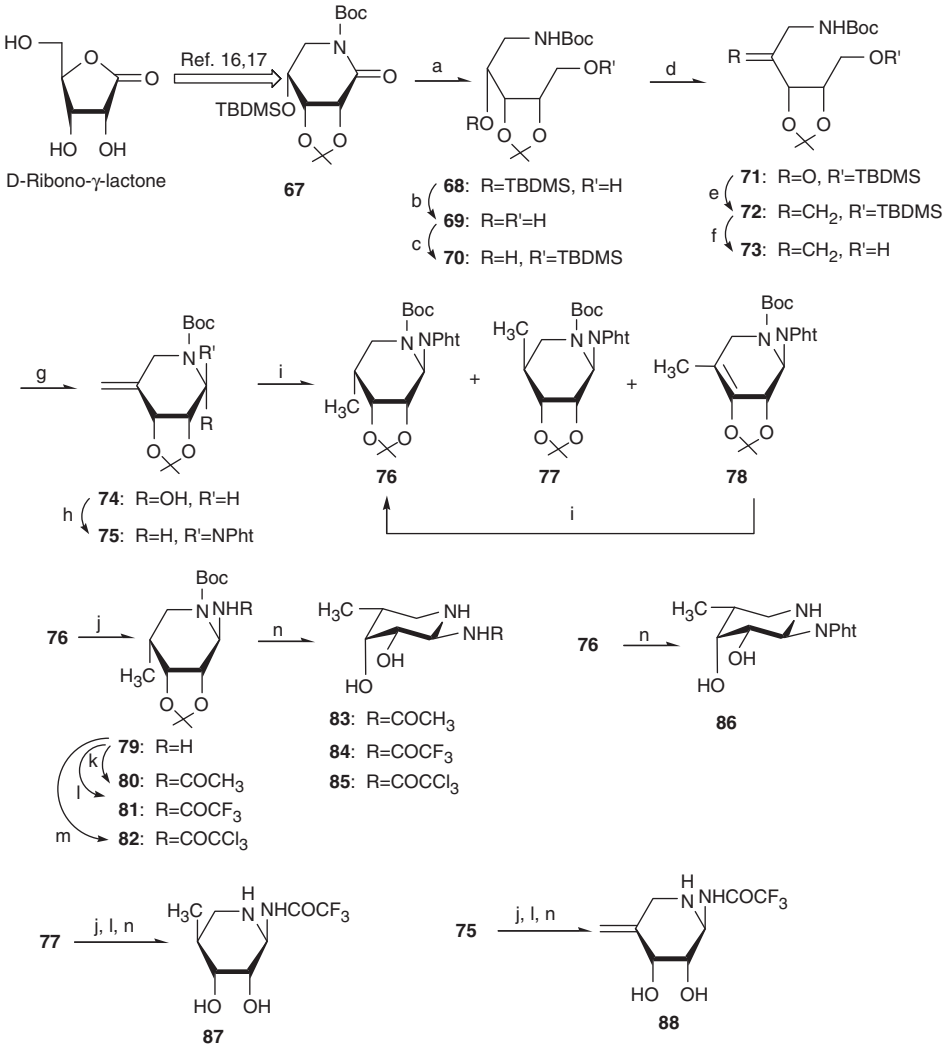

Scheme 6 Reagents and conditions: (a) $NaBH_4$, EtOH, 0 °C to rt; (b) *n*-Bu_4NF, THF, rt; (c) *t*-$BuMe_2SiCl$, imidazole, DMF, rt; (d) Dess–Martin periodinane, CH_2Cl_2; (e) Ph_3PMeBr, $(Me_3Si)_2NLi$, THF, 0 °C to rt; (f) *n*-Bu_4NF, THF, rt; (g) $(COCl)_2$, DMSO, Et_3N, CH_2Cl_2, −78 °C to rt; (h) phthalimide, Ph_3P, DEAD, DMF, rt; (i) H_2/Pd-C, MeOH, rt; (j) $H_2NNH_2{\cdot}xH_2O$, MeOH, rt; (k) Ac_2O, DMAP, py, rt; (l) $(CF_3CO)_2O$, py, CH_2Cl_2, rt; (m) CCl_3COCl, py, CH_2Cl_2, 0 °C; (n) 4 M HCl/dioxane, 0 °C to rt.

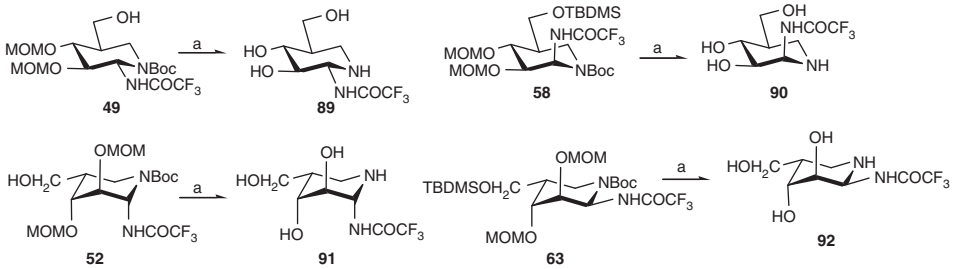

Scheme 7 Reagents and conditions: (a) 4 M HCl/dioxane.

The inhibitory activities of uronic acid-type *gem*-diamine 1-*N*-iminosugars against glycosidases are summarized in Table 2.[7,20–22,26,27]

D-glucuronic acid-type 2-trifluoroacetamido-1-*N*-iminosugar **51** shows a very strong inhibition against β-glucuronidase. D-uronic acid-type *gem*-diamine 1-*N*-iminosugars, similar to the L-fucose-type *gem*-diamine mentioned above, have been proven to smoothly undergo the Amadori rearrangement to yield the hydrated ketone **155** or its derivative **156** through a hemiaminal **154** at pH > 5.0 (Figure 4).[39] The time-course evaluation of the inhibitory activity in the medium also indicates that the hemiaminal and hydrated ketone generated in the medium strongly inhibits glycuronidases. It is reasonable to expect that the hemiaminal and hydrated ketone and

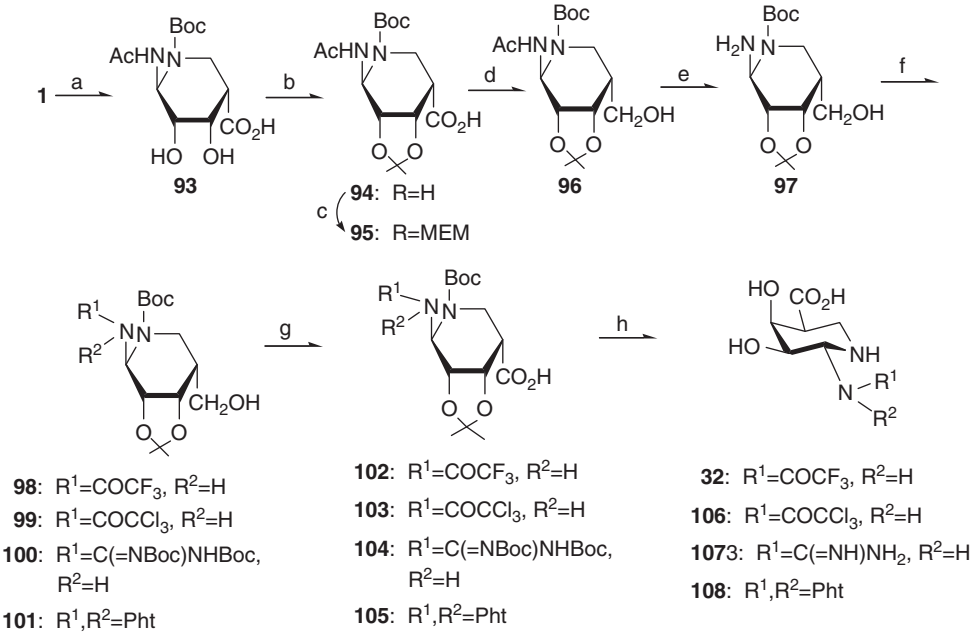

Scheme 8 Reagents and conditions: (a) $(t\text{-BuOCO})_2O$, $i\text{-Pr}_2NEt$, DMF (91%); (b) MeCH(OMe)CH_2OMe, TMSCl, DMF (98%); (c) MEMCl, $i\text{-Pr}_2NEt$, DMF (83%); (d) NaBH4, CF_3CH_2OH/THF (99%); (e) $H_2NNH_2{\cdot}xH_2O$ (54%; recovery, 80%); (f) CF_3CO_2Et, $i\text{-Pr}_2NEt$, DMF; or CCl_3COCl, py, CH_2Cl_2; or $(BocNH)_2CS$, $HgCl_2$, Et_3N, DMF; or Phthalic anhydride, Et3N, DMF, 120 °C (81, 88, 94, 60%); (g) RuO_2, $NaIO_4$, CCl_4/MeCN/H_2O (77, 76, 69, 75%); (h) 4 M HCl/dioxane (97, 100, 94, 95%).

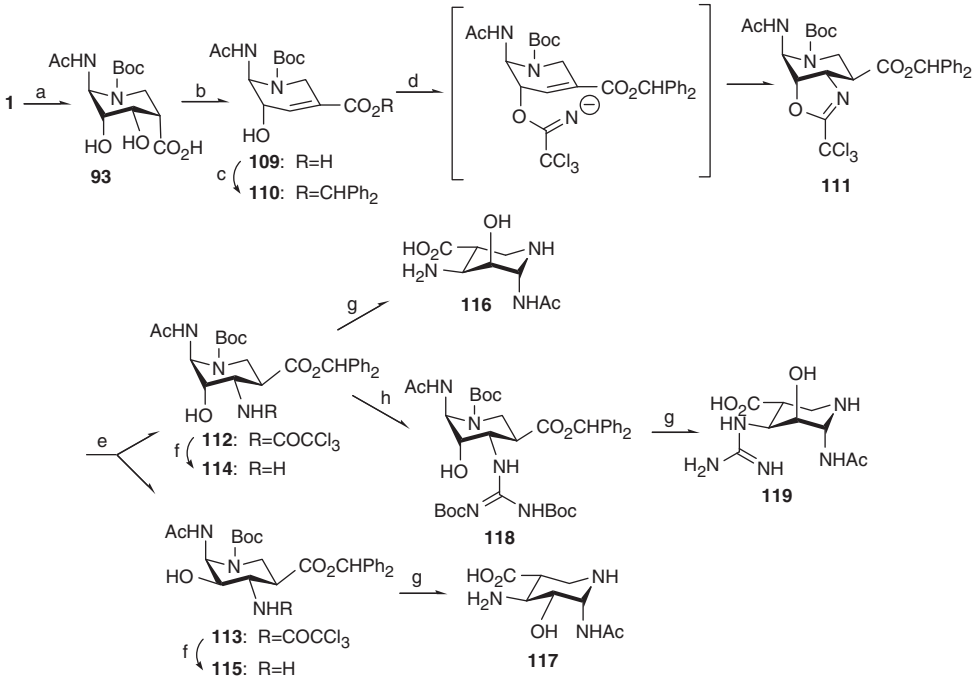

Scheme 9 Reagents and conditions: (a) $(t\text{-BuOCO})_2O$, $i\text{-Pr}_2NEt$, MeOH (93%); (b) Ac_2O, $i\text{-Pr}_2NEt$, DMF; MeONa, MeOH (90%); (c) $PhCN_2$, CH_2Cl_2/MeOH (92%); (d) CCl_3CN, DBU, CH_2Cl_2 (76%); (e) *p*-TsOH, py/H_2O (**112**, 77%; **113**, 9%); (f) $NaBH_4$, EtOH (~62%); (g) 4 M HCl/dioxane (~96%); (h) $(BocNH)_2CS$, $HgCl_2$, Et_3N, DMF (88%).

its equivalent generated from **51** in the medium should closely mimic a glycopyranosyl cation that could adapt either a chair-like or a flattened conformational **157** and **158**, respectively, in the putative transition state of β-glucuronidase hydrolysis (Figure 5). D-galacturonic acid-type 2-trifluoroacetamido-, 2-trichloroacetamido-, 2-guanidino- and 2-phthalimido-1-*N*-iminosugars **27b**, **32**, **106**, **107** and **108** also strongly inhibit glucuronidase. These results indicate that β-glucuronidase roughly recognizes the configuration of the 4-OH group of glycopyranose and/or that the binding group of β-glucoronidase to the 4-OH has no important role in the specificity. Interestingly, D-mannuronic acid-type 2-trifluoroacetamido-1-*N*-iminosugar **61** also shows a strong inhibition equivalent to those of

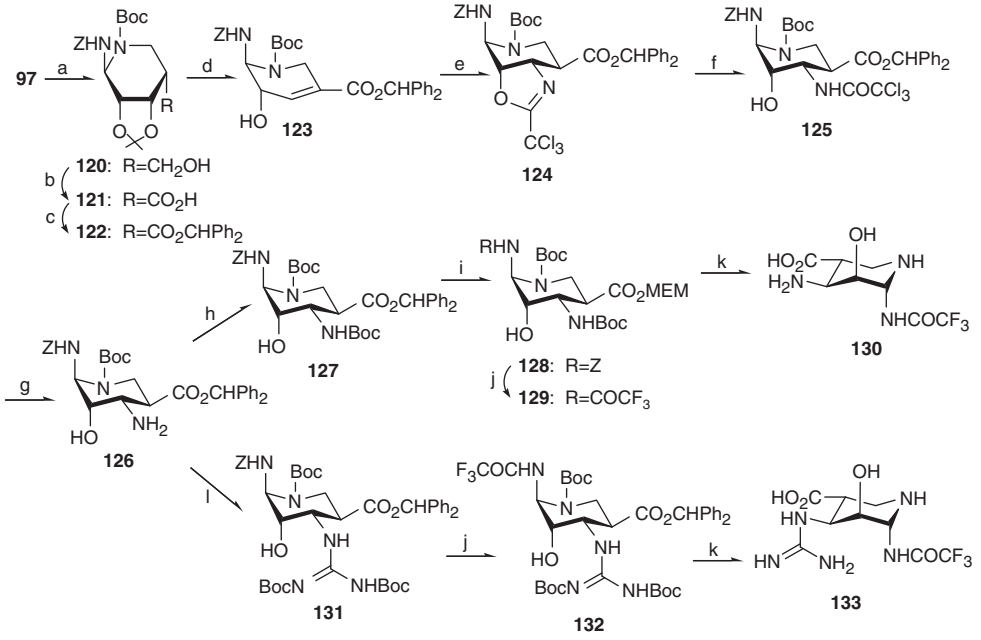

Scheme 10 Reagents and conditions: (a) $Ph_2CH_2CO_2Cl$, *i*-Pr_2NEt, MeOH (86%); (b) RuO_2, $NaIO_4$, $MeCN/CCl_4/H_2O$ (80%); (c) Ph_2CN_2, CH_2Cl_2/MeOH (94%); (d) *t*-BuOK, THF (70%); (e) CCl_3CN, DBU, C6H6 (70%); (f) *p*-TsOH, py/H_2O (95%); (g) $NaBH_4$, EtOH (68%); (h) $(t\text{-BuOCO})_2O$, *i*-Pr_2NEt, MeOH (91%); (i) 1 M NaOH/MeOH; MEMCl, *i*-Pr_2NEt, CH_2Cl_2 (83%); (j) H_2, 10% Pd/C, MeCN; $(CF_3CO)_2O$, py (~68%); (k) 4 M HCl/dioxane (~100%); (l) $(BocNH)_2CS$, $HgCl_2$, Et3N, DMF (98%).

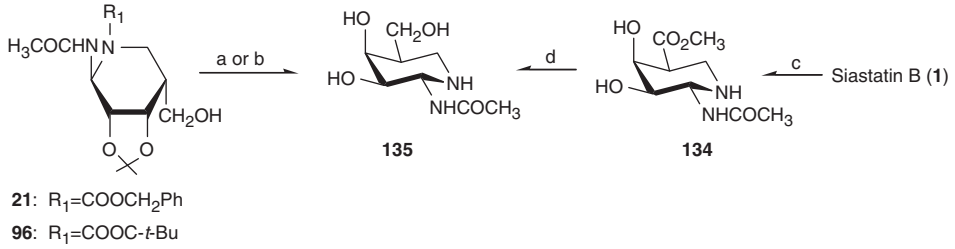

Scheme 11 Reagents and conditions: (a) H_2, 5% Pd/C, MeOH; 4 M HCl/dioxane (78%); (b) 4 M HCl/dioxane(63%); (c) Amberlist 15 (H^+), MeOH (84%); (d) $NaBH_4$, EtOH (90%).

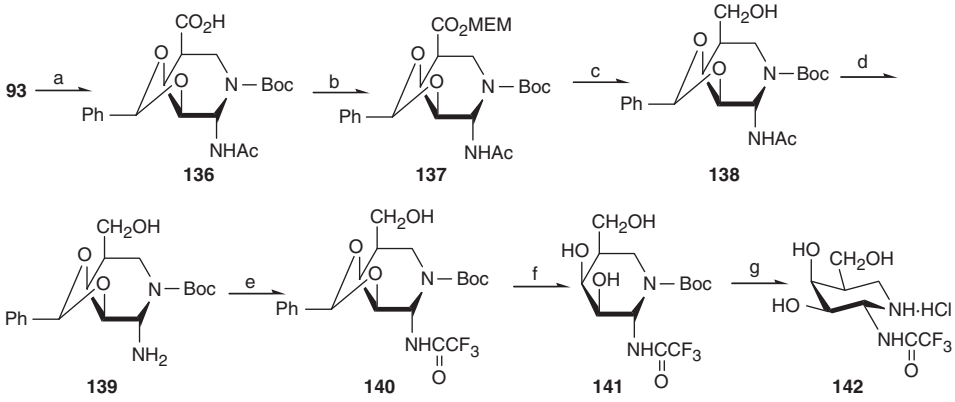

Scheme 12 Reagents and conditions: (a) $(MeO)_2CHPh$, TMSCl, DMF (92%); (b) $MeOCH_2CH_2OCH_2Cl$, *i*-Pr_2NEt, DMF, rt, 98%; (c) $NaBH_4$, CF_3CH_2OH/THF, rt, 94%; (d) $H_2NNH_2{\cdot}xH_2O$, 70 °C, 83%; (e) CF_3CO_2Et, *i*-Pr_2NEt, DMF, 60 °C, 73%; (f) H_2/10% Pd-C, MeOH, rt, 92%; (g) 4 M HCl/dioxane, rt, 80%.

D-glucuronic- and D-galacturonic acid-type 1-*N*-iminosugars **51**, **32**, **106**, **107** and **108**. The ^{1}H-NMR spectrum of **61** shows the adoption of a boat conformation that is different from the chair conformations of D-glucuronic acid- and D-galacturonic acid-type 1-*N*-iminosugars in solution, suggesting that the hemiaminal generated from **61** may mimic the flattened conformation of cation **158** in the transition state

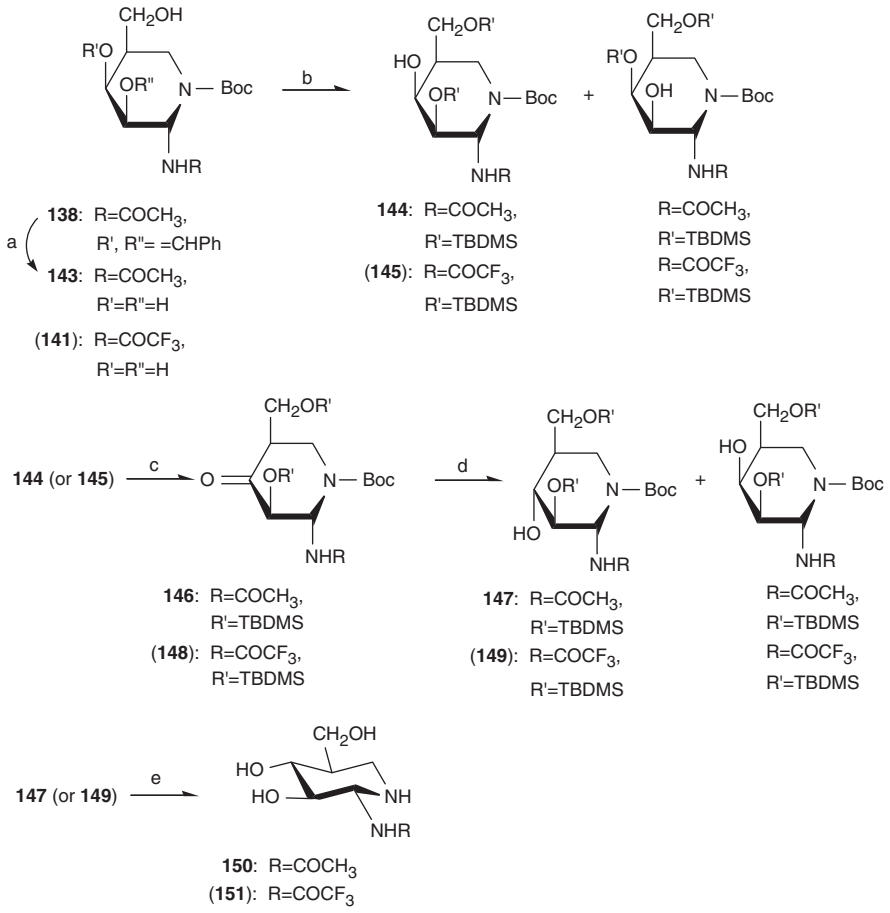

Scheme 13 Reagents and conditions: (a) H_2, 10% Pd/C, MeOH, 94%; (b) TBDMSCl, imidazole, DMF, rt, (**141** → **145**, 58%; **143** → **144**, 50%); (c) Dess–Martin periodinane, CH_2Cl_2, rt, (**145** → **148**,97%; **144** → **146**, 98%); (d) $LiBH_4$, MeCN, −50 °C, (**148** → **149**, 88%; **146** → **147**, 74%); (e) 4 M HCl/dioxane, rt, (**147** → **150**, 91%; **149** → **151**, 80%).

Table 1 Inhibitory activities (IC_{50} (M) and Ki (M)) of L-fucose-type *gem*-diamine 1-*N*-iminosugars against glycosidases

Enzyme	***83***	***84***	***85***	***86***	***87***	***88***
α-L-fucosidase[a]	4.8×10^{-7}	1.1×10^{-8} (5×10^{-9})[j]	9.0×10^{-9}	1.3×10^{-8}	1.8×10^{-6}	7.0×10^{-7}
α-D-glucosidase[b]	1.8×10^{-4}	4.7×10^{-5}	NT	NT	NT	NT
β-D-glucosidase[c]	1.0×10^{-5}	1.2×10^{-4}	NT	NT	NT	NT
α-D-mannosidase[d]	$>2.2\times10^{-4}$	$>1.8\times10^{-4}$	NT	NT	NT	NT
β-D-mannosidase[e]	$>2.2\times10^{-4}$	$>1.8\times10^{-4}$	NT	NT	NT	NT
α-D-galactosidase[f]	$>2.2\times10^{-4}$	$>1.8\times10^{-4}$	NT	NT	NT	NT
β-D-galactosidase[f]	$>2.2\times10^{-4}$	$>1.8\times10^{-4}$	NT	NT	NT	NT
β-D-glucuronidase[g]	$>2.2\times10^{-4}$	$>1.8\times10^{-4}$	NT	NT	NT	NT
α-D-NAc-galactosaminidase[h]	$>2.2\times10^{-4}$	$>1.8\times10^{-4}$	NT	NT	NT	NT
β-D-NAc-glucosaminidase[i]	$>2.2\times10^{-4}$	$>1.8\times10^{-4}$	NT	NT	NT	NT

Abbreviations: IC_{50}, half maximal inhibitory concentration; NT, not tested.
[a]Bovine kidney.
[b]Baker's yeast.
[c]Almonds.
[d]Jack beans.
[e]Snail.
[f]*Escherichia coli.*
[g]Bovine liver.
[h]Chicken liver.
[i]Bovine epididymis.
[j]Ki (M).

(Figure 5). On the other hand, the stable analogs **1** and **27a** in the media expectedly show only a weak inhibitory activity against β-glucuronidase.

The typical analogs (**32**, **51**, **61**) of D-uronic acid-type *gem*-diamine 1-*N*-iminosugars also inhibit recombinant human heparanase from human melanoma A375M cells transfected with

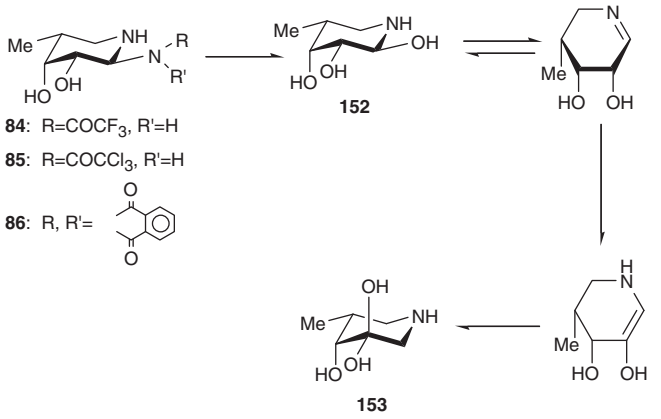

Figure 3 Structural changes of L-fucose-type *gem*-diamine 1-*N*-iminosugars in medium at pH 6.3.

pBK-CMV expression vectors containing the heparanase cDNA (Table 3).[22,41]

Heparanase is an *endo*-β-glucuronidase that specifically cleaves the β-1,4 linkage between D-glucuronic acid and *N*-acetyl-D-glucosamine of heparan sulfate (HS) side chains of HS proteoglycans (HSPGs). The relationships between activity against heparanase and the inhibitor structures are also similar to those discussed regarding the inhibition against *exo*-β-glucuronidase from bovine liver. The weaker activity against heparanase than that against *exo*-β-glucuronidase suggests that heparanase should simultaneously recognize D-glucuronic acid and the adjacent glycoses on both sides of D-glucuronic acid. As expected, all of the L-uronic acid-type *gem*-diamine 1-*N*-iminosugars (**54**, **66**, **116**, **117**, **119**, **130** and **133**) show no remarkable inhibition against these D-sugar hydrolases. These results indicate that glycohydrolases recognize precisely the absolute configurations of *gem*-diamine 1-*N*-iminosugars corresponding to the D- and L-sugars for specificity and potency.

Table 2 Inhibitory activities (IC_{50} (M)) of D-uronic acid-type *gem*-diamine 1-*N*-iminosugars against D-glycosidase

Enzyme	***1***	***27a***	***27b***	***32***	***106***	***107***	***108***	***51***	***61***
β-D-glucuronidase[a]	7.1×10^{-5}	1.2×10^{-4}	6.2×10^{-8}	6.5×10^{-8}	9.2×10^{-8}	1.3×10^{-7}	6.8×10^{-8}	6.5×10^{-8}	6.5×10^{-8}
α-D-glucosidase[b]	$>3.3\times10^{-3}$ (Ni)	Ni	2.4×10^{-7}	Ni	NT	NT	NT	Ni	Ni
β-D-glucosidase[c]	Ni	Ni	Ni	1.3×10^{-5}	NT	NT	NT	9.8×10^{-5}	3.6×10^{-5}
α-D-mannosidase[d]	Ni	Ni	Ni	Ni	NT	NT	NT	Ni	Ni
β-D-mannosidase[e]	Ni	Ni	Ni	Ni	NT	NT	NT	Ni	Ni
α-D-galactosidase[f]	Ni	Ni	Ni	1.3×10^{-6}	NT	NT	NT	Ni	Ni
β-D-galactosidase[f]	Ni	Ni	Ni	Ni	NT	NT	NT	Ni	Ni
α-D-NAc-galactosaminidase[g]	Ni	Ni	Ni	Ni	NT	NT	NT	Ni	Ni
β-D-NAc-glucosaminidase[h]	Ni	Ni	Ni	Ni	NT	NT	NT	Ni	Ni

Abbreviations: IC_{50}, half maximal inhibitory concentration; Ni, no inhibition at 3.3×10^{-3} M; NT: not tested.
[a]Bovine liver.
[b]Baker's yeast.
[c]Almonds.
[d]Jack beans.
[e]Snail.
[f]*Aspergillus niger.*
[g]Chicken liver.
[h]Bovine epididymis.

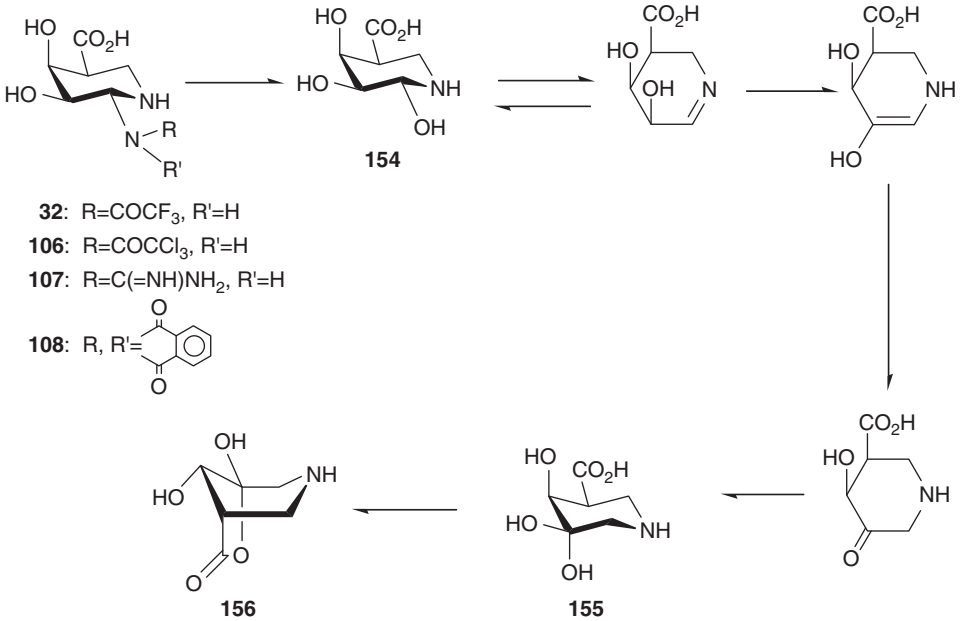

Figure 4 Structural changes of D-galacturonic acid-type *gem*-diamine 1-*N*-iminosugars in medium at pH 5.0.

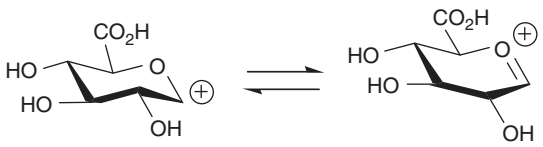

157 **158**

Figure 5 Possible conformations **157** and **158** of the glycosyl cation formed as an intermediate in β-glucuronidase hydrolysis.

Table 3 Inhibitory activities (IC_{50}) of uronic acid-type *gem*-diamine 1-*N*-iminosugars against human heparanase (endo β-D-glucuronidase)

Compounds	*IC_{50} (μM)*
32	1.02 ± 0.29
51	10.5 ± 1.07
54	Ni
61	28.99 ± 11.41
66	Ni

Abbreviations: IC_{50}, half maximal inhibitory concentration; FITC, fluorescein isothiocyanate.
Ni, no inhibition at 3.3 mM; buffer: 50 mM AcNA, pH 4.2, 0.02% CHAPS.
Enzyme: heparanase 0.26 μg protein per tube; substrate: FITC-heparan sulfate 0.5 μl (5 μg HS).
Incubation time: 37 °C, 2 h.

Table 4 Inhibitory activities (IC_{50} (M)) of D-glycose- and D-glycosamine-type *gem*-diamine 1-*N*-iminosugars against D-glycosidases

Enzyme	***135***	***142***	***150***	***151***
α-D-glucosidase[a]	$>3.9\times10^{-4}$	$>3.2\times10^{-4}$	2.9×10^{-6}	1.9×10^{-7}
β-D-glucosidase[b]	7.9×10^{-5}	4.8×10^{-7}	5.4×10^{-6}	4.2×10^{-7}
α-D-galactosidase[c]	2.5×10^{-5}	3.4×10^{-7}	$>3.9\times10^{-4}$	$>3.2\times10^{-4}$
β-D-galactosidase[c]	1.7×10^{-5}	1.7×10^{-7}	$>3.9\times10^{-4}$	1.9×10^{-4}
α-D-mannosidase[d]	$>3.9\times10^{-4}$	$>3.2\times10^{-4}$	2.5×10^{-4}	2.2×10^{-5}
β-D-mannosidase[e]	$>3.9\times10^{-4}$	1.3×10^{-4}	3.8×10^{-5}	3.2×10^{-6}
α-D-NAc-galactosaminidase[f]	3.3×10^{-7}	2.2×10^{-6}	$>3.9\times10^{-4}$	$>3.2\times10^{-4}$
β-D-NAc-glucosaminidase[g]	2.7×10^{-6}	$>3.2\times10^{-4}$	1.2×10^{-6}	$>3.2\times10^{-4}$
β-D-glucuronidase[h]	$>3.9\times10^{-4}$	$>3.2\times10^{-4}$	$>3.9\times10^{-4}$	$>3.2\times10^{-4}$

Abbreviations: IC_{50}, half maximal inhibitory concentration.
[a]Baker's yeast.
[b]Almonds.
[c]*Aspergillus niger.*
[d]Jack beans.
[e]Snail.
[f]Chicken liver.
[g]Bovine epididymis.
[h]Bovine liver.

The inhibitory activities of D-glycose- and D-glycosamine-type *gem*-diamine 1-*N*-iminosugars against glycosidases are summarized in Table 4.[30–32]

As expected, D-glucose-type 2-trifluoroacetamide **151** inhibits α- and β-D-glucosidases very strongly and specifically, and D-glucosamine-type 2-acetamide **150** shows a strong and specific inhibition against β-D-*N*-acetylglucosaminidase. On the other hand, D-galactose-type 2-trifluroacetamide **142** strongly inhibits not only α- and β-D-galactosidases but also β-D-glucosidase. D-galactosamine-type 2-acetamide **135** also strongly inhibits both α-D-*N*-acetylgalactosaminidase and β-D-*N*-acetylglucosaminidase. These results seem to indicate that the hemiaminals of the glycose-type inhibitors generated in the media mimic a transient intermediate **7** (Figure 2) in the hydrolysis of glycosidases, and that the glycosamine-type inhibitors themselves mimic a glycopyranoside in its grand state during the hydrolysis of glycosaminidases. These results also suggest that the axial 4-OH group is the main determinant for specificity and potency of the inhibitors against D-galacto-type hydrolases. However, D-gluco-type hydrolases may roughly recognize the stereochemistry of the 4-OH group and accept both axial and equatorial configurations. *N*-acetylglycosaminidases also recognize the 2-*N*-acetyl group precisely.

Table 5 Effects of 27b and CDP on [^{14}C]NeuAc incorporation into lactosylceramide (LacCer) as an exogenous acceptor

Compound	*Treatment*	*[^{14}C]NeuAc incorporated into GM3 c.p.m. mg^{-1} lipid added*	*%*
—	0	850	100
27b	1.3 mM	961	110
	4.3 mM	659	78
	13 mM	13	1.5
CDP	13 mM	7	0.82

Abbreviations: CDP, cytidine 5′-diphosphate.
The sialyltransferase activity was determined according to the method of Hakomori *et al.*[34] using mouse mammary carcinoma mutant cell line (FUA 169), which shows high activity of CMP-sialic acid:LacCer 2,3-sialosyltransferase.

D-galacturonic acid-type 2-trifluoroacetamido-1-*N*-iminosugar having a hydroxyl group at the C-5 position **27b** inhibits sialyltransferase nearly as well as cytidine 5′-diphosphate, a standard inhibitor, in the mouse mammary carcinoma mutant cell line (FUA169),[42] which has a high transfer activity of sialic acid to lactosylceramide [Galβ1—4Glcβ1—1Cer] to form ganglioside GM3 [NeuAcα2—3Galβ1—4Glcβ1—1Cer] (Table 5). This result suggests that **27b** may resemble a *gem*-diamine 5-*N*-iminosugar and mimic sialic acid (**4**) in the sialyltransferase reaction (Figure 6). This is similar to the method in which siastatin B (**1**) mimics **4** in NA (*N*-acetylsialidase) hydrolysis (Figure 1).

L-altruronic acid-type 2-acetamido-1-*N*-iminosugar **119** and its 1-*N*-2-ethlybutyrylamide (**159**) also inhibit HS 2-*O*-sulfotransferase (HS 2-*O*-ST) over 80% at 25 μM.[43] HS 2-*O*-ST transfers the sulfate group from the sulfate donor, adenosine 3′-phosphate-5′-phosphosulfate, to the 2-OH group of L-iduronic acid of HS, which is composed of a repeating disaccharide unit comprising glucosamine (GlcN) and hexuronic acid (D-glucuronic acid or its C-5 epimer, L-iduronic acid).[44] This result indicates that HS 2-*O*-ST recognizes **119** and **159** as L-iduronic acid. Molecular modeling using PM3 in MOPAC shows the structural similarity between α-L-iduronic acid and **119** (Figure 7).[29] As shown in Figure 7, **119** superimposes well on α-L-iduronic acid and the acetamido and guanidino moieties of **119** are also topographically equivalent to the hydroxyl moieties of α-L-iduronic acid.

Inhibition of esophageal keratinocyte differentiation

Recently, it has been clarified that heparanase is localized in the cell nucleus of the normal esophageal epithelium and esophageal cancer,[45] and that its expression is correlated with cell differentiation.[46] On esophageal cell differentiation, heparanase is translocated from the cytoplasm to the nucleus. On such translocation, heparanase degrades the glycan chain of HS in the nucleus, and changes in the expression of keratinocyte differentiation markers such as p27 and involucrin are observed. D-galacturonic acid-type *gem*-diamine 1-*N*-iminosugar **32** inhibits efficiently this degradation and induction in the nucleus.[47] It has been shown that heparanase regulates the

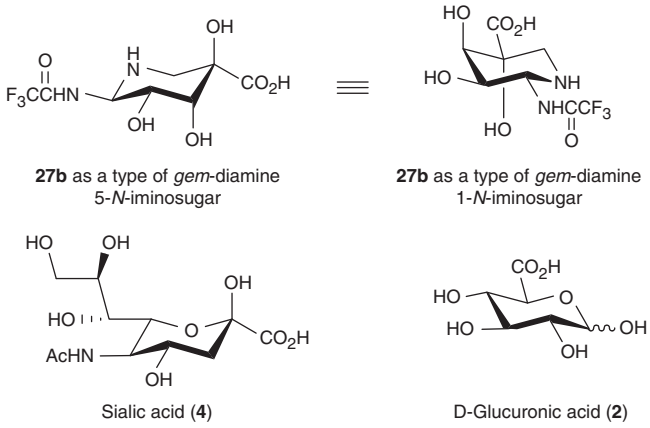

Figure 6 Structural similarity of **27b** to sialic acid (**4**) as *gem*-diamine 5-*N*-iminosugar and to D-glucuronic acid (**2**) as *gem*-diamine 1-*N*-iminosugar.

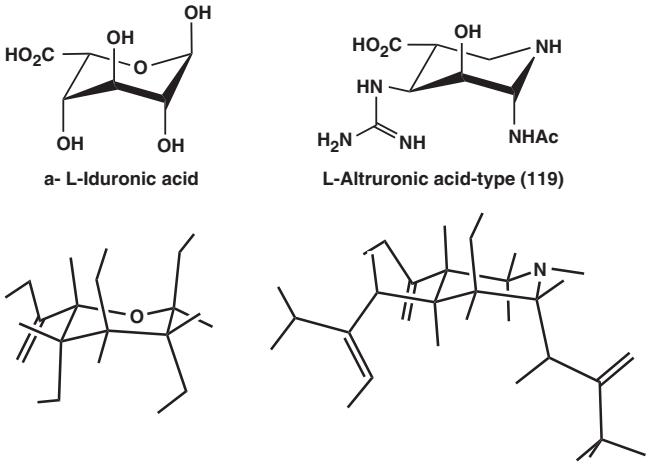

Figure 7 PM3/MOPAC-optimized structures of L-iduronic acid and **119**.

Table 6 Inhibition of experimental pulmonary metastasis of the B16BL6 by *in vitro* treatment with D-galacturonic acid-type *gem*-diamine 1-*N*-iminosugars in mice

Compound	*Dose ($\mu g\,ml^{-1}$)*	*Inhibition of metastasis (%)*
Saline (0.9%)	0	0
27b	10	11.9
	30	75.0
	50	80.5**
	100	90.4**
32	10	48.5
	30	61.9
	50	90.8**
106	10	26
	30	29.6
	50	67.3*
107	10	59.1*
	30	74.2*
	50	87.1*

The B16BL6 cells were cultured with or without compounds in Dulbecco's modified Eagle's medium supplemented with fetal bovine serum for 3 days.
The cells were harvested with 0.25% trypsin-1 mM ethylenediaminetetraacetic acid (EDTA) solution from culture dishes and washed twice with phosphate-buffered saline (PBS). The cell suspension (1×10^5) in PBS were implanted intravenously (i.v.) into the tail vein of BDF1 mice. Fourteen days later, the mice were autopsied and the numbers of pulmonary tumor nodules were counted.
*$P<0.01$; **$P<0.001$.

Table 7 Inhibition of experimental metastasis of the B16BL6 by *in vitro* treatment with L-altruronic acid-type *gem*-diamine 1-*N*-iminosugars in mice

Compound	*Dose ($\mu g\,ml^{-1}$)*	*Inhibition of metastasis (%)*
Saline (0.9%)	0	0
116	10	0
	30	12.1
	50	44.3*
119	10	40.1*
	30	91***
	50	97***
130	10	3.8
	30	38.1**
	50	75.5***
133	10	14.1
	30	58.8***
	50	81.0***

The B16BL6 cells were cultured with **116** and **119** for 3 days and with **130** and **133** for 1 day in Dulbecco's modified Eagle's medium supplemented with fetal bovine serum. The cells were harvested with 0.05% trypsin and 0.02% ethylenediaminetetraacetic acid (EDTA) solution. The cells (1×10^5) in 0.1 ml of divalent cation-free Dulbecco's phosphate-buffered saline were collected and injected intravenously (i.v.) into the tail vein of BDF1 mice. Fourteen days later, the mice were autopsied and the pulmonary tumor colonies were counted.
*$P<0.05$; **$P<0.01$; ***$P<0.001$.

Table 8 Inhibitory effect of D-galacturonic acid-type 2-trifluoroacetamide 1-*N*-iminosugar 32 on the spontaneous lung metastasis of 3LL cells in mice

Compound	*Administered dose ($mg\,kg^{-1}$)×days*	*Inhibition of metastasis (%)*
Saline (0.9%)	0×5	0
32	10×5	5.1
	50×5	23.5
	100×5	57.1*

Five female C57BL/6 mice per group inoculated with 3LL cells (1×10^6) by intra-footpad injection were administered intravenously (i.v.) with **32** for 5 days starting on the day of the surgical excision of primary tumors on day 9. Mice were killed 10 days after tumor excision.
*$P<0.01$.

differentiation of normal esophageal epithelium through nuclear translocation and nuclear HS cleavage and has an important role in the development of normal esophageal epithelium.

Inhibition of microglial cell migration

Very recently, microglia, the resident macrophages in the brain, have been found to express heparanase mRNA and protein, which can degrade the glycan chain of HSPGs.[48] Heparanase activity is correlated with the *in vitro* transmigration ability of microglia through an artificial basement membrane (BM)/extracellular matrix (ECM) containing HSPGs. D-galacturonic acid-type *gem*-diamine 1-*N*-iminosugar **32** inhibits this process in a dose-dependent manner.[48] The transmigration of microglia through BM/ECM appears to be associated with the degradation of HSPG, and this is also inhibited dose dependently by **32**. The results suggest the involvement of heparanase in the migration or invasion of microglia or brain macrophages across the BM around the brain vasculature.

Table 9 Inhibition of invasive activity of tumor cells by 32

Experimental	*Treatment ($\mu g\,ml^{-1}$)*	*Tumor cell line*	*Inhibition*
1	0	3LL	0
	100	3LL	72.4*
	200	3LL	80.1*
2	0	B16BL6	0
	100	B16BL6	29.1
	300	B16BL6	64.1*

Tumor cells were cultured in the presence of **32** for 72 h (B16BL6) or 15 h (3LL). Numbers of cells that invaded the reconstituted basement membrane Matrigel in 6 h (Experiment 1) or 3 h (Experiment 2) were counted. A laminin coated under the filter surface was used as a cell attractant.
*$P<0.05$.

Table 10 Inhibition of invasive activity of B16BL6 cell by 119 and 133

Experimental	*Compound*	*Treatment ($\mu g\,ml^{-1}$)*	*Inhibition %*
1	**119**	0	0
		200	44.8*
		300	58.9**
2	**133**	0	0
		100	44.4
		200	61.1***
		300	63.9*

The cells were cultured with **119** and **133** for 72 and 24 h, respectively. Numbers of invaded cells on the lower surface of the Matrigel/laminin-coated filters in 3 h (Experiment 1) or 6 h (Experiment 2) were counted.
*$P<0.05$; **$P<0.01$; ***$P<0.001$.

THERAPEUTIC POTENTIALS

Tumor metastasis

Recent biochemical studies have shown that cellular function and phenotype are highly influenced by HSPGs of ECM, and that the enzymatic degradation of ECM is involved in fundamental biological phenomena, including angiogenesis and cancer metastasis.[49–53] Proteolytic enzymes (heparanase and matrix metalloproteinases) secreted by tumor cells are capable of degrading ECM and BM components, and their activities are closely related to the metastasis potential of malignant cells.[54–60]

The inhibitory effects of uronic acid-type *gem*-diamine 1-*N*-iminosugars that have inhibitory activities against *exo*-uronidase, heparanase, sulfotransferase and sialyltransferase were also evaluated on tumor metastasis using the experimental and spontaneous pulmonary metastasis in mice.

D-galacturonic acid-type *gem*-diamine 1-*N*-iminosugars **27b**, **32**, **106** and **107** that have inhibitory activities against *exo*-uronidase and heparanase significantly suppress in a dose-dependent manner the number of colonies of pulmonary metastasis of B16BL6 cells in the experimental metastasis (Table 6).[6,7,26,27] Of these, 2-trifluoroacetamide **32** inhibits pulmonary metastasis most potently.

L-altruronic acid-type *gem*-diamine 1-*N*-iminosugars **116**, **119**, **130** and **133** that have inhibitory activity against HS 2-*O*-ST also reduce remarkably in a dose-dependent manner the pulmonary colonization of B16BL6 cells in the experimental metastasis (Table 7).[28] Of these, 2-acetamido-4-guanidino-1-*N*- iminosugar **119** inhibits the experimental metastasis very strongly.

As shown in Table 8, the inhibition of spontaneous lung metastasis in mice by the intravenous (i.v.) injection of **32** is more noticeable.[6,61] Compound **32** shows 57% inhibition of metastasis by the administration of 100 mg kg^{-1} per day for 5 days.

Table 11 Inhibitory activity (IC_{50} (M)) of 3-episiastatin B (160) and DDNA (161) against influenza virus *N*-acetylneuraminidase

	Influenza virus neuraminidase		
Compound	*A/FM/1/47 (H1N1)*	*A/Kayano/57 (H2N2)*	*B/Lee/40*
3-Episiastatin B	7.4×10^{-5}	$>1.0\times10^{-5}$ (25.6)	4.2×10^{-5}
DDNA	$<1.0\times10^{-5}$ (93.2)	2.9×10^{-5}	4.9×10^{-5}

Abbreviations: IC_{50}, half maximal inhibitory concentration;
( ): inhibition (%) at 1.0×10^{-5} M.
Neuraminidase inhibition assay was carried out using the method of Aminoff.[71,72]

Table 12 Inhibition (%) of 3-episiastatin B (160) and DDNA (161) against influenza virus A/FM/1/47 (H1N1) infection in MDCK cells

	Plaque forming units (PFU)			*Stained area*		
Compound	*40 μM*	*20 μM*	*10 μM*	*40 μM*	*20 μM*	*10 μM*
3-Episiastatin B	88.9	55.5	35.6	97.1	87.2	64.1
DDNA	100	100	89.6	100	100	98.7

Plaque assay was carried out using the modified method of Schulman and Palese.[71,73]

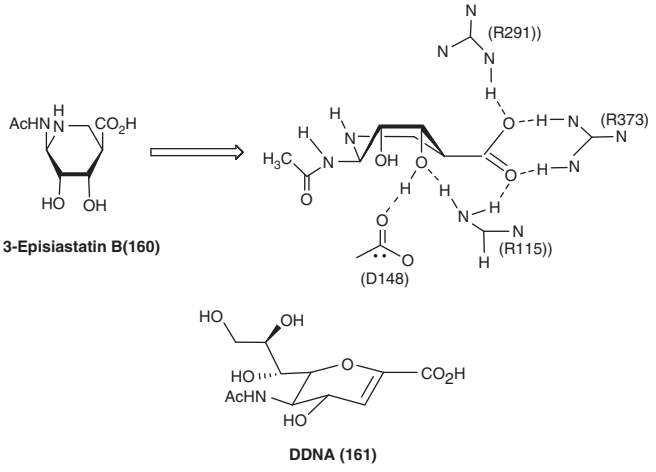

Figure 8 BIOCES[E] /AMBER minimized structure of 3-episiastatin B (**160**) in a pocket of active site residues of the crystal structure of influenza virus B/Beijin/1/87 and structure of DDNA (**161**).

On the other hand, D-galacturonic acid-type **32** and L-altruronic acid-types **119** and **133** inhibit in a dose-dependent manner the transmigration of B16BL6 and 3LL cells through the reconstituted BM (Matrigel) by *in vitro* treatment (Tables 9 and 10).[8,61]

Gem-diamine 1-*N*-iminosugars related to D-glucuronic and L-iduronic acids markedly inhibit the experimentally induced lung metastasis of B16BL6 and/or 3LL cells, and also the spontaneous lung metastasis of 3LL cells after i.v. administration. D-uronic acid-type iminosugars inhibit tumor heparanase activity, an effect that probably results from their resemblance to D-glucuronic acid as a substrate for tumor heparanase. L-uronic acid-type iminosugars inhibit HS 2-*O*-ST activity, an effect that probably results from their resemblance to L-iduronic acid as a substrate for HS 2-*O*-ST. Furthermore, *gem*-diamine 1-*N*-iminosugars prevent the transmigration of B16BL6 and/or 3LL cells through the reconstituted BM with no cytotoxicity. These results suggest that the anti-metastatic effect of the iminosugars may be due to their anti-invasive rather than their

anti-proliferative activities. It is likely that *gem*-diamine 1-*N*-iminosugars related to D-glucuronic and L-iduronic acids act as the mimic of respective uronic acids in the metabolism of ECM and/or BM involved in tumor metastasis. These iminosugars seem to modify the cell surface glycoconjugates of tumor cells simultaneously, thereby altering the cell properties involved in cellular recognition and adhesion.

Influenza virus infection

Some of the uronic acid-type *gem*-diamine 1-*N*-iminosugars could also mimic sialic acid (**4**) in the sialidase (*N*-acetyneuraminidase) reaction as an alternative type of *gem*-diamine 5-*N*-iminosugar such as siastatin B (**1**) (Figure 1).

Two integral membrane glycoproteins, hemagglutinin (HA) and NA, of the influenza virus were proved to have important roles at the beginning of infection and during the spread of the infection,[61–66] respectively, and it has been postulated that the inhibitors of HA and NA should have antiviral properties. NA is a glycosidase that cleaves the α-ketosidic bond linking the terminal sialic acid to the adjacent oligosaccharide residues of glycoproteins and glycolipids.[67,68] In 1992, the binding modes of sialic acid to NAs of the influenza virus B/Beijin/1/87 and A/Tokyo/3/67 were clarified to involve the characteristic α-boat conformation.[69,70]

3-Episiastatin B (**160**) shows specific potent inhibitory activities against influenza virus NAs and the influenza virus infection in the MDK cell *in vitro* (Tables 11 and 12).[71] Its activity is almost comparable with that of DDNA **161**, a standard inhibitor. The lowest energy boat conformer of **160** obtained by molecular modeling using PM3/MOPAC is superimposed onto the α-boat conformer of **4** in a pocket of the active site residue of the crystal structure of influenza virus B/Beijin/1/87 NA complex with **4** by a docking experiment using BIOCES/AMBER[6] (Figure 8). Compound **160** was shown to be a possible lead compound for anti-influenza virus agents.

Lysosomal storage disease

Lysosomal storage disease, in which specific enzymes of glycoconjugate degradation are deficient, is an inherited storage disorder characterized by the accumulation of partially degraded molecules in lysosomes, eventually resulting in cell, tissue and organ dysfunctions.[74] The strategies for overcoming the deficit in enzyme capacity is to provide an endogenous supply of completely functional enzymes by direct infusion or by cellular replacement with cells capable of secreting enzymes (bone marrow replacement) or by gene delivery.[75–77] An alternative to enzyme replacement is to reduce substrate influx to the lysosome by inhibiting the synthesis of glycoconjugates. This strategy has been called substrate reduction therapy.[78–80] By balancing the rate of glycoconjugate synthesis with the impaired rate of glycoconjugate breakdown, the substrate influx–efflux should be regulated to rates that do not lead to storage.

The enzyme deficient in Hunter's syndrome (MPS II) is iduronate 2-*O*-sulfatase, which functions by removing a 2-*O*-sulfate group from the iduronic acid unit of HS.[81–83] As mentioned above in the section 'Total synthetic route to *gem*-diamine 1-*N*-iminosugars,' compounds **119** and **159** inhibit strongly recombinant iduronate 2-*O*-ST over 80% at 25 μM.[43] Therefore, a partial inhibition of iduronate 2-*O*-ST by these iminosugars would reduce the build-up of the sulfated iduronic acid of HS in cells.

On the other hand, an alternative strategy, chemical chaperon therapy has been proposed for lysosomal storage disease, on the basis of a paradoxical phenomenon that states that an exogenous competitive inhibitor of low molecular weight stabilizes the target mutant protein and restores its catalytic activity as a molecular chaperon.[84–87] A competitive inhibitor binds to a misfolded mutant protein as a molecular chaperon in the endoplasmic reticulum/Golgi apparatus of the cell, resulting in the formation of a stable complex at neutral pH and transport of the catalytically active enzyme to lysosomes, in which the complex dissociates under acidic conditions and the mutant enzyme remains stabilized and functional. Some iminosugars have shown remarkable efficacy for chemical chaperon therapy of Fabry and Gaucher's disease in clinical trials.[88] *Gem*-diamine 1-*N*-iminosugars have proven to be highly potent and specific competitive inhibitors against glycosidases, glycosyltransferases and sulfotransferases. These facts suggest that *gem*-diamine 1-*N*-iminosugars would be reasonable candidates for chemical chaperon therapy in lysosomal storage diseases, and that they are in principle applicable to all types of lysosomal storage diseases.

The main advantage of these therapies is the potential ability of the inhibitors as small molecules to cross the blood–brain barrier (BBB) and elicit a favorable response in the central nervous system (CNS). The difficulties in delivering proteins (enzymes) or genes to the CNS are not apparent using a small molecule that can cross the BBB easily. The therapy using iminosugars has the potential to prevent and/or reverse the effects of lysosomal storage disease both in the body and in the brain.

CLOSING REMARKS

This article describes our current progress in the chemical, biochemical and therapeutic potential of *gem*-diamine 1-*N*-iminosugars, a new family of glycomimetics, with a nitrogen atom in place of the anomeric carbon. Mechanistically, the protonated form of new glycomimetics may act as a mimic of a glycopyranosy cation and/or the transition state formed during enzymatic glycosidic hydrolysis. New inhibitors that mimic the charge at the anomeric position of the transition state have proven to be potent and specific inhibitors of various kinds of glycosidases.

New inhibitors that affect some metabolic enzymes of glycoconjugates have been found to participate in tumor metastasis. Uronic acid-type *gem*-diamine 1-*N*-iminosugars certainly contribute to the study regarding the involvement of carbohydrates in malignant cell movement and seem to be a promising new drug candidate for cancer chemotherapy. The *N*-acetylneuraminic acid-type iminosugar has shown potency against influenza virus infection, indicating a possible drug candidate that inhibits NA. It is also likely that *gem*-diamine 1-*N*-iminosugar, a new family of glycomimetics, is a reasonable drug candidate for chemical chaperon therapy and/or substrate reduction therapy in lysosomal storage disorder.

Iminosugars have proven to be a rich source of therapeutic drug candidates in the past several years and have thus become the special focus of research attention. Of these, *gem*-diamine 1-*N*-iminosugars have been recently recognized as a new source of therapeutic drug candidates in a wide range of diseases associated with the carbohydrate metabolism of glycoconjugates.

ACKNOWLEDGEMENTS

A part of this work was supported by the Sumiki-Umezawa Memorial Award Research Grants from the Japan Antibiotic Research Association, by MPS Research Grants from the National MPS Society, USA and by Grants-in-Aid for Scientific Research from the Japan Society for the Promotion of Science (JSPS) (KAKENHI 14370761).

1 Compain, P. & Martin, O. R. ed. *Iminosugars: From Synthesis to Therapeutic Applications* 1–467 (John Wiley & Sons, West Sussex, (2007)).

2 Asano, N. Naturally occurring iminosugars and related compounds: structure, distribution, and biological activity. *Curr. Top. Med. Chem.* **3,** 471–484 (2003).
3 Inouye, S., Tsuruoka, T. & Niida, T. The structure of nojirimycin, a piperidinose sugar antibiotic. *J. Antibiot.* **19,** 288–292 (1966).
4 Cipolla, L., La Ferla, B. & Nicotra, F. General methods for iminosugar synthesis. *Curr. Top. Med. Chem.* **3,** 485–511 (2003).
5 Umezawa, H. *et al.* Purification and characterization of sialidase inhibitor, siastatin, produced by *Streptomyces*. *J. Antibiot.* **27,** 963–969 (1974).
6 Nishimura, Y. Synthesis and transformation of siastatin B, a novel glycosidase inhibitor, directed toward new drugs for viral infection and tumor metastasis in *Studies in Natural Products Chemistry* Vol. 16 (ed. Atta-ur-Rahman), 75–121 (Elsevier, Amsterdam, (1995)).
7 Nishimura, Y., Kudo, T., Kondo, S. & Takeuchi, T. Totally synthetic analogues of siastatin B. III. Trifluoroacetamide analogues having potent inhibitory activity for tumor metastasis. *J. Antibiot.* **47,** 101–107 (1994).
8 Nishimura, Y., Satoh, T., Kudo, T., Kondo, S. & Takeuchi, T. Synthesis and activity of 1-*N*-iminosugar inhibitors, siastatin B analogues for α-*N*-acetylgalactosaminnidase and β-*N*-acetylglucosaminidase. *Bioorg. Med. Chem.* **4,** 91–96 (1996).
9 McNaught, A. D. Nomenclature of carbohydrates. *Pure Appl. Chem.* **68,** 1919–2008 (1996)In the past many years, the incorrect terms 'azasugar' has been used by chemists refer to structures where oxygen is replaced by nitrogen. Use of the terms 'aza' should be restricted when carbon is replaced by nitrogen in the IUPAC rules of carbohydrate nomenclature. Thus, the 1-N-iminosugar described in this review is a true 1-aza-carbasugar. However, the terms '1-N-iminosugar' is expediential used for easy discrimination from the old incorrect azasugar in this review.
10 Jespersen, T. M. *et al.* Isofagomine, a potent, new glycosidae inhibitor. *Angew. Chem. Int. Ed. Engl.* **33,** 1778–1779 (1994).
11 Lillelund, V. H., Jensen, H. H., Liang, X. & Bols, M. Recent developments of transition-state analogue glycosidase inhibitors non-natural product origin. *Chem. Rev.* **102,** 515–553 (2002).
12 Butter, T. D. Iminosugar inhibitors for substrate reduction therapy for the lysosomal glycosphingolipidoses in *Iminosugars: From Synthesis to Therapeutic Applications* (eds. Compain, P. & Martin, O.R.) 249–268 (John Wiley & Sons, West Sussex, (2007)).
13 Look, G. C., Fotsh, C. H. & Wong, C.-H. Enzyme-catalyzed organic synthesis: practical routes to aza sugars and their analogs for use as glycoprocessing inhibitors. *Acc. Chem. Res.* **26,** 182–190 (1993).
14 Ganem, B. Inhibitors of carbohydrate-processing enzymes: design and synthesis of sugar-shaped heterocycles. *Acc. Chem. Res.* **29,** 340–347 (1996).
15 Hoos, R., Vasella, A., Rupitz, K. & Withers, S. G. D-glyconhydroximolactams strongly inhibit α-glycosidases. *Carbohydr. Res.* **298,** 291–298 (1997).
16 Nishimura, Y., Wang, W., Kondo, S., Aoyagi, T. & Umezawa, H. Siastatin B, a potent sialidase inhibitor: the total synthesis and absolute configuration. *J. Am. Chem. Soc.* **110,** 7249–7250 (1988).
17 Nishimura, Y., Wang, W., Kudo, T. & Kondo, S. Total synthesis and absolute configuration of siastatin B, neuraminidase inhibitor. *Bull. Chem. Soc. Jpn* **65,** 978–986 (1992).
18 Walker, T. E. Hogenkamp HPC. A new synthesis of L-ribofuranose derivatives. *Carbohyd. Res.* **32,** 413–417 (1974).
19 Mitsunobu, O. The use of diethyl azodicarboxylate and triphenylphosphine in synthesis and transformation of natural products. *Synthesis* 1–28 (1981).
20 Kudo, T., Nishimura, Y., Kondo, S. & Takeuchi, T. Totally synthetic analogues of siastatin B. I. Optically active 2-acetamidopiperidine derivatives. *J. Antibiot.* **45,** 954–962 (1992).
21 Nishimura, Y., Kudo, T., Kondo, S. & Takeuchi, T. Totally synthetic analogues of siastatin B. II. Optically active piperidine derivatives having trifluoroacetamide and hydroxyacetamide groups at C-2. *J. Antibiot.* **45,** 963–970 (1992).
22 Nishimura, Y. *et al.* Flexible synthesis and biological activity of uronic acid-type 1-*N*-iminosugars: a new family of glycosidase inhibitors. *J. Org. Chem.* **65,** 2–11 (2000).
23 Morgenlie, S. Synthesis of di-*O*-isopropylidene derivatives of L-fructose. *Carbohyd. Res.* **107,** 137–141 (1982).
24 Nishimura, Y., Shitara, E. & Takeuchi, T. Enantioselective synthesis of a new family of α-L-fucosidase inhibitors. *Tetrahedron Lett.* **40,** 2351–2354 (1999).
25 Shitara, E., Nishimura, Y., Kojima, F. & Takeuchi, T. *Gem*-diamine 1-*N*-iminosugars of L-fucose-type, the extremely potent L-fucosidase inhibitors. *Bioorg. Med. Chem.* **8,** 343–352 (2000).
26 Satoh, T., Nishimura, Y., Kondo, S. & Takeuchi, T. A practical synthesis of (3*S*,4*S*,5*R*,6*R*)-4,5-dihydroxy-6-(trifluoroacetamido)piperidine-3-carboxylic acid having antimetastatic activity in mice from siastatin B. *Carbohydr. Res.* **286,** 173–178 (1996).
27 Satoh, T. *et al.* Synthesis and antimetastatic activity of 6-trichloroacetamido and 6-guanidino analogues of siastatin B. *J. Antibiot.* **49,** 321–325 (1996).
28 Nishimura, Y. *et al.* The first L-iduronic acid-type 1-*N*-iminosugars having inhibitory activity of experimental metastasis. *J. Am. Chem. Soc.* **118,** 3051–3052 (1996).
29 Nishimura, Y. *et al.* Synthesis and antimetastatic activity of L-iduronic acid-type 1-*N*-iminosugars. *J. Med. Chem.* **40,** 2626–2633 (1997).
30 Nishimura, Y., Satoh, T., Kudo, T., Kondo, S. & Takeuchi, T. Synthesis and activity of 1-*N*-iminosugar inhibitors, siastatin B analogues for α-*N*-acetylgalactosaminidase and β-*N*-acetylglucosaminidase. *Bioorg. Med. Chem.* **4,** 91–96 (1996).
31 Shitara, E., Nishimura, Y., Kojima, F. & Takeuchi, T. A facile synthesis of D-galactose-type *gem*-diamine 1-*N*-iminosugr: a new family of galactosidase inhibitor. *J. Antibiot.* **52,** 348–350 (1999).
32 Shitara, E., Nishimura, Y., Kojima, F. & Takeuchi, T. A facile synthesis of D-glucose-type *gem*-diamine 1-*N*-iminosugars: a new family of glucosidase inhibitors. *Bioorg. Med. Chem.* **7,** 1241–1246 (1999).
33 Nishimura, Y. Glycosidase and glycosyltransferase inhibitors in *Studies in Natural Products Chemistry* Vol. 10 (ed. Atta-ur-Rahman), 495–583 (Elsevier, Amsterdam, (1992)).
34 Stütz, A. D. ed. *Iminosugars as Glycosidase Inhibitors: Nojirimycin and Beyond* 1–412 (Wiley-VCH, New York, (1999)).
35 Martin, O. R. & Compain, P. (ed.) Iminosugars: recent insights into their bioactivity and potential as therapeutic agents. *Curr. Top. Med. Chem.* **3,** 471–591 (2003).
36 Nishimura, Y. *Gem*-diamine 1-*N*-iminosugars and related iminosugars, candidate of therapeutic agents for tumor metastasis. *Curr. Top. Med. Chem.* **3,** 575–591 (2003).
37 Nishimura, Y. *Gem*-diamine 1-*N*-iminosugars, a new family of glycosidase inhibitors: synthesis and biological activity. *Heterocycles* **67,** 461–488 (2006).
38 Nishimura, Y. Iminosugar-based antitumoral agents in *Iminosugars: From Synthesis to Therapeutic Applications* (ed. Compain, P. & Martin, O.R.) 269–294 (John Wiley & Sons, West Sussex, (2007)).
39 Kondo, K., Adachi, H., Shitara, E., Kojima, F. & Nishimura, Y. Glycosidase inhibitors of *gem*-diamine 1-*N*-iminosugars: Structures in media of enzyme assays. *Bioorg. Med. Chem.* **9,** 1091–1095 (2001).
40 Lopez, O. & Bols, M. Isofagomine, noeuromycin and other 1-azasugars, iminosugar-related glycosidase inhibitors in *Iminosugars: From Synthesis to Therapeutic Applications* (ed. Compain, P. & Martin, O.R.) 131–151 John Wiley & Sons, West Sussex (2007).
41 Toyoshima, M. & Nakajima, M. Human heparanase. *J. Biol. Chem.* **274,** 24153–24160 (1999).
42 Tsuruoka, T., Tsuji, T., Nojiri, H., Holmes, H. & Hakomori, S. Selection of a mutant cell line based on differential expression of glycosphingolipid, utilizing anti-lactosylceramide antibody and complement. *J. Biol. Chem.* **268,** 2211–2216 (1993).
43 Brown, J. R., Nishimura, Y. & Esko, J. D. Synthesis and biological evaluation of *gem*-diamine 1-*N*-iminosugars related to L-iduronic acid as inhibitors of heparan sulfate 2-O-sulfotransferase. *Bioorg. Med. Chem. Lett.* **16,** 532–536 (2006).
44 Esko, J. D. & Lindahl, U. Molecular diversity of heparan sulfate. *J. Clin. Invest.* **108,** 169–173 (2001).
45 Ohkawa, T. *et al.* Localization of heparanase in esophageal cancer cells: respective roles in prognosis and differentiation. *Lab. Invest.* **84,** 1289–1304 (2004).
46 Nobuhisa, T. *et al.* Emergence of nuclear heparanase induces differentiation of human mammary cancer cells. *Biochem. Biophys. Res. Commun.* **331,** 175–180 (2005).
47 Kobayashi, M. *et al.* Heparanase regulates esophageal keratinocyte differentiation through nuclear translocation and heparan sulfate cleavage. *Differentiation* **74,** 235–243 (2006).
48 Takahashi, H. *et al.* Involvement of heparanase in migration of microglial cells. *Biochim. Biophys. Acta* **1780,** 709–715 (2008).
49 Esko, J. D. & Selleck, S. B. Order out of chaos: assembly of ligand binding sites in heparan sulfate. *Annu. Rev. Biochem.* **71,** 435–471 (2002).
50 Turnbull, J., Powell, A. & Guimond, S. Heparan sulfate: decoding a dynamic multifunctional cell regulator. *Trends Cell Biol.* **11,** 75–82 (2001).
51 Bernfield, M. *et al.* Function of cell surface heparan sulfate proteoglycans. *Annu. Rev. Biochem.* **68,** 729–777 (1999).
52 Iozzo, R. V. Matrix proteoglycans: from molecular design to cellular function. *Annu. Rev. Biochem.* **67,** 609–652 (1998).
53 Wight, T. N., Kinsella, M. G. & Qwarnstrom, E. E. The role of proteoglycans in cell adhesion, migration and proliferation. *Curr. Opin. Cell Biol.* **4,** 739–810 (1992).
54 Ilan, N., Elkin, M. & Vlodavsky, I. Regulation, function and clinical significance if heparanase in cancer metastasis and angiogenesis. *Int. J. Biochem. Cell Biol.* **38,** 2018–2039 (2006).
55 Goldshmidt, O. *et al.* Cell surface expression and secretion of heparanase markedly promote tumor angiogenesis and metastasis. *Proc. Natl Acad. Sci. USA* **99,** 10031–10036 (2002).
56 Vlodavsky, I. *et al.* Mammalian heparanase: gene cloning, expression and function in tumor progression and metastasis. *Nat. Med.* **5,** 793–802 (1999).
57 Hulett, M. D., Freemen, C., Hamdorf, B. J., Baker, R. T., Harris, M. J. & Parish, C. R. Cloning of mammalian heparanase, an important enzyme in tumor invasion and metastasis. *Nat. Med.* **5,** 803–809 (1999).
58 Nakajima, M., Morikawa, K., Fabra, A., Bucana, C. D. & Fidler, I. J. Influence of organ environment on extracellular matrix degradation activity and metastasis of human colon carcinoma cells. *J. Natl Cancer Inst.* **82,** 1890–1898 (1990).
59 Woolley, D. E. Collagenolytic mechanisms in tumor cell invasion. *Cancer Metastasis Rev.* **3,** 361–372 (1984).
60 Sloane, B. F. & Honn, K. V. Cystein proteinase and metastasis. *Cancer Metastasis Rev.* **3,** 249–263 (1984).
61 Nishimura, Y. *et al.* Effect on spontaneous metastasis of mouse lung carcinoma by a trifluoroacetamide analogues of siastatin B. *J. Antibiot.* **47,** 840–842 (1994).
62 Paulson, J. C. Interactions of animal viruses with cell surface receptors in *The Receptors* Vol. 2 (ed. Conn, P.M.) 131–219 (Academic Press, New York, (1985)).
63 Wiley, D. C. & Skehel, J. J. The structure and function of the hemagglutinin membrane glycoprotein of influenza virus. *Annu. Rev. Biochem.* **56,** 365–394 (1987).
64 Weis, W. *et al.* Structure of the influenza virus haemagglutinin complexed with its receptor, sialic acid. *Nature* **333,** 426–431 (1988).
65 Klenk, H. D. & Rott, R. The molecular biology of influenza virus pathogenicity. *Adv. Virus Res.* **34,** 247–281 (1988).
66 Colman, P. & Ward, C. W. Structure and diversity of influenza virus neuraminidase. *Curr. Top. Microbiol. Immunol.* **114,** 177–255 (1985).

67 Gottschalk, A. Neuraminidase: the specific enzyme of influenza virus and Vibrio cholera. *Biochem. Biophys. Acta* **23,** 645–646 (1957).
68 Schauer, R. Sialic acid and their role as biological masks. *Trends Biochem. Sci.* **10,** 357–360 (1985).
69 Burmeister, W. P., Ruigrok, R. W. H. & Cusack, S. The 2.2 Å resolution crystal structure of influenza B neuraminidase and its complex with sialic acid. *EMBO J.* **11,** 49–56 (1992).
70 Varghese, J. N. & Colman, P. M. Three-dimensional structure of the neuraminidase of influenza virus A/Tokyo/3/67 at 2.2 Å resolution. *J. Mol. Biol.* **221,** 473–486 (1991).
71 Nishimura, Y. *et al*. Synthesis of 3-episiastatin B analogues having anti-influenza virus activity. *J Antibiot.* **46,** 1883–1889 (1993).
72 Aminoff, D. Methods for the quantitative estimation of *N*-acetylneuraminic acid and their application to hydrolysates of sialomucoids. *Biochem. J.* **81,** 384–392 (1961).
73 Schulman, J. L. & Palese, P. Susceptibility of different strains of influenza A virus to the inhibitory effect of 2-deoxy-2,3-dehydro-*N*-trifluoroacetylneuraminic acid (FANA). *Virology* **63,** 98–104 (1975).
74 Winchester, B., Vellodi, A. & Young, E. The molecular basis of lysosomal storage diseases and their treatment. *Biochem. Soc. Trans.* **28,** 150–154 (2000).
75 Schiffmann, R. & Brady, R. O. New prospect for the treatment of lysosomal storage diseases. *Drugs* **62,** 733–742 (2002).
76 Ellinwood, N. M., Vite, C. H. & Haskins, M. E. Gene therapy for lysosomal storage diseases: the lessons and promise of animal models. *J. Gene. Med.* **6,** 481–506 (2004).
77 Eto, Y., Shen, J. S., Meng, X. L. & Ohashi, T. Treatment of lysosomal storage disorders: cell therapy and gene therapy. *J. Inherit. Metab. Dis.* **27,** 411–415 (2004).
78 Butters, T. D., Raymond, D. A. & Platt, F. M. Inhibition of glycosphingolipid: application to lysosomal storage disorder. *Chem. Rev.* **100,** 4683–4969 (2000).
79 Platt, F. M. *et al*. Inhibition of substrate synthesis as a strategy for glycolipids lysosomal storage disease therapy. *J. Inherit. Metab. Dis.* **24,** 275–290 (2001).
80 Cox, T. *et al*. Novel oral treatment of Gaucher's disease with N-butyldeoxynojirimycin (OGT918) to decrease substrate biosynthesis. *Lancet* **355,** 1481–1485 (2000).
81 Wraith, J. E. *et al*. Mucopolysaccharidosis type II (Hunter syndrome): a clinical review and recommendation for treatment in the era of enzyme replacement therapy. *Eur. J. Pediatr.* **167,** 267–277 (2008).
82 Hunter, C. A. A rare disease in two brothers. *Proc. R. Soc. Med.* **10,** 104–116 (1917).
83 Wilson, P. J. *et al*. Hunter syndrome: isolation of an iduronate-2-sulfatase cDNA clone and analysis of patient DNA. *Proc. Natl Acad. Sci. USA* **87,** 8531–8535 (1990).
84 Sawkar, A. R. *et al*. Chemical chaperones increase the cellular activity of N370S β-glucosidase: a therapeutic strategy for Gaucher disease. *Proc. Natl Acad. Sci. USA* **99,** 1528–15433 (2002).
85 Matsuda, J. *et al*. Chemical chaperon therapy for brain pathology in G(M_1)-gangliosidosis. *Proc. Natl Acad. Sci. USA* **100,** 15912–15917 (2003).
86 Perlmuntter, D. H. Chemical chaperones: a pharmacological strategy for disorders of protein folding and trafficking. *Pediatr. Res.* **52,** 832–836 (2002).
87 Suzuki, Y., Ogawa, S. & Sakakibara, Y. Chaperone therapy for neuronopathic lysosomal disease: competitive inhibitors as chemical chaperones for enhancement of mutant enzyme activities. *Perspectives in Medicinal Chemistry* **3,** 7–19 (2009).
88 Fan, J. Q. Iminosugars as active-site-specific chaperones for the treatment of lysosomal storage disorders in *Iminosugars: From Synthesis to Therapeutic Applications* (eds. Compain, P. & Martin, O.R.) 225–247 (John Wiley & Sons, West Sussex, (2007)).

The Journal of Antibiotics (2009) 62, 425–429

www.nature.com/ja

ORIGINAL ARTICLE

Oligomycin induced the proteasomal degradation of cyclin D1 protein

Mai Kanai, Satoru Iba, Ryoko Okada, Etsu Tashiro and Masaya Imoto

We searched for compounds that affect the cyclin D1/retinoblastoma protein pathway from the in-house natural product library using a recombinant adenovirus with the Cre/loxP-regulated cyclin D1 overexpression system, and we found that oligomycin inhibited cell growth more effectively in cyclin D1-overexpressing SW480 cells than in control SW480 cells. We also found that oligomycin reduced the expression levels of cyclin D1 protein and that this reduction is, at least in part, mediated by Thr-286 phosphorylation-dependent proteasomal degradation.
The Journal of Antibiotics (2009) **62,** 425–429; doi:10.1038/ja.2009.47; published online 3 July 2009

Keywords: cell growth inhibition; chemosensitivity; cyclin D1; pRB; E2F-1

INTRODUCTION

The transition from G1 to S phase is regulated by cyclins, cyclin-dependent kinases (CDK) and their inhibitor proteins. The proto-oncogenic function of cyclin D1 has been attributed in part to its role in promoting cell cycle progression. Cyclin D1 is a key cell cycle regulator of the G1 to S phase progression. The binding of cyclin D1 to cyclin-dependent kinase (cdk4 or cdk6) leads to the phosphorylation of retinoblastoma protein (pRB) subsequently triggering the release of E2F transcription factors to allow the transcription of genes required for the G1 to S phase progression of the cell cycle. In several types of human cancer, there is abundant evidence that disturbances of specific cyclins, CDKs or CDK inhibitory proteins enhance tumor cell growth.[1–3] In particular, disruption of the regulation of the cyclin D1/pRB/E2F pathway, overexpression of cylin D1, loss of pRB function and amplification of E2F-1 are often observed in several types of cancer.[2,4,5] Although recent reports have shown that some antitumor drugs may affect the cyclin D1/pRB/E2F pathway,[6–8] it is unclear which types of antitumor drugs induced the disruption of this pathway. In this study, we searched for compounds that inhibit cell growth selectively in cyclin D1-overexpressing human colorectal carcinoma cell lines (SW480 and LoVo) using a recombinant adenovirus with the Cre/loxP-regulated expression system.

MATERIALS AND METHODS

Cell culture and reagents

Human embryonic kidney HEK293 cells were grown in Dulbecco's Modified Eagle's Medium supplemented with 10% fetal bovine serum (FBS). Human colon cancer SW480 and LoVo cell lines were maintained in RPMI 1640 medium with 5% FBS. Adriamycin, camptothecin, etoposide, tunicamycin, wortmannin and bafilomycin A1 were purchased from Sigma Chemical (St Louis, MO, USA). Vinblastine and taxol were obtained from Wako Pure Chemical Industries, Ltd (Tokyo, Japan). Thapsigargin was obtained from Santa Cruz Biotechnology (Santa Cruz, CA, USA). Oligomycin was obtained from Calbiochem (San Diego, CA, USA). Leptomycin B was kindly supplied by Dr Minoru Yoshida (RIKEN, Japan). Inostamycin was isolated from the fermentation broth of *Streptomyces*.[9]

Adenoviral vectors and adenoviral vector-mediated expression

To exogenously express cyclin D1, we used adenovirus Cre/loxP-regulated expression vectors (TaKaRaBio, Shiga, Japan). In these vectors, pAxCALNLw, a stuffer DNA fragment sandwiched by two loxP sequences, is located just upstream of cyclin D1 cDNA and interferes with the expression of cyclin D1. Recombinant adenoviruses (adenovirus expressing wild-type cyclin D1 (Ad-cyclin D1) and adenovirus expressing Cre-recombinase (Ad-Cre)) were grown and concentrated in HEK293 cells. Infection was carried out by the addition of recombinant adenoviruses to serum-containing media following the manufacturer's instructions. SW480 and LoVo cells seeded on 6- or 96-well plates were incubated with virus-containing media at the indicated multiplicity of infection (MOI) at 37 °C for 1 h. After 1 h of incubation at 37 °C, the 1.5 ml (6-well plates) or 100 μl (96-well plates) of the fresh medium containing 5% FBS were added.

Western blotting

Cells were lysed in lysis buffer (50 mM HEPES (pH 7.2), 150 mM NaCl, 2.5 mM EGTA, 1 mM EDTA, 1 mM DTT, 0.1% Tween 20, 10 mM β-glycerophosphate, 1 mM NaF, 0.1 mM Na_3Vo_4, 10% glycerol and 0.1 mM PMSF) for 30 min on ice and centrifuged at 15 000 r.p.m. for 15 min to yield the soluble cell lysates. For immunoblotting, 50 μg proteins of cell lysates were subjected to 10% SDS-polyacrylamide gel electrophoresis. Proteins were transferred onto a polyvinylidene fluoride membrane and then incubated with appropriate antibodies for 1 h. Enhanced chemiluminescence (Millipore, Billerica, MA, USA) was used to visualize the immunoblot signals.

Department of Biosciences and Informatics, Faculty of Science and Technology, Keio University, Yokohama, Japan
Correspondence: Dr M Imoto, Department of Biosciences and Informatics, Faculty of Science and Technology, Keio University, 3-14-1 Hiyoshi, Kohoku-ku, Yokohama 223-8522, Japan.
E-mail: imoto@bio.keio.ac.jp
Received 17 April 2009; revised 22 May 2009; accepted 27 May 2009; published online 3 July 2009

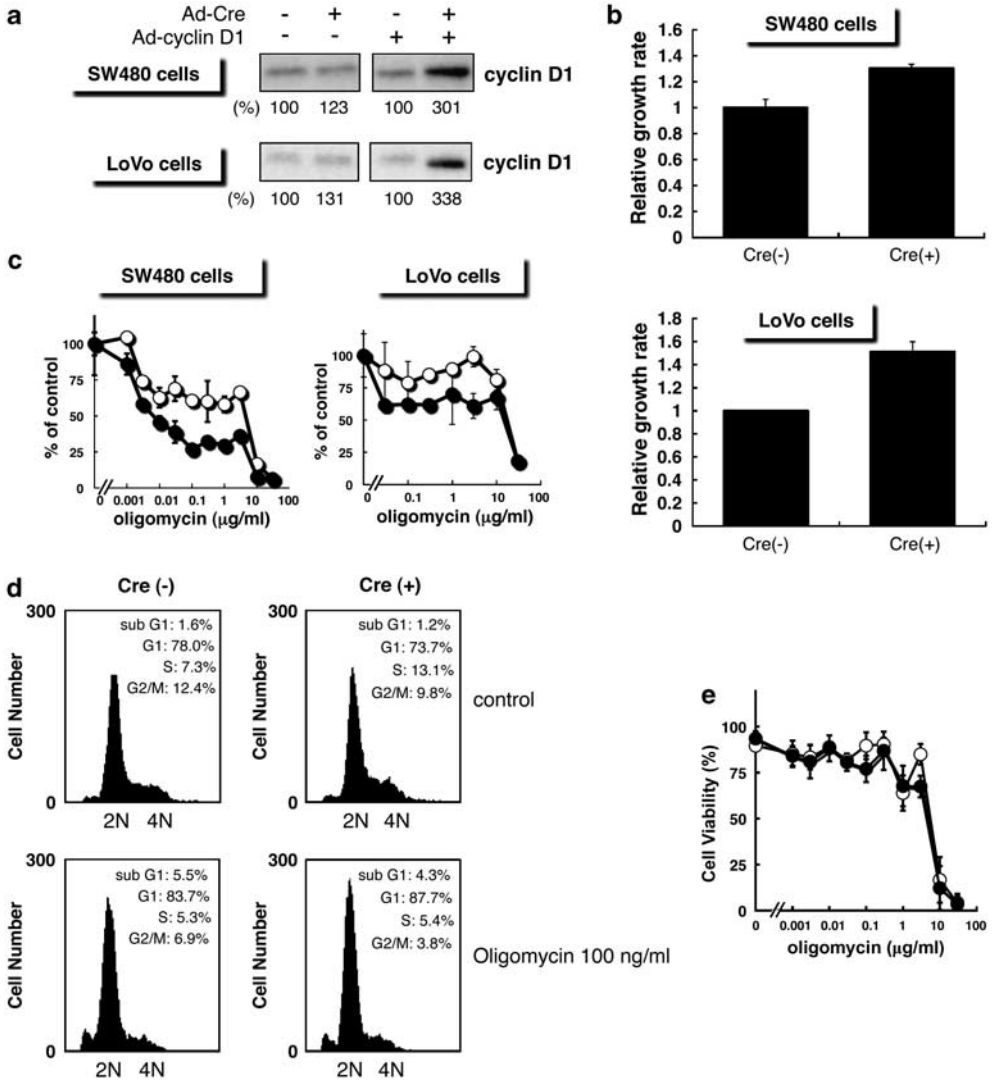

Figure 1 Effect of oligomycin on the growth of cyclin D1-overexpressing cells and control cells. SW480 cells and LoVo cells were infected with Ad-cyclin D1 (MOI 3) together with or without Ad-Cre (MOI 0.5). (**a**) At 48 h after infection, the protein expression of cyclin D1 was detected by western blotting using anti-cyclin D1 antibody (Santa Cruz Biotechnology). The bands of cyclin D1 were quantified by densitometry, and the results were normalized to control, which was arbitrarily set to 1.0 (below the panel). (**b**) At 48 h after infection, cell growth was measured by the MTT assay. Values represent the means ± s.d. (bars) obtained from triplicate determinations. (**c**) At 48 h after infection, cells were treated with oligomycin, and cells were further incubated for 48 h. Cell growth was measured by the MTT assay (Ad-cyclin D1 alone (Cre(−)); open circle, Ad-cyclin D1/Ad-Cre (Cre(+)); closed circle). Values represent the means ± s.d. (bars) obtained from triplicate determinations. (**d**) SW480 cells were infected with Ad-cyclin D1 (MOI 3) together with or without Ad-Cre (MOI 0.5). At 48 h after infection, cells were treated with 100 ng ml^{-1} of oligomycin and further incubated for 48 h, and the DNA contents were then analyzed by flow cytometer. (**e**) SW480 cells were infected with Ad-cyclin D1 (MOI 3) together with or without Ad-Cre (MOI 0.5). At 48 h after infection, cells were treated with the indicated concentration of oligomycin and further incubated for 48 h, and then the cell viability was determined by trypan blue dye exclusion assay (Ad-cyclin D1 alone (Cre(−)); open circle, Ad-cyclin D1/Ad-Cre (Cre(+)); closed circle).

Figure 2 Oligomycin induced the degradation of cyclin D1 protein. (**a**) SW480 cells were infected with Ad-cyclin D1 (MOI 3) together with or without Ad-Cre (MOI 0.5). At 48 h after infection, cells were treated with oligomycin at the indicated doses. At 48 h after treatment, cells were lysed and the expression levels of cell cycle progression-related proteins were detected by western blotting using anti-cyclin D1, anti-E2F-1 and anti-CDK2 (Santa Cruz Biotechnology), anti-pRB (BD Biosciences, Franklin Lakes, NJ, USA) and anti-cyclin E (Upstate, Charlottesville, VA, USA) antibodies. (**b**) SW480 cells were infected with Ad-cyclin D1 (MOI 3) together with Ad-Cre (MOI 0.5). At 48 h after infection, cells were treated with indicated concentrations of oligomycin for a further 24 and 48 h, and then cyclin D1 mRNA was analyzed by real-time quantitative RT-PCR. GAPDH mRNA was measured for internal control and relative Cyclin D1 mRNA was calculated as Cyclin D1/GAPDH. The data are expressed as means ± s.d. of three independent experiments. (**c**) SW480 cells were infected with Ad-cyclin D1 (MOI 3) together with Ad-Cre (MOI 0.5). At 48 h after infection, cells were treated with oligomycin in the presence or absence of MG132. At 48 h after treatment, cells were lysed and the expression levels of cyclin D1 protein were detected by western blotting using an anti-cyclin D1 antibody. Percentages represent the relative expression level of cyclin D1 compared with treatment with MeOH and normalization to tubulin.

Table 1 Effect of natural anti-tumor drugs on the growth of cyclin D1-overexpressing SW480 cells (Cre(+)) and control SW480 cells (Cre(−))

	IC_{50} (mg ml^{-1})		
Antitumor drug	*Cre (−)*	*Cre (+)*	*Cre (−)/Cre (+)*
Adriamycin	0.75	0.64	1.17
Camptothecin	0.78	0.89	0.88
Etoposide	47	20	2.35
Inostamycin	0.49	0.48	1.02
Thapsigargin	0.07	0.05	1.40
Tunicamycin	0.45	0.36	1.25
Leptomycin B	0.36	0.56	0.64
Vinblastine	>3	>3	—
Taxol	>10	>10	—
Wortmannin	25.6	32.8	0.78
Bafilomycin A1	2.17	1.03	2.11
Oligomycin	5.31	0.007	758.57

Abbreviation: MOI, multiplicity of infection.
SW480 cells were infected with Ad-cyclin D1 (MOI 3) together with or without Ad-Cre (MOI 0.5). Values are the means of three samples.

MTT cell growth assay

The cells were seeded at 3×10^3 cells (SW480 cells) or 1.5×10^3 cells (LoVo cells) in 100 µl of growth medium in 96-well plates. The following day, the cells were infected with Ad-Cyclin D1 with or without Ad-Cre. At 48 h after infection, drugs were added and the cells were further incubated for 48 h. A total of 10µl of 5 mg ml^{-1} 3-(4,5-dimethylthiazol-2-yl)-2,5-diphenyltetrazolium bromide (MTT) in phosphate-buffered saline was added to each well, and the plate was incubated at 37 °C for 4 h. Then, 100 µl of DMSO was added to the cells. The amount of Formazan formed was measured at 570 nm using a MRP-A4 microplate reader (Tosho, Tokyo, Japan).

Real-time RT-PCR

Total RNA (2 µg) isolated from cells with TRIzol reagent (Invitrogen, Carlsbad, CA, USA) was reverse transcribed with 2 µg oligo(dT) primer using MMLV-RT/HT point mutant reverse transcriptase (Promega, Madison, MA, USA) at 42 °C for 1 h. Real-time reverse transcriptase (RT)-PCR assay was performed using SYBR Premix Ex Taq (TaKaRaBio), and PCR amplification was carried out in a MJ mini personal thermal cycler (Bio-Rad, San Diego, CA, USA). Relative mRNA levels of Cyclin D1 were calculated by MJ opticon monitor analysis version 3.1 (Bio-Rad).

Plasmid construction and transfection

Flag-Cyclin D1 cDNA was generated from pcDNA3-Cyclin D1 by PCR using the synthetic primers 5′-GTGTCCTCGACCACAAGGTAGAACAGCAGCAG

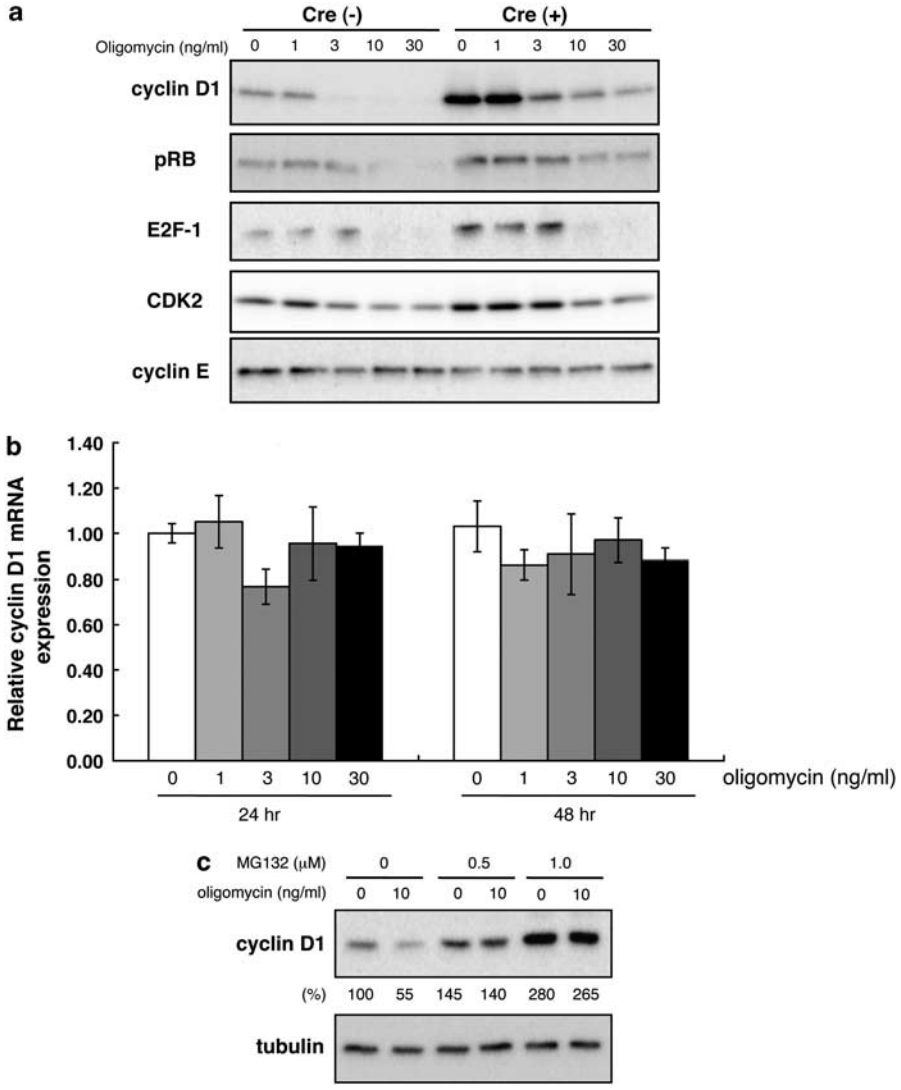

CAGGAACATCAGGTATCGAAGGG-3′ and 5′-TGGCTGCACGCCCTGCACC TGTAGACTTTCGAAGGG-3′. The amplified PCR product was inserted into the pBlueScript vector to construct pBS-Flag-Cyclin D1. Point mutant T286A of Flag-Cyclin D1 was generated by PCR using sense primer 5′-CGTGCAGC CACCCGCGCGTTCGGTCCGGT-3′ and antisense primer 5′-ACCTGGACC GAACGCGCGGGTGGCTGCACG-3′. Both pBS-Flag-Cyclin D1 and pBS-Flag-Cyclin D1 T286A were digested with *Hind*III and inserted into the pcDNA3 vector. For transient transfection, HEK293 T cells were seeded at 2.5×10^5 cells per well in 12-well plates. The following day, HEK293T cells were transfected with 0.3 μg of plasmid using lipofectamine 2000 (Invitrogen) in OPTIMEM according to the manufacturer's instructions.

Flow cytometry

The cells were collected by trypsinization, combined with cells floating in the medium, and then stained with propidium iodide. The cell suspension was analyzed using an EPICS Elite and EXPO32 software analysis program (Beckman Coulter, Fullerton, CA, USA).

RESULTS AND DISCUSSION

To overexpress cyclin D1 protein in human colon cancer cell lines SW480 and LoVo, we used the recombinant adenovirus with the Cre/loxP-regulated expression system. The cells were infected with a combination of Ad-cyclin D1/Ad-Cre (Cre(+)) or Ad-cyclin D1 alone (Cre(−)), and their cyclin D1 expression levels were evaluated by western blot analysis. We found that expression levels of cyclin D1 in SW480 and LoVo cells were increased 48 h after infection with a combination of recombinant adenovirus cyclin D1 (Ad-cyclin D1; MOI 3) and Cre-recombinase (Ad-Cre; MOI 0.5) (Figure 1a), and a high level of cyclin D1 expression was maintained for 96 h after adenovirus infection, as judged from western blotting experiments. In addition, the growth rate of Ad-cyclin D1/Ad-Cre (Cre(+)) cells was approximately 1.5-fold higher than that of Ad-cyclin D1 alone (Cre(−)) cells (Figure 1b). Using this system, we next examined the effects of twelve known natural antitumor drugs—adriamycin (topoisomerase II inhibitor), camptothecin (topoisomerase I inhibitor), etoposide (topoisomerase II inhibitor), inostamycin (phosphatidylinositol turnover inhibitor), thapsigargin (Ca^{2+}-ATPase inhibitor), tunicamycin (*N*-linked glycosylation inhibitor), leptomycin B (CRM1 inhibitor), vinblastine (microtubule inhibitor), taxol (tubulin inhibitor), wortmannin (PI3 kinase inhibitor), bafilomycin A1 (V-ATPase inhibitor) and oligomycin (F_0F_1-ATPase inhibitor)—on the growth of cyclin D1-overexpressing cells and control cells by the MTT cell growth assay. We found that oligomycin inhibited cell growth more effectively in cyclin D1-overexpressing SW480 cells (Cre(+)) than in control SW480 cells (Cre(−)) (Table 1 and Figure 1c). The IC_{50} value of oligomycin for cell growth inhibition in cyclin D1-overexpressing SW480 cells (Ad-cyclin D1; MOI 3, Ad-Cre; MOI 0.5) was approximately 750-fold lower than in control SW480 cells (Ad-cyclin D1; MOI 3). Similar results were observed in cyclin D1-overexpressing LoVo cells and control LoVo cells (Figure 1c).

The growth inhibition of cyclin D1-overexpressing SW480 cells caused by oligomycin (up to 1 μg ml^{-1}) did not relate to the cytotoxic effect of the drug, as determined by trypan blue dye exclusion assay and flow cytometric analysis (Figures 1d and e). Next, we examined the effect of oligomycin on the expression levels of cell cycle-related proteins in cyclin D1-overexpressing cells (Cre(+)) and control cells (Cre(−)). As shown in Figure 2a, oligomycin reduced the expression levels of cyclin D1 protein in both cyclin D1-overexpressing SW480 cells and control cells. The expressions of pRB, E2F-1 and CDK2 were also decreased by oligomycin with a similar profile in both cells, whereas the expression profiles of cyclin E were not affected by oligomycin. The growth rate of cyclin D1-overexpressing cells was higher than that of control cells (Figure 1b), indicating that the growth properties of cyclin D1-overexpressing cells might be more sensitive to the expression levels of cyclin D1 than that of control cells, which may explain the difference in the growth inhibition rate between cyclin D1-overexpressing cells and control cells.

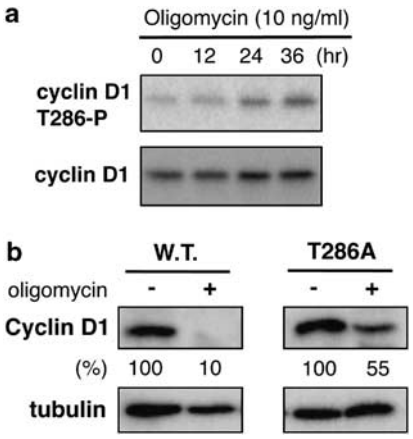

Figure 3 Involvement of T286 phosphorylation in oligomycin-induced decrease in cyclin D1 expression. (**a**) SW480 cells were treated with 10 ng ml^{-1} oligomycin. At the indicated times after treatment, cells were lysed and T286-phosphorylated cyclin D1 was detected by western blotting using anti-phospho-cyclin D1 (Thr-286) antibody (Cell Signaling Technology, Danvers, MA, USA). (**b**) HEK293T cells were transfected with Flag-tagged cyclin D1 wild-type (Flag-cyclin D1 WT) or Flag-tagged T286A mutant of cyclin D1 (Flag-cyclin D1 T286A) for 24 h, and they were also incubated with or without oligomycin (10 ng ml^{-1}) for 48 h. Protein samples were detected by western blotting using an anti-Flag antibody (M2; Sigma-Aldrich Corp., St Louis, MO, USA). Percentages represent the relative expression level of Flag-cyclin D1 compared with treatment with MeOH and normalization to tubulin.

Gemin *et al.* also reported that treatment of HL60 cells with oligomycin resulted in a reduction in the amount of endogenous cyclin D1 protein;[10,11] however, it has not yet been reported how oligomycin reduced the expression levels of cyclin D1. We found that the mRNA level of cyclin D1 was not affected by treatment with oligomycin when the cyclin D1 protein level was decreased (Figure 2b), indicating that decreased expression of cyclin D1 protein did not occur at the transcriptional level. On the other hand, oligomycin failed to reduce the expression level of cyclin D1 in cyclin D1-overexpressing SW480 cells when cells were treated with MG132, an inhibitor of proteasome (Figure 2c). These results indicated that the oligomycin-induced decrease in cyclin D1 expression levels was because of the proteasomal degradation of cyclin D1.

It is known that cyclin D1 is ubiquitinated and degraded through its phosphorylation at Thr-286 by glycogen synthase kinase-3β (GSK3β),[12] IκB kinase α (IKKα),[13] p38[14] or extracellular signal-regulated kinase 1/2 (ERK1/2).[15] As shown in Figure 3, oligomycin induced phosphorylation at Thr-286 in cyclin D1 (Figure 3a), and elimination of this site through point mutation (Ala for Thr-286 substitution: T286A) markedly but did not completely stabilize cyclin D1 (Figure 3b); therefore, although at present we do not know which kinase is responsible for phosphorylation at Thr-286 in cyclin D1 after oligomycin treatment, oligomycin-induced reduction of cyclin D1 expression is, at least in part, mediated by Thr-286 phosphorylation-dependent proteasomal degradation. Other degradation motifs of cyclin D1, such as the Arg-X-X-Leu destruction box,[16] may also be involved in oligomycin-induced degradation of cyclin D1 protein.

Apoptolidin as well as oligomycin is also reported to be an inhibitor of the F_0F_1-ATPase inhibitor, and is identified on the basis of its ability to selectively kill E1A- and E1A/E1B19K-transformed rat glial cells while not killing untransformed glial cells.[17] E1A alone is sufficient to activate the cell cycle, inducing the expression of genes required for DNA synthesis and repeated rounds of cell division. Binding of pRB by E1A is intimately linked with these activities. E1B products alone show no ability to induce proliferation; however, the proliferation of cells in response to E1A is often quite limited in the absence of E1B expression;[18] therefore, apoptolidin is also related to the cyclin D1/pRB/E2F pathway. Although further studies on the biological activities of oligomycin are required, the F_0F_1-ATPase inhibitors, such as oligomycin and apoptolidin, affect the disruption of the cyclin D1/pRB/E2F pathway.

ACKNOWLEDGEMENTS

This study was supported in part by the Global COE program for Human Metabolomic Systems Biology from MEXT, Japan.

1 Draetta, G. F. Mammalian G1 cyclins. *Curr. Opin. Cell Biol.* **6,** 842–846 (1994).
2 Hunter, T. & Pines, J. Cyclins and cancer. II: cyclin D and CDK inhibitors come of age. *Cell* **79,** 573–582 (1994).
3 Sherr, C. J. G1 phase progression: cycling on cue. *Cell* **79,** 551–555 (1994).
4 Nevins, J. R. The Rb/E2F pathway and cancer. *Hum. Mol. Genet.* **10,** 699–703 (2001).
5 Saito, M. *et al.* Amplification of the E2F1 transcription factor gene in the HEL erythroleukemia cell line. *Genomics* **25,** 130–138 (1995).
6 Endo, N. *et al.* Herbimycin A induces G1 arrest through accumulation of p27(Kip1) in cyclin D1-overexpressing fibroblasts. *Biochem. Biophys. Res. Commun.* **267,** 54–58 (2000).
7 Pirkmaier, A., Yuen, K., Hendley, J., O'Connell, M. J. & Germain, D. Cyclin d1 overexpression sensitizes breast cancer cells to fenretinide. *Clin. Cancer Res.* **9,** 1877–1884 (2003).
8 Dong, Y. B., Yang, H. L., Elliott, M. J. & McMasters, K. M. Adenovirus-mediated E2F-1 gene transfer sensitizes melanoma cells to apoptosis induced by topoisomerase II inhibitors. *Cancer Res.* **62,** 1776–1783 (2002).
9 Imoto, M. *et al.* Isolation and structure determination of inostamycin, a novel inhibitor of phosphatidylinositol turnover. *J. Nat. Prod.* **53,** 825–829 (1990).
10 Sweet, S. & Singh, G. Accumulation of human promyelocytic leukemic (HL-60) cells at two energetic cell cycle checkpoints. *Cancer Res.* **55,** 5164–5167 (1995).
11 Gemin, A., Sweet, S., Preston, T. J. & Singh, G. Regulation of the cell cycle in response to inhibition of mitochondrial generated energy. *Biochem. Biophys. Res. Commun.* **332,** 1122–1132 (2005).
12 Diehl, J. A., Cheng, M., Roussel, M. F. & Sherr, C. J. Glycogen synthase kinase-3beta regulates cyclin D1 proteolysis and subcellular localization. *Genes Dev.* **12,** 3499–3511 (1998).
13 Kwak, Y. T. *et al.* IkappaB kinase alpha regulates subcellular distribution and turnover of cyclin D1 by phosphorylation. *J. Biol. Chem.* **280,** 33945–33952 (2005).
14 Casanovas, O. *et al.* Osmotic stress regulates the stability of cyclin D1 in a p38SAPK2-dependent manner. *J. Biol. Chem.* **275,** 35091–35097 (2000).
15 Okabe, H. *et al.* A critical role for FBXW8 and MAPK in cyclin D1 degradation and cancer cell proliferation. *PLoS ONE* **1,** e128 (2006).
16 Agami, R. & Bernards, R. Distinct initiation and maintenance mechanisms cooperate to induce G1 cell cycle arrest in response to DNA damage. *Cell* **102,** 55–66 (2000).
17 Kim, J. W., Adachi, H., Shin-ya, K., Hayakawa, Y. & Seto, H. Apoptolidin, a new apoptosis inducer in transformed cells from Nocardiopsis sp. *J. Antibiot. (Tokyo)* **50,** 628–630 (1997).
18 Moran, E. Interaction of adenoviral proteins with pRB and p53. *FASEB J.* **7,** 880–885 (1993).

The Journal of Antibiotics (2009) 62, 431–434

www.nature.com/ja

ORIGINAL ARTICLE

Xanthoradones, new potentiators of imipenem activity against methicillin-resistant *Staphylococcus aureus*, produced by *Penicillium radicum* FKI-3765-2: I. Taxonomy, fermentation, isolation and biological properties

Hiroyuki Yamazaki[1], Kenichi Nonaka[2], Rokuro Masuma[2], Satoshi Ōmura[2] and Hiroshi Tomoda[1]

The fungal strain FKI-3765-2, identified as *Penicillium radicum*, was found to produce potentiators of imipenem activity against methicillin-resistant *Staphylococcus aureus* (MRSA). Two new compounds, designated xanthoradones A and B, were isolated from the fermentation broth of the producing strain by solvent extraction, octadecyl silyl column chromatography and preparative HPLC. Xanthoradones A and B potentiated imipenem activity against MRSA by decreasing the MIC value of imipenem from 16 μg ml^{-1} to 0.060 and 0.030 μg ml^{-1}, respectively.
The Journal Antibiotics (2009) **62,** 431–434; doi:10.1038/ja.2009.69; published online 24 July 2009

Keywords: fungal metabolites; imipenem potentiator; methicillin-resistant *Staphylococcus aureus* (MRSA); *Penicillium radicum*; xanthoradone; xanthoviridicatin

INTRODUCTION

Methicillin-resistant *Staphylococcus aureus* (MRSA), a major and widespread pathogen in hospitals, has developed resistance to many antibiotics.[1,2] Moreover, MRSA is reportedly becoming resistant to the last-resort antibiotic, vancomycin,[3] suggesting that resistance to vancomycin will increase in the near future. It is therefore increasingly important and necessary to find new antimicrobial agents and to devise new measures that are effective against MRSA infection.

During our continuous screening program for microbial potentiators of imipenem activity against MRSA,[4–7] the culture broth of a fungal strain FKI-3765-2 was found to show potentiating activity. Activity-guided purification led to the discovery of two new compounds, namely designated xanthoradones A and B (Figure 1). They showed moderate anti-MRSA activity, but strongly enhanced imipenem activity against MRSA. The structure elucidation of xanthoradones A and B will be described in an accompanying study.[8] In this study, the taxonomy of the producing strain, and fermentation, isolation and biological properties of xanthoradones are described.

RESULTS

Taxonomy of Strain FKI-3765-2

Colonies on Czapek yeast agar (CYA) after 7 days at 25 °C (Figure 2a) were 24–25 mm in diameter, dense, colliculose, floccose to funiculose, with a smooth margin, and white (a) in color. The center of the colony was a dusty olive (1 ie) conidial color, exuding clear drops. The reverse side was golden brown (3 pg). Colonies on malt extract agar (MEA) (Figure 2b) were 19–21 mm in diameter, dense, colliculose, floccose, with a smooth margin, and light yellow (1 ea) in color, without exudate drops. The reverse side was antique gold (1 ½ na). Colonies on 25% glycerol nitrate agar (G25N) (Figure 2c) were 9.0–10 mm in diameter, pulvinate, floccose, with a smooth margin, and sage gray (24 ih), without exudate drops. The reverse side was olive (1 ni) green in color. Colonies on CYA after 7 days at 37 °C were the same as those at 27 °C. The reverse was camel (3 ie) in color. The colony on CYA at 5.0 °C showed no growth.

Conidiophores on CYA formed basal hyphae, rarely branching, were of 65–180×2.5–3.0 μm in size, with a smooth wall. Penicilli from conidiophores were biverticillate (consisting of metulae and phialides) (Figure 2d). Metulae were of 2–6 branches, which were usually rather appressed or sometimes slightly divergent of larger size, being 7.5–10×2.3–2.7 μm in size. Phialides were acerose, 12.5–15×2.3–2.5 μm in size, with smooth walls. Conidia were subglobose to globose, slightly roughened or sometimes smooth-walled, 2.7–3.5 (5.0)×2.3–2.7 μm in size and with divergent long chains (Figure 2e).

From the above-mentioned morphological characteristics, the strain FKI-3765-2 was considered to belong to genus *Penicillium* in the subgenus *Biverticillium* section *Simplicia*.[9] Furthermore, from the characteristics of the colony colors on CYA, the rapid growth at

[1]Graduate School of Pharmaceutical Sciences, Kitasato University, Minato-ku, Tokyo, Japan and [2]Kitasato Institute for Life Sciences, Kitasato University, Minato-ku, Tokyo, Japan
Correspondence: Professor H Tomoda, Graduate School of Pharmaceutical Sciences, Kitasato University, 5-9-1 Shirokane, Minato-ku, Tokyo 108-8641, Japan.
E-mail: tomodah@pharm.kitasato-u.ac.jp
Received 16 April 2009; revised 3 July 2009; accepted 3 July 2009; published online 24 July 2009

37 °C on CYA and the length of conidiophores, the strain was considered to be a member of *Penicillium radicum*. In addition, the internal transcribed spacer (ITS) rDNA sequence (593 nucleotides) of the strain FKI-3765-2 showed 100% similarity to that of *P. radicum* (strain name) (accession no. AY256855). Thus, the producing strain FKI-3765-2 was identified as *P. radicum*.

Isolation

A thirteen-day-old rice cake (1000 g) was extracted with 2.0 l of acetone. After the acetone extracts were filtered and concentrated to remove acetone, the aqueous solution was extracted with ethyl acetate. The extracts were dried over Na_2SO_4 and concentrated *in vacuo* to dryness to yield a reddish brown material (1.8 g). The material was dissolved in 30% CH_3CN, applied to an octadecyl silyl (ODS) column (100 g) and eluted stepwise with 30, 50, 70, 100% CH_3CN containing 0.050% TFA (200 ml×4 tubes for each solvent, respectively). The active fractions (third and fourth tubes of 70% CH_3CN) were concentrated *in vacuo* to dryness to yield a reddish brown material (385 mg). The material was finally purified using preparative HPLC (column, PEGASIL ODS, 20×250 mm, Senshu Scientific, Tokyo, Japan; solvent, 80% CH_3CN containing 0.050% TFA; detection, UV at 210 nm; flow rate, 8.0 ml min^{-1}). Under these conditions, xanthoradones A and B were eluted as peaks with a retention time of 20.7 and 21.2 min, respectively (Figure 3). The fractions were concentrated *in vacuo* to dryness to yield pure xanthoradones A (7.3 mg) and B (5.6 mg) as yellow materials.

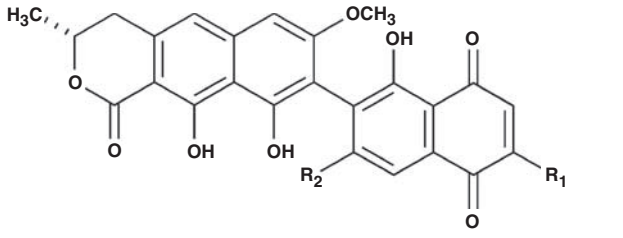

Xanthoradone	R_1	R_2
A	$-OCH_3$	$-CH_3$
B	$-CH_3$	$-OCH_3$

Figure 1 Structures of xanthoradones A and B.

Antimicrobial activity of xanthoradones

First, the antimicrobial activity of xanthoradones was tested using the paper disc method. At a concentration of 5.0 μg per disc, xanthoradone A showed inhibition zones of 8 and 9 mm against *S. aureus* and *Bacillus subtilis*, respectively. Xanthoradone B showed an inhibition zone of 9 mm against *B. subtilis*; however, neither xanthoradones inhibited the growth of MRSA K24 at 10 μg per disc.

Second, the anti-MRSA activity of xanthoradones was tested using the liquid microdilution method.[10] Xanthoradones A and B showed moderate anti-MRSA activity with an MIC of 4.0 and 2.0 μg ml^{-1}, respectively.

Potentiation of imipenem activity against MRSA by xanthoradones

Using the paper disc assay, xanthoradones A and B showed potent anti-MRSA activity with inhibition zones of 10 and 13 mm, respectively, on agar medium A (AMA) plates containing imipenem (10 μg ml^{-1}). Next, the potentiating effect of xanthoradones on the activity of imipenem and of other typical antibiotics against MRSA was investigated using the liquid microdilution method.[10] Concentrations of xanthoradones A and B were set up at 1.0 and 0.50 μg ml^{-1} for these experiments, respectively, which showed no effect on the growth of the MRSA K-24 strain. As summarized in Table 1, xanthoradones A and B markedly reduced the MIC value of imipenem from 16 to 0.060 and 0.030 μg ml^{-1}, indicating a 266- and 533-fold potentiation, respectively; however, the anti-MRSA activity of streptomycin, vancomycin, tetracycline, erythromycin or ciprofloxacin was

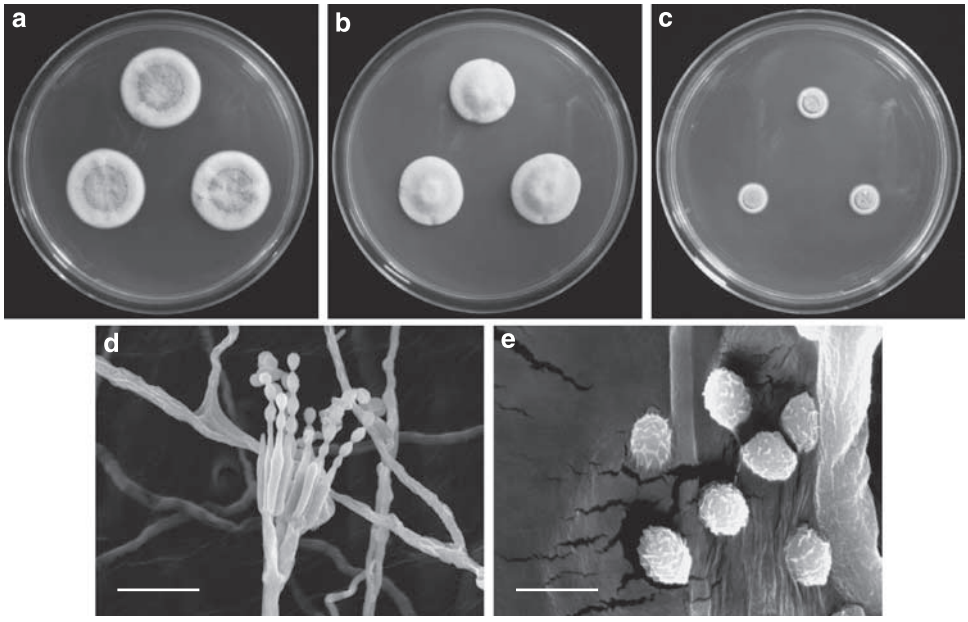

Figure 2 Morphological characteristics of xanthoradone-producing *Penicillium radicum* FKI-3765-2. (**a**) Colonies grown on Czapek yeast agar (CYA) after 7 days. (**b**) Colonies grown on malt extract agar (MEA) after 7 days. (**c**) Colonies grown on 25% glycerol nitrate agar (G25N) after 7 days. (**d**) Scanning electron micrograph of conidiophores grown on MEA. Scale bar, 10 μm. (**e**) Micrograph of synnemata and conidia grown on MEA. Scale bar, 10 mm.

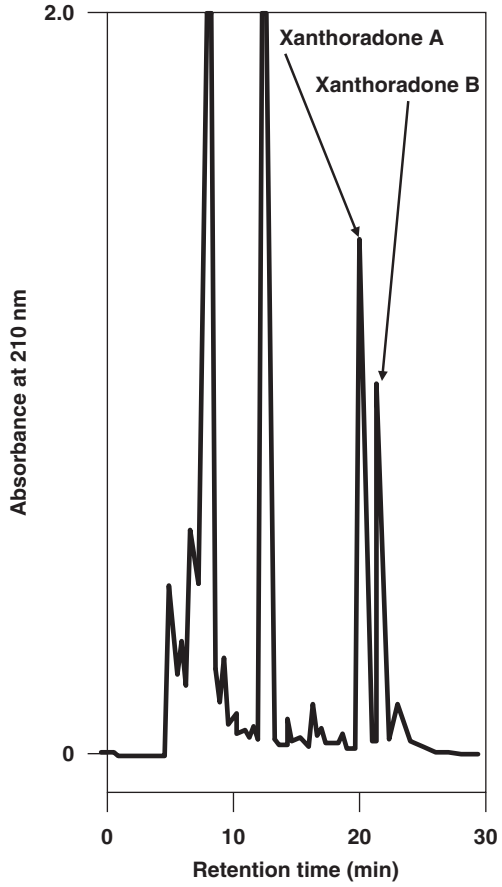

Figure 3 A chromatographic profile of xanthoradones A and B purification by preparative HPLC. Column, PEGASIL octadecyl silyl (ODS) (20×250 mm); solvent, 80% aqueous acetonitrile; detection, UV at 210 nm; flow rate, 8.0 ml min^{-1}; sample, 10 mg of active materials (obtained through ODS column chromatography) dissolved in 200 µl methanol.

Table 1 MIC of imipenem (IPM) against MRSA in the presence of xanthoradones and cytotoxic effect of xanthoradones on Jurkat cells

	MIC of IPM	*Potentiation ratio*	*IC_{50}*
In combination with	*(µg ml^{-1})*	*(None/xanthoradone)*	*µg ml^{-1}*
None	16	1	N.T.
Xanthoradone			
A	0.060	266	23.2
B	0.030	533	2.6

Abbreviation: MRSA,methicillin-resistant *Staphylococcus aureus*.
Concentrations of xanthoradones A and B are 1.0 and 0.50 µg ml^{-1}, respectively.

not enhanced or was only slightly potentiated (twofold with streptomycin) in combination with xanthoradones (data not shown).

Other biological activity

Xanthoradones A and B showed cytotoxicity on Jurkat cells with an IC_{50} value of 23.2 and 2.6 µg ml^{-1}, respectively (Table 1).

DISCUSSION

As described in this study, two xanthoradones (Figure 1) were isolated from the culture broth of *P. radicum* strain FKI-3765-2 and were found to potentiate imipenem inhibition against MRSA K-24. Several compounds have been reported to potentiate β-lactam activity against MRSA: polyoxotungstates,[11] polyphenols such as epigallocatechin gallate isolated from tea,[12] corilagin from *Arctostaphylos uva-urs*,[13] tellimagrandin I from rose red (*Rosa canina*),[13] diterpenes such as totarol isolated from totara tree[14] and synthetic MC-200,613.[15] Our research group has discovered microbial potentiators, such as stemphones from *Aspergillus* sp.[4,5] and cyslabdan from *Streptomyces* sp.[6,7] These potentiators have a polyphenol- or terpene-derived core structure. However, xanthoradones have a different core structure, a polyketide-derived heterodimer containing an aromatic ring.

The action mechanism of these potentiators is important for the development of a new type of anti-infective drug.[16] Polyphenols and MC-200,613, as described above, were reported to affect penicillin-binding protein-2′ (PBP2′).[15,17] The potentiators discovered by our groups, including xanthoradones, showed no affinity to PBP2′ and no effect on PBP2′ expression and β-lactamase activity (data not shown); therefore, their action mechanisms seemed different from those of polyphenols and MC-200,613. Further studies are in progress.

METHODS

Materials

Vancomycin, tetracycline and ciprofloxacin were purchased from Wako Pure Chemical Industries (Osaka, Japan). Streptomycin was purchased from Meiji Seika Kaisha (Tokyo, Japan). Imipenem was purchased from Banyu Pharmaceutical (Tokyo, Japan). Erythromycin was purchased from Sigma-Aldrich (St Louis, MO, USA).

Microorganisms

The fungal strain FKI-3765-2 was isolated from a soil sample collected from Hilo, Hawaii, USA. This strain was used to produce xanthoradones. The following microorganisms were used for antimicrobial tests: *B. subtilis* ATCC 6633, *S. aureus* FDA 209P (MSSA), *Micrococcus luteus* PCI 1001, *Escherichia coli* NIHJ, *Xanthomonas campestris* pv. *oryzae* KB 88, *Mucor racemosus* IFO 4581 and *Candida albicans* KF 1. MRSA K-24 was clinically isolated in Japan.

General experimental procedures

SSC-ODS-7515-12 (Senshu Scientific) was used for ODS column chromatography. HPLC was carried out using the L-6200 system (Hitachi, Tokyo, Japan). To determine the amounts of xanthoradones A and B in culture broths, samples of ethyl acetate extracts were dissolved in methanol and analyzed using the HP1100 system (Hewlett-Packard, Palo Alto, CA, USA) under the following conditions: column, symmetry (2.1×150 mm; Waters Corporation, Milford, MA, USA); flow rate (0.20 ml min^{-1}); mobile phase (a 20-min linear gradient from 60% CH_3CN to 100% CH_3CN containing 0.050% H_3PO_4); and detection (UV at 210 nm). Under these conditions, xanthoradones A and B were eluted with retention times of 6.3 and 6.8 min, respectively.

Taxonomic study of the producing strain FKI-3765-2

Taxonomic study of the fungal strain FKI-3765-2 was conducted according to the procedures described by Pitt.[9] Morphological characteristics of the strain growing on CYA, MEA and G25N were observed under a light microscope (Vanox-S AH-2; Olympus, Tokyo, Japan) and a scanning electron microscope (JSM-5600; JEOL, Tokyo, Japan). Color names and hue numbers were determined according to the Color Harmony Manual.[18] For molecular phylogenetic study, genomic DNA was extracted using the PrepMan Ultra Sample Preparation Reagent (Applied Biosystems, Foster City, CA, USA) according to the manufacturer's protocol. The rDNAITS regions, including the 5.8S rDNA gene, were amplified by PCR using primers ITS1 and ITS4.[19] Amplifications were performed using a PCR Thermal Cycler Dice mini Model TP100 (Takara Bio, Shiga, Japan). The amplified PCR products were purified using a QIAquick PCR DNA Purification Kit (Qiagen, Valencia, CA, USA). Sequencing reactions were directly performed using a BigDye Terminator v3.1 Cycle Sequencing Kit (Applied Biosystems), and the products were purified using a DyeEX 2.0 Spin Kit (Qiagen). DNA sequences were read on an ABI PRISM 3130 Genetic

Analyzer (Applied Biosystems) and assembled using the programs SeqMan and SeqBuilder from the Lasergene7 package (DNAStar, Madison, WI, USA). The ITS region of the rDNA sequence was compared with the database of the National Center for Biotechnology Information, Japan. ITS was deposited in DDBJ (accession no. AB457008).

Fermentation

A slant culture of the strain FKI-3765-2 grown on LCA (0.10% glycerol, 0.080% KH_2PO_4, 0.020% K_2HPO_4, 0.020% $MgSO_4 \cdot 7H_2O$, 0.020% KCl, 0.20% $NaNO_3$, 0.020% yeast extract and 1.5% agar, adjusted to pH 6.0 before sterilization) was inoculated into a 50-ml tube containing 10 ml of the seed medium (2.0% glucose, 0.50% polypeptone, 0.050% $MgSO_4 \cdot 7H_2O$, 0.20% yeast extract, 0.10% KH_2PO_4 and 0.10% agar, adjusted to pH 6.0 before sterilization). The tube was shaken reciprocally for 3 days at 27 °C. A 1-ml portion of the seed culture was then inoculated into a 500-ml Erlenmeyer flask (IWAKI, Tokyo, Japan) containing the production medium (50 g Italian rice; Japan Europe Trading, Tokyo, Japan). The production medium was prepared as follows; Italian rice (50 g) was soaked in water for 2 h and then collected in a colander. The sodden rice was put into a 500-ml Elenmeyer flask and sterilized by an autoclave. Fermentation was carried out at 27 °C for 13 days under static conditions.

Assay for potentiating imipenem activity against MRSA

The assay for potentiating imipenem (or other antibiotics) activity against MRSA in combination with a sample (xanthoradones) was carried out using two methods:[10] (1) The paper disc method, in which MRSA K-24 was cultured in a Mueller–Hinton broth (MHB; Sanko Junyaku, Tokyo, Japan) at 37 °C for 20 h and adjusted to 1.0×10^8 CFU ml^{-1}. The inoculum (100 μl) was spread in a plate (10×14 cm; Eiken Chemical, Tokyo, Japan) on the respective AMA or agar medium B (AMB) containing MHB and 1.5% agar (Shimizu Shokuhin, Shizuoka, Japan) with or without imipenem (10 μg ml^{-1}, which has no effect on the growth of MRSA). Paper discs (6 mm i.d.; Toyo Roshi Kaisha, Tokyo, Japan) containing various concentrations of a sample were placed on AMA and AMB and incubated at 37 °C for 20 h. Anti-MRSA activity was expressed as the diameter (mm) of the inhibitory zone on the agar media. (2) Liquid microdilution method,[10] in which xanthoradone A or B dissolved in CH_3OH (5.0 μl) was added to prepare the final concentration of 1.0 or 0.50 μg ml^{-1}, respectively, after MHB (85 μl) was added to each well of a 96-well microplate (Corning, Corning, NY, USA). Imipenem dissolved in distilled water (5.0 μl) was then added to each well at a final concentration of 0.015 to 512 μg ml^{-1}. Finally, MRSA (5.0 μl) was added at a concentration of 1.0×10^7 CFU ml^{-1}. The microplates were incubated at 37 °C for 20 h without shaking. MIC was defined as the lowest concentration of imipenem (or other antibiotics) in which MRSA cannot grow.

Antimicrobial assay

Antimicrobial activity against the seven microorganisms was measured using the paper disc method. Media for microorganisms were as follows: Nutrient agar (Sanko Junyaku) for *B. subtilis*, *S. aureus*, *M. luteus*, *E. coli* and *X. campestris*; a medium composed of glucose 1.0%, yeast extract 0.50% and agar 0.80% for *M. racemosus* and *C. albicans*. A paper disc (6 mm i.d.; Toyo Roshi Kaisha) containing 10 μg of the sample was placed on an agar plate. Bacteria, except *X. campestris*, were incubated at 37 °C for 24 h. *C. albicans* and *X. campestris* were incubated at 27 °C for 24 h. *M. racemosus* was incubated at 27 °C for 48 h. Antimicrobial activity was expressed as the diameter (mm) of the inhibitory zone.

Cytotoxic assay

The cytotoxicity of xanthoradones to Jurkat cells (a kind gift from Dr M Suganuma, CanBas, Shizuoka, Japan) was evaluated by the MTT assay.[20] Cells (2.0×10^4 cells per 100 μl per well) were cultured in 96-well plates in the presence of a sample (xanthoradones) at the indicated concentrations at 37 °C in 5.0% CO_2 atmosphere. After 48 h incubation, they received MTT solution (10 μl to each well, 5.5 mg ml^{-1} in phosphate-buffered saline; Sigma-Aldrich) and were incubated at 37 °C for 4 h. A 90-μl aliquot of the extraction solution (40% (v/v) *N*,*N*-dimethylformamide, 2.0% (v/v) CH_3COOH, 20% (w/v) SDS and 0.03 *N* HCl) was added to each well, and the cells were incubated at room temperature for 2 h. Cytotoxicity was determined by measuring the optical density at 550 nm using a plate reader (Elx-808; Central Scientific Commerce, Tokyo, Japan).

ACKNOWLEDGEMENTS

This work was supported by a grant-in-aid for Scientific Research (B) 21310146 (to HT) from the Ministry of Education, Culture, Sports, Science and Technology, Japan and by the Sasakawa Scientific Research Grant (to HY) from The Japan Science Society.

1 Tomasz, A. Multiple-antibiotic resistant pathogenic bacteria. *N. Engl. J. Med.* **330,** 1247–1251 (1994).
2 Hiramatsu, K. *et al.* Methicillin-resistant *Staphylococcus aureus* clinical strain with reduced vancomycin susceptibility. *J. Antimicrob. Chemother.* **40,** 135–136 (1997).
3 Centers for Disease Control and Prevention. *Staphylococcus aureus* with reduced susceptibility to vancomycin-United States, 1997. *MMWR Morb. Mortal. Wkly. Rep.* **46,** 765–766 (1997).
4 Koyama, N. *et al.* Stemphones, novel potentiators of imipenem activity against methicillin-resistant *Staphylococcus aureus*, produced by *Aspergillus* sp. FKI-2136. *J. Antibiot.* **58,** 695–703 (2005).
5 Yamazaki, H., Koyama, N., Ōmura, S. & Tomoda, H. Structure-activity relationships of stemphones, potentiators of imipenem activity against methicillin-resistant *Staphylococcus aureus*. *J. Antibiot.* **61,** 426–441 (2008).
6 Fukumoto, A. *et al.* Cyslabdan, a new potentiator of imipenem activity against methicillin-resistant *Staphylococcus aureus*, produced by *Streptomyces* sp. K04-0144 I. Taxonomy, fermentation, isolation and structural elucidation. *J. Antibiot.* **61,** 1–6 (2008).
7 Fukumoto, A. *et al.* Cyslabdan, a new potentiator of imipenem activity against methicillin-resistant *Staphylococcus aureus*, produced by *Streptomyces* sp. K04-0144 II. Biological activities. *J. Antibiot.* **61,** 7–10 (2007).
8 Yamazaki, H., Ōmura, S. & Tomoda, H. Xanthoradones, new potentiators of imipenem activity against methicillin-resistant *Staphylococcus aureus*, produced by *Penicillium radicum* FKI-3765-2 II. Structure elucidation. *J. Antibiot.* **62,** 435–437 (2009).
9 Pitt, J. I. *The Genus Penicillium, and its Teleomorphic States Eupenicillium and Talaromyces* 1–634 (Academic Press, London, 1979).
10 Committee for Antimicrobial Susceptibility Testing Method. Standard methods of Japanese Society of Chemotherapy. *Chemotherapy* **38,** 102–105 (1990) (in Japanese).
11 Fukuda, N., Yamase, T. & Tajima, Y. Inhibitory effect of polyoxotungstates on the production of penicillin-binding proteins and β-lactamase against methicillin-resistant *Staphylococcus aureus*. *Biol. Pharm. Bull* **22,** 463–470 (1999).
12 Zhao, W. H., Hu, Z. Q., Okubo, S., Hara, Y. & Shimamura, T. Mechanism of synergy between epigallocatechin gallate and β-lactams against methicillin-resistant *Staphylococcus aureus*. *Antimicrob. Agents Chemother.* **45,** 1737–1742 (2001).
13 Shiota, S. *et al.* Mechanisms of action of corilagin and tellimagrandin I that remarkably potentiate the activity of β-lactams against methicillin-resistant *Staphylococcus aureus*. *Microbiol. Immunol.* **48,** 67–73 (2004).
14 Nicolson, K., Evans, G. & O'Toole, P. W. Potentiation of methicillin activity against methicillin-resistant *Staphylococcus aureus* by diterpenes. *FEMS Microbiol. Lett.* **179,** 233–239 (1999).
15 Chamberland, S. *et al.* MC-207,252 Abolishes PBP2a mediated β-lactam resistance in Staphylococci. Abstract in 35th Interscience Conference on Antimicrobial Agents and Chemotherapy (ICAAC). pp F138–F144 (1995).
16 Ōmura, S. Antiinfective drugs into the 21st century. *Nippon Saikingaku Zasshi* **54,** 795–813 (1999) (in Japanese).
17 Yamase, T., Fukuda, N. & Tajima, Y. Synergistic effect of polyoxotungstates in combination with beta-lactam antibiotics on antibacterial activity against methicillin-resistant *Staphylococcus aureus*. *Biol. Pharm. Bull* **19,** 459–465 (1996).
18 Jacobson, E., Granville, W. C. & Foss, C. E. *Color Harmony Manual*, 4th edn (Container of America, Chicago, 1958).
19 White, T. J., Bruns, T., Lee, S. & Taylor, J. W. Amplification and direct sequencing of fungal ribosomal RNA genes for phylogenetics. in *PCR Protocols: A Guide to Methods and Applications* (eds. Innis, M.A., Gelfand, R.H., Sninsky, J.J. & White, T.J.) 315–332 (Academic Press, New York, 1990).
20 Mosmann, T. Rapid colorimetric assay for cellular growth and survival: application to proliferation and cytotoxicity assays. *J. Immunol. Methods* **65,** 55–63 (1983).

The Journal of Antibiotics (2009) 62, 435–437

www.nature.com/ja

ORIGINAL ARTICLE

Xanthoradones, new potentiators of imipenem activity against methicillin-resistant *Staphylococcus aureus*, produced by *Penicillium radicum* FKI-3765-2 II. Structure elucidation

Hiroyuki Yamazaki[1], Satoshi Ōmura[2] and Hiroshi Tomoda[1]

The structures of xanthoradones A and B, new potentiators of imipenem activity against methicillin-resistant *Staphylococcus aureus* produced by *Penicillium radicum* FKI-3765-2, were elucidated by spectroscopic studies, including various NMR experiments. These compounds have an asymmetric biaryl skeleton, which contains dihydronaphthopyranone and naphthoquinone moieties.
The Journal of Antibiotics (2009) **62,** 435–437; doi:10.1038/ja.2009.61; published online 17 July 2009

Keywords: fungal metabolites; imipenem potentiator; methicillin-resistant *Staphylococcus aureus* (MRSA); structure elucidation; xanthoradone; xanthoviridicatin

INTRODUCTION

Two new compounds, designated xanthoradones A and B (Figure 1), were isolated as potentiators of imipenem activity against methicillin-resistant *Staphylococcus aureus* from the culture broth of *Penicillium radicum* strain FKI-3765-2.[1] The taxonomy of the producing strain, fermentation, isolation and biological properties of the xanthoradones were described in a previous paper.[1] In this study, the physico-chemical properties and structure elucidation of xanthoradones are described.

RESULTS

Physico-chemical properties

The physico-chemical properties of xanthoradones A and B are summarized in Table 1. They had similar UV spectra with absorption maxima at 218 nm, 263–267 nm and 373–375 nm. The IR absorption at 1606–1778 cm^{-1} and 3403–3407 cm^{-1} suggested the presence of carbonyl and hydroxyl groups in their structures. These data indicated that they share the same skeleton.

Structure elucidation of xanthoradone A

The molecular formula of xanthoradone A was determined to be $C_{27}H_{22}O_9$ on the basis of high-resolution electrospray ionization time-of-flight mass spectrum (HRESI-TOF-MS) measurement. The ^{13}C NMR spectrum (in $CDCl_3$) showed 27 resolved signals, which were classified into two methyl carbons, one methylene carbon, four sp^2 methine carbons, two oxygenated methyl carbons, one oxygenated methine carbon, nine sp^2 quaternary carbons, five oxygenated sp^2 quaternary carbons and three carbonyl carbons by analyzing the DEPT and heteronuclear single quantum coherence (HSQC) spectra. The ^1H NMR spectrum (in $CDCl_3$) displayed 22 proton signals, nine of which were suggested to be three hydroxy protons (δ 9.73, 12.5 and 13.9) and two oxygenated methyl protons (δ 3.84 and 3.92), as reported for xanthoviridicatin F.[2] These results supported the molecular formula. The connectivity of proton and carbon atoms was established by the ^{13}C–^1H HSQC spectrum (Table 2). Analyses of ^1H–^1H COSY revealed the presence of the partial structure I, as shown in Figure 2a. Furthermore, ^{13}C–^1H long-range couplings of ^2J and ^3J observed in the ^{13}C–^1H heteronuclear multiple bond coherence (HMBC) spectrum gave the following linkages (Figure 2b): (1) Cross peaks from H_2-3 (δ 3.00, 3.06) to C-4 (δ 133.5), C-5 (δ 116.1) and C-13 (δ 99.7); from H-5 (δ 6.99) to C-3 (δ 34.7), C-6 (δ 140.0), C-7 (δ 98.1), C-11 (δ 108.4) and C-13; from H-7 (δ 6.71) to C-5, C-8 (δ 160.3), C-9 (δ 109.0) and C-11; from OH-10 (δ 9.73) to C-9, C-10 (δ 154.7) and C-11; from OH-12 (δ 13.9) to C-11, C-12 (δ 162.7) and C-13; and from H_3-15 (δ 3.84) to C-8 indicated that a naphthalene skeleton connects the partial structure I at C-4. Furthermore, the findings that the chemical shift of C-2 (δ 76.8) corresponds to that of an oxygenated carbon and that the OH-12 proton (δ 13.9) shifted to a lower field because of hydrogen bonding indicated that C-2 and C-13 are connected through an ester bond. This connection was supported by the chemical shift of C-1 (δ 171.5) corresponding to an ester bond and the long-range coupling of ^4J observed from H-5 to C-1 in ^{13}C–^1H HMBC (Figure 2). Thus, these data indicated that xanthoradone A was found to have a dihydronaphthopyranone skeleton. (2)

[1]Graduate School of Pharmaceutical Sciences, Kitasato University, Tokyo, Japan and [2]Kitasato Institute for Life Sciences, Kitasato University, Tokyo, Japan
Correspondence: Professor H Tomoda, Graduate School of Pharmaceutical Sciences, Kitasato University, 5-9-1 Shirokane, Minato-ku, Tokyo 108-8641, Japan.
E-mail: tomodah@pharm.kitasato-u.ac.jp
Received 16 April 2009; revised 29 May 2009; accepted 25 June 2009; published online 17 July 2009

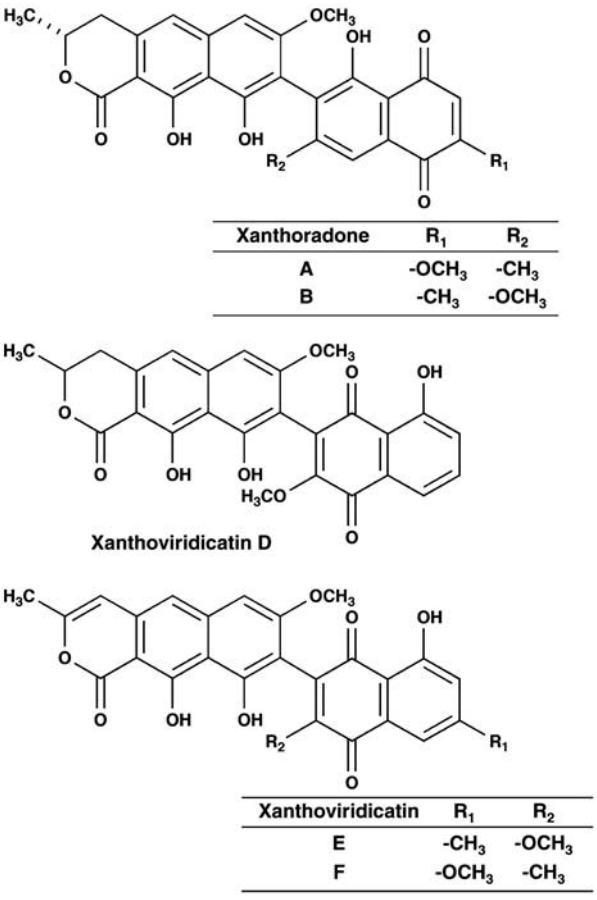

Figure 1 Structures of xanthoradones A, B and xanthoviridicatins D to F.

Table 1 Physico-chemical properties of xanthoradones A and B

	Xanthoradone A	*Xanthoradone B*
Appearance	Orange crystal	Orange crystal
Molecular weight	490	490
Molecular formula	$C_{27}H_{22}O_9$	$C_{27}H_{22}O_9$
HRESI-TOF-MS (m/z)		
Calculated	489.1186 $(M-H)^-$	489.1186 $(M-H)^-$
Found	489.1136 $(M-H)^-$	489.1149 $(M-H)^-$
UV (MeOH), λ_{max}	218 (32 600), 263	218 (55 300), 267
nm (ε)	(53 400), 375 (15 100)	(34 700), 373 (13 000)
$[\alpha]_D^{26}$	+320.1° (*c*=0.1, $CHCl_3$)	+167.9° (*c*=0.1, $CHCl_3$)
IR (KBr), ν_{max} (cm^{-1})	3407, 2971, 1778, 1681, 1631, 1598	3403, 2967, 1641, 1606, 1579, 1542

Cross peaks from H-2′ (δ 6.08) to C-1′ (δ 190.6), C-3′ (δ 160.9), C-4′ (δ 179.8) and C-10′ (δ 112.0); from H-6′ (δ 7.67) to C-4′, C-5′ (δ 129.8), C-7′ (δ 147.2), C-8′ (δ 130.6), C-10′ and C-12′ (δ 20.5); from OH-9′ (δ 12.5) to C-8′, C-9′ (δ 159.7) and C-10′; from H_3-11′ (δ 3.92) to C-3′; and from H_3-12′ (δ 2.21) to C-6′ (δ 121.3), C-7′ and C-8′ indicated that xanthoradone A has another naphthoquinone skeleton. This was supported by the chemical shifts of two carbonyl carbons (C-1′ (δ 190.6) and C-4′ (δ 179.8)) derived from a quinone skeleton and the UV absorption (263 nm). Finally, the correlations observed between H_3-15 and OH-9′, and between OH-10 and H_3-12′ in

Table 2 ^{1}H- and ^{13}C NMR chemical shifts of xanthoradones A and B

	Xanthoradone A		*Xanthoradone B*	
Position	δ_C	δ_H	δ_C	δ_H
1	171.5	—	171.5	—
2	76.8	4.79m	76.6	4.75m
3	34.7	ax: 3.00dd (*J*=17.0, 10.0 Hz) eq: 3.06dd (*J*=17.0, 4.0 Hz)	34.7	ax: 2.98dd (*J*=17.0, 10.0 Hz) eq: 3.05dd (*J*=17.0, 4.0 Hz)
4	133.5	—	133.3	—
5	116.1	6.99s	116.1	6.94s
6	140.0	—	140.3	—
7	98.1	6.71s	98.1	6.67s
8	160.3	—	160.8	—
9	109.0	—	106.4	—
10	154.7	—	155.2	—
10-OH		9.73s		9.69s
11	108.4		108.4	—
12	162.7	—	162.8	—
12-OH		13.9s		13.8s
13	99.7	—	99.5	—
14	20.7	1.57d (*J*=7.0 Hz)	20.7	1.53d (*J*=7.0 Hz)
15	56.0	3.84s	56	3.82s
1′	190.6	—	189.0	—
2′	109.6	6.08s	135.8	6.73q (*J*=2.0 Hz)
3′	160.9	—	148.3	—
4′	179.8	—	185.0	—
5′	129.8	—	133.0	—
6′	121.3	7.67s	163.2	7.33s
7′	147.2	—	163.6	—
8′	130.6	—	110.3	—
9′	159.7	—	161.1	—
9′-OH		12.5s		12.3s
10′	112.0	—	116.1	—
11′	56.6	3.92s	16.4	2.16d (*J*=2.0 Hz)
12′	20.5	2.21s	56.5	3.88s

Abbreviations: *ax*, axial; *eq*, equatorial.

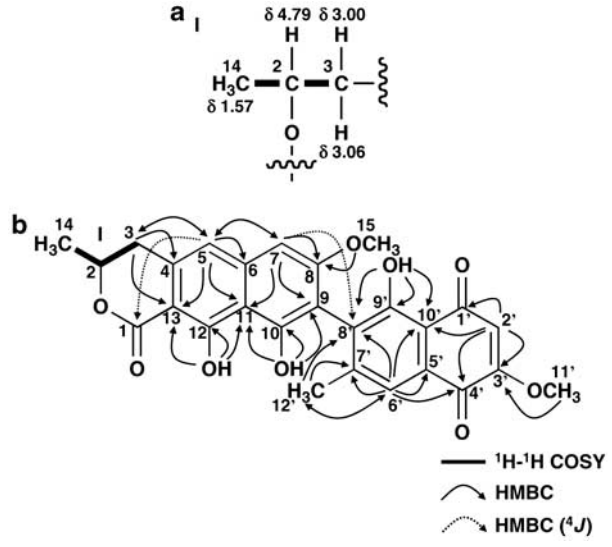

Figure 2 Partial structure (**a**) and ^{1}H–^{1}H COSY and ^{13}C–^{1}H HMBC experiments (**b**) of xanthoradone A.

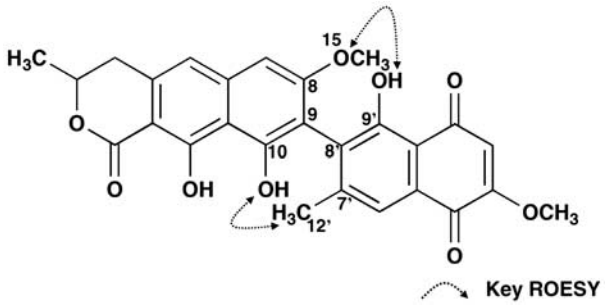

Figure 3 ROESY experiments of xanthoradone A.

rotating frame nuclear overhauser effect spectroscopy (ROESY) experiments (Figure 3), and the long-range coupling of ^4J observed from H-7 to C-8′ in ^{13}C–^1H HMBC experiments (Figure 2b) indicated that the two substructures of dihydronaphthopyranone and naphthoquinone are connected at C-9–C-8′. Taken together, the structure of xanthoradone A was elucidated as shown in Figure 1. The structure satisfied the degree of unsaturation and the molecular formula.

Structure elucidation of xanthoradone B

The molecular formula $C_{27}H_{22}O_9$ of xanthoradone B was the same as that of xanthoradone A. The ^1H NMR spectrum of xanthoradone B was almost identical to that of xanthoradone A except for a weak coupling constant (J=2.0 Hz) between H-2′ and H-11′ in xanthoradone B, which was not observed in xanthoradone A. In fact, cross peaks observed from H-2′ (δ 6.73) to C-4′ (δ 185.0), C-10′ (δ 116.1) and C-11′ (δ 16.4); from H-6′ (δ 7.33) to C-4′, C-5′ (δ 133.0), C-7′ (δ 163.6), C-8′ (δ 110.3) and C-10′; from OH-9′ (δ 12.3) to C-8′, C-9′ (δ 161.1) and C-10′; from H_3-11′ (δ 2.16) to C-2′ (δ 135.8), C-3′ (δ 148.3) and C-4′; and from H_3-12′ (δ 3.88) to C-7′ in the ^{13}C–^1H HMBC experiments indicated the presence of a naphthoquinone skeleton (Figure 4). This was also supported by the chemical shifts of two carbonyl carbons (C-1′ (δ 189.0) and C-4′ (δ 185.0)) derived from a quinone skeleton and the UV absorption (267 nm). Taken together, the structure of xanthoradone B was elucidated as shown in Figure 1; the oxygenated methyl group at R1 and the methyl group at R2 in xanthoradone A are reversed in xanthoradone B (Figure 1). The structure satisfied the degree of unsaturation and the molecular formula.

DISCUSSION

In this study, xanthoradones A and B were isolated from *Penicillium radicum* strain FKI-3765-2, and their planar structures were elucidated by NMR studies (Figure 1). They were found to have a common asymmetric biaryl skeleton containing a dihydronaphthopyranone and a naphthoquinone. Regarding the stereochemistry of xanthoradones, both xanthoradone A and B have one chiral carbon at C-2 in the structure. The orientation of the methyl group at C-2 of the δ-lactone in xanthoradone A was investigated by ^1H–^1H spin decoupling experiments. On irradiation at H_3-14 (δ 1.57), a complex multiplet at H-2 (δ 4.79) became a simple doublet of doublets with $J_{2,3}$=10.0 and 4.0 Hz. The large coupling constant ($J_{2,3}$=10.0 Hz) indicated that H-2 and H_{ax}-3 (δ 3.00) are oriented in an axial–axial direction. This was supported by the coupling constants of H_{ax}-3 (J=17.0, 10.0 Hz). Thus, the methyl group at C-2 of the δ-lactone in xanthoradone A was determined to be equatorial in orientation as shown in Figure 1. Similarly, the orientation of the methyl group at C-2 of the δ-lactone in xanthoradone B was also deduced, as shown in Figure 1.

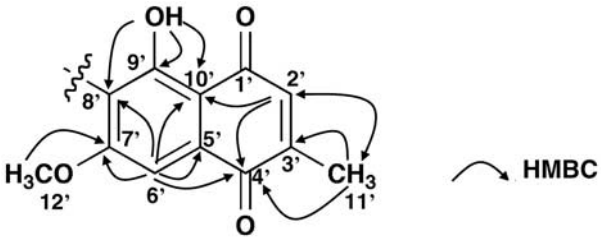

Figure 4 ^{13}C–^1H HMBC experiments of xanthoradone B.

Some structurally related natural products, such as xanthoviridicatin D produced by *Penicillium viridicatum*[3] and xanthoviridicatins E and F, as HIV-1 integrase inhibitors, produced by *Penicillium chrysogenum*,[2] have been reported previously (Figure 1). However, the binding pattern of the two substructures differs between xanthoradones and xanthoviridicatins; C-9 of a dihydronaphthopyranone moiety connects with C-8′ of the aromatic site of the naphthoquinone moiety in xanthoradones, whereas the former connects with C-2′ of the quinone site of the naphthoquinone moiety in known xanthoviridicatins.

By comparison with fungal biaryl compounds containing a dihydronaphthopyranone moiety, such as vioxanthin,[4] rubrosulphin,[5] viomellein[5] and luteosporin,[6] the absolute configuration of xanthoradones at C-2 can be deduced to be in 2*R* configuration. Furthermore, xanthoradones A and B have a chiral axis in the structures. The configuration of the axis might be *M* by comparing the CD spectra of (*P*) and (*M*)-vioxanthins;[4] xanthoradones show a negative cotton effect at 281–289 nm and a positive cotton effect at 266–269 nm similar to (*M*)-vioxanthin.

METHODS

General experimental procedures

The UV spectra were recorded on a spectrophotometer (8453 UV-Visible spectrophotometer; Agilent Technologies, Santa Clara, CA, USA). IR spectra were recorded on a Fourier transform infrared spectrometer (FT-710; Horiba, Kyoto, Japan). Optical rotations were measured using a digital polarimeter (DIP-1000; JASCO, Tokyo, Japan). ESI-TOF-MS and HRESI-TOF-MS spectra were recorded on a mass spectrometer (JMS-T100LP; JEOL, Tokyo, Japan). Various NMR spectra were measured using a spectrometer (XL-400; Varian, Palo Alto, CA, USA).

ACKNOWLEDGEMENTS

This work was supported by a grant-in-aid for Scientific Research (B) 21310146 (to HT) from the Ministry of Education, Culture, Sports, Science and Technology, Japan and the Sasakawa Scientific Research Grant (to HY) from The Japan Science Society. We express our thanks to Ms N Sato for performing NMR experiments, and Dr K Nagai and Ms A Nakagawa for measuring mass spectra.

1 Yamazaki, H., Nonaka, K., Masuma, R., Ōmura, S. & Tomoda, H. Xanthoradones, new potentiators of imipenem activity against methicillin-resistant *Staphylococcus aureus*, produced by *Penicillium radicum* FKI-3765-2 I. Taxonomy, fermentation, isolation and biological properties. *J. Antibiot.* **62,** 431–434 (2009).
2 Singh, S. B. *et al.* Isolation, structure, and HIV-1 integrase inhibitory activity of xanthoviridicatin E and F, two novel fungal metabolites produced by *Penicillium chrysogenum*. *Helv. Chim. Acta.* **86,** 3380–3385 (2003).
3 Stack, M. E., Mazzola, E. P. & Eppley, R. M. Structure of xanthoviridicatins D and xanthoviridicatin G, metabolites of *Penicillium viridicatum*: application of proton and carbon-13 NMR spectroscopy. *Tetrahedron Lett.* **52,** 4989–4992 (1979).
4 Bode, S. E., Drochner, D. & Muller, M. Synthesis, biosynthesis, and absolute configuration of vioxanthin. *Angew. Chem. Int. Ed. Engl.* **46,** 5916–5920 (2007).
5 Durley, R. C., MacMillan, J., Simpson, T. J., Glen, A. T. & Turner, W. B. Fungal products. Part XIII. Xanthomegnin, viomellin, rubrosulphin, and viopurpurin, pigments from *Aspergillus sulphureus* and *Aspergillus melleus*. *J. Chem. Soc. Perkin. Trans. 1* **2,** 163–169 (1975).
6 Mori, H., Kawai, K., Ohbayashi, F., Kitamura, J. & Nozawa, Y. Genotoxicity of quinone pigments from pathogenic fungi. *Mutat. Res.* **122,** 29–34 (1983).

The Journal of Antibiotics (2009) 62, 439–444

www.nature.com/ja

ORIGINAL ARTICLE

A comprehensive view on 4-methyl-2-quinazolinamine, a new microbial alkaloid from *Streptomyces* of TCM plant origin

Daniel Vollmar[1], Andrea Thorn[2], Ingrid Schuberth[1] and Stephanie Grond[1]

In the course of our chemical and biological screening program for yet unidentified microbial metabolites, we selected plants of Traditional Chinese Medicine (TCM) as habitats for talented Streptomycetes producer strains for the first time. Liquid pure cultures of strain *Streptomyces* sp. GS DV232 were found to contain 4-methyl-2-quinazolinamine (1), a potent alkaloid yet unknown from nature. In this study, we investigated the chemical and crystal structure of 1, as well as its antiproliferative bioactivity, and addressed the unusual biosynthesis using feeding experiments.
The Journal of Antibiotics (2009) **62,** 439–444; doi:10.1038/ja.2009.68; published online 7 August 2009

Keywords: antiproliferative agent; biosynthesis; feeding experiments; natural products; quinazoline alkaloids; *Streptomyces*; TCM

INTRODUCTION

On the basis of knowledge of traditional medicine, natural products as extracts or pure compounds make a crucial contribution to the health precautions of about 80% of the world's population today.[1] In addition to plants being the main category, selective groups of microorganisms such as actinomycetes, myxobacteria and various fungi are called 'talented producers' of secondary metabolites. They provide important drugs for clinical use, such as antibiotics, anti-tumor agents or especially immunosuppressive compounds; in these fields of applications, natural products are by far unmatched by synthetic chemicals. Furthermore, microbial metabolites are a source of research biochemicals and agrochemicals and are continuously investigated worldwide. To a significant extent, expertise in modern organic chemistry in terms of structural diversity, reaction types and mechanisms is driven by exploring natural products.[2–4] In addition to the indispensable use for medicinal and agricultural applications, the innovative potential of natural products lies in the discovery of manifold ecological interactions, which are presently unknown. These are explored in interdisciplinary research networks of biology, ecology and chemistry.[5] Screening for new metabolite structures by the 'ethnobotanical approach' takes advantage of the tradition of using medicinal plants by indigenous people.[6,7] Ethnobotany is considered as the science of transferring knowledge of historical therapy into active principles of drug agents. Thus, drug discovery benefits from rare or yet unexplored habitats, reinforcing this research strategy.[1,8]

Our ongoing screening project for yet unknown microbial metabolites comprises the isolation of microorganisms from Traditional Chinese Medicinal (TCM) herbs with the aim of isolating strains, establishing laboratory cultivations and giving access to bioactive substances from a thus renewable resource. Among 51 bacterial isolates, *Streptomyces* sp. GS DV232 was isolated from leaves (*folium*) of *Filipendula palmata* (Pall.) Maxim. (bot. syn.: *Spiraea palmata Pall.*, Chinese: *wen zi cao*). Traditionally, the dried rhizome or herb is used to treat the respiratory system and is also used against rheumatic and renal diseases.[9,10] From strain GS DV232, quinazolinamine **1** could be isolated as the main secondary metabolite.

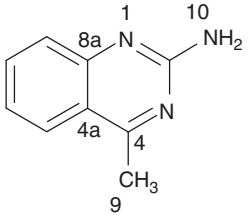

4-Methyl-2-quinazolinamine (1)

Hitherto, the structurally uncommon **1** has not been found in nature, and has only been described as a synthetic chemical product.[11,12] Among plant alkaloids, small quinazolines are well known. However, only a few single reports deal with quinazolines as secondary metabolites of microorganisms.[13,14] In this study, cultivation, isolation, structural elucidation, crystal structure and biological activity of **1** are presented. Feeding experiments allow for insights into the unusual biosynthetic pathway of microbial quinazoline **1**.

[1]Institute of Organic and Biomolecular Chemistry, Georg-August-Universität Göttingen, Göttingen, Germany and [2]Institute of Inorganic Chemistry, Georg-August-Universität Göttingen, Göttingen, Germany
Correspondence: Dr S Grond, Institute of Organic and Biomolecular Chemistry, Georg-August-Universität Göttingen, Tammannstr. 2, Göttingen D-37077, Germany.
E-mail: sgrond@gwdg.de
Received 23 June 2009; revised 1 July 2009; accepted 2 July 2009; published online 7 August 2009

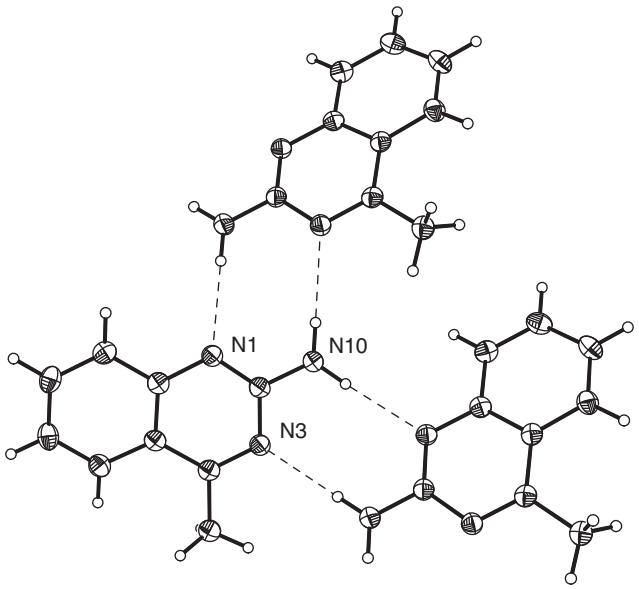

Figure 1 Structure **1** as determined by X-ray crystallographic analysis.[15] The atoms are shown as ORTEP plots with 50% probability displacement ellipsoids. Dashed lines mark hydrogen bonds.

RESULTS AND DISCUSSION

Isolation and structural elucidation

Streptomyces sp. GS DV232 was isolated from leaf surfaces of traditionally used plants of the *Filipendula palmata* (Pall.) Maxim. Owing to 16S rDNA analysis, it could be taxonomically classified as *Streptomyces zaomyceticus* or *S. venezuelae*. According to the chemical screening strategy, strain GS DV232 was cultivated in different media to analyze its metabolite pattern. The obtained extracts showed several metabolites using high performance thin layer chromatography, but only one gave an intense red color reaction on TLC plates after staining with anisaldehyde. Chromatography gave a white solid with an overall yield of 2 mg l^{-1}, the molecular formula ($C_9H_9N_3$) of which was determined by mass spectral analysis (HRESI mass spectrometry, $[M+H]^+$ 160.08692). ^{1}H-NMR spectra exhibited four aromatic protons, a methyl group (2.72 p.p.m.) with distinct NOESY correlations to the aromatic proton at 7.94 p.p.m. and a broad singlet at 6.08 p.p.m. for an amino group. From ^{13}C-NMR, HSQC and HMBC data, the compound was identified as the alkaloid 4-methyl-2-quinazolinamine (**1**). Hitherto, **1** has not been described from any natural source. Given that the number of synthetic quinazoline derivatives exceeds the number of 'natural' quinazolines,[13] **1** was first synthesized by Theiling and McKee[12] during their studies on heterocyclic compounds carrying guanidine substituents.

For further investigations, **1** was synthesized according to Hynes *et al.*[11] and physicochemical properties were verified. Crystals suitable for X-ray structure determination were obtained from a CD_2Cl_2 solution of the synthetic material by evaporation. The crystal structure underlined the formula of **1** (Figure 1).[15] Nitrogen N-10 was found to bind two hydrogen atoms, the positions of which were clearly visible in the electron density. Although potential hydrogen positions at N-1 and N-3 also showed a slight residual density, the crystal structure is mainly based on amine **1**. The crystal lattice is based on hydrogen bonds between the amino hydrogen atoms and the free electron pairs at N-1 and N-3, as shown in Figure 1. At present, only one related crystal structure can be found in the CSD (Cambridge Structural Database), which resembles [1,2,4]triazoloquinazolinium betaine (**2**).[16]

Feeding experiments

So far, only very few reports have addressed the biosynthesis of the small bicyclic quinazolines. Among the known quinazoline alkaloids from plants, arborine (**3**) and peganine/vasicine (**4**) were examined by *in vivo* feeding experiments.[17–19] Anthranilic acid has been suggested to be the putative precursor of the aromatic ring system and phenylalanine for the pyrimidine fragment. Yet, the metabolic origin of this aminobenzoic acid has only been discussed. Incorporation of labeled tryptophan [U-$^{14}C_6$] benzene ring into **4** fueled questions whether anthranilic acid derives *de novo* from the shikimate pathway or from the catabolism of tryptophan.[19,20] 4-Methylquinazolines from *Pseudomonas* sp. have been suggested to originate from the so-called 'quinazoline pathway', starting from tryptophan through *N*-formylacetophenone to yield 4-methylquinazolines of type **5**.[21] Therefore, we are fascinated to have a bacterial 4-methyl-2-quinazolinamine (**1**) at hand and to investigate the biosynthesis that presumably encloses anthranilic acid, some urea-like nitrogen source and possibly methionine for the C-4 methyl group. Our feeding experiments with unlabeled anthranilic acid, glycerol and urea should show whether these compounds increased the production of **1**. No alteration for quinazoline (**1**) production has been detected by TLC and HPLC-MS analysis.

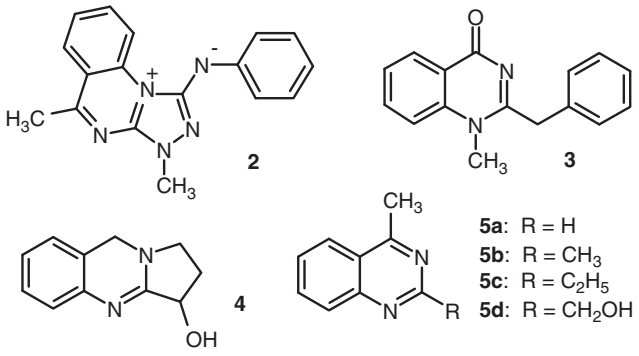

Quinazolinium salt (2) and natural quinazolines (3-5)

Shikimate generally incorporates glycerol from phosphoenolpyruvate (PEP) and erythrose-4-phosphate (E4P) of the pentose phosphate pathway and gives rise to specifically labeled anthranilic acid (Figure 2). Therefore, $^{13}C_3$-labeled glycerol was administered to growing cultures, and ^{13}C-NMR spectra of purified **1** clearly showed a distinct ^{13}C-^{13}C coupling between C-5/C-6/C-7 and C-4a/C-8a and a single enrichment at methyl group C-9 (Supplementary information). This indicates an intact incorporation of glycerol through the shikimate pathway (Figure 2). Levels of [$^{13}C_3$]glycerol are unbalanced in the metabolic pools of PEP and E4P, and therefore C-8 (C-1 of E4P) might not be significantly labeled.[22]

Previous speculations about the incorporation of methionine into quinazoline alkaloids revolve around the origin of the methyl group at N-1 of **3**. Gröger and collaborators[17] isolated labeled *N*-methylanthranilic acid as a degradation product during their studies. [Methyl-^{13}C]methionine did not significantly label any carbon atom of **1**, and *N*-methylanthranilic acid has not been isolated from feeding studies with strain GS DV232 (data not shown), but in earlier experiments. Uncommonly, 4-methyl-2-quinazolinamine (**1**) bears a third nitrogen atom in the pyrimidine fragment, which strongly invited for biosynthetic experiments. [^{13}C]Urea was fed to the producing strain and gave

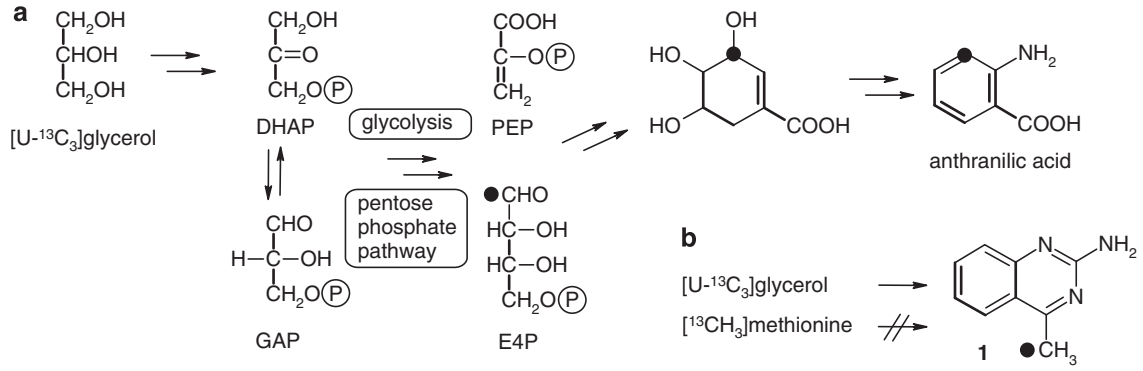

Figure 2 Labeling patterns of (**a**) shikimate from glycerol metabolism in general; and (**b**) quinazoline **1** from [U-$^{13}C_3$]glycerol and [methyl-^{13}C]methionine.

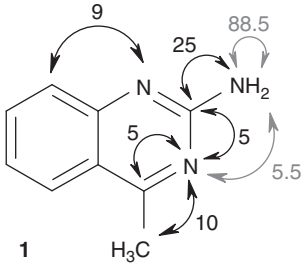

Figure 3 Coupling constants (in Hz) of **1** from ^{1}H-NMR (J_{NH}: gray) and ^{13}C-NMR data (J_{NC}: black) after feeding [^{13}C,$^{15}N_2$]urea.

no significant enrichments. However, consistent labeling patterns for **1** were observed from feeding [$^{15}N_2$]urea and [^{13}C,$^{15}N_2$]urea. The ^{1}H-NMR spectra revealed new high field-shifted multiplet signals, δ_H=6.07 p.p.m. ($^1J_{NH}$ 88.5 Hz, $^3J_{NH}$ 5.5 Hz), pointing to an incorporation rate of about 14% of ^{15}N into the NH_2-group. ^{1}H-^{15}N-HMBC studies (with optimization on J_{NH} 5 Hz) gave only a significant cross-correlation of N-3 (δ_N= −110 p.p.m.) and 9-CH_3 (δ_H=2.72 p.p.m.). In addition, several J_{NC} couplings are deduced from ^{13}C-NMR data (Figure 3), suggesting a distinguished, moderate ^{15}N incorporation into all N-atoms of **1** because of a vital catabolism of ^{15}N-labeled urea, but no incorporation of an intact [^{13}C,^{15}N]urea moiety.

From our data of the comprehensive feeding experiments, we suggest the following biosynthetic pathway for the uncommon microbial 2-quinazolinamine metabolite **1**:

(1) Tryptophan originates from anthranilic acid from the shikimic acid pathway by means of PEP and E4P. Three sources form the tryptophan skeleton, anthranilate (shikimic acid pathway), 5-phosphoribosylpyrophosphate (pentose phosphate pathway) and serine (3-phosphoglycerate from glycolysis), which in turn are formed from glycerol (Figure 4).[23]

(2) Cleavage of tryptophan by tryptophan pyrrolase/tryptophan-2,3-dioxygenase could form *N*-formylkynurenine (**6**), which is transformed into **7** by a 2-oxoglutarate aminotransferase. Possibly, a reduction at the 2-keto group gives **8,** which is converted into 2-aminoacetophenone (**9**) and glyoxylate through a keto-hydroxyglutarate aldolase reaction type (Figure 4).[24]

(3) The significant high incorporation of labeled urea in NH_2-10 and the indicated weak labeling of N-1 and N-3 should be the result of urea catabolism by urease—already known from *Streptomyces*—to NH_3 and CO_2. The resulting ^{15}N-labeled ammonium represents a source for each of the three nitrogens in **1** in individual degrees. Hence, no [^{13}C]label is transferred directly from [^{13}C,^{15}N]urea into carbon C-2 of **1**. That is, N-3–C-2–N-10 does not come from an intact urea-moiety (Figure 4).

(4) We suggest that inorganic ammonium labels carbamoyl phosphate (**10**), which mediates ^{15}N transfer to **1**. We consequently assume *N*-carbamoyl aspartate (**11**) carrying ^{15}N isotopic labels derived from **10** and from glutamate in the course of aspartate biosynthesis by transamination. Generally, glutamate in turn is biosynthetically close to the ammonia pool, and is therefore strongly ^{15}N labeled in respective feeding experiments.

(5) It is also feasible that N-1 is ^{15}N labeled, as glutamate also provides the anthranilic acid and indole nitrogen at an early stage of biosynthesis (Figure 4). To conclude, labeling of the three nitrogen atoms in different intensities reflects the dynamic metabolism (time, sites, substrate specificities).

(6) Finally, the quinazoline ring system is formed from **9** and **11** by a double nucleophilic attack (Figure 4). Transamination and release of oxaloacetate could result in the new quinazoline metabolite **1**.

Biological activity

For biological screening, crude extracts of strain GS DV232 were tested against different test organisms in a plate diffusion assay. A weak growth inhibition of *Bacillus subtilis* and *Escherichia coli* was observed, but no growth inhibition of any testorganisms could be detected for the pure 4-methyl-2-quinazolinamine (**1**). Cytotoxicity cell assays with **1** indicated a moderate activity against different tumor cell lines (Table 1). Furthermore, **1** showed antiproliferating properties on bronchial carcinoma cells (line A549), which can be compared with known chemotherapeutic agents such as doxorubicin and melphalan (Figure 5) (Supplementary information). Currently, ongoing assays are concerned with the possible mode of action of **1**, and thus the morphological effects on tumor cells were investigated. After incubating breast adenocarcinoma cells (line MCF 7) with **1** in a concentration of 5 μg ml^{-1}, the cells showed a deformation of the nuclei combined with hollows in the network of microtubules (Supplementary information).

Conclusion

The concept of our screening has its seeds in TCM plants as habitats for potent antibiotic-producing Streptomycetes, one of them producing 4-methyl-2-quinazolinamine (**1**), not known as a natural product before. Significant enrichments of 2-quinazolinamine **1** from feeding experiments indicated the biosynthetic pathway of **1** to originate from a tryptophan-derived core. The three nitrogen atoms are an uncommon feature of the bacterial quinazoline **1**; in this study, we present

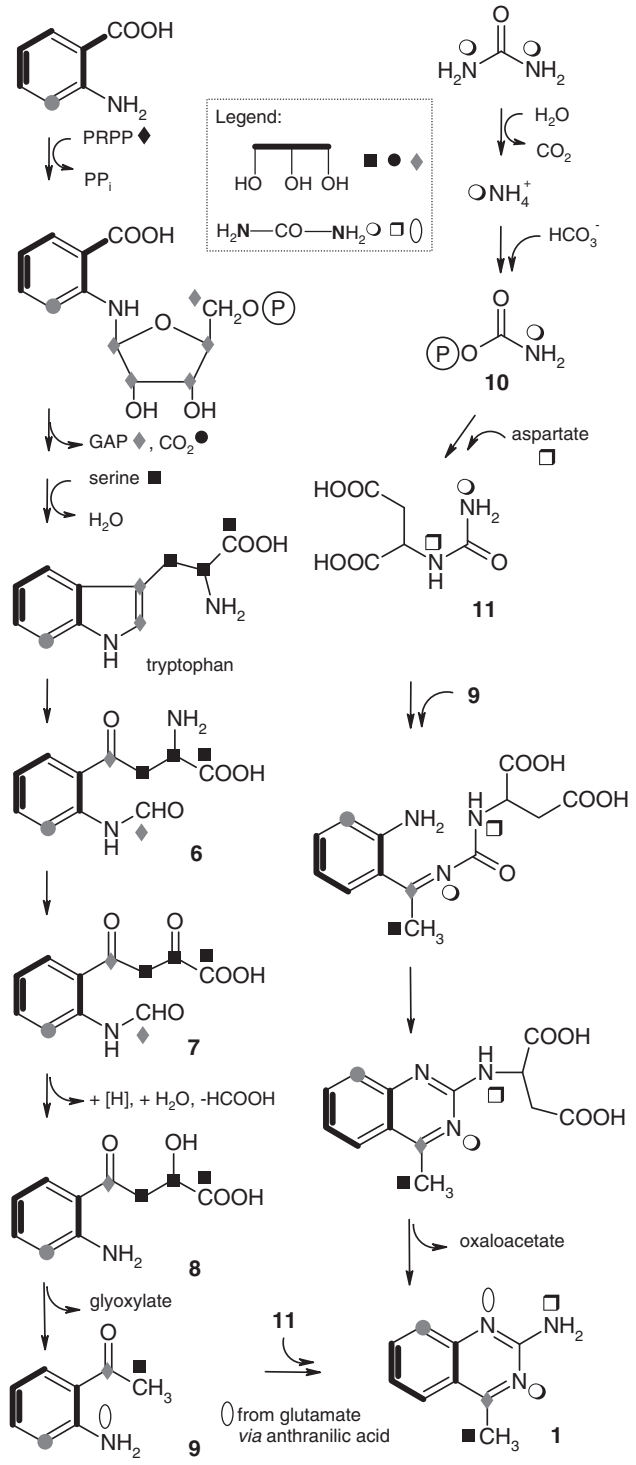

Figure 4 The proposed biosynthetic pathway for 4-methyl-2-quinazolinamine (**1**) in accordance with labeling patterns derived from ^{13}C- and ^{15}N-labeled precursors (black: significant, grey: weak/not detectable incorporation).

a conclusive biosynthetic pathway. In different biological tests for antitumor activity, **1** showed a moderate antiproliferating potential on cancer cells in comparison with known compounds. Thus, ongoing research revolves around the synthesis and biological evaluation of 2-amino-substituted quinazolines.

Although alkaloids—mainly of plant origin—have been intensively investigated, quinazolines especially are still in the focus of research.

Table 1 Cytotoxicity of quinazoline 1 against different tumor cell lines: AGS, HM02 (gastric adenocarcinoma), HepG2 (hepatocellular carcinoma) and MCF 7 (breast adenocarcinoma)

	AGS		*HM02*		*HepG2*		*MCF 7*	
Cell line	GI_{50}	*TGI*	GI_{50}	*TGI*	GI_{50}	*TGI*	GI_{50}	*TGI*
$\mu g\,ml^{-1}$	1.3	4.1	1.25	9.1	4.9	>10	2.5	4.9
$\mu mol\,l^{-1}$	8.18	25.8	7.86	57.2	30.8	>63	15.7	30.8

GI_{50} is the concentration at which half of the cells were inhibited in their growth, and TGI is the concentration at which a total inhibition of cell growth was observed.

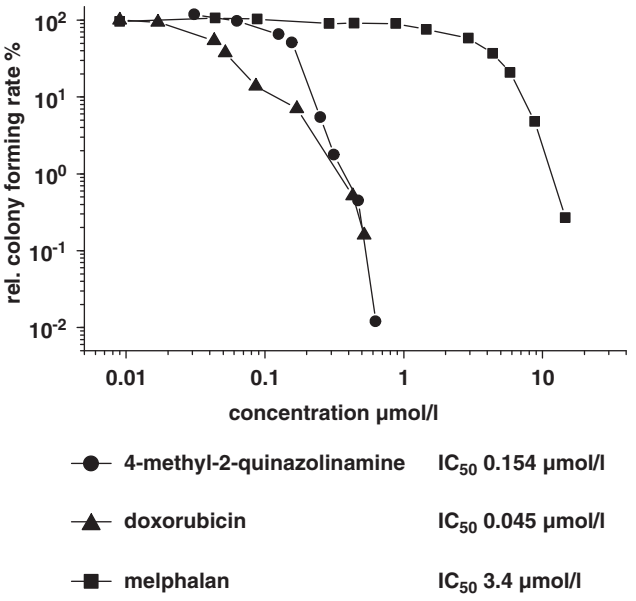

Figure 5 Antiproliferative potential of **1** against bronchial carcinoma cells (line A549) compared with doxorubicin and melphalan (Supplementary information). Relative colony-forming rates (%) were obtained as follows: average of treated colonies/average of untreated colonies $\times 100$.

Streptomycetes have been observed to produce known alkaloids and the strikingly simple quinazoline-4-one.[25] We learn that (synthetically) known quinazoline structures have been also invented by nature: 4-methylquinazoline (**5a**), first discovered from *Pseudomonas* sp.,[21] was recently identified as a sex pheromone in the parasitoid wasp *Nasonia vitripennis*.[26] Synthetic efforts on 2-guanidino quinazolines as adenosine receptor antagonists add on the picture of actual quinazoline research fields.[27]

EXPERIMENTAL SECTION

General

Electron impact and HREI mass spectra were recorded on Finnigan MAT 95 (70 eV; Thermo Scientific, Dreieich, Germany); relative intensities in parenthesis refer to the highest peak of the spectrum. HRESI-MS spectra were obtained using Bruker Apex IV (FTICR, 7 T; Bruker Daltonik GmbH, Bremen, Germany). All NMR spectra were measured in acetone-d_6 or CD_2Cl_2, with the solvent as internal reference. Chemical shifts are expressed in δ-values. ^1H-NMR spectra were recorded on Varian Inova-600, and ^{13}C-NMR spectra on Varian Inova-500 (125.7 MHz) equipped with Varian PFG Cold Probe (with helium cooling system). ^{15}N-NMR spectra were recorded on Varian VNMR-S 600 equipped with a 3 mm triple-resonance inverse probehead (temperature 25 °C, 600 MHz for ^1H and 60 MHz for ^{15}N). UV spectra were obtained in methanol from a

Varian Cary 3E spectrometer (Varian GmbH, Darmstadt, Germany), and IR spectra from a PerkinElmer model 1600 as KBr pellets (PerkinElmer LAS GmbH, Rodgau, Germany). M.p.s were measured with a Reichert (Vienna, Austria) hot-stage microscope (not corrected).

Producer strain

The producing strain *Streptomyces* sp. GS DV232 was isolated from the leaf (*folium*) of the meadowsweet *Filipendula palmata* (Pall.) Maxim. family of *Rosaceae*, which was collected near Harbin, Heilongjiang Province, PR of China in 2005. Taxonomic investigations suggest strain GS DV232 to be *S. zaomyceticus* and *S. venezuelae* (100% identity by 16S rDNA analysis).

Chemical screening and isolation

Chemical screening was performed by the cultivation of strain GS DV232 in different media with oat meal (HF), soybean meal (SGG) and yeast/malt/glucose (YMG), and subsequent chemical and biological analyses of the extracts (Supplementary information). Fermentations were carried out in liquid cultures (1 l baffled Erlenmeyer flasks with 250 ml broth volumes) that were incubated in a shake incubator at 28 °C, 180 r.p.m. for 72 h. After adjusting the pH to 5.0, culture broths were filtrated. Filtrates were extracted thrice with ethyl acetate, and combined organic phases were evaporated. Crude extracts were subjected to chromatography on silica gel (eluent: chloroform/methanol 9:1), followed by MPLC (medium pressure liquid chromatography) on RP-18 (Merck LiChroprep column; Merck KGaA, Darmstadt, Germany; eluent: methanol/water 8:2). Optional further purification was achieved by HPLC (high performance liquid chromatography): Jasco PU-2080plus pump, Jasco MD-210plus UV-detector, Rheodyne manual injection valve, software Jasco Borwin (version 1.50) with Jasco HSS-2000 (version 3.5.2) (Jasco GmbH, Gross-Umstadt, Germany); column: Phenomenex Aqua (Hydro-RP; Phenomenex, Aschaffenburg, Germany) C18 endc., 5 µm, 250×10 mm, flow rate 2.7 ml min^{-1}; isocratic solvent system: MeOH/H_2O 15:85; UV detection at 274 and 339 nm; retention time of 7 min for **1**. The overall yield of **1** was 2 mg l^{-1} from liquid cultures.

Feeding experiments

For feeding experiments, the producer strain was cultivated in a 2 l fermenter (Biostat B; B.Braun AG, Melsungen, Germany) containing 1.5 l YMG medium for 54 h. A 48 h preculture in 1 l baffled Erlenmeyer flasks with 150 ml YMG medium was used as inoculum. From the twelfth to the twenty-third hour of fermentation, feeding reagents were added continuously as sterile-filtered solutions (40 ml each). Feeding reagents: anthranilic acid 7.3 mM, glycerol 5.4 mM, [U-$^{13}C_3$]glycerol (99% ^{13}C) 5.4 mM, urea 4.0 mM, [^{13}C]urea (99% ^{13}C) 4.0 mM, [$^{15}N_2$]urea (95% ^{15}N) 4.0 mM, [^{13}C,$^{15}N_2$]urea (99% ^{13}C, >98% ^{15}N) 4.0 mM and [methyl-^{13}C]methionine (99% ^{13}C) 1.2 mM. Labeled glycerol, [^{13}C]urea and [$^{15}N_2$]urea were obtained from Campro Scientific GmbH (Berlin, Germany), and [^{13}C,$^{15}N_2$]urea and methionine from Cambridge Isotope Laboratories (Euriso-top GmbH, Saarbrücken, Germany). Isolation of pure **1** was performed by subjecting the crude extract to chromatography on Sephadex LH-20 (Sigma-Aldrich Chemie GmbH, Munich, Germany; eluent: methanol), followed by MPLC and HPLC as described above.

Biological tests

In plate diffusion tests, crude extracts and pure compounds were tested against *B. subtilis*, *Candida albicans*, *E. coli* and *Staphylococcus aureus* (Supplementary information).

In a first test series, cytotoxic activity was determined according to NCI (USA) protocol with tumor cell lines AGS, HM02 (gastric adenocarcinoma), HepG2 (hepatocellular carcinoma) and MCF 7 (breast adenocarcinoma) (Supplementary information).[28] In the second study, **1** was tested with regard to its toxic potential on the colony-forming rate of human bronchial carcinoma cells (line A549) (Supplementary information). For morphological studies, MCF 7 (breast adenocarcinoma) cells were incubated for 24 h after adding **1** in a concentration of 5 µg ml^{-1}. Microtubules were colored green by immunofluorescence, nuclei and chromosomes were stained blue with 4,6-diamidino-2-phenylindole (Supplementary information).

Crystal structure determination

1 was crystallized in a Ø 3 mm glass vial by evaporation from CD_2Cl_2. A suitable crystal (0.27×0.22×0.18 cm) was mounted at 100 K on a Bruker Smart 6000 CCD diffractometer (Bruker AXS GmbH, Karlsruhe, Germany) equipped with mirror-system-monochromated Cu Kα radiation (λ 1.54178 Å). A total of 8189 reflections were measured, of which 1197 were independent. Data reduction and processing was carried out with SAINT (Bruker AXS), empirical absorption correction with SADABS (Bruker AXS) and phasing with SHELXS.[29] The asymmetric unit contained two molecules and the measured crystal belonged to the orthorhombic space group P 2_1 2_1 2_1. The structure was determined by direct methods. All atoms except hydrogens were refined anisotropically by the full-matrix least-squares method on F2 using SHELXL97[29] to give a final R-factor of 0.0226. The amino hydrogen atoms were refined, all other hydrogen atoms were calculated in riding positions.

4-Methyl-2-quinazolinamine (1)

$C_9H_9N_3$ (159.19);. white solid; m.p. 112 °C; R_f 0.47 (RP-18, MeOH/H_2O 8:2); EI-MS (70 eV) *m/z* (%) 159 (100) $[M]^+$, 144 (12) $[M\text{-}CH_3]^+$, 132 (18), 119 (17); HREI-MS calcd., found *m/z* 159.0797; HRESI-MS calcd., found *m/z* 160.08692 $[M+H]^+$; UV (MeOH) λ_{max} nm (log ε) 202 (4.04), 235 (4.28), 349 (3.31); UV (MeOH+HCl) λ_{max} nm (log ε) 201 (3.96), 230 (4.14), 246 (4.01), 275 (3.43), 342 (3.34); UV (MeOH+NaOH) λ_{max} nm (log ε) 211 (3.81), 236 (4.31), 350 (3.57); IR ν_{max} (KBr) cm^{-1} 3329, 3176, 1650, 1617, 1565, 1480, 1441, 1392, 1363, 1263, 1142, 1037; ^{1}H-NMR (600 MHz, acetone-d_6): δ p.p.m. 2.72 (s, 3H, 9-H_3), 6.08 (bs, 2H, 2-N$\underline{H}_2$), 7.21 (ddd, *J*=8.5, 7.0, 1.5 Hz, 1H, 6-H), 7.44 (dd, *J*=8.5, 1.5 Hz, 1H, 8-H), 7.63 (ddd, *J*=8.5, 7.0, 1.5 Hz, 1H, 7-H), 7.94 (dd, *J*=8.5, 1.5 Hz, 1H, 5-H); ^{1}H-NMR (600 MHz, CD_2Cl_2) (see Supplementary information); ^{13}C-NMR (125.7 MHz, acetone-d_6) δ p.p.m. 21.5 (q, C-9), 120.3 (s, C-4a), 122.9 (d, C-6), 126.4 (d, C-5), 126.7 (d, C-8), 134.3 (d, C-7), 153.2 (s, C-8a), 161.4 (s, C-2), 170.6 (s, C-4); ^{13}C-NMR (125.7 MHz, CD_2Cl_2) (see Supplementary information); ^{15}N-NMR (60 MHz, acetone-d_6) δ p.p.m. −110.4 (N-3), −164.2 (N-1), −303.1 (N-10). Chemical shifts were obtained from ^{1}H-^{15}N-HMQC resp. ^{1}H-^{15}N-HMBC correlations. Chemical synthesis of **1** was performed considering the results of Hynes *et al.*[11] (Supplementary information).

ACKNOWLEDGEMENTS

We thank Prof Dr W Beil (Institute of Pharmacology, Medizinische Hochschule Hannover/Germany) and Dr F Sasse (Helmholtz Centre for Infection Research, Braunschweig/Germany) for performing cell assays. We thank Prof Dr Fu Yu-jie and Mei An (Northeast Forestry University, Harbin/China) for valuable discussions about TCM. Furthermore, we thank Dr T Paululat (Institute of Organic Chemistry, Universität Siegen/Germany) for measurement of ^{15}N-NMR spectroscopic data.

1 Gurib-Fakim, A. Medicinal plants: traditions of yesterday and drugs of tomorrow. *Mol. Aspects Med.* **27,** 1–93 (2006).
2 Newman, D. J. & Cragg, G. M. Natural products as sources of new drugs over the last 25 years. *J. Nat. Prod.* **70,** 461–477 (2007).
3 Cordell, G. A. Natural products in drug discovery—creating a new vision. *Phytochem. Rev.* **1,** 261–273 (2002).
4 Wilson, R. M. & Danishefsky, S. J. Small molecule natural products in the discovery of therapeutic agents: the synthesis connection. *J. Org. Chem.* **71,** 8329–8351 (2006).
5 Lam, K. S. New aspects of natural products in drug discovery. *Trends Microbiol.* **15,** 279–289 (2007).
6 Heinrich, M. Ethnobotany and natural products. *Curr. Top. Med. Chem.* **3,** 141–154 (2003).
7 Strobel, S. A. & Strobel, G. A. Plant endophytes as a platform for discovery-based undergraduate science education. *Nat. Chem. Biol.* **3,** 356–359 (2007); and citations therein.
8 Izzo, A. A. & Ernst, E. Interactions between herbal medicines and prescribed drugs: a systematic review. *Drugs* **61,** 2163–2175 (2001).
9 Traversier, R., Staudinger, K. & Friedrich, S. TCM in westlichen Pflanzen, Phytotherapie, Akupunktur, Diätetik. Sonntag Verlag Stuttgart (2005) (*in German*).
10 Wu, Z. Y., Raven, P. H. & Hong, D. Y. (eds). *Flora of China* Vol. 9 (*Pittosporaceae* through *Connaraceae*). (Science Press, Beijing, China and Missouri Botanical Garden Press, St Louis, MO, USA, 2003).

11 Hynes, J. B., Campbell, J. P. & Hynes, J. D. Synthesis of 2-aminoquinazolines from ortho-fluoroketones. *J. Heterocyclic Chem.* **32,** 1185–1187 (1995).
12 Theiling, L. F. & McKee, R. L. 2-Guanidinoquinazolines. *J. Am. Chem. Soc.* **74,** 1834–1836 (1952).
13 D'yakonov, A. L. & Telezhenetskaya, M. V. Quinazoline alkaloids in nature. *Chem. Nat. Compd.* **33,** 221–267 (1997).
14 Michael, J. P. Quinoline, quinazoline and acridone alkaloids. *Nat. Prod. Rep.* **25,** 166–187 (2008).
15 CCDC reference number 737855 contains the supplementary crystallographic data for this structure. These data can be obtained free of charge via www.ccdc.cam.ac.uk/conts/retrieving.html (or from the CCDC, 12 Union Road, Cambridge CB2 1EZ, UK; fax: +44 1223 336033; e-mail: deposit@ccdc.cam.sc.uk).
16 Crabb, D. L. *et al.* Preparation of [1,2,4]triazoloquinazolinium betaines and molecular rearrangements of putative [1,2,4]triazolo[4,3-a][1,3,5]triazinium betaines. *J. Chem. Soc., Perkin Trans.* **1,** 1517–1525 (1999).
17 Johne, S., Waiblinger, K. & Gröger, D. Zur Biosynthese des Chinazolinalkaloids Arborin. *Eur. J. Biochem.* **15,** 415–420 (1970) (*in German*).
18 O'Donovan, D. G. & Horan, H. The biosynthesis of arborine. *J. Chem. Soc. (C)* **1970,** 2466–2470 (1970).
19 Liljegren, D. R. Biosynthesis of quinazoline alkaloids of *Peganum harmala*. *Phytochemistry* **10,** 2661–2669 (1971).
20 Liljegren, D. R. The biosynthesis of quinazoline alkaloids of *Peganum harmala* L. *Phytochemistry* **7,** 1299–1306 (1968).
21 Mann, S. Chinazolinderivate bei Pseudomonaden. *Arch. Mikrobiol.* **56,** 324–329 (1967) (*in German*).
22 Wenzel, S. C. *et al.* On the biosynthetic origin of methoxymalonyl-acyl carrier protein, the substrate for incorporation of 'glycolate' units into ansamitocin and soraphen. *J. Am. Chem. Soc.* **128,** 14325–14336 (2006).
23 Berg, J. M., Tymoczko, J. L. & Stryer, L. *Biochemistry*, International 6th edition. (W.H. Freeman & Co Ltd, New York, USA, 2006).
24 Nishihara, H. & Dekker, E. E. Purification, substrate specifity and binding, β-decarboxylase activity, and other properties of *Escherichia coli* 2-keto-4-hydroxyglutarate aldolase. *J. Biol. Chem.* **241,** 5079–5087 (1972).
25 Maskey, R. P., Shaaban, M., Grün-Wollny, I. & Laatsch, H. Quinazoline-4-one derivatives from Steptomyces isolates. *J. Nat. Prod.* **67,** 1131–1134 (2004).
26 Ruther, J., Steiner, S. & Garbe, L.-A. 4-Methylquinazoline is a minor compound of the male sex pheromone in *Nasonia vitripennis*. *J. Chem. Ecol.* **34,** 99–102 (2008).
27 Webb, T. R. *et al.* Quinazolines as adenosine receptor antagonists: SAR and selectivity for A_{2B} receptors. *Bioorg. Med. Chem.* **11,** 77–85 (2003).
28 Grever, M. R., Schepartz, S. A. & Chabner, B. A. The National Cancer Institute: cancer drug discovery and development program. *Semin. Oncol.* **19,** 622–638 (1992).
29 Sheldrick, G. M. A short history of SHELX. *Acta. Cryst.* **A64,** 112–122 (2008).

Supplementary Information accompanies the paper on The Journal of Antibiotics website (http://www.nature.com/ja)

The Journal of Antibiotics (2009) 62, 445–452

www.nature.com/ja

ORIGINAL ARTICLE

Gombapyrones, new α-pyrone metabolites produced by *Streptomyces griseoruber* Acta 3662*

Soleiman Helaly[1], Kathrin Schneider[1], Jonny Nachtigall[1], Sabaratnam Vikineswary[2], Geok Yuan Annie Tan[2], Heidi Zinecker[3], Johannes F Imhoff[3], Roderich D Süssmuth[1] and Hans-Peter Fiedler[4]

Gombapyrones A–D, new members of the α-pyrone family of secondary metabolites, were produced by *Streptomyces griseoruber* Acta 3662, which was isolated from bamboo tree rhizosphere. The strain was characterized by its morphological and chemotaxonomical features and by 16S rDNA sequencing as *S. griseobuber*. The gombapyrone structures were determined by mass spectrometry and by NMR experiments, and were found to have an inhibitory activity against protein tyrosine phosphatase 1B and glycogen synthase kinase 3β.
The Journal Antibiotics (2009) **62,** 445–452; doi:10.1038/ja.2009.70; published online 31 July 2009

Keywords: fermentation; isolation; α-pyrone; protein-tyrosine phosphatase inhibitor; *Streptomyces*; structure elucidation

INTRODUCTION

In our screening program to detect novel secondary metabolites from actinomycetes for pharmaceutical applications (http://www. actapharm.org) freshly isolated strains from selected European and Malaysian ecosystems were included. The strains were grown as submerged cultures in different complex media, extracts were prepared from mycelia and from culture filtrates at various fermentation times and were screened by HPLC-diode array analysis to determine their chemical diversity. Evaluation of chromatograms was performed using our in-house developed HPLC-UV-Vis database, which contains 933 entries, most of them being antibiotics.[2] Strain Acta 3662, which was isolated from soil collected from the rhizosphere of bamboo trees in the tropical rainforest of the University of Malaya Field Station at Gombak, Selangor, Malaysia, was of interest because of the presence of a family of metabolites in the mycelium extract having nearly congruent UV-Vis spectra, which were unlike those of all reference compounds of the database. This study describes the taxonomy of the producing strain, the fermentation, isolation, structural elucidation and biological activity of the new family of metabolites from strain Acta 3662, which were named gombapyrones, composed from the collection site Gombak and the α-pyrone scaffold of their structures, which are shown in Figure 1.

RESULTS

Taxonomy of the producing strain

Strain Acta 3662 was isolated from a rhizospheric soil sample from a patch of bamboo trees at the University of Malaya Field Station in Gombak, Selangor on the West Coast of Malaysia. The putative *Streptomyces* strain was characterized for growth morphology on inorganic salt–starch agar (ISP 4) by electron microscopic studies. The aerial mycelium of strain Acta 3662 grown on ISP 2 agar was extensively branched and the ends of the hypha had spiral arthrospore chains. No sclerotic granules, sporangia or zoospores were observed (Figure 2). Furthermore, the strain contained L,L-diaminopimelic acid in petidoglucan. The cultural and phenotypic properties of the strain are given in Tables 1 and 2.

Strain Acta 3662 grew on a wide range of media and its cultural characteristics are given in Table 1. The color of the spore mass was gray on yeast extract–malt extract agar and on inorganic salt–starch agar. Melanoid pigment was observed when Acta 3662 was grown on peptone–yeast extract–iron agar. There was no pigment production by the strain in tyrosine agar. The carbon source utilization pattern and physiological properties are summarized in Table 2. The strain was positive for H_2S formation, had strong proteolytic activity, coagulated milk, reduced nitrate to nitrite and could grow in concentrations of sodium chloride up to 6% (w/v) in media ISP 2. The carbon sources utilized are given in Table 2. Growth of strain Acta 3662 was observed from 25 to 35 °C, but the strain failed to grow at 45 °C. On the basis of growth and physiological characteristics, strain Acta 3662 was assigned to the genus *Streptomyces*. 16S rDNA analysis indicated that the strain is the same as *Streptomyces griseoruber* JCM 4642 (AY999750) with 100% similarity (Figure 3).

Screening, fermentation and isolation

Strain Acta 3662 was cultivated in 500-ml Erlenmeyer flasks in various complex media, and extracts from the mycelium and culture filtrates

[1]Institut für Chemie, Technische Universität Berlin, Berlin, Germany; [2]Institute of Biological Sciences, University of Malaya, Kuala Lumpur, Malaysia; [3]Leibniz-Institut für Meereswissenschaften IFM-GEOMAR, Kiel, Germany and [4]Mikrobiologisches Institut, Universität Tübingen, Tübingen, Germany
Correspondence: Professor H-P Fiedler, Mikrobiologisches Institut, Auf der Morgenstelle 28, Tübingen 72076, Germany.
E-mail: hans-peter.fiedler@uni-tuebingen.de or Professor RD Süssmuth, Institut für Chemie, Technische Universität Berlin, Straße des 17. Juni 124, Berlin 10623, Germany.
E-mail: suessmuth@chem.tu-berlin.de
*Article no. 52 in 'Biosynthetic Capacities of Actinomycetes'. Article no. 51: see reference 1.
Received 3 June 2009; revised 2 July 2009; accepted 3 July 2009; published online 31 July 2009

were prepared at 72 and 120 h, respectively, to investigate their secondary metabolite pattern by HPLC-diode array analysis. Evaluation by means of our in-house developed HPLC-UV-Vis database revealed the presence of elaiophylin and bafilomycins in the mycelium extract besides a family of metabolites of which the UV-Vis spectra differed from those of all reference compounds stored in the database. The HPLC elution profile of the mycelium extract is shown in Figure 4.

A scale-up of the cultivation of strain Acta 3662 was performed to the 10-l fermentor scale in a complex medium in which maximal biomass was reached after incubation for 120 h. Production of **1–5** started at 72 h, reaching a maximal yield of 40 mg l^{-1} in the case of the

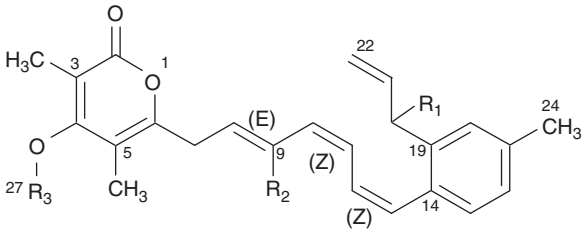

A (**2**): $R_1 = OH$, $R_2 = CH_3$, $R_3 = CH_3$
B (**3**): $R_1 = H$, $R_2 = CH_3$, $R_3 = H$
C (**4**): $R_1 = H$, $R_2 = H$, $R_3 = CH_3$
D (**5**): $R_1 = H$, $R_2 = CH_3$, $R_3 = CH_3$

Figure 1 Structures of gombapyrones A–D (**2**–**5**).

Table 2 Physiological properties of strain Acta 3662

Temperature range of growth (ISP 2)	15–35 °C
Optimum temperature for growth (ISP 2)	25–35 °C
Formation of melanoid pigments	
Peptone–yeast extract–iron agar (ISP 6)	+
Tyrosine agar (ISP 7)	–
Liquefaction of gelatin	+
Soluble pigment production	+
Coagulation of milk	+
Peptonization of milk (medium skim milk agar)	–
Hydrolysis of starch	+
Reduction of nitrate	+
H_2S production	+
NaCl tolerance (ISP 2)	⩽6%
Carbon source utilization (ISP 2)	
L(+) Arabinose	+
D(+) Xylose	+
D(+) Glucose	+
D-Fructose	+
Sucrose	±
myo-Inositol	+
α-L-Rhamnose	+
Raffinose	±
D-Mannitol	±
D-Sorbitol	–
Maltose	±
β-Lactose	+

+, positive; ±, slightly positive; –, negative.

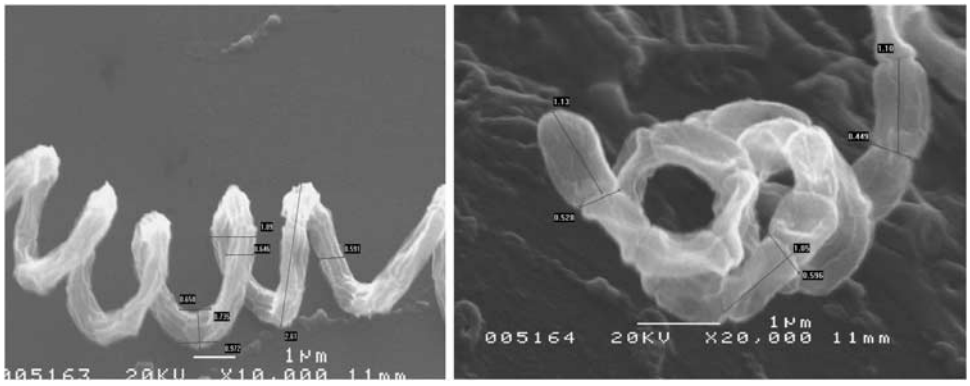

Figure 2 Micrograph of the aerial mycelium of strain Acta 3662 with long spore per chain classified in the spiral and *Rectiflexibiles* section; scale bar: 1 µm.

Table 1 Growth and cultural characteristics of strain Acta 3662 on selected agar media

Medium	*Yeast extract–malt extract agar*	*Oatmeal agar*	*Inorganic salts–starch agar*	*Glycerol– asparagine agar*	*Peptone–yeast-extract agar*	*Tyrosine agar*
Growth	+++	++	++	+	+	+
Spore chain morphology	Spirales	Spirales	Spirales	Spirales	Spirales	Spirales
Spore surface ornamentation	Smooth	Smooth	Smooth	Smooth	Smooth	Smooth
Colony of spore mass	Gray	Silver mist	Gray	Ash gray to white	Blue black	Ash gray to white
Pigmentation of substrate	Red orange to violet	–	Osprey to red purple	Impian red	Blue black	Orange to signal red
Diffusible pigment	Red orange to violet	Honeypine	–	Honeypine on ramin	Blue black	Wicker

–, no growth; +, poor growth; ++, moderate growth; +++, good growth. Observation after incubation at 28 °C for 7 days.

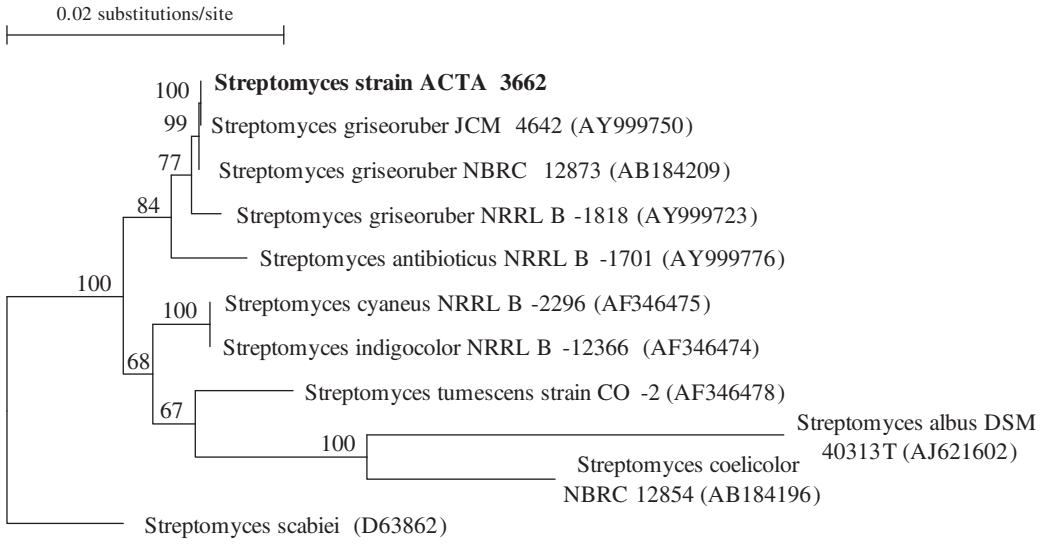

Figure 3 Neighbor-joining tree of streptomycetes based on 16S rDNA sequence. The numbers at the nodes indicate the level of bootstrap support (%) based on the analysis; scale bar: substitutions per nucleotide position.

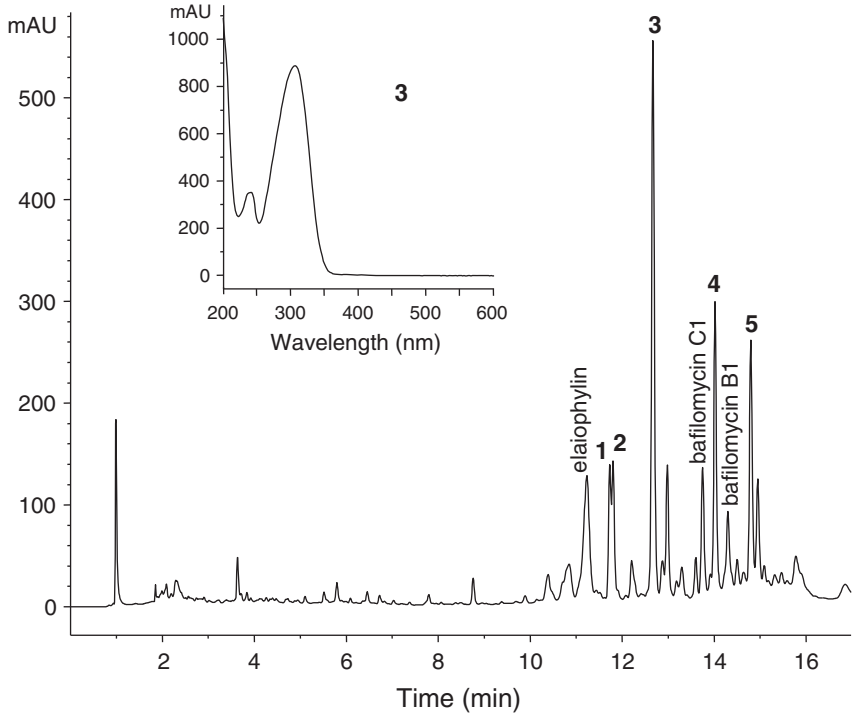

Figure 4 HPLC analysis of a mycelium extract from *S. griseoruber* Acta 3662 at a cultivation time of 120 h, monitored at 280 nm. Insert: UV-VIS spectrum of gombapyrone B (**3**).

main component **3** after incubation for 120 h. Compounds **1–5** were isolated from mycelium by extraction with MeOH-Me_2CO. Extracts were concentrated to an aqueous residue and were re-extracted with cyclohexane to separate elaiophylin, which is not soluble in cyclohexane. The crude product was purified by subsequent chromatography on a silica gel and Sephadex LH-20 column (Amersham, Freiburg, Germany). Pure gombapyrones were obtained by preparative reversed-phase HPLC as yellow powders after concentration to dryness.

Structural elucidation

The physio-chemical properties of compounds **1–5** are summarized in Table 3. The mass spectrum derived from HPLC-ESI-MS chromatograms for **1–5** showed molecular masses at $[(M+H\text{-}H_2O)^+=389.2]$, $[(M+H\text{-}H_2O)^+=389.2]$, $[(M+H)^+=377.2]$, $[(M+H)^+=377.2]$ and $[(M+H)^+=391.2]$, respectively. The exact molecular masses were determined by high-resolution electrospray ionization fourier transform ion cyclotron resonance MS (ESI-FT-ICR-MS) as 389.211273 Da

Table 3 Physico-chemical properties of BE 51068 (1) and gombapyrones A–D (2–5)

	1	2	3	4	5
Appearance	Yellow powder	Yellow powder	Yellow powder	Yellow powder	Yellow powder
Molecular mass	406.2	406.2	376.2	376.2	390.2
Molecular formula	$C_{26}H_{30}O_4$	$C_{26}H_{30}O_4$	$C_{25}H_{28}O_3$	$C_{25}H_{28}O_3$	$C_{26}H_{30}O_3$
ESI-FT-ICR MS (m/z)					
Found	389.211273 $(M+H-H_2O)^+$	389.211169 $(M+H-H_2O)^+$	377.21054 $(M+H)^+$	377.21000 $(M+H)^+$	391.226793 $(M+H)^+$
Calc.	389.21176	389.21176	377.21167	377.21167	391.22732
UV λ_{max}^{MeOH} (nm)	311	311	309	307	307
$[\alpha]_D^{20}$ (c=0.32, MeOH)	—	+3.75	—	—	—
IR ν1)	3420, 2925, 2856, 1706, 1638, 1643, 1567, 1450, 1380, 1360, 1222, 1099, 1037, 988	3427, 2926, 2856, 1707, 1648, 1643, 1567, 1451, 1380, 1359, 1222, 1098, 1039, 988	3272, 2926, 2856, 1673, 1639, 1569, 1495, 1446, 1379, 1233, 1202, 1104, 1075, 992	2924, 2853, 1712, 1687, 1639, 1570, 1456, 1379, 1359, 1328, 1251, 1223, 1071, 991	2999, 2926, 2856, 1709 1639, 1569 1449, 1380, 1359, 1327 1221, 1098, 1280, 988

$[(M+H-H_2O)^+]$ (**1**), 389.211169 Da $[(M+H-H_2O)^+]$ (**2**), 377.21054 Da $[(M+H)^+]$ (**3**), 377.21000 Da $[(M+H)^+]$ (**4**) and 391.226793 Da $[(M+H)^+]$ (**5**); this corresponds to the molecular formulae $C_{26}H_{30}O_4$ (**1**) $[(M+H-H_2O)^+_{theor}$=389.21176, Δm=0.39 p.p.m.], $C_{26}H_{30}O_4$ (**2**) $[(M+H-H_2O)^+_{theor}$=389.21176, Δm=0.12 p.p.m.], $C_{25}H_{28}O_3$ (**3**) $[(M+H)^+_{theor}$=377.21167, Δm=1.54 p.p.m.], $C_{25}H_{28}O_3$ (**4**) $[(M+H)^+_{theor}$=377.21167, Δm=0.28 p.p.m.] and $C_{26}H_{30}O_3$ (**5**) $[(M+H)^+_{theor}$=391.22732, Δm=0.06 p.p.m.].

The ^{1}H-NMR spectrum of **1** showed 10 signals in the olefinic/aromatic region, two signals between 4 and 5 p.p.m. and five signals in the aliphatic region. An integration of the signals revealed that the signal at Δ_H 1.89 p.p.m. in the aliphatic region corresponded to six protons, and each of three other signals in the same region corresponded to three protons, suggesting the presence of five methyl groups in the compound. The ^{13}C-NMR and distortionless enhancement by polarization transfer (DEPT) spectra confirmed the assumption of the presence of five methyl groups, including one methoxy group at Δ_C 60.4 p.p.m. In addition, the DEPT spectrum revealed the presence of two methylene, 10 methine and nine quaternary carbons. The correlation of ^{1}H-NMR signals to the corresponding C-atoms was carried out by the heteronuclear single quantum correlation (HSQC) NMR experiment and the signal at Δ_H 1.89 p.p.m. was assigned to the corresponding ^{13}C-chemical shifts for two methyl groups. One signal in the ^{1}H-NMR-spectrum at Δ_H 4.85 p.p.m. could not be assigned to any C-atom, suggesting the presence of a hydroxyl group. The structure of **1** was fully elucidated using COSY and heteronuclear multibond correlation (HMBC) spectra. The ^{1}H-^{1}H-COSY experiment showed correlations between H_2-7 to H-8, H-10 to H-11, H-11 to H-12, H-12 to H-13, H-15 to H-16, H-20 to H-21, H-21 to H_2-22 and H_2-22 to OH-23 (Figure 5). The HMBC spectrum of **1,** for which selected correlations are shown in Figure 5, provides evidence for an α-pyrone that is linked to an aromate by three conjugated double bonds. This core structure is decorated by methyl groups (C-3, C-5, C-9, C-17), one methoxy group (C-4) and a hydroxypropenyl residue (C-19), respectively. As a conclusion from the NMR-spectrometric data, compound **1** was found to be identical with the BE 51068 described previously.[3] On the basis of coupling constants, the above-mentioned report has established the geometry of the double bonds at C-10/C-11 (J=15.6 Hz) as E, at C-12/C-13 (J=11.6 Hz) as Z and at C-20/C-21 (J=15.6 Hz) as E, which is identical to those determined for compound **1**. These configurations have been confirmed by our groups by ^{1}H/^{1}H-NOESY experiments (correlations from H-8/H-10, H-10/H-15 and H-13/H-20) and, as a consequence, we could establish the E-configuration for C-8/C-9.

Compound **2** has the same molecular formula as **1** ($C_{26}H_{30}O_4$): however, the comparison of the ^{1}H-NMR and ^{13}C-NMR chemical shifts revealed minor structural differences (see Table 4). The ^{13}C-NMR spectra with signals for C-22 at Δ_C 61.6 p.p.m. (**1**) and at Δ_C 113.3 p.p.m. (**2**) indicate that the latter clearly corresponds to an olefinic methylene group, whereas the methylene group in **1** is attached to an oxygen atom. In the ^{1}H-NMR spectrum, methylene protons H_2-22 of **2** appeared at Δ_H 4.99/5.15 p.p.m. (d, d, J=10.3, 17.1 Hz), whereas for **1,** they were assigned at Δ_H 4.09 p.p.m. (t, J=5.3 Hz). Furthermore, signals of H-20/C-20 of **1** appeared at Δ_H 6.65 p.p.m. (d, J=15.8) and 129.7 p.p.m. compared with Δ_H 5.19 p.p.m. (t, J=4.9) and Δ_C 70.1 p.p.m. for **2,** which is an oxygenated methine carbon. The ^{1}H-^{1}H-COSY, HSQC and HMBC spectra for **2** provided proof of the deduced structure, particularly by HMBC correlations from H_2-22 to C-20 and C-21, from H-20 to C-14, C-18, C-21 and C-22, and from the hydroxyl proton to C-20 and C-21 (Figure 5). As compound **2** has a stereocenter at C-20 and is therefore supposed to be optically active, the optical activity of **2** was determined as shown in Table 3.

Compound **5** with a molecular formula of $C_{26}H_{30}O_3$ lacks one oxygen atom compared with **2** ($C_{26}H_{30}O_4$). The corresponding ^{1}H-NMR spectrum of **5** showed an absence of hydroxymethine signals and the appearance of one methylene signal in the aliphatic region, which suggests the replacement of the hydroxyl of **2** with a hydrogen proton in **5**. Similarly, the absence of oxygen leads to a high-field shift of carbon C-20 in the ^{13}C-NMR spectrum from Δ_C 70.1 p.p.m. (**2**) to Δ_C 37.2 p.p.m. (**5**), and minor signal shifts of aromatic ring carbons. 2D NMR experiments, including ^{1}H-^{1}H-COSY, HSQC and HMBC, confirmed the structure as shown in Figure 5.

The molecular formula determined for **3** ($C_{25}H_{28}O_3$) suggests the lack of a methyl group compared with that of **5**. Structural difference was located at carbon C-4, by the absence of the characteristic signals of the methoxy group in the ^{1}H-NMR spectrum Δ_H 3.78 p.p.m., (s, 3H)

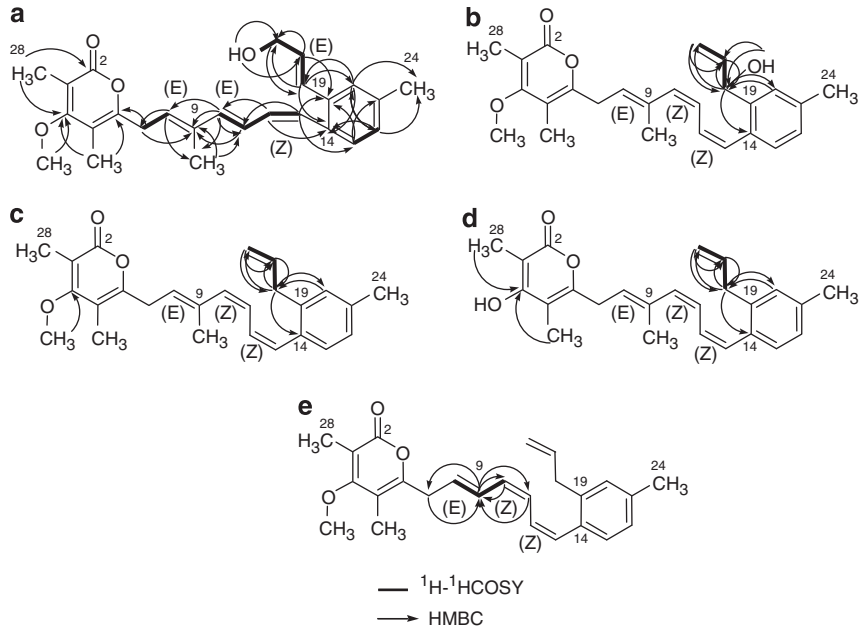

Figure 5 (a) 1H-1H COSY and HMBC correlations of BE 51068 (**1**); **(b)** selected 1H-1H COSY and HMBC correlations of gombapyrone A (**2**); **(c)** selected ^{1}H-^{1}H COSY and HMBC correlations of gombapyrone D (**5**); **(d)** selected 1H-1H COSY and HMBC correlations of gombapyrone B (**3**); **(e)** selected ^{1}H-^{1}H COSY and HMBC correlations of gombapyrone C (**4**).

and the ^{13}C-NMR spectrum Δ_C 60.4 p.p.m. The expected signal for the hydroxyl group proton in the ^{1}H-NMR spectrum of **3** was not detected. HSQC and HMBC spectra confirmed the structure of **3** (Figure 5).

Comparison of the molecular formulae of **4** ($C_{25}H_{28}O_3$) and **5** ($C_{26}H_{30}O_3$) suggested the lack of a methyl group in **4**. In the aliphatic region of the ^{1}H-NMR of **4,** three signals assigned to three methyl carbons are found, whereas the same region of the ^{1}H-NMR of **5** has three signals equivalent to four methyl carbons. In addition, the ^{1}H-NMR spectrum of **4** shows a new signal at Δ_H 6.21 p.p.m., (m, H). The ^{13}C-NMR and DEPT spectra of **4** revealed the presence of three methyl, one methoxy, three methylene, three aromatic, seven methine and eight quaternary carbons. Compared with **5**, signals for the methyl group (C-25) and the quaternary carbon (C-9) are replaced by an additional methine signal at Δ_C 132.8 p.p.m. The HSQC, ^{1}H-^{1}H COSY and HMBC spectra confirmed the structure of **4** (Figure 5).

The structural element unifying compounds **2–5** is the configuration of the double bonds at C-8/C-9, C-10/C-11 and C-12/C-13. The configuration has been determined as *Z* for the double bonds at C-10/C-11 and C-12/C-13, on the basis of the coupling constants for H-10/H-11 (J=7.4 Hz (**2**), 5.6 Hz (**3**), 9.7 Hz (**4**) and 5.8 Hz (**5**)), and for H-12/H-13 (J=11.2 Hz (**2–5**)), as shown in Table 2. In addition, the geometry of the C-8/C-9 double bonds of compounds **2**, **3** and **5** was assigned as *E* on the basis of the chemical shifts of a related system,[4] and the configuration of compound **4** was assigned as *E* on the basis of the coupling constant for H-8/H-9 (J=15.2 Hz). The NOESY spectrum of compound **2** showed correlations for H-20 to H-13 and H-18, H-11 showed correlations to H-15 and H-10 showed correlations to H_3-25. As a consequence, these correlations confirm the suggested configurations of the double bonds of compounds **2–5**.

Biological activity

Except for gombapyrone A (**2**), no growth inhibitory activities against Gram-negative and Gram-positive bacteria or against the yeast *Candida glabrata* could be detected. Compound **2** inhibited the growth of *Propionibacterium acnes* and *Staphylococcus lentus* slightly with IC_{50} values of 100 μM.

All of the tested compounds **1–5** inhibited glycogen synthase kinase 3β (GSK-3β) with an IC_{50} >100 μM (inhibition at 100 μM was 23% for **1**, 42% for **2**, 35% for **3**, 45% for **4** and 30% for **5**). GSK-3 is an important regulator of glycogen synthesis and acts as a signal-transduction element, regulating several intracellular processes such as Wnt signaling.[5] In addition, the β-isoform GSK-3β is supposed to be responsible for the hyperphosphorylation of the tau protein observed in pathogenesis of Alzheimer's disease.[6] Only **2** showed a weak activity also at 10 μM (27% inhibition).

Gombapyrones A (**2**), B (**3**) and D (**5**) also exhibited a weak inhibitory activity with IC_{50} > 100 μM against human recombinant protein tyrosine phosphatase 1B (PTPN1), which is a major negative regulator of insulin signaling, by regulating the phosphorylation state of the insulin receptor and possibly insulin receptor substrate.[7] Only **1** is more active compared with the others (57% inhibition at 100 μM and 23% inhibition at 50 μM), but **4** lacked activity against PTPN1. For comparison, inhibition at 100 μM was 22% for **3**, 31% for **3** and 39% for **5**.

DISCUSSION

Gombapyrones A–D (**2–5**) represent new members of secondary metabolites bearing an α-pyrone subunit as a characteristic structural feature. Although their biological activities are, in general, weak, some differences in their inhibitoring properties seemed remarkable. Antibiotic activities were found only in the case of gombapyrone A (**2**) and specifically against two species of bacteria. Inhibition of GSK-3β and PTPN1 was found for all gombapyrones at a high concentration level of 100 μM (except gombapyrone C, which was inactive against PTPN1). Compound BE 51068 (**1**) was significantly more active against PTPN1, and gombapyrone A (**2**) was more active against GSK-3β than were **1** and **3–5**. The minor congener **1** produced by

Table 4 ^{1}H and ^{13}C-NMR spectral data of BE 51068 (1) and gombapyrones A–D (2–5) in DMSO-d_6 and $CDCl_3$

	1 in DMSO-d_6		*2 in DMSO-d_6*		*3 in $CDCl_3$*				*5 in DMSO-d_6*	
No.	*δ (^{1}H) (p.p.m.) J in Hz*	*δ (^{13}C) (p.p.m.)*	*δ (^{1}H) (p.p.m.) J in Hz*	*δ (^{13}C) (p.p.m.)*	*δ (^{1}H) (p.p.m.) J in Hz*	*δ (^{13}C) (p.p.m.)*		*4 in DMSO-d_6*	*δ (^{1}H) (p.p.m.) J in Hz*	*δ (^{13}C) (p.p.m.)*
2	—	165.1 C	—	164.6 C	—	165.7 C	—	164.6 C	—	164.6 C
3	—	108.3 C	—	108.3 C	—	98.6 C	—	108.4 C	—	108.3 C
4	—	168.4 C	—	167.9 C	—	164.4 C	—	167.8 C	—	167.9 C
5	—	108.9 C	—	108.9 C	—	106.6 C	—	109.4 C	—	108.9 C
6	—	156.5 C	—	156.5 C	—	157.3 C	—	156.8 C	—	156.5 C
7	3.41 d (7.4)	30.0 CH_2	3.41 d (7.4)	30.0 CH_2	3.35 d (7.4)	30.8 C	3.33 d (6.5)	33.77 CH_2	3.4 d (7.4)	30.3 CH_2
8	5.60 t (7.3)	126.1 CH	5.60 t (7.3)	126.7 CH	5.54 t (7.3)	125.7 CH	5.77 dt (15.2, 6.8)	128.6 CH	5.6 t (7.3)	126.7 CH
9	—	135.3 C	—	135.9 C	—	136.8 C	6.21 m	132.8 CH	—	135.9 C
10	6.44 d (14.6)	138.7 CH	6.44 d (7.4)	138.6 CH	6.45 d (5.6)	138.5 CH	6.41 d (9.7)	134.3 CH	6.45 d (5.8)	138.7 CH
11	6.43 m	123.7 CH	6.45 d (2.4)	123.7 CH	6.46 d (4.8)	124.8 CH	6.40 d (4.7)	128.2 CH	6.46 d (4.3)	123.7 CH
12	6.36 m	130.4 CH	6.33 m	130.3 CH	6.33 m	130.7 CH	6.30 m	129.9 CH	6.33 m	130.4 CH
13	6.52 d (11.2)	128.3 CH	6.58 d (11.2)	127.9 CH	6.49 d (11.2)	128.9 CH	6.5 d (11.2)	128.7 CH	6.50 d (11.2)	128.2 CH
14	—	132.1 C	—	131.6 C	—	133.7 C	—	132.9 C	—	132.9 CH
15	7.13 d (7.7)	129.7 CH	7.11 d (7.8)	129.3 CH	7.17 d (7.8)	130.0 CH	7.10 d (7.8)	129.6 CH	7.15 d (7.8)	129.4 CH
16	7.06 d (7.7)	128.3 CH	7.07 d (7.8)	127.2 CH	7.01 d (7.8)	126.9 CH	7.04 d (7.8)	126.7 CH	7.06 d (7.8)	126.8 CH
17	—	136.7 C	—	136.5 C	—	137.4 C	—	136.7 CH	—	136.7 C
18	7.36 s	126.8 CH	7.27 s	126.9 CH	6.99 s	130.3 CH	7.02 s	130.0 CH	7.02 s	130.2 CH
19	—	135.9 C	—	141.8 C	—	138.2 C	—	136.6 C	—	137.6 C
20	6.65 d (15.8)	129.7 CH	5.19 t (4.9)	70.1 CH_2	3.32 d (6.6)	37.9 CH_2	3.29 d (6.5)	37.1 CH_2	3.30 d (6.5)	37.2 CH_2
21	6.26 dt (15.8, 5.0)	132.3 CH	5.87 m	140.9 CH	5.90 m	137.0 CH	5.87 m	136.8 CH	5.88 m	136.9 CH
22	4.09 t (5.3)	61.6 CH_2	4.99, 5.15 dd (10.3, 17.1)	113.3 CH_2	4.96, 5.00 d, d (17.1, 10.2)	115.9 CH_2	4.95, 4.99 d, d (17.1, 10.2)	115.7 CH_2	4.96, 5.00 d, d (17.1, 10.2)	115.8 CH_2
23	4.85 t (5.4) OH	—	5.42 d (4.3) OH	—	—	—	—	—	—	—
24	2.31 s	20.8 CH_3	2.30 s	20.9 CH_3	2.31 s	21.4 CH_3	2.28 s	20.8 CH_3	2.28 s	20.8 CH_3
25	1.72 s	12.4 CH_3	1.72 s	12.4 CH_3	1.75 s	12.9 CH_3	—	—	1.73 s	12.4 CH_3
26	1.89 s	9.7 CH_3	1.90 s	9.7 CH_3	1.94 s	8.6 CH_3	1.88 s	9.6 CH_3	1.90 s	9.7 CH_3
27	3.78 s	60.4 OCH_3	3.78 s	60.3 OCH_3	—	—	3.78 s	60.3 CH_3	3.78 s	60.4 OCH_3
28	1.89 s	9.9 CH_3	1.90 s	9.9 CH_3	1.96 s	9.8 CH_3	1.89 s	10.0 CH_3	1.90 s	10.0 CH_3

S. griseoruber Acta 3662 was found to be identical with the antitumor compound BE 51068 produced by a *Streptomyces* strain, which showed growth inhibition of various tumor cell lines.[3]

α-Pyrone metabolites are highly abundant in bacteria, fungi, plants and animals.[8] They exhibit a wide range of biological activities, such as antifungal, cytotoxic, neurotoxic and phytotoxic properties, and treatment of Alzheimer's disease and high cholesterol is discussed.[8,9,10] Furthermore, 4-hydroxy-2-pyrones have become one of the most important classes of anti-human immunodeficiency virus (HIV) agents in recent years.[8] These non-peptide compounds seem to be promising candidates for the treatment of AIDS. In comparison with peptides, small α-pyrones are interesting lead candidates for synthetic strategies because of their lack of chiral centers.[8,11]

Recently, we described albidopyrone, a new α-pyrone metabolite substituted in position 6 with a phenyl group, produced by a marine-derived *Streptomyces* strain. Albidopyrone showed an inhibitory activity against protein-tyrosine phosphatase B1, similar to gombapyrones.[12] Diemenensins A and B, two polypropionate antibiotics isolated from marine pulmonate *Siphonaria diemenensis,* were reported to have antimicrobial activity against *S. aureus* and *Bacillus subtilis*.[13] Furthermore, 11 α-pyrones, tentatively named TT-1–11, have been isolated from the imperfect fungus *Trichurus terrophilus*, from which compounds TT-1–4 exhibited considerably high immunosuppressive activities.[14] The α-pyrone derivative, 6-[(E)-hept-1-enyl]-α-pyrone, isolated from a marine *Botrytis* species, exhibited a tyrosinase inhibitory activity with an IC_{50} value of 4.5 μM, which is more active than kojic acid showing an IC_{50} value of 15.5 μM, which is currently being used as a preservative in cosmetics and food.[15] However, the most structurally related compounds are probably lehualides, which are isolated from a marine sponge of the genus *Plakortis*.[16] Lehualide A is an α-pyrone with a carbon side chain resembling that of gombapyrones. Lehualides B, C and D, which also bear carbon side chains, are, however, γ-pyrones. Lehualides exhibited a broad range of biological activities; for example, lehualide A showed a mild brine shrimp toxicity (LD_{50} 50 μg ml^{-1}). A further structurally highly related α-pyrone metabolite from a *Streptomyces* strain is represented by antibiotic CRP-2504-1 from which antibacterial properties are reported.[17] The new α-pyrone compounds gombapyrones A–D (**2–5**) extend the structural diversity of this group of natural products exhibiting enzyme-inhibitoring activities.

METHODS

Producing organism and taxonomy

Strain Acta 3662 was isolated from a rhizospheric soil sample collected from a bamboo patch at the University of Malaya Field Station in Gombak, Selangor. The sample was air-dried for 3 days before dry heat treatment at 60 °C for 40 min. The heat-treated samples were then serially diluted in 0.9% (w/v) NaCl, and 0.1 ml of the 10^{-3} sample was plated on the surface of starch–casein agar incorporated with cycloheximide and nystatin at 50 μg ml^{-1} each and 20 μg ml^{-1} of nalidixic acid to suppress fungal and heterotrophic bacterial growth. The inoculated plates were incubated at 27 °C and observed periodically, and putative actinomycete colonies were transferred to an ISP 4 agar medium.

Cultural characteristics were determined by the methods of Shirling and Gottlieb[18] and Takashi *et al.*[19] The strain was lawned on various media such as yeast extract–malt extract agar (ISP 2), oatmeal agar (ISP 3), inorganic salts–starch agar (ISP 4), glycerol–asparagine agar (ISP 5), peptone–yeast extract–iron agar (ISP 6) and tyrosine agar (ISP 7) and incubated at 28 °C for 14–21 days. Color grouping was carried out by observing the aerial mycelium, substrate mycelium and pigmentation. The color was compared under fluorescent light and categorized on the basis of the DULUX color chart, which was used as a standard color chart.

Coverslip culture was observed for aerial and substrate mycelia and spore morphology by light and scanning electron microscope (Philips SEM 15; FEI, Singapore). Spores and spore chains on 14-day-old coverslip culture were exposed to 2% osmium tetroxide vapor for about 2 h. The coverslips were then mounted onto aluminum stubs, sputter-coated with gold and examined by s.e.m.

The hydrolysates of whole cells of strain Acta 3662 grown on ISP 2 medium were analyzed for diaminopimelic acid type.[20]

Carbohydrate utilization was studied by lawning the strain on ISP 2 medium (without the carbon source) and incorporated with 1% (w/v) concentrations of a range of carbon sources.[18] The effect of temperature on growth was determined by streaking strain Acta 3662 on its optimum growth medium and incubating for 7 days at temperatures 15, 25, 35 and 45 °C. Tolerance against sodium chloride concentrations was determined in the same manner as for temperature studies by lawning the strain on ISP agar. Strain Acta 3662 grown on peptone–yeast extract–iron agar (ISP 6) and tyrosine agar (ISP 7) and incubated at 28 °C for 14 days was observed for melanoid formation after 7 and 14 days. Acta 3662 was grown on ISP 4 and examined for starch hydrolysis after 7 days of incubation at 28 °C. Hydrolysis of 12% (w/v) gelatin and determination of the color of the soluble pigment produced were carried out for up to 21 days of incubation. Cultures lawned on peptone–iron agar supplemented with 0.1% yeast extract were observed for hydrogen sulfide production after 6 and 18 h of incubation.

Genomic DNA extraction and polymerase chain reaction-mediated amplification of the 16S rDNA gene were carried out as described previously.[21] The 16S rDNA gene sequence of the strain was aligned against 16S rRNA gene sequences of representatives of *Streptomyces* spp. by Basic Local Alignment Search Tool analysis.

Fermentation and isolation

Batch fermentations of strain Acta 3662 were carried out in a 10-l stirred tank fermentor (Biostat S; B. Braun, Melsungen, Germany) in a complex medium that consisted of (per liter deionized water) glucose 10 g, starch soluble 20 g, yeast extract (Ohly Kat; Deutsche Hefewerke, Hamburg, Germany) 5 g, casein peptone (Fermtech; E. Merck, Darmstadt, Germany) 5 g and $CaCO_3$ 1 g; pH was adjusted to 7.6 (5 M HCl) before sterilization. The fermentor was inoculated with 5% by volume of a shake flask culture grown in a seed medium at 27 °C in 500 ml-Erlenmeyer flasks with a single baffle for 48 h on a rotary shaker at 120 r.p.m. The seed medium consisted of glucose 10 g, glycerol 10 g, oatmeal (Neuform, Zarrentin, Germany) 5 g, soybean meal (Schoenenberger, Magstadt, Germany) 10 g, yeast extract 5 g, Bacto Casamino acids 5 g and $CaCO_3$ 1 g in 1 l tap water. Fermentation was carried out for 5 days with an aeration rate of 0.5 volume air per volume per minute and agitation at 250 r.p.m.

Hyphlo Super-cel (2%) was added to the fermentation broth and separated by multiple sheet filtration into culture filtrate and mycelium. Mycelium was extracted three times, each time with 2 l MeOH–Me_2CO (1:1). The mycelium extracts were concentrated *in vacuo* to an aqueous residue (500 ml) that was re-extracted three times each with 350 ml cyclohexane and concentrated *in vacuo* to dryness. The crude extract was dissolved in CH_2Cl_2 and applied to a silica gel column (40×2.6 cm, silica gel SI 60; E. Merck). Separation was accomplished by a linear gradient from CH_2Cl_2 to CH_2Cl_2–MeOH (9:1) within 4 h at a flow rate of 5 ml min^{-1}. Fractions containing gombapyrones (**1–5**) were separated on a Sephadex LH-20 column (75×4 cm; Amersham, Freiburg, Germany) using MeOH as eluent. To obtain pure compounds **1–5,** each fraction was subjected to preparative RP-HPLC using a C-18 column (Grom-Sil 300 ODS-5 ST, 10 μm, 250×20 mm; Alltech Grom, Rottenburg, Germany) with CH_3CN–0.1% HCOOH (gradient from 65 to 75% CH_3CN over 45 min, increased to 100% CH_3CN at 50 min) at a flow rate of 15 ml min^{-1}.

HPLC-diode array analyses

The chromatographic system consisted of an HP 1090M liquid chromatograph equipped with a diode-array detector and an HP Kayak XM 600 ChemStation (Agilent, Waldbronn, Germany). Multiple wavelength monitoring was performed at 210, 230, 260, 280, 310, 360, 435 and 500 nm, and UV-Vis spectra were measured from 200 to 600 nm. A 10-ml aliquot of the fermentation broth

was centrifuged, and the supernatant was adjusted to pH 5 and extracted with the same volume of EtOAc. After centrifugation, the organic layer was concentrated to dryness *in vacuo* and resuspended in 1 ml MeOH. Aliquots of 10 µl of samples were injected onto an HPLC column (125×4.6 mm) fitted with a guard column (20×4.6 mm) filled with 5-µm Nucleosil-100 C-18 (Maisch, Ammerbuch, Germany). The samples were analyzed by linear gradient elution using 0.1% *ortho*-phosphoric acid as solvent A and CH_3CN as solvent B at a flow rate of 2 ml min^{-1}. The gradient was from 0 to 100% for solvent B in 15 min with a 2-min hold at 100% for solvent B.

Structure elucidation

LC-MS experiments were performed on a QTrap 2000 (Applied Biosystems, Darmstadt, Germany) coupled to an Agilent 1100 HPLC system (Agilent). High-resolution ESI-FT-ICR mass spectra were recorded on an APEX II FTICR mass spectrometer (4.7 T, Bruker-Daltonics, Bremen, Germany) and NMR experiments were performed on a DRX 500 NMR spectrometer (Bruker, Karlsruhe, Germany) equipped with a broadband inverse detection probe head with z gradients. DMSO-d_6 and $CDCl_3$ were used as solvents for NMR experiments and chemical shifts were referenced to tetramethyl silane.

Biological activity

Antimicrobial assays were performed using *B. subtilis* (DSM 347), *S. epidermidis* (DSM 20044), *S. lentus* (DSM 6672), *Erwinia amylovora* (DSM 50901), *Escherichia coli* K12 (DSM 498), *Pseudomonas fluorescens* (NCIMB 10586), *P. acnes* (DSM 1897), *P. aeruginosa* (DSM 50071), *P. syringae* pv. aptata (DSM 50252), *Ralstonia solanacearum* (DSM 9544), *Xanthomonas campestris* (DSM 2405) and yeast *C. glabrata* (DSM 6425). The assays were prepared by transferring 50 µl of a 2 mM methanolic solution of the sample compounds into one well of a 96-well microtiter plate, evaporating the solvent in a vacuum centrifuge. Overnight cultures of the test organisms in tryptic soy broth were diluted to an OD_{600} of 0.02–0.06, and 200 µl of the resulting suspension was added to the wells. After incubating the microtiter plates for 15 h at 28 °C, 10 µl of a resazurin solution (0.2 mg ml^{-1} phosphate-buffered saline) was added to each well and the plate was incubated at 28 °C for 30 min. For evaluation of cell viability, the transformation of resazurin was assessed by measuring the intensity of fluorescence at $560_{Ex}/590_{Em}$ nm.[22] The resulting values were compared with a positive (50 mg chloramphenicol for bacteria; 50 mg nystatin for yeast) and a negative control (no compound) on the same plate. *P. acnes* were grown anaerobically (Anaerocult A mini, E. Merck) in PYG medium (modified DSMZ-medium 104) at 37 °C for 24–48 h. The bacterial culture was diluted to an OD_{600} of 0.03, 200 µl of the inoculum was added to each well and the microtiter plate was incubated anaerobically at 37 °C for 48 h.

To discover specific enzyme inhibitory activities, isolated compounds were screened in several enzyme activity tests including prominent drug targets such as GSK-3β, PTPN1, phosphodiesterase 4 (PDE4), HIV-1 reverse transcriptase (HIV-1-RT) and acetylcholinesterase (AchE). Analysis of the effect on human recombinant PTPN1 was carried out with final concentrations of the substance of 10–100 µM in PTP1B assay buffer containing 100 mM Hepes buffer (pH 7.2), 2 mM EDTA, 2 mM DTT, 0.1% nonylphenylpolyethylene glycol (NP-40), 5 ng bovine serum albumin and 3 ng (150 µU) recombinant human PTP1B (Cat. no. SE332-0050, Biomol, Hamburg, Germany) in a volume of 45 µl per well. The reaction was started with 5 µl of the 1.5 mM PTP1B phosphopeptide substrate EGFR (988–998) (Cat. no. P323-0001, Biomol) dissolved in PTP1B assay buffer. After an incubation period of 15 min at 30 °C, the reaction was stopped by adding 100 µl of Biomol green (Cat. no. AK111-9090, Biomol); the ortho-phosphate concentration was quantified after incubating for 20 min at room temperature. Optimal density was measured at 620 nm using the microtiter plate reader Infinite M200 (Tecan, Crailsheim, Germany). As a positive control for inhibition of PTP1B, 50 µM of RK-682 (Cat. no. 557322–200UG, Calbiochem, Darmstadt, Germany) was added instead of the test substance.

Enzyme assays to determine GSK-3β activity were carried out as described by Baki *et al*.[23] Measurement of AchE activity was adapted from the colorimetric assay described by Ellman *et al*.[24] for a microplate test system. Reverse transcriptase activity was assayed using a colorimetric reverse transcriptase enzyme-linked immunosorbent assay kit (Cat. no. 11468120910, Roche, Mannheim, Germany) according to the manufacturer's instructions. Activity of PDE4 was measured by using the PDELight HTS cAMP phosphodiesterase kit (Cat. no. LT07-600, Lonza, Wuppertal, Germany) according to the manufacturer's instructions.

ACKNOWLEDGEMENTS

Financial support from the European Commission (project ACTAPHARM, 5th framework, QLK3-CT-2001-01783, and project ACTINOGEN, 6th framework, LSHM-CT-2004-005224) and from Bayer Schering Pharma AG (Berlin, Germany) is gratefully acknowledged.

1 Schneider, K. *et al*. Lipocarbazoles, new secondary metabolites from *Tsukamurella pseudospumae* Acta 1857 with antioxidative activity. *J. Nat. Prod.* submitted (2009).
2 Fiedler, H.-P. Biosynthetic capacities of actinomycetes. 1. Screening for novel secondary metabolites by HPLC and UV-visible absorbance libraries. *Nat. Prod. Lett.* **2,** 119–128 (1993).
3 Yamauchi, T., Nakashima, S., Hirayama, M., Ojiri, K. & Suda, K. Antitumor pyrone derivative BE 51068, its microbial manufacture, *Streptomyces spp.* therefore, and antitumor agents. *Jpn. Kokai Tokkyo Koho* (1998) 7 pp. JP 10101663, A 19980421 Heisei, AN 1998:236772.
4 Hengartner, U., Bernhard, K., Meyer, K., Englert, G. & Glinz, E. Synthesis, isolation, and NMR-spectroscopic characterization of fourteen (Z)-isomers of lycopene and of some acetylenic didehydro- and tetradehydrolycopenes. *Helv. Chim. Acta.* **75,** 1848–1865 (1992).
5 Forde, J. E. & Dale, T. C. Glycogen synthase kinase 3: a key regulator of cellular fate. *Cell. Mol. Life Sci*. **64,** 1930–1944 (2007).
6 Mattson, M. P. Neuronal death and GSK-3beta: a tau fetish? *Trends Neurosci.* **24,** 255–256 (2001).
7 Zhang, S. & Zhang, Z.-Y. PTP1B as a drug target: recent developments in PTP1B inhibitor discovery. *Drug Discov. Today* **12,** 373–381 (2007).
8 McGlacken, G. & Fairlamb, I. J. S. 2-Pyrone natural products and mimetics: isolation, characterisation and biological activity. *Nat. Prod. Rep.* **22,** 369–385 (2005).
9 Fairlamb, I. J., Marrison, L. R., Dickinson, J. M., Lu, F. J. & Schmidt, J. P. 2-Pyrones possessing promising antimicrobial and cytotoxic activities. *Bioorg. Med. Chem.* **12,** 4285–4299 (2004).
10 Katritzky, A. R., Wang, Z., Wang, M., Hall, C. D. & Suzuki, K. Facile syntheses of 2,2-dimethyl-6-(2-oxoalkyl)-1,3-dioxin-4-ones and the corresponding 6-substituted 4-hydroxy-2-pyrones. *J. Org. Chem.* **70,** 4854–4856 (2005).
11 Tummino, P. J., Ferguson, D., Huper, L. & Hupe, D. Competitive inhibition of HIV-1 protease by 4-hydroxy-benzopyran-2-ones and by 4-hydroxy-6-phenylpyran-2-ones. *Biochem. Biophys. Res. Commun.* **200,** 1658–1664 (1994).
12 Hohmann, C. *et al*. Albidopyrone, a new α-pyrone-containing metabolite from marine-derived *Streptomyces* sp. NTK 227. *J. Antibiot.* **62,** 75–79 (2009).
13 Hochlowski, J. E. & Faulkner, D. J. Antibiotics from the marine pulmonate *Siphonaria Diemenensis*. *Tetetrahedron Lett.* **24,** 1917–1920 (1983).
14 Fujimoto, H. *et al*. Eleven new 2-pyrones from a fungi imperfecti, *Trichurus terrophilus*, found in a screening study guided by immunomodulatory activity. *Chem. Pharm. Bull.* **53,** 923–929 (2005).
15 Zhang, D., Li, X., Kang, S. J., Choi, H. D. & Son, B. W. A new α-pyrone derivative, 6-[(E)-hept-1-enyl]-α-pyrone, with tyrosinase inhibitory activity from a marine isolate of the fungus *Botrytis*. *Bull. Korean Chem. Soc.* **28,** 887–888 (2007).
16 Sata, N. *et al*. Lehualides A-D, metabolites from a Hawaiian sponge of the genus *Plakortis,*. *J. Nat. Prod.* **68,** 1400–1403 (2005).
17 Doi, S. *et al*. Antibiotic CRP-2504-1 manufacture with *Streptomyces*. *Jpn. Kokai Tokkyo Koho* (1998) 8 pp. JP 10287666, A 19981027 Heisei, AN1998:696722.
18 Shirling, E. B. & Gottlieb, D. Methods for charcaterisation of *Streptomyces* species. *Int. J. Syst. Bacteriol.* **16,** 313–340 (1966).
19 Takashi, S. *et al*. Pladienolides, new substances from culture of *Streptomyces platensis* Mer-11107. *J. Antibiot.* **57,** 173–179 (2004).
20 Lechevalier, M. P. & Lechevalier, H. The chemotaxonomy of actinomycetes In *Actinomycetes Taxonomy* Vol. 6 (eds Dietz A. &Thayer D.W.) 227–291 (Society for Industrial Microbiology, 1980).
21 Rainey, F. A., Rainey, N. W., Kroppenstedt, R. M. & Stackebrandt, E. The genus *Nocardiopsis* represents a phylogenetically coherent taxon and a distinct actinomycetes lineage: proposal of *Nocardiopsaceae* fam.nov. *Int. J. Syst. Bacteriol*. **46,** 1088–1092 (1996).
22 Collins, L. A. & Franzblau, S. G. Microplate alamar blue assay versus BACTEC 460 system for high-throughput screening of compounds against *Mycobacterium tuberculosis* and *Mycobacterium avium*. *Antimicrob. Agents Chemother.* **41,** 1004–1009 (1997).
23 Baki, A., Bielik, A., Molnár, L., Szendrei, G. & Keserü, G. M. A high throughput luminescent assay for glycogen synthase kinase-3b inhibitors. *Assay Drug Develop. Technol.* **5,** 75–83 (2007).
24 Ellman, G. L., Courtney, K. D., Andres, Jr. V. & Featherstone, R. M. A new and rapid colorimetric determination of acetylcholesterinesterase activity. *Biochem. Pharmacol.* **7,** 88–90 (1961).

The Journal of Antibiotics (2009) 62, 453–460

www.nature.com/ja

ORIGINAL ARTICLE

Nitro derivatives from the Arctic ice bacterium *Salegentibacter* sp. isolate T436*

Imelda Schuhmann[1], Clarisse B Fotso-Fondja Yao[1], Wael Al-Zereini[2], Heidrun Anke[2], Elisabeth Helmke[3] and Hartmut Laatsch[1]

Twenty-five aromatic nitro, dinitro and trinitro compounds were isolated in low yields of less than 1 mg l^{-1} from a *Salegentibacter* sp. strain T436 derived from Arctic pack ice. Their structures were elucidated by MS and NMR techniques. Seven of these compounds, namely, 2-hydroxy-3-(4′-hydroxy-3′-nitrophenyl)-propionic acid methyl ester (6), 2-chloro-3-(4′-hydroxy-3′-nitrophenyl)propionic acid methyl ester (7), 3-(4′-hydroxy-3′,5′-dinitrophenyl)-propionic acid methyl ester (14), 4′-hydroxy-3′,5′-dinitrophenylethylchloride (16), (4′-hydroxy-3′,5′-dinitrophenyl)-2-chloropropionic acid methyl ester (17), *N*-acetyl-3′,5′-dinitrotyramine (18) and 2,6-dinitro-4-(2′-nitroethenyl)phenol (19) are new, and five are reported in this study from a natural source for the first time.
The Journal of Antibiotics (2009) **62,** 453–460; doi:10.1038/ja.2009.71; published online 31 July 2009

Keywords: aromatic nitro compounds; marine bacteria; *Salegentibacter*

INTRODUCTION

During our investigation of secondary metabolites produced by microorganisms in Arctic and Antarctic habitats, we isolated from Arctic pack ice a psychrotolerant, Gram-negative bacterium T436, which was assigned to a distinct group within the genus *Salegentibacter* on the basis of 16S rRNA gene profile and physiological characteristics.[1] Our interest in this strain was attracted by an antimicrobial activity of crude extracts against *Bacillus brevis*, *B. subtilis*, *Nematospora coryli* and *Micrococcus luteus*, as well as by an intensively yellow color.[1] On TLC, numerous yellow zones were visible over the whole polarity range, which were not because of quinones, xanthones, phenazines, polyenes or other common chromophores. On spraying with tin(II) chloride solution, the yellow spots were reduced to colorless or faintly yellow products, which gave intensively yellow or orange Schiff bases on treatment with 4-dimethylaminobenzaldehyde, as an indication of aromatic nitro compounds. This interpretation was confirmed by two IR signals in the range of ν 1510–1570 and 1320–1350 cm^{-1}, and by typical fragments in the EI mass spectra (see Supplementary Figure 1). Nitro compounds are widespread in microorganisms, but are rather rare in nature. Recent examples are nitrobenzyl alcohols from an endophytic mangrove fungus,[2] or nitroresorcinols from myxobacteria.[3]

On TLC, the mononitrophenols isolated in this study absorbed UV light at 254 nm and showed an absorption maximum at $\lambda_{max} \sim 350$ nm in solution (see Supplementary Figure 2). In contrast, the dinitrophenols emitted a yellow UV fluorescence on TLC at 366 nm, and showed a long-wavelength absorption at $\lambda_{max} \sim 430$ nm. A further specialty in the spectroscopic characterization of nitro compounds was with regard to the ^{13}C NMR signals of the quaternary carbon atoms carrying the nitro group, which were only visible at long relaxation delays (1 s).

So far, 25 nitro, dinitro and trinitrophenols were isolated from this strain.[4–6] Compounds **2–6**, **8**, **10**, **11–17**, **23** and **24** were already mentioned in our previous report.[1] In this study, we describe their chemical properties in detail and report additional metabolites obtained on re-fermentation.

RESULTS AND DISCUSSION

Mononitrophenols

For the isolation of further nitro derivatives, a 20 l fermentation conducted under the same conditions as described before[1] was extracted at weakly acidic pH; under basic conditions, the extraction was very ineffective. Chromatographic separation on silica gel, Sephadex LH-20 and by HPLC (Supplementary Figure 3) delivered 10 mononitrophenols. The de-replication of known

[1]Institute for Organic and Biomolecular Chemistry, Georg-August University Göttingen, Göttingen, Germany; [2]Institute for Biotechnology and Drug Research, Kaiserslautern, Germany and [3]Alfred-Wegener Institute for Polar and Marine Research, Bremerhaven, Germany
Correspondence: Professor H Laatsch, Department of Organic Chemistry, Georg-August University, Tammannstrasse 2, Göttingen D-37077, Germany.
E-mail: hlaatsc@gwdg.de
*Art. no. XXXIX on Marine Bacteria. Art. XXXVIII. Ling D, Pfoh R, Rühl S, Qin S, Laatsch H. T-Muurolol Sesquiterpenes from Marine *Streptomyces* sp. Qd491 and Revision of the Configuration of Previously Reported Amorphanes. *J Nat Prod* **72**: 99–101 (2009).
Received 30 June 2009; revised 4 July 2009; accepted 5 July 2009; published online 31 July 2009

compounds was performed by MS and HRMS, and by comparison with AntiBase data;[7] new compounds were elucidated by additional 2D NMR measurements. *p*-Nitrophenol (**1**),[8] isolated previously from carrot truffle (*Stephanaspora caroticolor*), was easily identified in this manner. It is a widespread environmental contaminant.

A group of nine compounds, **2–10,** showed the characteristic ^{1}H NMR signal pattern of 1,2,4-trisubstituted benzene derivatives. The downfield shift of aromatic ^{1}H NMR signals, the pH-dependent yellow color and the IR data pointed to a group of 4-substituted *o*-nitrophenols with differences in a side chain at C-4. Compounds **1**, **7** and **9** have not been described in our previous report on *Salegentibacter* sp. T436.[1]

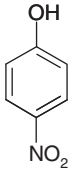

1

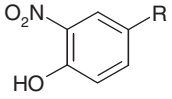

2: R = COOH
3 R = CH_2COOH
4: R = CH_2COOCH_3
5: R = CH_2CH_2COOH
6: R = $CH_2CH(OH)COOMe$
7: R = $CH_2CHClCOOMe$
8: R = CH_2CH_2OH
9: R = CH_2CH_2NHAc
10: R = $CH=CHNO_2$

Beside the signals for a 1,2,4-trisubstituted aromatic ring, the ^{1}H NMR spectrum of **6** revealed an oxymethine multiplet at δ 4.38, a methoxy group at δ 3.70, as well as the AB part of an ABX system at δ 3.10 and 2.98. (−)-APCI mass spectra gave an $[M\text{-}H]^-$ ion at *m/z* 240. 2D NMR data revealed the structure of 2-hydroxy-3-(4′-hydroxy-3′-nitrophenyl)propionic acid methyl ester (**6**). The NMR data of 2-chloro-3-(4′-hydroxy-3′-nitrophenyl)-propionic acid methyl ester (**7**) were very similar, but were downfield shifted. Both compounds are reported in this study for the first time. *N*-Acetyl-3′-nitrotyramine (**9**, 0.4 mg l^{-1}) was new in *Salegentibacter* sp. T436, but had been isolated previously from *Pyricularia oryzae*,[9] the causative agent of pyriculariosis, a widespread disease of rice.

Dinitro and trinitro derivatives

Seven simple dinitro compounds **11–17** had already been isolated previously from *Salegentibacter* T436.[1] Two further compounds **18** and **19** have been added now; all are new from natural sources but some had been obtained by synthesis. Their UV maxima (λ_{max} 432 nm) showed a strong bathochromic shift in alkaline solution similar to mononitro-phenols; however, ^{1}H NMR data indicated clearly symmetrically tetrasubstituted benzene derivatives by 2H singlets as the only aromatic signal; the structural differences were again localized in the side chain.

Their structures were derived from 2D NMR measurements and HR mass spectra as 4′-hydroxy-3′,5′-dinitrophenylacetic acid methyl ester (**12**, 0.02 mg l^{-1}), 4′-hydroxy-3′,5′-dinitrophenylacetic acid (**11**),[10] 4′-hydroxy-3′,5′-dinitrophenylpropionic acid (**13**, 0.05 mg l^{-1}), 4′-hydroxy-3′,5′-dinitrophenylpropionic acid methyl ester (**14**)[11] and dinitro-tyrosol (**15**).[12]

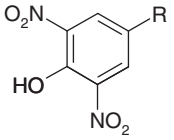

11: R = CH_2COOH
12: R = CH_2COOCH_3
13: R = CH_2CH_2COOH
14: R = CH_2CH_2COOMe
15: R = CH_2CH_2OH
16: R = CH_2CH_2Cl
17: R = $CH_2CHClCOOCH_3$
18: R = $CH_2CH_2NHCOCH_3$
19: R = $CH=CHNO_2$

The ^{1}H NMR spectrum of compound **16** (0.03 mg l^{-1}) was similar to that of **13**, although the methylene triplets were at different shifts. The ESI mass spectrum showed molecular ions at *m/z* 246/248 (EIMS) in the ratio of *ca.* 3:1, typical for chlorine. The IR spectrum gave no hints for carboxy or ester groups. From these data and from the empirical formula (by HRMS), the structure of 4′-hydroxy-3′,5′-dinitrophenylethyl chloride (**16**) was derived, which was finally confirmed by heteronuclear multibond correlation (HMBC) data (Supplementary Figure 4). Compound **16** is a new natural product and is also unknown from synthesis.

Compound **17** was obtained in the low yield of 0.04 mg l^{-1}. Its ^{1}H NMR spectrum showed signals of a methine group at δ 4.56, a methoxy group at δ 3.73 and signals of diastereotopic methylene protons at δ 3.18 and 3.06. In the APCI mass spectrum, an $[M\text{–}H]^-$ ion at *m/z* 303 indicated chlorine by its isotope pattern. The IR spectrum showed a strong absorption at 701 cm^{-1}, which is characteristic of a C-Cl bond. These data were in agreement with the structure of 4′-hydroxy-3′,5′-dinitrophenyl-2-chloropropionic acid methyl ester (**17**), and HRESIMS confirmed the respective formula, $C_{10}H_9ClN_2O_7$. Compound **17** had not been described before, but the mononitro derivative has been synthesized.[13]

The ^{1}H NMR spectrum of **18** (0.14 mg l^{-1}) resembled that of **16** in the aromatic region, whereas the aliphatic signals corresponded with those of **9**; moreover, the IR spectrum was very similar to that of **9**. The ESI mass spectrum showed an $[M\text{–}H]^-$ ion at *m/z* 268. It follows that **18** is the new *N*-acetyl-3′,5′-dinitrotyramine. The structure was further confirmed by HMBC correlations (see Supplementary Figure 5).

The ESI mass spectrum of **19** indicated an odd number of nitrogen atoms by a pseudomolecular ion at *m/z* 254 $[M\text{–}H]^-$; HRMS delivered the formula $C_8H_5N_3O_7$. In the ^{1}H NMR spectrum, two 1H doublets of a *trans*-configured double bond appeared at a similar shift as in **10**, which resulted in 2,6-dinitro-4-(2′-nitroethenyl)phenol (**19**); the latter is the first natural trinitro derivative.

Simple dinitro-phenols

A further separation by HPLC yielded two isomeric methoxy-dinitrophenols with the formula $C_7H_6N_2O_6$ (APCI HRMS). Both compounds showed two doublets of *meta*-coupled protons with strong HMBC correlations to the phenolic carbon, but only one proton in both isomers coupled with the carbon connected with the methoxy group). Therefore, in one isomer, the OH group has to be positioned at 1,3-distance with respect to both protons as in **20**, and at 1,2-distance in the other phenol as in **21**. Placing the methoxy group in *para* position to the OH group would result in two symmetrical dinitro compounds and can be excluded: one phenol must therefore be 2-methoxy-4,6-dinitrophenol (**20**) and the other is 3-methoxy-4,5-dinitrophenol (**21**). A direct comparison with synthetic materials[14,15] identified the slightly more polar isomer as **20**. Both assignments were further confirmed by HMBC data. The NMR data of 2-methoxy-3,5-dinitrophenol and 2-methoxy-4,5-dinitrophenol are additionally listed

in the experimental part. It is worth mentioning that the aromatic proton signals of **20** varied up to $\Delta\delta$ 0.2 ($\Delta\delta$ 4 for ^{13}C), depending on the concentration and purity of the sample and the solvent.

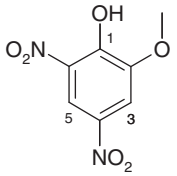

20

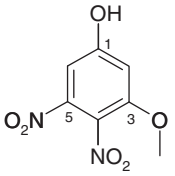

21

4,6-Dinitroguaiacol (**20**)[16] and isomeric 3,5-dinitroguaiacol[17] are known as metabolites of the red alga *Marginisporum aberrans*; they showed antimicrobial activity against *B. subtilis*. The dinitroresorcinol ether **21** had not been described before.

Additional fermentation products

The isoflavones daidzein and genistein are common by-products in the fermentation of bacteria, if soybean flour or malt extract was used for cultivation. Surprisingly, these compounds were found now in the nitrated form as 3′-nitro-daidzein (**22**, 0.06 mg l^{-1}; see Supplementary Figure 6), 3′-nitrogenistein (**23**) and 3′,5′-dinitro-genistein (**24**, see Supplementary Figure 7). All three compounds had been isolated previously from the genetically engineered *Streptomyces* sp. K_3.[18,19] They showed no significant antimicrobial or phytotoxic activities. In addition, the nitro-diketopiperazine pyriculamide (**25**, 0.3 mg l^{-1}) was found.[7]

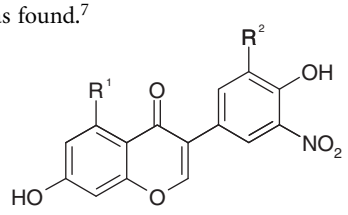

22: $R^1 = R^2 = H$
23: $R^1 = OH, R^2 = H$
24: $R^1 = OH, R^2 = NO_2$

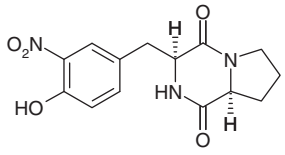

25

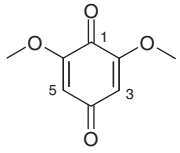

26

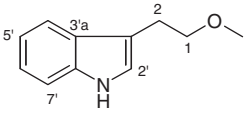

27

A yellow compound with a mass of *m/z* 168 was identified as 2,6-dimethoxy-1,4-benzoquinone (**26**) and was confirmed by literature data. It is known as a plant metabolite with antitumor activity.[20] Metabolite **27** was identified as tryptophol methyl ether, which was known only from synthesis.[21] Its spectroscopical data were in accordance with literature. Further polar UV absorbing fractions contained thymine, uracil and *p*-hydroxybenzoic acid.

ESI fragmentation of aromatic nitro compounds

The MS analysis of nitro compounds was performed best in the negative ESI mode. Under EI conditions, phenolic mononitrocarboxylic acids showed a loss of carbon dioxide and of a 30 Da fragment, a phenomenon that had already been observed in the early 1980s in CIMS experiments[22–25] (see Supplementary Figure 1). This fragmentation may be explained by the reduction of the aromatic nitro group into an amino function in the source during measurement. A better explanation, however, is based on an NO elimination, which was already known from EI experiments.[26] This assumption is further supported by the fact that in the full-scan spectra, no $[M\text{-}H\text{-}30]^-$ ions were detected, whereas these signals appeared after the fragmentation process. In several cases, a signal at $[M\text{-}47\text{-}H]^-$ was observed, which indicates the loss of an HNO_2 molecule.

The dinitro derivatives investigated in this study showed similar fragmentation patterns as those of mononitro compounds. If the nitrophenols contained further leaving groups, such as chlorine atoms, these were eliminated first (in this study as HCl); thereafter, the elimination of NO occurred.

In the positive ESI mode, only those nitro compounds were detectable, which carried a functional group which can be easily protonated, as in **9** or **18**. In these cases, usually an elimination of a 46 Da fragment was observed, which was most likely NO_2.

Biosynthetic considerations

For the biosynthesis of natural nitro groups, at least three different pathways are known: the oxidation of anilines, the direct nitration of phenols with reactive nitrogen species (RNS) and the oxidation of nitroso precursors.

By means of feeding experiments, it was shown that *p*-aminophenylalanine is the precursor of the *p*-nitrophenylserinol part in chloramphenicol,[27,28] as well as of the nitrophenyl unit of aureothin.[29] In the last step of pyrrolnitrin biosynthesis, an amino function is converted into a nitro group by a chloroperoxidase.[30,31] For most of the nitro compounds described in this study, potential amino precursors are, however, not known, and therefore this pathway seems less plausible.

An alternative biosynthetic route to nitro compounds is the oxidation of nitroso precursors,[32] which themselves could be formed with nitrite, NO^+ or $NO^\bullet$ radicals under physiological conditions. Several nitroso compounds related to the nitro compounds isolated in this study were described, for example, 4′-hydroxy-3′-nitrosobenzoic acid from *Streptomyces murayamaensis*.[33] Nitroso compounds such as viridomycin E[34] and others[7] are strong siderophores and are involved in the accumulation of iron, which is a limiting factor for phytoplankton growth in offshore surface waters of the Antarctic[35,36] and northeast Subarctic Pacific Ocean.[37] A search by HPLC/MS in the crude extract of *Salegentibacter* sp. T436 for nitroso compounds corresponding to the nitro derivatives isolated in this study was, however, not successful.

Fermentation under various conditions has shown that nitrate is a precondition for the production of these nitro compounds. As in the brine channel system of the Arctic bottom sea ice increased nitrate concentrations occur,[38] it can be assumed that another pathway is used: the direct nitration by RNS such as peroxynitrite and NO_2, formed as secondary products of NO metabolism in the presence of oxidants including superoxide, hydrogen peroxide and transition metal centres. 3′-Nitrotyrosine formed in such a process has been

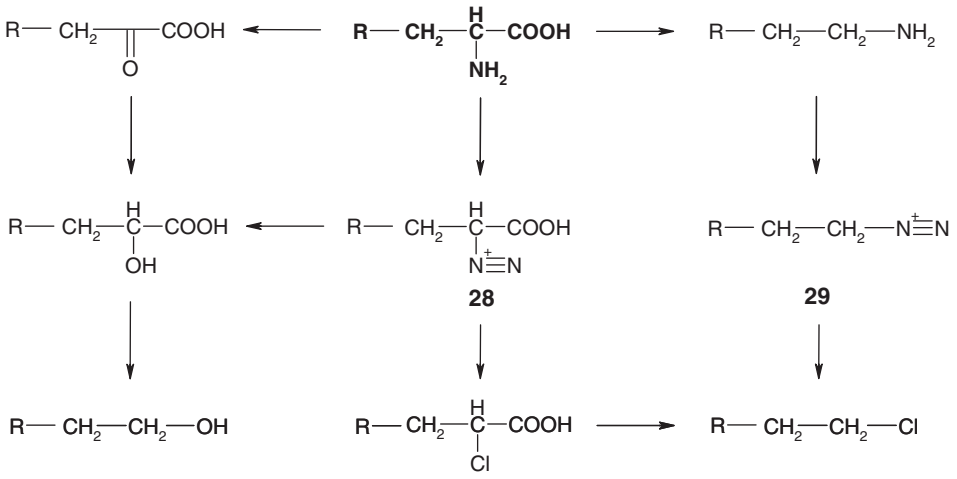

Figure 1 Sidechain transformations in nitrotyrosines by postulated diazonium intermediates **28**/**29**, R = 4′-hydroxy-3′-nitrophenyl and 4′-hydroxy-3′,5′-dinitrophenyl, respectively.

discussed as a biomarker of NO-dependent oxidative stress;[39,40] 3′-nitrogenistein is formed under the influence of peroxynitrite,[41] and in the case of dioxapyrrolomycin, such a nitration by RNS was proven on the basis of isotope labeling with an $^{15}N/^{18}O$-enriched nitrate.[42,43]

It seems that tyrosine is the parent compound for most of the nitro aromates described here. Starting with tyrosine, first a mono- and dinitration by RNS occur in the benzene ring. The following formation of nitrated phenylpropionic acids (for example, **5**), tyramines, *N*-acetyltyramines (such as **9**), phenyllactic acids and tyrosols (**8**) is easily explained by reduction, oxidative deamination, decarboxylation and acetylation, and a combination thereof. A similar mechanism has been found for the enzymatic degradation of stephanosporin.[8]

Even the chloro derivatives **16** and **17**, as well as the respective hydroxy derivatives **6** and **8**/**15**, may be produced in this way: It has been shown that diazonium ions can be formed under physiological conditions by the reaction of amines with RNS,[44] and more than 30 stable diazonium salts have been reported as natural products.[7,45] The formation of chloro derivatives may be explained by intermediates **28**/**29**, which could react with water or with chloride in the sense of a Sandmeyer reaction (Figure 1). Furthermore, the formation of **27** could be explained by the reaction of tryptamine through the respective diazonium ion with methanol. Further investigations with isotope labeling to confirm these assumptions are, however, presently not realistic because of the very low yield.

EXPERIMENTAL SECTION

Materials and methods

Nuclear magnetic resonance spectra were measured on Varian Unity 300 (300.145 MHz) and Varian Inova 600 (599.740 MHz) spectrometers with tetramethylsilane as internal standard (Varian Dentschland GmbH, Darmstadt, Germany). ESI mass spectra were recorded on a Quattro Triple Quadrupole Mass Spectrometer, Finnegan TSQ 7000 (Thermo Scientific, Dreieich, Germany) with nano-ESI-API-ion source. ESI-HRMS was measured on a 7 Tesla-Fourier Transform Ion Cyclotron Resonance (FTICR) mass spectrometer (APEX IV, Bruker Daltonik GmbH, Bremen, Germany). IR spectra were recorded on a Perkin-Elmer 1600 Series FT-IR spectrometer as KBr pellets. UV-VIS spectra were recorded on a Perkin-Elmer Lambda 15 UV/vis spectrometer (Wallthem, MA, USA). Flash chromatography was carried out on silica gel (230–400 mesh). TLC and determination of R_f values were performed on Polygram SIL G/UV_{254} (Macherey-Nagel & Co., Düren, Germany). Size exclusion chromatography was carried out on Sephadex LH-20 (Lipophilic Sephadex, Amersham Bioscience Ltd; purchased from Sigma-Aldrich Chemie, Steinheim, Germany).

HPLC Two Jasco Intelligent Prep. pumps PU-987 (Jasco, Easton, MD, USA) with high-pressure mixer, Vertex 4×250 mm column with 4×4 mm pre-column, Merck Lichrosorb RP C18 7 µm (Merck, Darmstadt, Germany); and preparative separations on Eurochrom Europrep RP 60–10 C18 60 Å 7–12 µm (Knauer, Berlin, Germany) aceotrope (83.7% acetonitrile 16.3% water, b.p. 78.5 °C) were used.

Taxonomy, fermentation and isolation

Details on the producing strain and its cultivation in Erlenmeyer flasks and in a 20-1 fermenter have been published previously.[1]

Isolation and characterization of metabolites

The crude extract from a 20 l batch fermentation was separated on silica gel with a stepwise CH_2Cl_2/MeOH gradient as described before;[1] the fractions obtained were further separated by chromatography on Sephadex LH-20 (CH_2Cl_2/MeOH 2:1 und MeOH). Subsequent flash chromatography on silica gel (CH_2Cl_2/MeOH) afforded 0.4 mg *p*-nitrophenol (**1**), 1.8 mg 4′-hydroxy-3′-nitrobenzoic acid (**2**), 3.0 mg 4′-hydroxy-3′-nitrophenylacetic acid (**3**), 1.7 mg 4′-hydroxy-3′-nitrophenylpropionic acid (**5**), 1.7 mg 4′-hydroxy-3′-nitrophenylacetic acid methyl ester (**4**), 2.6 mg 3′-nitrotyrosol (**8**), 7.1 mg *N*-acetyl-3′-nitrotyramine (**9**), 0.4 mg 2-nitro-4-(2′-nitroethenyl)phenol (**10**), 0.4 mg 4′-hydroxy-3′,5′-dinitrophenylacetic acid methyl ester (**12**), 1.1 mg 4′-hydroxy-3′,5′-dinitrophenylpropionic acid (**13**), 0.6 mg 4′-hydroxy-3′,5′-dinitrophenylethyl chloride (**16**), 0.7 mg 4′-hydroxy-3′,5′-dinitrophenyl-2-chloropropionic acid methyl ester (**17**), 2.7 mg *N*-(4′-hydroxy-3′,5′-dinitrophenylethyl)-acetamide (**18**), 0.4 mg 2,6-dinitro-4-(2′-nitroethenyl)phenol (**19**), 6.1 mg pyriculamide (**25**), 1.1 mg 3′-nitro-daidzein (**22**), 3.9 mg 3′,5′-dinitrogenistein (**24**), 1.2 mg 2-methoxy-4,6-dinitrophenol (**20**), 1.8 mg 3-methoxy-4,5-dinitrophenol (**21**), 2.1 mg 2,6-dimethoxy-1,4-benzoquinone (**26**), 1.1 mg 3′-indolylethyl-methylether (**27**), 4.7 mg thymine, 4.2 mg uracil and 2.2 mg *p*-hydroxybenzoic acid.

The crude extract (1.5 g) obtained from a second 20 l fermentation was separated on silica gel with ethyl acetate/hexane and then with Sephadex LH-20 (MeOH), followed by preparative HPLC (MeCN+0.001% H_3PO_4). The following compounds were obtained: 4′-hydroxy-3′-nitrophenyl-propionic acid (**5**, 1.2 mg), 2-hydroxy-3-(4′-hydroxy-3′-nitrophenyl)propionic acid methyl ester (**6**, 2 mg), 2-chloro-3-(4′-hydroxy-3′-nitrophenyl)propionic acid methyl ester (**7**, 2.1 mg), 4′-hydroxy-3′,5′-dinitrophenylacetic acid (**11**, 2.0 mg), 3-(4′-hydroxy-3′,5′-dinitrophenyl)propionic acid methyl ester (**14**, 0.7 mg), dinitrotyrosol (**15**, 2.7 mg), and 3′-mononitrogenistein (**23**, 1.4 mg). The retention

time of an individual compound corresponds to the elution profile, shown in Supplementary Figure 3.

4′-Hydroxy-3′-nitrobenzoic acid (2)

Yellow solid, UV absorbing (254 nm), R_F 0.25 (CH_2Cl_2/MeOH 9:1), R_t 11.9 min (LC-MS). UV/vis (MeOH) λ_{max} (lg ε) 237 (4.38), 340 (3.51) nm. IR (KBr) ν_{max} 3307, 2924, 2853, 1685, 1626, 1574, 1541, 1433, 1338, 1312, 1257, 1175, 1112, 923, 854, 827, 762, 704, 639, 532 cm^{-1}. ^1H NMR (CD_3OD, 600 MHz) δ 8.66 (d, ^4J 1.8 Hz, 1H, 2-H), 8.15 (dd, ^4J 1.8 Hz, ^3J 8.4 Hz, 1H, 6-H), 7.13 (d, ^3J 8.4 Hz, 1H, 5′-H). ^{13}C NMR (CD_3OD, 150 MHz) δ 169.8 (COOH), 158.0 (C_q-4), 137.9 (CH-6), 135.5 (C_q-3), 127.8 (CH-2), 126.9 (C_q-1), 120.8 (CH-5). EI-MS (70 eV) *m/z* (%) 183 ([M]$^{\bullet+}$, 100), 167 (12), 166 (18), 153 (16), 119 (22), 81 (23), 63 (61), 53 (28). (−)-APCI MS *m/z* 182 [M–H]$^-$.

4′-Hydroxy-3′-nitrophenylacetic acid (3)

Yellow solid, UV absorbing (254 nm), R_F 0.39 (CH_2Cl_2/MeOH 9:1), R_t 11.3 min (LC-MS). UV/vis (MeOH) λ_{max} (lg ε) 274 (3.84), 354 (3.52) nm. IR (KBr) ν_{max} 3432, 2930, 1698, 1632, 1581, 1493, 1434, 1412, 1331, 1258, 1216, 1180, 1132, 1084, 922, 848, 764 cm^{-1}. ^1H NMR (CD_3OD, 300 MHz) δ 8.01 (d, ^4J 2.1 Hz, 1H, 2-H), 7.54 (dd, ^3J 8.5 Hz, ^4J 2.1 Hz, 1H, 6-H), 7.10 (d, ^3J 8.5 Hz, 1H, 5′-H), 3.63 (s, 2H, CH_2COO). EI MS (70 eV) *m/z* (%) 198 (38), 197 ([M]$^{\bullet+}$, 23), 152 (100), 106 (20), 77 (19), 51 (18).

4′-Hydroxy-3′-nitrophenylacetic acid methyl ester (4)

Yellow solid, UV absorbing (254 nm), R_F 0.76 (CH_2Cl_2/MeOH 9:1), R_t 13.6 min (LC-MS). UV/vis (MeOH) λ_{max} (lg ε) 273 (4.00), 354 (3.68) nm. IR (KBr) ν_{max} 3480, 3280, 1736, 1634, 1581, 1537, 1486, 1430, 1420, 1356, 1330, 1307, 1262, 1172, 1083, 1002, 918, 926 cm^{-1}. – ^1H NMR (CD_3OD, 300 MHz) δ 7.99 (d, ^4J 2.4 Hz, 1H, 2-H), 7.52 (dd, ^3J 8.7 Hz, ^4J 2.4 Hz, 1H, 6-H), 7.09 (d, ^3J 8.7 Hz, 1H, 5′-H), 3.69 (s, 3H, COOMe), 3.67 (s, 2H, CH_2). EI MS (70 eV) *m/z* (%) 211 ([M]$^{\bullet+}$, 16), 165 (11), 152 (100), 135 (12), 106 (44), 77 (36), 59 (23), 51 (35).

4′-Hydroxy-3′-nitrophenylpropionic acid (5)

Yellow solid, UV absorbing (254 nm), R_F 0.82 (CH_2Cl_2/MeOH 9:1), R_t 11.4 min (LC-MS). UV/vis (MeOH) λ_{max} (lg ε) 274 (3.65), 356 (3.31) nm. IR (KBr) ν_{max} 3404, 2922, 1714, 1630, 1581, 1539, 1483, 1430, 1404, 1327, 1244. 1180, 1081, 907, 850, 762, 661, 600 cm^{-1}. ^1H NMR ($CDCl_3$, 300 MHz) δ 10.46 (s, 1H, 4′-OH), 7.93 (d, ^4J 2.1 Hz, 1H, 2-H), 7.43 (dd, ^3J 8.4 Hz, ^4J 2.1 Hz, 1H, 6-H), 7.08 (d, ^3J 8.4 Hz, 1H, 5′-H), 2.93 (t, ^3J 7.0 Hz, 2H, CH_2CH_2COO), 2.67 (t, ^3J 7.0 Hz, 2H, CH_2CH_2COO); (MeOH-d_4, 600 MHz) δ 7.96 (d, *J* 2.1 Hz, 1H, 2-H), 7.52 (dd, *J* 8.4, 2.1 Hz, 1H, 6-H), 7.08 (d, *J* 8.4 Hz, 1H, 5′-H), 2.90 (t, *J* 7.0 Hz, 2H, CH_2CH_2COO), 2.59 (t, *J* 7.0 Hz, 2H, CH_2CH_2COO). EI MS (70 eV) *m/z* (%) 211 ([M]$^{\bullet+}$, 32), 193 (46), 175 (20), 152 (100), 151 (56), 147 (38), 106 (15).

2-Hydroxy-3-(4′-hydroxy-3′-nitrophenyl)-propionic acid methyl ester (6)

Yellow solid, R_F 0.59 (CH_2Cl_2/MeOH 9:1), R_t 9.14 min (LC-MS). UV/vis (MeOH) λ_{max} nm (lg ε) 274 (3.45), 354 (3.07). IR (KBr) ν_{max} 3433, 2925, 2853, 1740, 1630, 1538, 1489, 1431, 1384, 1329, 1253, 1181, 1098, 824, 765, 678 cm^{-1}. ^1H NMR (MeOH-d_4, 600 MHz) δ 7.96 (d, ^4J 2.1 Hz, 1H, 2-H), 7.50 (dd, ^3J 8.4 Hz, ^4J 2.1 Hz, 1H, 6-H), 7.08 (d, ^3J 8.4 Hz, 1H, 5′-H), 4.38 (ABX, 1H, 2-H), 3.70 (s, 3H, 1-OCH_3), 3.06, 2.94 (ABX, J_{AB} 13, J_{AX} 8.4, J_{BX} 4.2 Hz, 2H, 3-H_2); see Supplementary Figure 8. EI (70 eV) *m/z* (%) 241 ([M]$^{\bullet+}$, 8), 223 (24), 192 (3), 152 (100), 135 (11), 106 (20), 77 (21). (−)-APCI MS *m/z* 240 [M-H]$^-$. (−)-ESI-HRMS *m/z* 240.05147 ([M-H]$^-$, calcd. 240.05135 for $C_{10}H_{10}NO_6$).

2-Chloro-3-(4′-hydroxy-3′-nitrophenyl)propionic acid methyl ester (7)

Yellow solid, UV absorbing (254 nm), R_t 10.54 min (LC-MS). –UV/vis (MeOH) λ_{max} (lg ε) 270 (3.75), 348 (3.42) nm. IR (KBr) ν_{max} 3423, 2926, 1746, 1631, 1540, 1491, 1436, 1328, 1256, 1177, 824, 765 cm^{-1}. ^1H NMR (MeOH-d_4, 600 MHz) δ 7.96 (d, ^4J 2.1 Hz, 1H, 2-H), 7.50 (dd, ^3J 8.4 Hz, ^4J 2.1 Hz, 1H, 6-H), 7.08 (d, ^3J 8.4 Hz, 1H, 5′-H), 4.63 (t, 1H, ^3J 7 Hz, 2-H), 3.73 (s, 3H, 1-OCH_3), 3.75, 3.10 (2 m, 2H, 3-H_2). – EI (70 eV) *m/z* (%) 259, 261 ([M]$^{\bullet+}$, 6, 2), 223 (100), 192 (50), 152 (87), 106 (19), 77 (17). (−)-APCI MS *m/z* 258, 260 [M-H]$^-$. (−)-ESI-HRMS *m/z* 258.01767 ([M+-H]$^-$, calcd. 258.01747 for $C_{10}H_9ClNO_5$).

3′-Nitrotyrosol (8)

Yellow solid, UV absorbing (254 nm), R_F 0.59 (CH_2Cl_2/MeOH 9:1), R_t 13.2 min (LC-MS). UV/vis (MeOH) λ_{max} (lg ε) 275 (3.93), 358 (3.59) nm. IR (KBr) ν_{max} 3300, 2929, 2847, 1632, 1586, 1540, 1488, 1427, 1326, 1253, 1179, 1058, 1026, 904, 836, 764 cm^{-1}. ^1H NMR ($CDCl_3$, 300 MHz) δ 10.46 (s, 1H, 4′-OH), 7.96 (d, ^4J 2.2 Hz, 1H, 2-H), 7.46 (dd, ^3J 8.5 Hz, ^4J 2.2 Hz, 1H, 6-H), 7.08 (d, ^3J 8.5 Hz, 1H, 5′-H), 3.86 (t, ^3J 6.5 Hz, 2H, CH_2CH_2OH), 2.84 (t, ^3J 6.5 Hz, 2H, CH_2CH_2OH). EI MS (70 eV) *m/z* (%) 183 ([M]$^{\bullet+}$, 35), 152 (100), 135 (39), 106 (31), 77 (20), 51 (9).

N-Acetyl-3′-nitrotyramine (9)

Yellow solid, UV absorbing (254 nm), R_F 0.51 (CH_2Cl_2/MeOH 9:1), R_t 11.1 min (LC-MS). UV/vis (MeOH) λ_{max} (lg ε) 275 (3.86), 357 (3.56) nm. IR (KBr) ν_{max} 3400, 3290, 3079, 2934, 1634, 1558, 1532, 1489, 1424, 1321, 1291, 1257, 1171, 850, 766 cm^{-1}. ^1H NMR ($CDCl_3$, 300 MHz) δ 10.44 (s, H/D exchangeable, 1H, 4′-OH), 7.89 (d, ^4J 2.1 Hz, 1H, 2-H), 7.41 (dd, ^3J 8.4 Hz, ^4J 2.1 Hz, 1H, 5′-H), 7.08 (d, ^3J 8.4 Hz, 1H, 6-H), 5.72 (br s, H/D exchangeable, 1H, NH), 3.46 (q, ^3J 6.9 Hz, 2H, CH_2CH_2NH), 2.79 (t, ^3J 6.9 Hz, 2H, CH_2CH_2NH), 1.93 (s, 3H, Ac). EI MS (70 eV) *m/z* (%) 206 ([M]$^{\bullet+}$, 60), 165 (100), 135 (23), 105 (19), 77 (15), 72 (18), 60 (17), 43 (41).

2-Nitro-4-(2′-nitroethenyl)phenol (10)

Yellow solid, UV absorbing (254 nm), R_F 0.83 (CH_2Cl_2/MeOH 9:1), R_t 13.7 min (LC-MS). UV/vis (MeOH) λ_{max} (lg ε) 222 (4.20), 269 (4.04), 325 (4.20), 435 (sh) (3.54) nm. IR (KBr) ν_{max} 3436, 3110, 2927, 1640, 1624, 1537, 1513, 1504, 1489, 1342, 1275, 1174, 972, 836, 766 cm^{-1}. ^1H NMR (CD_3OD, 600 MHz) δ 8.36 (d, ^4J 2.4 Hz, 1H, 2-H), 8.04 (d, ^3J 13.5 Hz, 1H, $CHNO_2$), 7.86 (d, ^3J 13.5 Hz, 1H, $CHCHNO_2$), 7.85 (dd, ^4J 2.4 Hz, ^3J 8.7 Hz, 1H, 6-H), 7.09 (d, ^3J 8.7 Hz, 1H, 5′-H). ^{13}C NMR (CD_3OD, 150 MHz) δ 160.8 (C_q-4), 145.8 (C_q-3), 138.4 ($CHCHNO_2$), 138.0 ($CHCHNO_2$), 136.5 (CH-6), 129.0 (CH-2), 122.5 (CH-5), 121.8 (C_q-1); see Supplementary Figure 9. EI MS (70 eV) *m/z* (%) 210 ([M]$^{\bullet+}$, 24), 163 (100), 118 (38), 89 (70), 63 (58).

4′-Hydroxy-3′,5′-dinitrophenylacetic acid (11)

Yellow solid, R_F 0.55 (CH_2Cl_2/MeOH 9:1), R_t 12.8 min (LC-MS). UV/vis (MeOH/HCl) λ_{max} (lg ε) 338, (3.97), 350 (3.65) nm. IR (KBr) ν_{max} 3433, 1696, 1641, 1580, 1544, 1431, 1401, 1352, 1305, 1261, 1155, 910, 729, 609 cm^{-1}. ^1H NMR (MeOH-d_4, 600 MHz) δ 8.22 (s, 2H, 2′,6′-H), 3.72 (s, 2H, 2-CH_2). EI-MS (70 eV) *m/z* (%) 242 ([M]$^{\bullet+}$, 65), 197 (100), 151 (20), 105 (16), 76 (16). (−)-APCI *m/z* 241 [M-H]$^-$. (−)-ESI HRMS *m/z* 241.01027 ([M-H]$^-$, calcd. 241.00997 for $C_8H_5N_2O_7$).

4′-Hydroxy-3′,5′-dinitrophenylacetic acid methyl ester (12)

Yellow solid, UV absorbing (254 nm), R_F 0.36 (CH_2Cl_2/MeOH 9:1), R_t 12.8 min (LC-MS). UV/vis (MeOH) λ_{max} (lg ε) 228 (4.33), 432 (3.85) nm. IR (KBr) ν_{max} 3437, 2925, 1738, 1631, 1553, 1439, 1406, 1384, 1338, 1265, 1238, 1198, 1177, 1116, 900, 784 cm^{-1}. ^1H NMR (CD_3OD, 600 MHz) δ 7.96 (s, 2H, 2,6-H), 3.70 (s, 3H, $COOCH_3$), 3.60 (s, 2H, CH_2COO). ^{13}C NMR (CD_3OD, 150 MHz) δ 173.7 (COO), 159.4 (C_q-4), 143.9 (C_q-3,5), 132.4 (CH-1), 114.6 (CH-2,6), 52.6 (CH_2COO), 39.6 ($COOCH_3$). EI MS (70 eV) *m/z* (%) 256 ([M]$^{\bullet+}$, 14), 226 (13), 197 (12), 59 (16), 44 (100). EI HRMS *m/z* 256.03330 ([M]$^{\bullet+}$, calcd. 256.03315 for $C_9H_8N_2O_7$); (+)-ESI-HRMS *m/z* 279.02252 ([M+Na]$^+$, calcd. 279.02238 for $C_9H_8N_2O_7Na$).

4′-Hydroxy-3′,5′-dinitrophenylpropionic acid (13)

Yellow solid, UV absorbing (254 nm), R_f 0.16 (CH_2Cl_2/MeOH 9:1), R_t 11.9 min (LC-MS). UV/vis (MeOH) λ_{max} (lg ε) 356 (3.16), 436 (3.39) nm. IR (KBr) ν_{max} 3412, 1712, 1638, 1542, 1428, 1343, 1262 cm^{-1}. ^1H NMR (CD_3OD, 600 MHz) δ 8.04 (s, 2H, 2,6-H), 2.89 (t, ^3J 7.0 Hz, 2H, CH_2CH_2COO), 2.62 (t, ^3J 7.0 Hz, 2H, CH_2CH_2COO). ^{13}C NMR (CD_3OD, 150 MHz) δ 176.2 (COOH), 152.7 (C_q-4), 141.7 (C_q-3,5), 131.4 (CH-2,6), 128.4 (C_q-1), 36.1 (CH_2CH_2COO), 30.3

(CH_2CH_2COO). (−)-ESI MS *m/z* (%) 533 [2M-2H+Na]$^-$ (29), 255 [M-H]$^-$ (100). EI-HRMS *m/z* 256.03320 ([M]$^{\bullet+}$, calcd. 256.03261 for $C_9H_8N_2O_7$).

3-(4′-Hydroxy-3′,5′-dinitrophenyl)-propionic acid methyl ester (14)

Yellow solid, R_F 0.62 (CH_2Cl_2/MeOH 9:1). EI MS (70 eV) *m/z* (%) 270 ([M]$^{\bullet+}$, 20), 260 (45), 210 (100), 187 (10), 180 (10). (−)-ESI HRMS *m/z* 269.04160 ([M-H]$^-$, calcd. 269.04097 for $C_{10}H_9N_2O_7$).

Dinitrotyrosol (15)

Yellow solid, R_F 0.55 (CH_2Cl_2/MeOH 9:1). R_t 10.34 min (LC-MS). UV/vis (MeOH/HCl) λ_{max} (lg ε) 248 sh (3.80), 351 (3.51) nm. IR (KBr) ν_{max} 3395, 2945, 2834, 1639, 1545, 1384, 1029, 618 cm^{-1}. ^{1}H NMR (CD_3OD, 600 MHz) δ 8.14 (s, 2H, 2′,6′-H), 3.78 (t, 2H, ^3J 6.8 Hz, 2-H$_2$), 2.82 (t, ^3J 6.8 Hz, 2H, 2-H$_2$). EI MS (70 eV) *m/z* (%) 228 ([M]$^{\bullet+}$, 32), 197 (28), 180 (100), 151 (28), 105 (12). (−)-APCI MS *m/z* 227 [M-H]$^-$. (−)-ESI HRMS *m/z* 227.03102 ([M-H]$^-$, calcd. 227.03095 for $C_8H_7N_2O_6$).

4′-Hydroxy-3′,5′-dinitrophenylethylchloride (16)

Yellow solid, UV absorbing (254 nm), R_F 0.44 (CH_2Cl_2/MeOH 9:1), R_t 15.6 min (LC-MS). UV/vis (MeOH) λ_{max} (lg ε) 231 (4.16), 435 (3.68) nm; λ_{max} 350 nm in acidic solution. IR (KBr) ν_{max} 3407, 2926, 1719, 1638, 1543, 1459, 1338, 1246, 1111, 10455, 914, 783 cm^{-1}. ^{1}H NMR (CD_3OD, 600 MHz) δ 7.86 (s, 2H, 2,6-H), 3.70 (t, ^3J 7.2 Hz, 2H, CH_2CH_2Cl), 2.93 (t, ^3J 7.2 Hz, 2H, CH_2CH_2Cl). ^{13}C NMR (CD_3OD, 150 MHz) δ 159.6 (C_q-4), 144.2 (C_q-3,5), 132.2 (CH-2,6), 119.1 (C_q-1), 46.0 (CH_2CH_2Cl), 38.2 (CH_2CH_2Cl). EI MS (70 eV) *m/z* (%) 246 ([M]$^{\bullet+}$, 16), 197 (100), 151 (16), 91 (98). EI HRMS *m/z* 246.00430 ([M]$^{\bullet+}$, calcd. 246.00381 for $C_8H_7N_2O_5Cl$).

(4′-Hydroxy-3′,5′-dinitrophenyl)-2-chloropropionic acid methyl ester (17)

Orange solid, UV absorbing (254 nm), R_F 0.41 (CH_2Cl_2/MeOH 9:1), R_t 17.0 min (LC-MS). UV/vis (MeOH) λ_{max} (lg ε) 348 (2.89) nm. IR (KBr) ν_{max} 3427, 2925, 2854, 1740, 1621, 1545, 1399, 1258, 1098, 701 cm^{-1}. ^{1}H NMR (CD_3OD, 600 MHz) δ 7.82 (s, 2H, 2′,6′-H), 4.58 (t, 1H, ^3J 8.9 Hz, 2-H), 3.73 (s, 3H, 1-OCH$_3$), 3.18, 3.06 (ABX, ^2J 15.1 Hz, J_{AX}, J_{BX} 8.9 Hz, 3-H$_2$). (−)-APCI MS *m/z* 303 [M-H]$^-$. (−)-ESI-HRMS *m/z* 303.00254 ([M-H]$^-$, calcd. 303.00254 for $C_{10}H_8ClN_2O_7$).

N-Acetyl-3′,5′-dinitrotyramine (18)

Yellow solid, UV absorbing (254 nm), R_F 0.19 (CH_2Cl_2/MeOH 9:1), R_t 10.3 min (LC-MS). UV/vis (MeOH) λ_{max} (lg ε) 225 (3.80), 443 (3.21) nm. IR (KBr) ν_{max} 3421, 2928, 1637, 1543, 1460, 1384, 1362, 1338, 1310, 1253, 1205, 1027, 1002, 910, 785 cm^{-1}. – ^{1}H NMR (DMSO-d_6, 300 MHz) δ 7.82 (t br, 1H, NH), 7.64 (s, 2H, 2,6-H), 3.17 (m, 2H, CH_2CH_2NH), 2.48 (m, 2H, CH_2CH_2NH), 1.77 (s, 3H, Ac). ^{13}C NMR (DMSO-d_6, 150 MHz) δ 169.0 (CH_3CO), 158.5 (C_q-4), 142.6 (C_q-3,5), 130.7 (CH-2,6), 114.4 (C_q-1), 40.0 (CH_2CH_2NH), 33.2 (CH_2CH_2NH), 22.5 (CH_3CO). (−)-ESI-MS *m/z* (%) 537 [2M-H]$^-$ (45), 268 [M-H]$^-$ (100). EI HRMS *m/z* 269.06480 ([M], calcd. 269.06425 for $C_{10}H_{11}N_3O_6$); (+)-ESI HRMS *m/z* 270.07206 ([M+H]$^+$, calcd. 270.07206 for $C_{10}H_{12}N_3O_6$).

2,6-Dinitro-4-(2′-nitroethenyl)phenol (19)

Orange solid, UV absorbing (254 nm), R_F 0.53 (CH_2Cl_2/MeOH 9:1). ^{1}H NMR (CD_3OD, 600 MHz) δ 8.24 (s, 2H, 3-H, 5′-H), 7.99 (d, ^3J 13.5 Hz, 1H, 2′-H), 7.76 (d, ^3J 13.5 Hz, 1H, 1′-H). (−)-ESI MS *m/z* 531 [2M-2H+Na]$^-$, 254 [M-H]$^-$; (−)-ESI HRMS *m/z* 254.00545 ([M-H]$^-$, calcd. 254.00546 for $C_8H_4N_3O_7$).

2-Methoxy-4,6-dinitrophenol (20)

Orange solid, UV absorbing (254 nm), R_F 0.50 (CH_2Cl_2/MeOH 9:1), R_t 14.1 min (LC-MS). UV/vis (MeOH) λ_{max} (lg ε) 268 (3.78), 377 (3.89), 420 sh (3.75) nm. IR (KBr) ν_{max} 3440, 1608, 1554, 1493, 1385, 1345, 1235, 1094, 1049, 798, 785, 735, 711 cm^{-1}. ^{1}H NMR (CD_3OD, 300 MHz) δ 8.51 (d, ^4J 2.7 Hz, 1H, 5-H), 7.75 (d, ^4J 2.7 Hz, 1H, 3-H), 3.94 (s, 3H, 2-OCH$_3$). ^{13}C NMR (CD_3OD, 150 MHz) δ 157.8 (C_q-1), 153.7 (C_q-2), 135.5 (C_q-6), 134.2 (C_q-4), 116.4 (CH-5), 108.3 (CH-3), 57.1 (2-OCH$_3$). EI MS (70 eV) *m/z* (%) 214 ([M]$^{\bullet+}$, 100), 197 (70), 166 (22), 121 (28), 53 (29), 50 (33).

Compound **20** by synthesis according to Ehrlich and Bogert[14]: ^{1}H NMR (CD_3OD, 300 MHz) δ 8.42 (d, ^4J 2.8 Hz, 1H, 5-H), 7.97 (d, ^4J 2.8 Hz, 1H, 3-H), 4.03 (s, 3H, 2-OCH$_3$); (acetone-d_6) δ 8.53 (d, ^4J 2.8 Hz, 1H, 5-H), 7.73 (d, ^4J 2.8 Hz, 1H, 3-H), 4.02 (s, 3H, 2-OCH$_3$); ^{13}C NMR (CD_3OD, 75 MHz) δ 151.4 (C_q-1), 150.3 (C_q-2), 139.9 (C_q-6), 136.4 (C_q-4), 114.0 (CH-5), 110.4 (CH-3), 57.7 (2-OCH$_3$); ($CDCl_3$) δ 150.8 (C_q-1), 150.5 (C_q-2), 139.2 (C_q-6), 132.4 (C_q-4), 112.6 (CH-5), 111.0 (CH-3), 57.0 (2-OCH$_3$); (acetone-d_6) δ 157.4 (C_q-1), 153.0 (C_q-2), 139.2 (C_q-6), 132.4 (C_q-4), 112.6 (CH-5), 111.0 (CH-3), 57.3 (2-OCH$_3$).

3-Methoxy-4,5-dinitrophenol (21)

Orange solid, UV absorbing (254 nm), R_F 0.51 (CH_2Cl_2/MeOH 9:1), R_t 14.1 min (LC-MS). UV/vis (MeOH) λ_{max} (lg ε) 213 (4.22), 266 (3.92), 342 (3.68) nm. IR (KBr) ν_{max} 3391, 3109, 2946, 2835, 1778, 1607, 1556, 1449, 1344, 1261, 1092, 1027, 946, 918, 804, 711 cm^{-1}. ^{1}H NMR (CD_3OD, 600 MHz) δ 8.59 (d, ^4J 2.4 Hz, 1H, 6-H), 7.55 (d, ^4J 2.4 Hz, 1H, 2-H), 3.87 (s, 3H, 3-OCH$_3$). ^{13}C NMR (CD_3OD, 150 MHz) δ 164.6 (C_q-1), 155.6 (C_q-3), 135.2 (C_q-5), 132.2 (C_q-4), 118.3 (CH-6), 106.7 (CH-2), 57.0 (3-OCH3). (−)-APCI MS *m/z* 213 [M-H]$^-$. (−)-ESI HRMS *m/z* 213.01535 ([M-H]$^-$, calcd. 213.01529 for $C_7H_5N_2O_6$).

2-Methoxy-3,5-dinitrophenol

Nitration of guaiacol acetate (2 g) according to Hynning *et al.*[15] resulted in a mixture of 3- and 5-nitroguaiacol acetate of similar polarity. After drying, the orange resin was dissolved at 0 °C in 5 ml fuming nitric acid and the product precipitated after 5 min by the addition of water. The dinitro acetate was hydrolyzed by dissolving in 2N NaOH. After 5 min at room temperature, the orange-red solution was acidified with diluted HCl and extracted with ether. Some polar impurities were separated by filtration over silica gel (column 4×10 cm, CH_2Cl_2). ^{1}H NMR (CD_3OD, 300 MHz) δ 8.08 (d, ^4J 2.7 Hz, 1H, 4-H), 7.88 (d, ^4J 2.7 Hz, 1H, 6-H), 4.02 (s, 3H, 2-OCH$_3$). ^{13}C NMR (CD_3OD, 75 MHz) δ 153.7 (C_q-1), 147.6 (C_q-2), 145.2 (C_q-3), 143.7 (C_q-5), 115.3 (CH-6), 111.3 (CH-4), 62.4 (2-OCH$_3$); assignment on the basis of 2D spectra.

2-Methoxy-4,5-dinitrophenol

2-Methoxy-4,5-dinitrophenol was obtained by nitration of veratrole and ether cleavage, according to Ehrlich and Bogert[14]. –^{1}H NMR (CD_3OD, 300 MHz) δ 7.80 (s, 2H, 3, 6-H), 6.96 (s, 3H, 2-OCH$_3$). –^{13}C NMR (CD_3OD, 125 MHz) δ 152.8 (C_q-1), 149.3 (C_q-2), 141.9 (C_q-5), 132.9 (C_q-4), 107.7 (CH-3,6), 57.6 (2-OCH$_3$).

3′-Nitro-daidzein (22)

Yellow solid, UV absorbing 254 nm). R_F 0.59 (CH_2Cl_2/MeOH 9:1). R_t 16.0 min (LC-MS). UV/vis (MeOH) λ_{max} (lg ε) 243 (3.99), 300 (sh, 3.67), 359 (3.22) nm. IR (KBr) ν_{max} 3429, 3281, 1620, 1588, 1578, 1537, 1426, 1385, 1310, 1266, 1240, 1179, 1101, 864, 766 cm^{-1}. ^{1}H NMR (DMSO-d_6, 300 MHz) δ 10.90 (s br, 1H, OH), 8.45 (s, 1H, 2-H), 8.15 (d, ^4J 2.1 Hz, 1H, 2′-H), 7.97 (d, ^3J 8.8 Hz, 1H, 5′-H), 7.71 (dd, ^3J 8.8 Hz, ^4J 2.1 Hz, 1H, 6′-H), 7.12 (d, ^3J 8.8 Hz, 1H, 5′-H), 6.94 (dd, ^3J 8.8 Hz, ^4J 2.1 Hz, 1H, 6-H), 6.88 (d, ^4J 2.1 Hz, 1H, 8-H). ^{13}C NMR (DMSO-d_6, 150 MHz) δ 174.3 (C_q-4), 162.8 (C_q-7), 157.4 (C_q-8a), 153.7 (CH-2), 153.0 (C_q-4′), 136.5 (C_q-3′), 135.3 (CH-6′), 127.2 (CH-5), 125.2 (CH-2′), 122.0 (C_q-1′), 121.4 (C_q-3), 119.6 (CH-5′), 116.4 (C_q-4a), 115.3 (CH-6), 102.1 (CH-8). (+)-ESI MS *m/z* (%) 621 [2M+Na]$^+$ (78), 300 [M+H]$^+$ (18). (−)-ESI MS *m/z* (%) 597 [2M-H]$^-$ (40), 298 [M-H]$^-$ (100). DCI MS (NH_3) *m/z* (%) 456 [2M+NH$_4$]$^+$ (14), 237 [M+NH$_4$]$^+$ (100). (+)-ESI HRMS *m/z* 300.05020 ([M+H]$^+$, calcd. 300.05027 for $C_{15}H_{10}NO_6$).

3′-Nitrogenistein (23)

Yellow solid, R_F 0.55 (CH_2Cl_2/MeOH 9:1), R_t 12.49 min (LC-MS). UV/vis (MeOH) λ_{max} (lg ε) 265 nm. IR (KBr) ν_{max} 3432, 2963, 2926, 1628, 1537, 1382, 1261, 1092, 1030, 803 cm^{-1}. ^{1}H NMR (MeOH-d_4, 600 MHz) δ 8.20 (s, 1H, 2-H), 8.15 (d, *J* 2.1 Hz, 1H, 6′-H), 7.60 (dd, *J* 8.8, 1.9 Hz, 1H, 2′-H), 7.01 (d, *J* 8.8 Hz, 1H, 3′-H), 6.28 (d, *J* 2.1 Hz, 1H, 8-H), 6.18 (d, *J* 2.1 Hz, 1H, 6-H); see Supplementary Figure 10. (−)-ESI MS *m/z* (%) 314.3 [M-H]$^-$ (100). (−)-ESI

MS/MS (45 eV) *m/z* (%) 314 $[M-H]^-$ (45), 297 (100). (−)-ESI MS/MS (35 eV) *m/z* (%) 297 (100), 280 (90), 267 (80). (+)-APCI MS *m/z* 316 $[M+H]^+$. (−)-APCI MS *m/z* 314 $[M-H]^-$.

3′,5′-Dinitro-genistein (24)

Orange solid, UV absorbing (254 nm), R_F 0.21 (CH_2Cl_2/MeOH 9:1), R_t 12.46 min (LC-MS). –UV/vis (MeOH) λ_{max} (lg ε) 268 (4.12), 434 (3.29) nm. IR (KBr) ν_{max} 3410, 1632, 1552, 1503, 1346, 1258, 1108, 1028, 1006, 822, 557, 450 cm^{-1}. ^1H NMR (DMSO-d_6, 300 MHz) δ 12.78 (br, 1H, OH), 8.27 (s, 1H, 2-H), 8.03 (s, 2H, 2′,6′-H), 6.15 (d, ^4J 2.1 Hz, 1H, 8-H), 6.03 (d, ^4J 2.1 Hz, 1H, 6-H). ^{13}C NMR (DMSO-d_6, 150 MHz) δ 178.9 (C_q-4), 161.6 (C_q-5), 159.0 (C_q-4′), 157.9 (C_q-8a), 152.6 (CH-2), 142.9 (C_q-3′,5′), 130.4 (CH-2′,6′), 119.9 (C_q-1′), 105.7 (C_q-3), 102.3 (C_q-4a), 100.2 (CH-6), 94.3 (CH-8). (−)-APCI MS *m/z* (%) 359 $[M-H]^-$ (100). (+)-ESI HRMS *m/z* 361.03046 ($[M+H]^+$, calcd. 361.03027 for $C_{15}H_9N_2O_9$); (−)-ESI HRMS *m/z* 359.01580 ($[M-H]^-$, calcd. 359.01569 for $C_{15}H_7N_2O_9$).

Pyriculamide (25)

Yellow solid, UV absorbing (254 nm), R_F 0.45 (CH_2Cl_2/MeOH 9:1), R_T 9.5 min (LC-MS). UV/vis (MeOH) λ_{max} 273, 354 nm. IR (KBr) ν_{max} 3439, 3191, 3081, 2930, 2862, 1655, 1623, 1524, 1472, 1445, 1356, 1335, 1280 cm^{-1}. ^1H NMR (DMSO-d_6, 300 MHz) δ 10.7 (s br, 1H, OH), 8.14 (d, ^3J 4.0 Hz, 1H, NH), 7.70 (d, ^4J 2.3 Hz, 1H, 5′-H), 7.34 (dd, ^3J 8.4 Hz, ^4J 2.3 Hz, 1H, 9-H), 7.08 (d, ^3J 8.4 Hz, 1H, 8-H), 3.94 (m, 1H, 2-H), 3.48 (m, 1H, 2′-H), 3.46 (m, 1H, 3-H_A), 3.27 (m, 1H, 3-H_B), 3.03, 2.96 (ABX, ^2J 13, ^3J 7 Hz, 2H, 5′-H_2), 2.06 (m, 1H, 3′-H_A), 1.83 (m, 1H, 4′-H_A), 1.68 (m, 2H, 3′-H_A, 4′-H_B). ^{13}C NMR (DMSO-d_6, 150 MHz) δ 168.2 (C_q-1), 164.5 (C_q-1′), 151.1 (C_q-7), 136.6 (CH-5), 136.2 (C_q-6), 127.4 (C_q-4), 125.7 (CH-9), 119.1 (CH-8), 57.8 (CH-2), 57.3 (CH-2′), 44.7 (CH_2-3), 37.7 (CH_2-5′), 28.5 (CH_2-3′), 21.4 (CH_2-4′). (+)-ESI MS *m/z* (%) 655 $[2M-H+2Na]^+$ (100), 633 $[2M+Na]^+$ (25). (−)-ESI MS *m/z* (%) 631 $[2M-2H+Na]^-$ (100), 304 $[M-H]^-$ (55).

2,6-Dimethoxy-1,4-benzoquinone (26)

Yellow solid, ^1H NMR ($CDCl_3$, 300 MHz) δ 5.84 (s, 2H, 3′,5′-H), 3.80 (s, 6H, 2 OCH_3). ^{13}C NMR ($CDCl_3$, 150 MHz) δ 186.8 (C_q-1), 176.7 (C_q-4), 157.3 (C_q-2,6), 107.4 (CH-3,5), 56.5 (2 OCH_3). EI MS (70 eV) *m/z* (%) 168 ($[M]^{\bullet+}$, 5), 104 (39), 91 (21), 80 (20), 69 (100), 53 (29).

3′-Indolylethyl-methyl ether (27)

Colorless oil, UV absorbing at 254 nm, R_F 0.80 (CH_2Cl_2/MeOH 9:1), with anisaldehyde/sulfuric acid red, with Ehrlich's reagent violet. R_t 15.7 min (LC-MS). UV/vis (MeOH) λ_{max} 221, 281 nm. IR (KBr) ν_{max} 3415, 2926, 1620, 1457, 1384, 1339, 1228, 1107, 742 cm^{-1}. ^1H NMR (CD_3OD, 600 MHz) δ 7.51 (d, ^3J 7.8 Hz, 1H, 7′-H), 7.31 (d, ^3J 7.8 Hz, 1H, 4′-H), 7.06 (t, ^3J 7.8 Hz, 1H, 6′-H), 7.05 (s, 1H, 2′-H), 6.98 (t, ^3J 7.8 Hz, 1H, 5′-H), 3.66 (t, ^3J 7.2 Hz, 2H, 1-H), 3.37 (s, 3H, OCH_3), 2.99 (t, ^3J 7.2 Hz, 2H, 2-H). EI MS (70 eV) *m/z* (%) 175 ($[M]^{\bullet+}$, 20), 130 (100), 103 (7), 77 (10), 45 (12). EI HRMS *m/z* 175.0997 ($[M]^{\bullet+}$, calcd. 175.09917 for $C_{11}H_{13}NO$).

ACKNOWLEDGEMENTS

We thank H Frauendorf and R Machinek for mass and NMR spectra, and F Lissy and A Kohl for technical assistance. This investigation was supported by the Ministry of Education and Research (BMBF, 03F0348A).

1 Al-Zereini, W., Schuhmann, I., Laatsch, H., Helmke, E. & Anke, H. New aromatic nitro compounds from *Salegentibacter* sp. T436, an Arctic sea ice bacterium. Taxonomy, fermentation, isolation and biological activities. *J. Antibiot.* **60,** 301–308 (2007).
2 Shao, C. L. *et al*. Five nitro-phenyl compounds from the South China Sea mangrove fungus. *J Asian Nat Prod Res* **9,** 643–648 (2007).
3 Hoefle, G. & Irschik, H. Isolation and biosynthesis of aurachin P and 5-nitroresorcinol from *Stigmatella erecta*. *J Nat Prod* **71,** 1946–1948 (2008).
4 Schuhmann, I. Aufbau einer HPLC-UV-ESI-MS/MS-Datenbank und ihre Anwendung im Screening arktischer und antarktischer Meeresbakterien. PhD Thesis, University of Göttingen, Germany (2005).
5 Fotso Fondja Yao, C. B. Aqabamycins, Rare Nitro Maleimides and other Novel Metabolites from Microorganisms; Generation and Application of an HPLC-UV-ESI MS/MS Database. PhD Thesis, University of Göttingen, Germany (2008).
6 Al-Zereini, W. Natural Products from Marine Bacteria. PhD Thesis, Technical University Kaiserslautern (2006).
7 Laatsch, H. AntiBase 2008. A Data Base for Rapid Dereplication and Structure Determination of Microbial Natural Products, Wiley-VCH, Weinheim, Germany; see http//wwwuser.gwdg. de/~ucoc/laatsch/AntiBase.htm.
8 Lang, M., Spiteller, P., Hellwig, V. & Steglich, W. Stephanosporin, a 'traceless' precursor of 2-chloro-4-nitrophenol in the gasteromycete *Stephanospora caroticolor*. *Angew. Chem. Int. Ed.* **40,** 1704–1705 (2001).
9 Sviridov, S. I. & Ermolinskii, B. S. Secondary metabolites of *Pyricularia oryzae*. I. Derivatives of *o*-nitrophenol. *Khim. Prirod. Soed.* 811–18 (1990) *Chem. Nat. Comp.* **26,** 691–696 (1990).
10 Fleifel, A. M. Syntheses of β-aroyl-α- and β-methylacrylic acids. *J. Org. Chem.* **24,** 1343–1345 (1959).
11 Bruice, T. C. A new 'meta' analog of thyroxine. *J. Org. Chem.* **19,** 333–337 (1954).
12 Tomita, K. & Lardy, H. A. Enzymic conversion of iodinated thyronines to iodinated thyroacetic acids. *J. Biol. Chem.* **235,** 3292–3297 (1960).
13 Svensson, M., Helgee, B., Skarp, K., Andersson, G. & Hermann, D. Phase properties in relation to mesogen length in chiral side-chain polysiloxanes. *Polymer* **38,** 3269–3278 (1997).
14 Ehrlich, J. & Bogert, M. T. Experiments in the veratrole and quinoxaline groups. *J. Org. Chem.* **12,** 522–534 (1947).
15 Hynning, P. A., Remberger, M. & Neilson, A. H. Synthesis, gas-liquid chromatographic analysis and gas-chromatographic-mass spectrometric identification of nitrovanillins, chloronitrovanillins, nitroguaiacols and chloronitroguaiacols. *J. Chromatogr.* **467,** 99–110 (1989).
16 Ohta, K. Chemical studies on biologically-active substances in seaweeds. *Proc. Int. Seaweed Symp.* **9,** 401–411 (1979).
17 Ohta, K. & Takagi, M. Antimicrobial compounds of the marine red alga *Marginisporum aberrans*. *Phytochemistry* **16,** 1085–1086 (1977).
18 Shangguan, D., Jiang, R., Li, B., Xiao, C. & Wu, J. Production, isolation and structure elucidation of novel isoflavonoid compounds K3-D4, K3-D5, K3-D6. *Zhongguo Kangshengsu Zazhi* **24,** 254–257 (1999).
19 Jiang, R., Li, B., Xiao, C., Yang, D. & Wu, J. Production, isolation and structure elucidation of new isoflavonoid compound K3-D3. *Zhongguo Kangshengsu Zazhi* **22,** 81–83 (1997).
20 Cordell, G. A., Chang, P. T. O., Fong, H. H. S. & Farnsworth, N. R. Xylosmacin, a new phenolic glucoside ester from *Xylosma velutina* (Flacourtiaceae). *Lloydia* **40,** 340–343 (1977).
21 Robinson, G. C. Production of Indoles US 3534059. *Chem. Abstr.* **74,** 53516 (1970).
22 Yinon, J. & Laschever, M. Reduction of trinitroaromatic compounds in water by chemical ionization mass spectrometry. *Org. Mass Spectrom.* **16,** 264–266 (1981).
23 Harrison, A. G. & Kallury, R. K. M. R. Chemical ionization mass spectra of mononitroarenes. *Org. Mass Spectrom.* **15,** 284–288 (1980).
24 Brophy, J. J., Diakiw, V., Goldsack, R. J., Nelson, D. & Shannon, J. Anomalous ions in the chemical ionization mass spectra of aromatic nitro and nitroso compounds. *Org. Mass Spectrom.* **14,** 201–203 (1979).
25 Karancsi, T. & Slegel, P. Reliable molecular mass determination of aromatic nitro compounds elimination of gas-phase reduction occurring during atmospheric pressure chemical ionization. *J. Mass. Spectrom.* **34,** 975–977 (1999).
26 Gillis, R. G., Lacey, M. J. & Shannon, J. S. Chemical ionisation mass spectra of explosives. *Org. Mass Spectrom.* **9,** 359–364 (1974).
27 Vats, S., Stuttard, C. & Vining, L. C. Transductional analysis of chloramphenicol biosynthesis genes in *Streptomyces venezuelae*. *J. Bacteriol.* **169,** 3809–3813 (1987).
28 Siddiqueullah, M., McGrath, R. M., Vining, L. C., Sala, F. & Westlake, D. W. S. Biosynthesis of chloramphenicol. II. p-Aminophenylalanine as a precursor of the p-nitrophenylserinol moiety. *Can. J. Biochem.* **45,** 1881–1889 (1967).
29 Cardillo, R. *et al*. Biosynthesis of aureothin. *Tetrahedron* **30,** 459–461 (1974).
30 Kirner, S. & van Pée, K. H. Biosynthesis of nitro compounds: enzymic oxidation of a precursor with an amino group to pyrrolnitrin. *Angew. Chem.* **106,** 346–347 (1994); Angew Chem, Int Ed Engl 33: 351-352 (1994).
31 van Pée, K. H., Salcher, O. & Lingens, F. Formation of pyrrolnitrin and 3-(2-amino-3-chlorophenyl)pyrrole from 7-chlorotryptophan. *Angew. Chem.* **92,** 855–856 (1980); Angew Chem Int Ed Engl 19: 828–829 (1980).
32 Hütter, K. *et al*. Viriplanin A, a new anthracycline antibiotic of the nogalamycin group. I. Isolation, characterization, degradation reactions and biological properties. *J. Antibiot.* **39,** 1193–1204 (1986).
33 Li, Y., Gould, S. J. & Proteau, P. J. Biosynthesis of 3-amino-4-hydroxybenzoic acid in *Streptomyces murayamaensis* incorporation of [4-13C]oxalacetate. *Tetrahedron Lett.* **41,** 5181–5185 (2000).
34 Kurobane, I., Dale, P. L. & Vining, L. C. Characterization of new viridomycins and requirements for production in cultures of *Streptomyces griseus*. *J. Antibiot.* **40,** 1131–1139 (1987).
35 Martin, J. H., Gordon, R. M. & Fitzwater, S. E. Iron in Antarctic waters. *Nature* **345,** 156–158 (1990).
36 Guan, L. L., Kanoh, K. & Kamino, K. Effect of exogenous siderophores on iron uptake activity of marine bacteria under iron-limited conditions. *Appl. Environ. Microbiol.* **67,** 1710–1717 (2001).

37 Martin, J. H. & Fitzwater, S. E. Iron deficiency limits phytoplankton growth in the north-east Pacific subarctic. *Nature* **331,** 341–343 (1988).
38 Rysgaard, S. & Glud, R. N. Anaerobic N_2 production in Arctic sea ice. *Limnol. Oceanogr.* **49,** 86–94 (2004).
39 Radi, R. Nitric oxide, oxidants, and protein tyrosine nitration. *Proc. Natl Acad. Sci. USA* **101,** 4003–4008 (2004).
40 Greenacre, S. A. B. & Ischiropoulos, H. Tyrosine nitration: localization, quantification, consequences for protein function and signal transduction. *Free Radical Res.* **34,** 541–581 (2001).
41 Prasain, J. K. *et al.* Mass spectrometric methods for the analysis of chlorinated and nitrated isoflavonoids A novel class of biological metabolites. *J. Mass Spectrom.* **38,** 764–771 (2003).
42 Carter, G. T. *et al.* Direct biochemical nitration in the biosynthesis of dioxapyrrolomycin. A unique mechanism for the introduction of nitro groups in microbial products. *J. Chem. Soc., Chem. Commun.* **17,** 1271–1273 (1989).
43 Ratnayake, A. S. *et al.* Investigating the biosynthetic origin of the nitro group in pyrrolomycins. *J. Nat. Prod.* **71,** 1923–1926 (2008).
44 Backhaus, C., Rahman, H., Scheffler, S., Laatsch, H. & Hardeland, R. NO scavenging by 3-hydroxyanthranilic acid and 3-hydroxykynurenine N-nitrosation leads to oxadiazoles and their tautomers, *o*-quinone diazides. *Nitric Oxide Biol. Chem.* **19,** 227–244 (2008).
45 Dornberger, K. *et al.* Antibiotics from basidiomycetes. Evidence for the occurrence of the 4-hydroxybenzenediazonium ion in the extracts of *Agaricus xanthodermus* Genevier (Agaricales). *Tetrahedron Lett.* **27,** 559–560 (1986).

Supplementary Information accompanies the paper on The Journal of Antibiotics website (http://www.nature.com/ja)

The Journal of Antibiotics (2009) 62, 461–464

www.nature.com/ja

NOTE

Production of Avilamycin A is regulated by AviC1 and AviC2, two transcriptional activators

Yuriy Rebets[1,3], Raija Boll[1,3], Liliya Horbal[1,2,3], Victor Fedorenko[2] and Andreas Bechthold[1]

The Journal of Antibiotics (2009) **62,** 461–464; doi:10.1038/ja.2009.63; published online 17 July 2009

Keywords: avilamycin; regulation; secondary metabolite; *Streptomyces*

Streptomycetes are typical soil-dwelling bacteria with intricate morphological and biochemical differentiation of colonies, resulting in onset of secondary metabolite production. Compounds produced during these stages of differentiation comprise nearly two-thirds of bioactive molecules synthesized by microorganisms, including antibiotics, antitumor agents and immunosuppressants.[1,2] The biosynthesis of antibiotics and other secondary metabolites is controlled by interactions of both global and pathway-specific regulators. However, in all cases, the influence of the environment is reflected by the activity of pathway-specific regulatory genes, which are located within a biosynthetic gene cluster and which control the expression of biosynthetic genes.[3] On account of high structural and functional similarity, such regulators were grouped into two families, namely *Streptomyces* antibiotics regulatory proteins (SARP), mostly found within the aromatic polyketides clusters, and large ATP-binding regulators of LuxR family (LAL), controlling the production of macrolides and glycopeptides.[4–6] Recent efforts in cloning and characterization of biosynthetic gene clusters for new groups of secondary metabolites revealed novel classes of transcriptional factors that differ from typical SARPs or LAL representatives.[7,8]

Avilamycins are secondary metabolites produced by *Streptomyces viridochromogenes* Tu57. They are active against Gram-positive bacteria. It is known that avilamycins bind to the 23S rRNA in the region proximal to the channel, where tRNA enters the A-site and blocks the protein synthesis.[9] Avilamycin resistance is mediated by 23S rRNA methylation and active avilamycin transport.[10]

The avilamycin resistance genes together with the structural genes were identified and cloned as an entire biosynthetic gene cluster containing 54 open reading frames.[11] The biosynthetic steps leading to the formation of the avilamycin molecule were established by the analysis of secondary metabolites produced by mutants.[11,12] Within the cluster also, two putative regulatory genes named *aviC1* and *aviC2* were identified. Both genes are located in close proximity to each other and are transcribed in the same direction (Figure 1). Genes are separated by a 271-bp non-coding region. We succeeded in identifying the presence of putative bacterial promoter sequences upstream of *aviC1* initiation codon by the use of BPROM bacterial promoter prediction server (Softberry Inc., Mount Kisco, NY, USA). It consists of a putative −10 box GGTTTTCAT (Score 34) and a −35 box ATGCGA (Score 12). Another putative promoter sequence is located upstream of the *aviC2* translation start site consisting of a −10 box GCCCATGAT (Score 31) and a −35 box at TTTCTA (Score 34) similar to consensus *Streptomycetes* promoters.[13]

AviC1 consists of 206 amino acid (aa) residues. The C-terminal region of the putative *aviC1* product is similar to response regulators, which contain a LuxR-type DNA-binding domain.[14] Examples are CitB from *Frankia* sp. EAN1pec (53% identical aa) and NarQ, a nitrate/nitrite response regulator from *Escherichia coli* (43% identical aa).[15] All these proteins possess common CheY-like N-terminal sensor domains that undergo phosphorylation by protein kinases and C-terminal LuxR-type Helix-Turn-Helix (HTH) DNA-binding domains.[14] However, the AviC1 N terminus does not resemble CheY-like signal receiver domains, supposing that AviC1 responds to some other signals than phosphorylation.

The product of *aviC2* consists of 192 aa residues. The C-terminal region of AviC2 exhibits similarity to proteins involved in the control of nystatin production in *S. noursei* (NysRIV, 56% identical aa)[7] and pimaricin production in *S. natalensis* (PimM, 53% identical aa).[16] These proteins contain N-terminal PAS domains and sense internal and external signals, such as redox potential or light.[17] The C-terminal part of these proteins represents a LuxR type of HTH DNA-binding motif, which is formed by two α-helixes (R145-E157 and R164-L174

[1]Institut für Pharmazeutische Wissenschaften, Pharmazeutische Biologie und Biotechnologie, Universität Freiburg, Freiburg im Breisgau, Germany and [2]Department of Genetics and Biotechnology of Ivan Franko National University of L'viv, L'viv, Ukraine
[3]These authors contributed equally to this work.
Correspondence: Professor A Bechthold, Institut für Pharmazeutische Wissenschaften, Pharmazeutische Biologie und Biotechnologie, University of Freiburg, Stefan-Meier-Str. 19, Freiburg D-79104, Germany.
E-mail: andreas.bechthold@pharmazie.uni-freiburg.de
This manuscript is dedicated to Professor Dr Hans Zähner who died in 2008.
Received 21 April 2009; revised 19 June 2009; accepted 22 June 2009; published online 17 July 2009

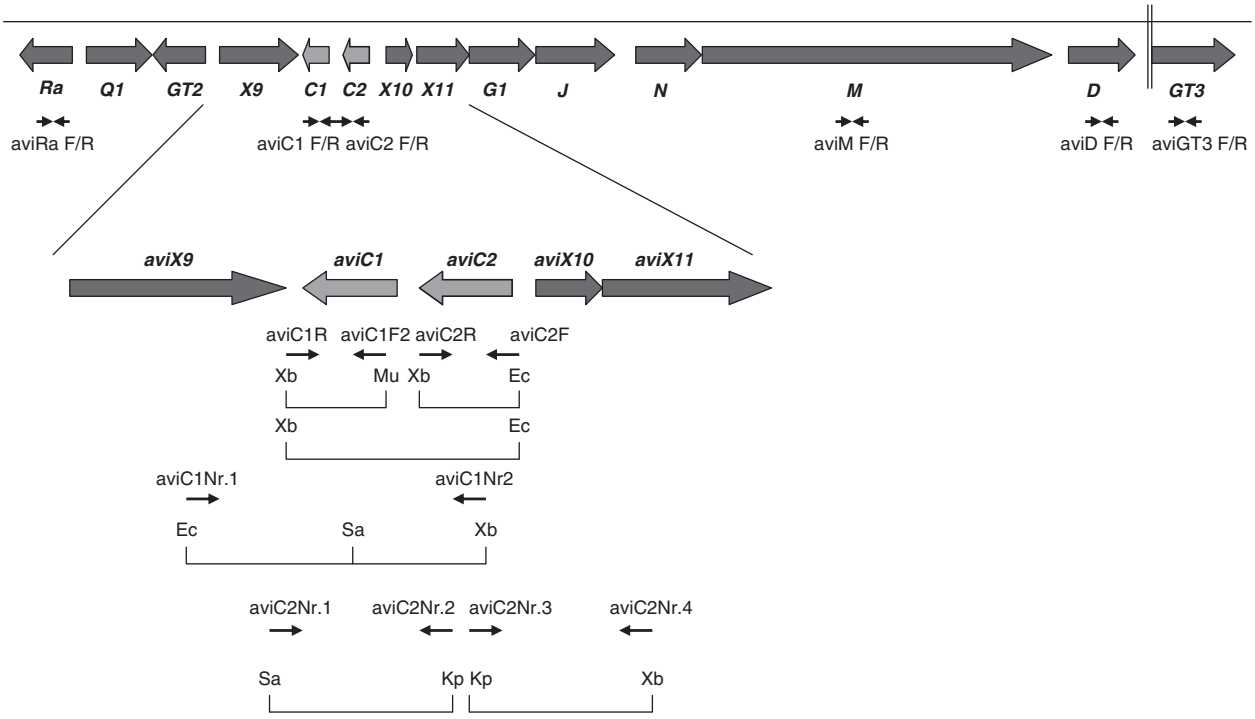

Figure 1 Genetic organization of a part of the avilamycin biosynthesis gene cluster in *S. viridochromogenes* Tu57. Open reading frames are shown as arrows. DNA fragments used for *aviC1* and *aviC2* disruption and expression experiments are shown below the genes. Primers used for gene cloning and reverse transcriptase PCR are indicated as small arrows. Sites for restriction endonucleases are abbreviated as follows: *Eco*RI (Ec), *Sac*I (Sa), *Xba*I (Xb), *Mun*I (Mu), *Kpn*I (K), *Pst*I (P).

in the case of AviC2). BLASTP search for homologs of the N-terminus of AviC2 did not give any significant matches.

To investigate the function of *aviC1* and *aviC2* genes, respective mutants were generated. For this purpose, plasmids pSPaviC1X and pSPaviC2X, were obtained. For inactivation of *aviC1*, the entire gene and flanking DNA regions were amplified by PCR using cosmid F4 as template, and primers aviC1Nr.1 (TCGCCACCGAATTCGGGCTG GACC) and aviC1Nr.2 (ACGTCATCTAGATGATGGAGCGCTTC) (Figure 1). The 1.5 kb PCR fragment was cloned into the *Eco*RI and *Xba*I sites of pSP1. The resulting plasmid pSPaviC1 was restricted by *Sac*I and treated with T4 DNA polymerase. After ligation, pSPaviC1X was obtained. Sequencing confirmed an insertion of 4 bp in the *aviC1*-coding region. To inactivate *aviC2*, two PCR fragments containing parts of *aviC2* were amplified using primers aviC2Nr.1 (TATGAGCG TGAGCTCCTTGCATGC), aviC2Nr.2 (GGTGAGGGTACCACCTG CATCG) and aviC2Nr.3 (ACTCCTTGGTACCCAACACTCGTTC), aviC2Nr.4 (CAGGGTCTAGATGGCGTGGACGG), respectively (Figure 1). PCR products were T/A cloned into pGEM vector (Promega, Mannheim, Germany) to yield pGEMaviC2l and pGEMaviC2r. Fragment aviC2r was restricted using *Kpn*I and *Xba*I, and cloned into the respective sites of pGEMaviC2l. The resulting plasmid was digested using *Sac*I and *Xba*I, and the fragment containing *aviC2* with a deletion of 153 bp was subcloned into pSP1 to give pSPaviC2X.

For gene inactivation, *S. viridochromogenes* GW4 was used as a host. This strain lacks *aviGW4*, a methyltransferase gene involved in methylation of the orsellinic acid moiety of avilamycin A. Desmethyl-avilamycin derivatives are, namely, gavibamycin A1 (desmethyl-avilamycin A) and A3 (desmethyl-avilamycin C).[18] pSPaviC1X and pSPaviC2X were introduced into *S. viridochromogenes* GW4 by protoplast transformation and selection for erythromycin resistant strains. Integration of the plasmids into the chromosome was shown by PCR analysis using primers aviC1F and aviC1R, and aviC2Nr.1 and aviC2Nr.4.

For the generation of *S. viridochromogenes* GW4-C1 and *S. viridochromogenes* GW4-C2 single-crossover mutants were screened for loss of resistance as a consequence of a double-crossover event. Insertion and deletions of the respective genes were confirmed by PCR and Southern hybridization. Analysis of secondary metabolites produced by *S. viridochromogenes* GW4-C1 and *S. viridochromogenes* GW4-C2 verified that both mutants did not produce either gavibamycin A derivatives or its intermediates, as analyzed by HPLC–MS.[12] For complementation and 'overexpression' experiments, *aviC1* and *aviC2* genes were PCR amplified using primers aviC1F (AACGCGT CAATTGAGCCACTGTCAC), aviC1R (CTGTACGTCTAGACGCGG TACACC) and aviC2F (ACGCCACGAATTCGCAGGCGTCGAGGA) aviC2R (GATGCACCTCTAGAAATCCGGCATCC), respectively (Figure 1). PCR products were cloned behind the P_{ErmE} promoter into the *Mun*I and *Xba*I sites of pSET-1cerm. The resulting plasmids were named pSETerm-aviC1 and pSETerm-aviC2. For simultaneous expression of *aviC1* and *aviC2*, plasmid pSETerm-C1C2 was constructed. A 1.7-kb fragment containing both genes was amplified using primers, aviC1F and aviC2R, and using cosmid F4 as a template. Introduction of pSETerm-aviC1 and pSETerm-aviC2 into *S. viridochromogenes* GW4-C1 and *S. viridochromogenes* GW4-C2, respectively, restored production of gavibamycin derivatives, indicating that the mutations did not have any polar effect on other genes of the cluster. On the basis of the results obtained, we suppose that both *aviC1* and *aviC2* gene products are positively controlling avilamycin production.

To establish the hierarchy of both regulatory proteins, cross-complementation experiments were performed. However neither *aviC1* in *S. viridochromogenes* GW-C2 nor *aviC2* in *S. viridochromogenes* GW-C1 were able to restore antibiotic production. The absence

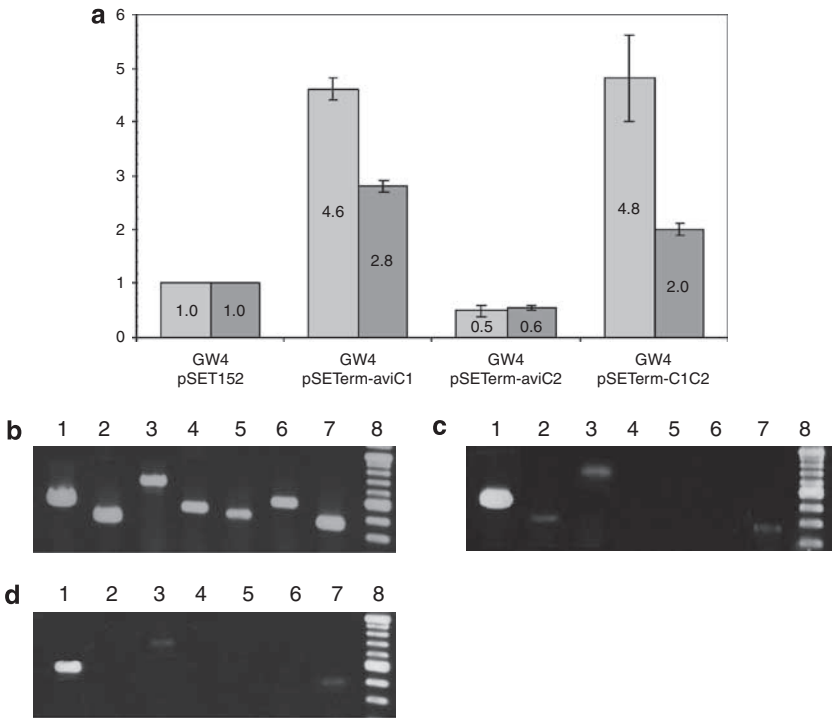

Figure 2 Production of gavibamycin derivatives by *S. viridochromogenes* GW4 strains harboring extra copies of *aviC1* and *aviC2* (**a**), and agarose gel electrophoresis of fragments obtained by reverse transcriptase PCR using total RNA of *S. viridochromogenes* GW4 (**b**), *S. viridochromogenes* GW4-C1 (**c**) and *S. viridochromogenes* GW4-C2 (**d**) as templates. (**a**: Level of gavibamycin A1 is shown in light gray, level of gavibamycin A3 is shown in dark gray; **b**, **c**, **d**: Results obtained by PCR using primers specific for 16S rRNA amplification (lane1), for *aviRa* amplification (lane 2), for *aviD* amplification (lane 3), for *aviM* amplification (lane 4), for *aviGT3* amplification (lane 5), for *aviC2* amplification (lane 6), for *aviC1* amplification (lane 7) and marker (8–100 bp) (lane8)).

of cross-complementation between *aviC1* and *aviC2* suggests that both genes are acting at the same level of regulation.

As *aviC1* and *aviC2* encode positive regulatory proteins, both proteins were also expressed in *S. viridochromogenes* GW4. A strain containing *aviC1* was producing significantly increased levels of gavibamycin A1 (4.6 times higher compared with *S. viridochromogenes* GW4) and gavibamycin A3 (2.8 times higher), major products of *S. viridochromogenes* GW4 (Figure 2a). Interestingly, production of gavibamycins was reduced to twofold compared with the wild type when *aviC2* was expressed in *S. viridochromogenes* GW4 (Figure 2a). Overexpression of AviC2 causes repression of avilamycin biosynthesis either by unspecific binding or by binding to low affinity sites within the *avi* promoters. This phenomenon was described for GerE, a transcriptional factor of the LuxR family controlling spore formation in *Bacillus.*[19] GerE can act both as activator and repressor of the same gene depending on its level of expression. AviC2 might control avilamycin production by a precise expression of *avi* genes depending on the physiological state of the producer strain. When both genes *aviC1* and *aviC2* were introduced into *S. viridochromogenes* GW4, the productivity of the strain was increased again (4.8-fold increase in gavibamycin A1 production and twofold increase in gavibamycin A3 production) (Figure 2a).

To prove that AviC1 and AviC2 act as transcriptional regulators of structural avilamycin biosynthesis genes, reverse transcriptase (RT)-PCR was performed. Total RNA of *S. viridochromogenes* GW4, *S. viridochromogenes* GW4-C1 and *S. viridochromogenes* GW4-C2 were isolated using the hot-phenol extraction method.[20] RT-PCR was performed using the ImProm II Reverse Transcription System (Promega). Total RNA was extracted from the mycelia after 72 h of culture growth that coincides with the active phase of antibiotic production by the wild-type strain. We performed the transcription analysis of *aviM*, encoding a polyketide synthase type I (primers avMF (CTGCACCTACGACTATGGC) and avMR (CAGCAGCTTGATGAC CAGC)), *aviD* encoding a dTDP glucose synthetase (primers avDF (ATTACGCATACCTCGGCCAA) and avDR (CTTCCAGTACCGGTC GATC)), *aviGT3* encoding a glycosyltransferase (primers avGT3F (TCTGCTACGTCGACAACGAC) and avGT3R (GTGAAGAGGTAG TAGTAGCG)), *aviC1* (primers avC1F (ATGGTCGGATCCCTCTGCA) and avC1R (CATGCAAGGACCACACGCT)), *aviC2* (primers avC2F (TCAATTGACGCGTTCCTGCA) and avC2R1 (ATGATCGTGAA GTCCGGTCA)) and resistance gene *aviRa* encoding a rRNA methyl-transferase (primers avRaF (GCGGATCGACAGTTCCGAT) and avRaR (AGATAGGAGGGCTTGCCGA)) (Figure 1). Primers specific to the 16S rRNA of *S. coelicolor* (rrnAF (CACATGCAAGTCGAAC GATG) and rrnAR (GCTGCTGGCACGTAGTTAG)) were used as positive control. Samples were analyzed by 2% agarose gel electro-phoresis, scanned and band density was measured using ImageJ 1.34s software (NIH, Bethesda, MD, USA).

In *S. viridochromogenes* GW4, both regulatory genes as well as biosynthetic and resistance genes were actively transcribed (Figure 2b). The transcription of *aviM* seemed to be much weaker than the activity of other structural genes, which might be explained either by the instability of the long *aviM* transcripts or by a low level of the *aviM* promoter activity. The latter has been described for PKSI-encoding genes from the nystatin biosynthesis gene cluster of *S. norsei.*[7]

In the case of *S. viridochromogenes* GW4-C1, no PCR fragment was obtained for *aviM, aviGT3* and *aviC2*, whereas very tiny fragments

were obtained for *aviD, aviRa and aviC1* (Figure 2c). In the case of *S. viridochromogenes* GW4-C2, no PCR fragment was obtained for *aviM, aviRa, aviGT3* and *aviC2*, whereas very tiny fragments were obtained for *aviD* and *aviC1* (Figure 2d).

On the basis of the obtained results, we suggest that both *aviC1* and *aviC2* gene products are positively controlling avilamycin production at the level of transcription of structural genes. Surprisingly, in both mutants, transcripts of *aviC1* were detectable at a very low level, but transcripts of *aviC2* were not. This might indicate that AviC1 can control *aviC2* expression and that AviC2 acts as autoregulator influencing its own gene transcription.

In conclusion, we have studied two novel regulatory genes controlling avilamycin production in *S. viridochromogenes* Tu57 that differ from the well-characterized SARP and LAL families of antibiotic biosynthesis regulators.

ACKNOWLEDGEMENTS

This work was supported by the BMBF (GenomicPlus), grant to Andreas Bechthold and by the DAAD, fellowships to Yuriy Rebets (PKZ - A/05/28943) and Liliya Horbal (PKZ – A/07/99406).

1 Lam, K. S. Discovery of novel metabolites from marine actinomycetes. *Curr. Opin. Microbiol.* **9,** 245–251 (2006).
2 Chng, Ch., Lum, A. M., Vroom, J. & Kao, C. M. A key developmental regulator controls the synthesis of the antibiotic erythromycin in *Saccharopolyspora erythraea. Proc. Natl Acad. Sci. USA* **105,** 11346–11351 (2008).
3 Rodriguez, M. *et al.* Identification of transcriptional activators for thienamycin and cephamycin C biosynthetic genes within the thienamycin gene cluster from *Streptomyces cattleya. Mol. Microbiol.* **69,** 633–645 (2008).
4 Wietzorreck, A. & Bibb, M. A novel family of proteins that regulates antibiotic production in streptomycetes appears to contain an OmpR-like DNA binding fold. *Mol. Microbiol.* **25,** 1181–1184 (1997).
5 Bibb, M. J. Regulation of secondary metabolism in streptomycetes. *Curr. Opin. Microbiol.* **8,** 208–215 (2005).
6 Nuria, A., Mendes, M. V., Martin, J. F. & Aparicio, J. F. Identification of pimR as a positive regulator of pimaricin biosynthesis in Streptomyces natalensis. *J. Bacteriol.* **186,** 2567–2575 (2004).
7 Sekurova, O. N. *et al. In vivo* analysis of the regulatory genes in the nystatin biosynthetic gene cluster of *Streptomyces noursei* ATCC 11455 reveals their differential control over antibiotic biosynthesis. *J. Bacteriol.* **186,** 1345–1354 (2004).
8 Eustaquio, A. S., Li, S. M. & Heide, L. NovG, a DNA-binding protein acting as a positive regulator of novobiocin biosynthesis. *Microbiology* **151,** 1949–1961 (2005).
9 Kofoed, C. B. & Vester, B. Interaction of avilamycin with ribosomes and resistance caused by mutations in 23S rRNA. *Antimicrob. Agents Chemother.* **46,** 3339–3342 (2002).
10 Weitnauer, G. *et al.* An ATP-binding cassette transporter and two rRNA methyltransferases are involved in resistance to avilamycin in the producer organism *Streptomyces viridochromogenes* Tu57. *Antimicrob. Agents Chemother.* **45,** 690–695 (2001b).
11 Gaisser, S., Trefzer, A., Stockert, S., Kirschning, A. & Bechthold, A. Cloning of an avilamycin biosynthetic gene cluster from *Streptomyces viridochromogenes* Tu57. *J. Bacteriol.* **179,** 6271–6278 (1997).
12 Weitnauer, G. *et al.* Biosynthesis of the orthosomycin antibiotic avilamycin A: deductions from the molecular analysis of the avi biosynthetic gene cluster of *Streptomyces viridochromogenes* Tu57 and production of new antibiotics. *Chem. Biol.* **8,** 569–581 (2001a).
13 Bourn, W. R. & Babb, B. Computer assisted identification and classification of streptomycete promoters. *Nucleic Acids Res.* **23,** 3696–3703 (1995).
14 Galperin, M. Y., Nikolskaya, A. N. & Koonin, E. V. Novel domains of the prokaryotic two-component signal transduction systems. *FEMS Microbiol. Lett.* **203,** 11–21 (2001).
15 Stewart, V., Chen, L. L. & Wu, H. C. Response to culture aeration mediated by the nitrate and nitrite sensor NarQ of *Escherichia coli* K-12. *Mol. Microbiol.* **50,** 1391–1399 (2003).
16 Nuria, A. *et al.* PimM, a PAS domain positive regulator of pimaricin biosynthesis in *Streptomyces* natalensis. *Microbiology* **153,** 3174–3183 (2007).
17 Taylor, B. L. & Zhulin, I. B. PAS domains: internal sensors of oxygen, redox potential, and light. *Microbiol. Mol. Biol. Rev.* **63,** 479–506 (1999).
18 Weitnauer, G. *et al.* Novel avilamycin derivatives with improved polarity generated by targeted gene disruption. *Chem. Biol.* **11,** 1403–1411 (2004).
19 Ichikawa, H., Halberg, R. & Kroos, L. Negative regulation by the *Bacillus subtilis* GerE protein. *J. Biol. Chem.* **274,** 8322–8327 (1999).
20 Kieser, T., Bibb, M. J., Buttner, M. J., Chater, K. F. & Hopwood, D. A. *Practical Streptomyces Genetics*, John Innes Foundation, Norwich, United Kingdom, (2000).

The Journal of Antibiotics (2009) 62, 465–468

www.nature.com/ja

NOTE

The kirromycin gene cluster of *Streptomyces collinus* Tü 365 codes for an aspartate-α-decarboxylase, KirD, which is involved in the biosynthesis of the precursor β-alanine

Kristina J Laiple, Thomas Härtner, Hans-Peter Fiedler, Wolfgang Wohlleben and Tilmann Weber

The Journal of Antibiotics (2009) **62,** 465–468; doi:10.1038/ja.2009.67; published online 17 July 2009

Keywords: kirromycin; antibiotics; β-alanine; aspartate-α-decarboxylase; PanD

In 1972, Heinz Wolf and Hans Zähner[1] described the isolation and characterization of the narrow-host range antibiotic kirromycin from the actinomycete *Streptomyces collinus* Tü 365. Soon after its discovery, it was shown that the observed inhibitory effect of protein biosynthesis[2] is caused by the binding of kirromycin to the bacterial elongation factor EF–Tu,[3] a rare molecular target for antibiotics. Kirromycin binding inhibits the conformational shift that EF–Tu normally undergoes when GTP is hydrolyzed to GDP.[4] This prevents dissociation of EF–Tu from the ribosomal complex and thus blocks translation. Owing to their target, 'elongation factor EF–Tu' kirromycin and related antibiotics such as aurodox[5] or kirrothricin[6] are also referred as elfamycins.

In our previous work, the kirromycin biosynthetic gene cluster was identified, isolated and analyzed.[7,8] The linear carbon skeleton of kirromycin is synthesized by a highly complex hybrid type I polyketide synthase (PKS)/non-ribosomal peptide synthetase machinery encoded by the genes *kirAI–kirAVI* and *kirB*. The hybrid PKS/non-ribosomal peptide synthetase thereby combines trans-AT PKS architecture represented in the enzymes KirAI–KirAV with *cis*-AT architecture in the PKS KirAVI. Extender unit selection and loading are presumably carried out by two discrete acyltransferase enzymes, KirCI and KirCII, which are encoded in the gene cluster.[8] Sequence analysis of the kirromycin biosynthetic gene cluster led to the proposal that β-alanine might be a building block for the typical pyridone moiety of kirromycin. This hypothesis was confirmed by feeding studies. Isotope-labeled β-alanine was efficiently incorporated at the expected positions in the kirromycin molecule.[8]

β-Alanine is an important primary metabolite that is required for vitamin B_5 (pantothenate) biosynthesis. Pantothenate itself is a precursor of coenzyme A and phosphopantetheine, the prosthetic group of fatty acid or polyketide acyl carrier proteins and peptidyl carrier proteins of non-ribosomal peptide synthetases. In bacteria, β-alanine is mainly synthesized by the decarboxylation of aspartate catalyzed by aspartate-α-decarboxylases (ADC), usually designated as PanD.[9] ADC enzymes undergo a remarkable post-translational modification, which finally leads to the formation of an N-terminal pyruvoyl group that is required for catalytic activity.[10] Owing to their essential function in pantothenate biosynthesis, ADC enzymes are ubiquitous in bacteria.

To our surprise, a putative ADC, designated as KirD, is encoded within the boundaries of the kirromycin biosynthetic gene cluster. KirD is highly similar to putative ADCs of other actinobacteria (for example, amino acid sequence identity 65%, similarity 82% to PanD of *Corynebacterium amycolatum* SK46 (GenBank: ZP_03393336)). Although the site of post-translational processing at the N terminus is very high, the C terminus of the enzyme is less conserved and differs from other known streptomycete ADC sequences.

As typical primary metabolism genes within biosynthetic gene clusters are often accompanied by a second gene encoding an isoenzyme elsewhere in the genome, it was tested whether KirD is the only ADC present in *S. collinus*. Conserved regions were identified in a multiple sequence alignment of streptomycete PanD enzymes and degenerate primers PanDscreen5′ (aagtcsaagatycaccg)/PanDscreen3′ (acggcctgmgggctgcg) were deduced and used in a PCR with *S. collinus* genomic DNA. The resulting PCR products were subsequently cloned into the vector pJET (Fermentas, St Leon-Rot, Germany) and sequenced. Sequence analysis revealed the presence of a second putative ADC gene, designated as *panD* in *S. collinus*. Its gene product, PanD, forms a clade with other ADC (PanD) enzymes from strepto-

Fakultät für Biologie, Lehrstuhl für Mikrobiologie/Biotechnologie, Auf der Morgenstelle, Universität Tübingen, Tübingen, Germany
Correspondence: Dr T Weber, Fakultät für Biologie, Lehrstuhl für Mikrobiologie/Biotechnologie, Universität Tübingen, Auf der Morgenstelle 28, 72076 Tübingen, Germany.
E-mail: tilmann.weber@biotech.uni-tuebingen.de
This paper is dedicated to late Professor Hans Zähner.
Received 8 June 2009; revised 1 July 2009; accepted 2 July 2009; published online 17 July 2009

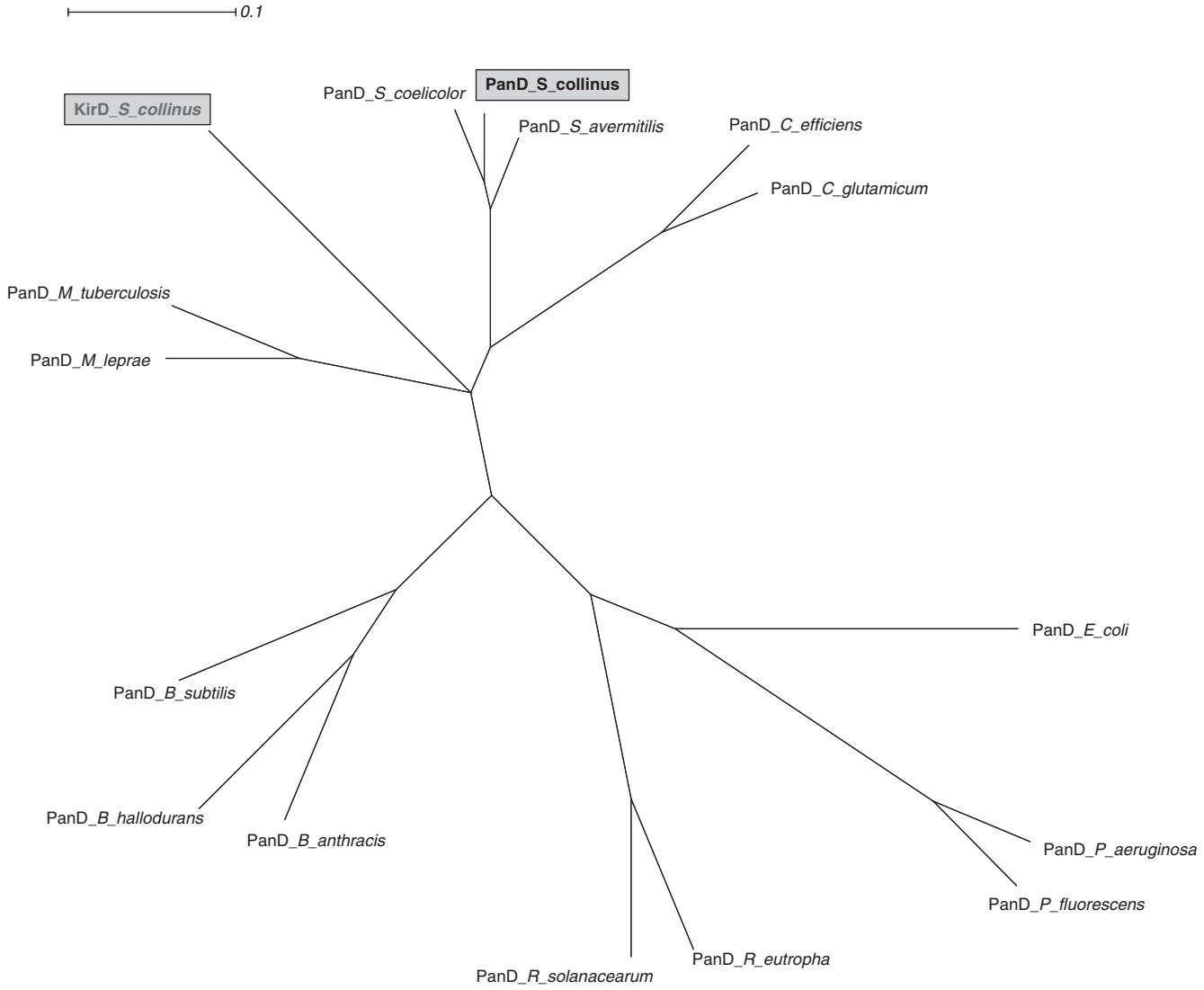

Figure 1 Consensus tree of aspartate-β-decarboxylases (PanD) of different bacteria. KirD and PanD of *S. collinus* Tü 365 are marked with a gray box. The sequences of the other PanD proteins were obtained from the UniProt database, aligned using muscle.[18] The tree was calculated using Splitstree[19] (BioNJ, 1000 bootstrap replicates, consensus tree).

mycetes, whereas KirD forms its own clade more closely related to enzymes from mycobacteria or corynebacteria than to enzymes from streptomycetes (Figure 1).

To test the involvement of KirD in kirromycin biosynthesis, the *S. collinus* mutant TL–D1 was constructed. As double crossover frequency is very low in *S. collinus,* the chromosomal *kirD* gene was inactivated by insertional inactivation with plasmid pTL–Dl, a pA18 derivative[8] that contains a 265 bp internal fragment of *kirD* and an *ermE**-promoter to avoid polar effects on downstream genes. Correct integration of the plasmid was confirmed by Southern hybridization (Supplementary Figure S1, Supplementary information). HPLC-diode array[11] and HPLC–MS analysis of the extracts of *S. collinus* TL–D1 revealed that only traces of kirromycin were produced. These can be explained by residual activity of the primary metabolism equivalent to PanD, which may also be able to provide β-alanine for kirromycin biosynthesis. To confirm that this effect was due to the inactivation of *kirD* and not due to polar effects on essential downstream genes, exogenous β-alanine (final concentration 1 mg ml^{-1}) was supplemented with the production broth. This led to a low but detectable increase in kirromycin production, although wild-type production levels were not reached. The absence of a full complementation may be caused by the fact that, in the mutant, the transcription of the downstream genes, the putative methyltransferase gene *kirM* and the putative acyltransferase gene *kirCII,* is under the control of the *ermE**-promoter instead of their native promoter.

To further investigate the function of KirD in kirromycin biosynthesis, the *kirD* gene was amplified by PCR using the primers KirDoe5′ (cgcgcaagcttaggaggatttaaaatgtaccgagagatgctcaagtcg; *Hin*dIII site+ Shine Dalgarno sequence) and KirDoe3′ (gcgctctagatcacgcgt cgacggtgtcgccgcg; *Xba*I site) from cosmid 1C24,[8] which carries the *kirD* region of the gene cluster, and cloned into pBlueskript II SK through the introduced restriction sites resulting in plasmid pTL–kirD1. Two β-alanine auxotrophic *E. coli* strains (*E. coli* SJ16[12] and *E. coli* DV9[13]), which are mutated in *panD* and thus are unable to decarboxylate aspartate to β-alanine, were transformed with pTL–kirD1 or the empty vector, respectively. Their growth was monitored in a minimal medium with glucose and citrate as carbon sources. Neither strain grew in minimal medium if transformed with

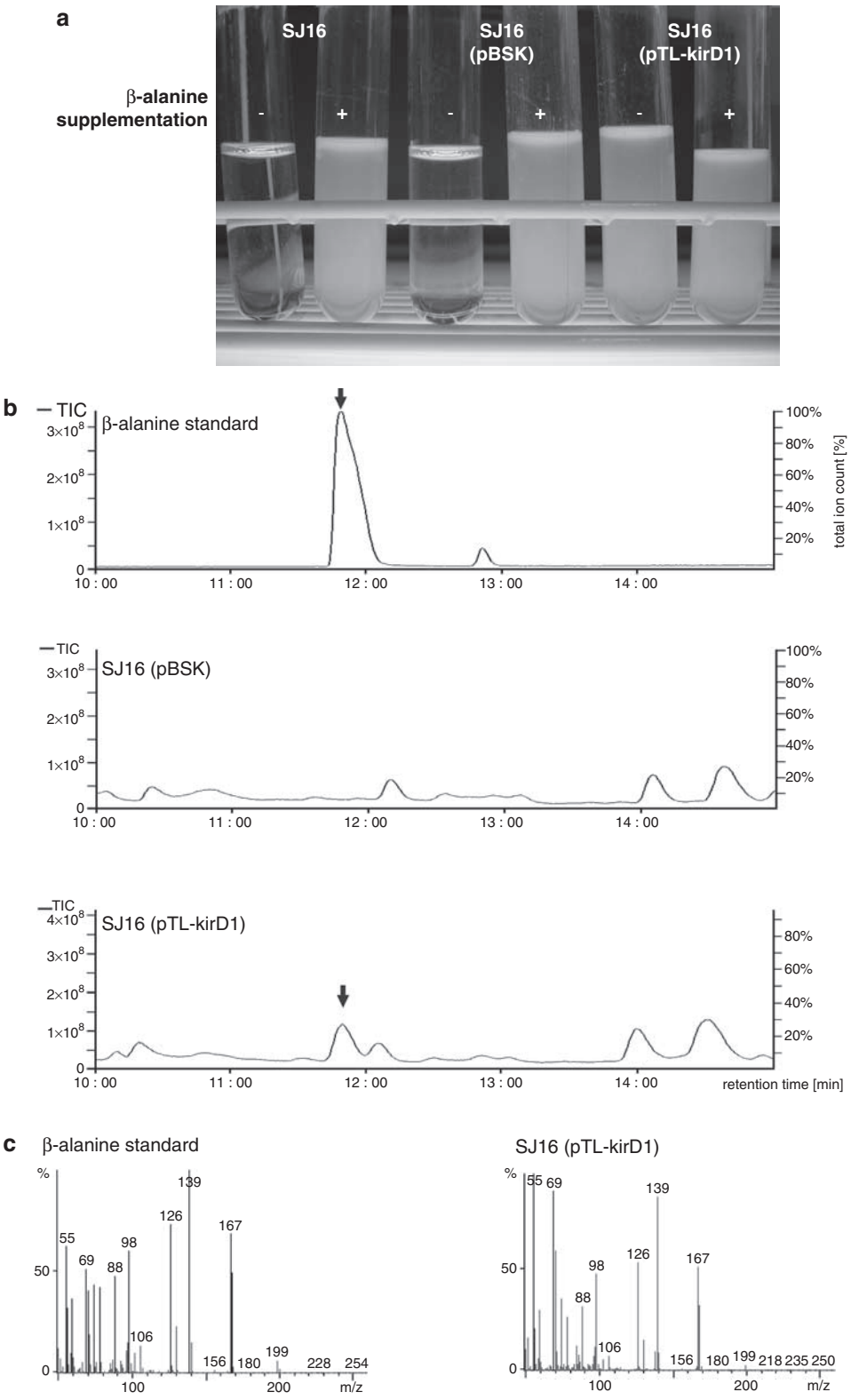

Figure 2 (**a**) Growth of *E. coli* SJ16, *E. coli* SJ16 (pBluescript) and *E. coli* SJ16 (pTL–D1). As a control, the different clones were also complemented with exogenously added β-alanine (end concentration 0.1 mg ml^{-1}). (**b**) GC traces of a β-alanine standard and ADC assays using a crude extract from the control strain transformed with an empty pBluescript SK plasmid (SJ16 (pBSK)) and a crude extract of the *kirD*-expressing strain SJ16 (pTL–kirD1). β-alanine peak is marked with an arrow. The minimal differences of the retention times among the different samples are due to manual injection to the GC. (**c**) Mass spectrum of the peaks at retention time 11.8 min of the β-alanine standard and the ADC assay SJ16 (pTL–kirD1).

the empty vector. Growth was only observed when transformants expressing *kirD* were analyzed (Figure 2a). This shows that *kirD* was successfully expressed and post-translationally processed in *E. coli*, and catalyzes the formation of β-alanine. Thus, a full complementation of the *panD* deficiency of *E. coli* SJ16 and DV9 was achieved by heterologously expressing *kirD* from the kirromycin biosynthetic gene cluster.

To finally prove that the effect observed in the growth experiments is due to the formation of β-alanine by KirD, assays for the *in vitro* conversion of aspartate to β-alanine were carried out. Crude protein extracts of *E. coli* SJ16 (pTL–kirD1) expressing the putative ADC from the kirromycin gene clusters cultivated in complex Luria Bertani medium and induced at an OD_{580} of 0.2 with 1 mM isopropyl-β-D-thio-galactopyranoside (IPTG) were prepared and used in slightly modified aspartate decarboxylase activity assays as described by Dusch *et al.*[14] 2 mM aspartate was used as substrate and 50 µg protein extract was applied per 200 µl reaction volume. The reactions were carried out for 48 h at 37 °C and stopped with the same volume of 3% perchloric acid and evaporated in a vacuum centrifuge. For gas chromatographic analysis, the samples were then hydrolyzed, derivatized with trifluoroacetic anhydride (TFAA), and finally resuspended in 100 µl CH_2Cl_2. Analysis was performed on a Shimadzu GC-17A gas chromatograph with coupled QP5000 mass detector on a Lipodex-E capillary column (diameter 0.25 mm×25 m; film thickness 0.25 µm). By comparison with an β-alanine standard, it was shown that a substance with retention time 11.8 min, which exactly corresponds to the retention time of β-alanine, is accumulated when using crude extracts of the complemented strain SJ16 (pTL–kirD1). No peak at this retention time was observed when using crude extracts of the control strain SJ16 carrying the empty pBluescript SK vector (Figure 2b). Mass spectrometric analysis of the substance eluting at 11.8 min revealed a mass peak of 199, which corresponds to the mass of the TFAA-derivatized β-alanine. The observed fragmentation pattern of both the accumulated metabolite and the β-alanine standard was identical, indicating that the accumulating substance in fact is β-alanine (Figure 2c). This finally proved that KirD is a functional aspartate-α-decarboxylase catalyzing the conversion of aspartic acid to β-alanine.

The presence of KirD in the gene cluster indicates that β-alanine might be a limiting factor in kirromycin production. Therefore, the effect of β-alanine supplementation on kirromycin production with wild-type *S. collinus* was investigated under controlled conditions in a 5 l fermenter using kirromycin production broth (soybean flour 10 g, mannitol 10 g, $CaCO_3$ 5 g, in 1.0 l tap water, pH 7.3). No effect was observed under optimized conditions in the fermenter.

Although the presence of typical 'primary metabolism' genes within antibiotic biosynthetic gene clusters has also been described for other biosynthesis pathways (for example, Shawky *et al.*, 2007[15]), only few experimental data concerning their function in antibiotic production exist. However, some reports have been published on the effects of inactivation or overexpression of primary metabolism genes that are involved in secondary metabolite precursor supply (for a review, see Olano *et al.*, 2008[16]) but are not encoded within secondary metabolite gene clusters. For example, in the actinorhodin biosynthesis of *S. coeliocolor* A3(2), the overexpression of acetyl-CoA carboxylase, which catalyzes the formation of the polyketide precursor malonyl-CoA, led to a six-fold increase of actinorhodin yield,[17] indicating a strong correlation between precursor availability and secondary metabolite production. This shows that maintaining precursor supply is important and may have an important function in the evolution of the gene clusters. Although the supplementation with β-alanine in rich media under controlled fermentation conditions did not lead to an increase of kirromycin production in *S. collinus* Tü 365, it is likely that this β-amino acid is still a limiting factor and its supply during secondary metabolite production may be required for efficient kirromycin production in the natural environment. To our knowledge, this is the first report of a cluster-encoded aspartate-α-decarboxylase that is directly involved in providing β-alanine for antibiotic biosynthesis.

ACKNOWLEDGEMENTS

This work was supported by the German Federal Ministry of Education and Research (BMBF) with grant 0313805J (GenoMikPlus). We thank D Worbs for technical assistance.

1 Wolf, H. & Zähner, H. Metabolic products of microorganisms. 99. Kirromycin. *Arch. Microbiol.* **83,** 147–154 (1972).
2 Wolf, H., Zähner, H. & Nierhaus, K. Kirromycin, an inhibitor of the 30 S ribosomal subunits function. *FEBS Lett.* **21,** 347–350 (1972).
3 Wolf, H., Chinali, G. & Parmeggiani, A. Kirromycin, an inhibitor of protein biosynthesis that acts on elongation factor Tu. *Proc. Natl Acad. Sci. USA* **71,** 4910–4914 (1974).
4 Vogeley, L., Palm, G. J., Mesters, J. R. & Hilgenfeld, R. Conformational change of elongation factor Tu (EF-Tu) induced by antibiotic binding. Crystal structure of the complex between EF-Tu.GDP and aurodox. *J. Biol. Chem.* **276,** 17149–17155 (2001).
5 Liu, C. M., Williams, T. H. & Pitcher, R. G. ^{13}C-NMR studies on the biosynthesis of aurodox (antibiotic X-5108). *J. Antibiot.* **32,** 414–417 (1979).
6 Thein-Schranner, I., Zähner, H., Hoppe, H. U., Hummel, I. & Zeeck, A. Metabolic products of microorganisms. 209 Kirrothricin, a new member of the kirromycin-group. *J. Antibiot.* **35,** 948–956 (1982).
7 Weber, T., Welzel, K., Pelzer, S., Vente, A. & Wohlleben, W. Exploiting the genetic potential of polyketide producing streptomycetes. *J. Biotechnol.* **106,** 221–232 (2003).
8 Weber, T. *et al.* Molecular analysis of the kirromycin biosynthetic gene cluster revealed β-alanine as precursor of the pyridone moiety. *Chem. Biol.* **15,** 175–188 (2008).
9 Cronan, Jr. J. E. ß-Alanine synthesis in *Escherichia coli*. *J. Bacteriol.* **141,** 1291–1297 (1980).
10 Schmitzberger, F. *et al.* Structural constraints on protein self-processing in L-aspartate-α-decarboxylase. *EMBO J.* **22,** 6193–6204 (2003).
11 Fiedler, H. P. Biosynthetic capacities of actinomycetes: 1. Screening for secondary metabolite products by HPLC and UV-visible absorbance spectral libraries. *Nat. Prod. Lett.* **2,** 119–128 (1993).
12 Jackowski, S. & Rock, C. O. Regulation of coenzyme A biosynthesis. *J. Bacteriol.* **148,** 926–932 (1981).
13 Vallari, D. S. & Rock, C. O. Isolation and characterization of *Escherichia coli* pantothenate permease (*panF*) mutants. *J. Bacteriol.* **164,** 136–142 (1985).
14 Dusch, N., Pühler, A. & Kalinowski, J. Expression of the *Corynebacterium glutamicum panD* gene encoding L-aspartate-α-decarboxylase leads to pantothenate overproduction in *Escherichia coli*. *Appl. Environ. Microbiol.* **65,** 1530–1539 (1999).
15 Shawky, R. M. *et al.* The border sequence of the balhimycin biosynthesis gene cluster from *Amycolatopsis balhimycina* contains *bbr*, encoding a StrR-like pathway-specific regulator. *J. Mol. Microbiol. Biotechnol.* **13,** 76–88 (2007).
16 Olano, C., Lombo, F., Mendez, C. & Salas, J. A. Improving production of bioactive secondary metabolites in actinomycetes by metabolic engineering. *Metab. Eng.* **10,** 281–292 (2008).
17 Ryu, Y. G., Butler, M. J., Chater, K. F. & Lee, K. J. Engineering of primary carbohydrate metabolism for increased production of actinorhodin in *Streptomyces coelicolor*. *Appl. Environ. Microbiol.* **72,** 7132–7139 (2006).
18 Edgar, R. C. MUSCLE: a multiple sequence alignment method with reduced time and space complexity. *BMC Bioinformatics* **5,** 113 (2004).
19 Huson, D. H. SplitsTree: analyzing and visualizing evolutionary data. *Bioinformatics* **14,** 68–73 (1998).

Supplementary Information accompanies the paper on The Journal of Antibiotics website (http://www.nature.com/ja)

The Journal of Antibiotics (2009) 62, 469–470

www.nature.com/ja

COMMUNICATION TO THE EDITOR

The first total synthesis of nidulalin A, a dihydroxanthone possessing multiple bioactivities

The Journal of Antibiotics (2009) **62,** 469–470; doi:10.1038/ja.2009.52; published online 3 July 2009

Nidulalin A (**1**) was isolated by Kawahara's group from the rice culture of an ascomycetous fungus, *Emericella nidulans* (Eidam) Vuill. var. lata (Thom and Raper) Subram. (anamorph: *Aspergillus nidulellus*, Samon and W Gams), strain IN-68.[1] The structure of nidulalin A (**1**) was determined by X-ray crystallography and Mosher's method as well as by comparison of CD spectra with known xanthone derivatives.[1] In the later studies, nidulalin A (**1**) was found to possess potent inhibitory activity against DNA topoisomerase II and immunomodulatory activity.[2,3] Although natural products having the dihydroxanthone skeleton have been seen to be widespread,[4–8] only a few total syntheses have been achieved.[9,10] Interested in the structure and bioactivities of nidulalin A, we embarked on the synthetic studies of the natural product.

An overview of our total synthesis of nidulalin A (**1**) including the ORTEP drawing of X-ray crystallography of the key intermediates is disclosed in Scheme 1. (The spectrum

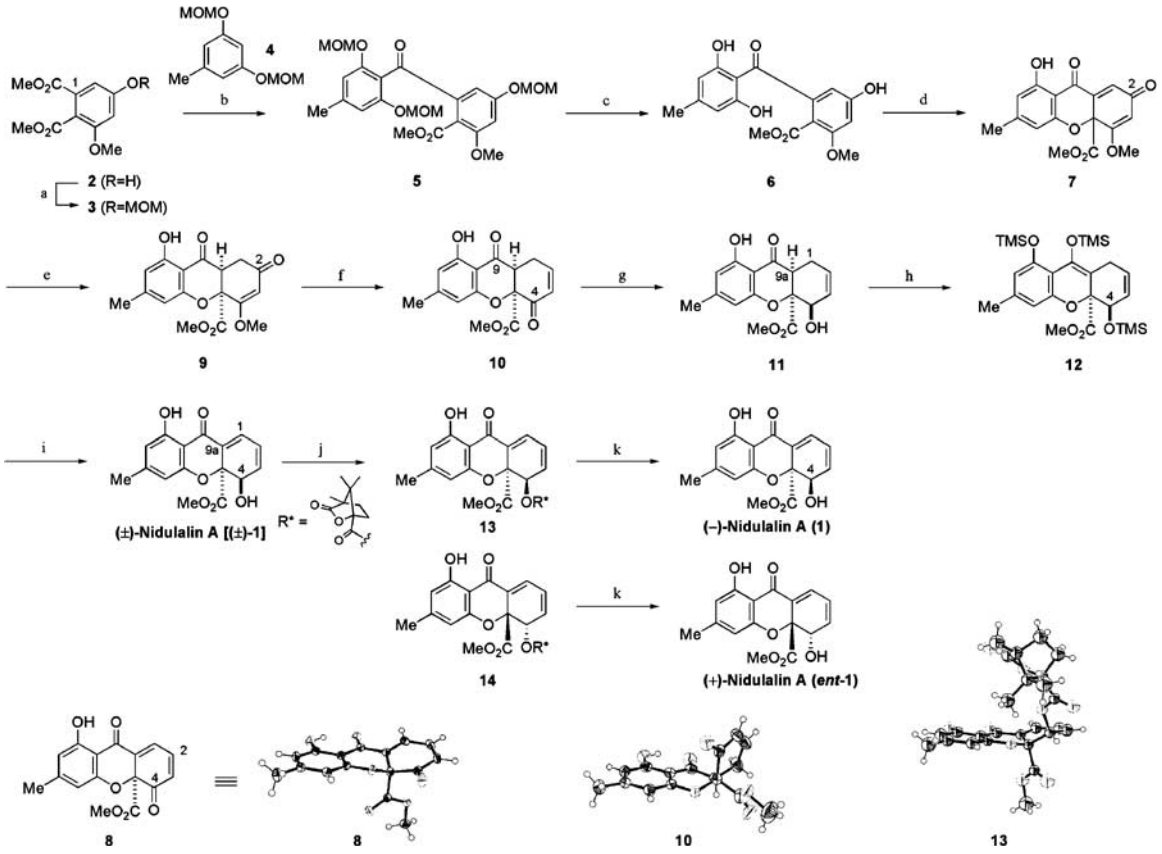

Scheme 1 *Reagents and conditions*: (**a**) MOMCl, NaH, DMF, 0 °C to rt, 40 min, quant.; (**b**) *t*-BuLi, TMEDA, Et_2O-THF, −78 to −20 °C, 2 h, 90%; (**c**) TsOH•H_2O, MeOH, reflux, 5 h, quant.; (**d**) $Pb(OAc)_4$, AcONa, $MeNO_2$, rt, 10 min, 39%; (**e**) $NaBH(OAc)_3$, $B(OAc)_3$, THF, rt, 30 min, 79%; (**f**) DIBAL, THF, −78 °C, 10 min then, 6 N HCl, rt, 14 h, quant.; (**g**) $LiAlH_4$, THF, −60 °C, 2 h, 60% (recovery of SM, 30%); (**h**) TMSOTf, Et_3N, CH_2Cl_2, 0 °C, 1 h; (**i**) SeO_2, 1,4-dioxane, 50 °C, 20 h (60% from **11**); (**j**) (−)-camphanic acid, WSCI-HCl, 4-DMAP, CH_2Cl_2, rt, 30 min, 75% (1:1); (**k**) K_2CO_3, MeOH, 0 °C, 5 h, 80% for (−)-nidulalin A (**1**), 76% for (+)-nidulalin A (*ent*-**1**).

data of compounds in Scheme 1 as well as ^{1}H and ^{13}C NMR spectra of synthetic (−)-nidulalin A (**1**) are provided as supplementary information.) The total synthesis started with dimethyl 5-hydroxy-3-methoxyphthalate (**2**).[11] The hydroxy group of **2** was protected as methoxymethyl ether to provide **3**, which was submitted to regioselective coupling to give ketone **5**. Treatment of bis(methoxymethyl ether) **4** with *t*-BuLi in the presence of *N,N′*-tetramethylethylene diamine (TMEDA) at −78 °C produced regioselectively lithiated **4**, which reacted with diester **3** regioselectively at the C-1 carbonyl group at −20 °C to provide ketone **5** in 90% yield. Acid hydrolysis of **5** gave trihydroxyketone **6** in quantitative yield. Oxidative cyclization of **6** was performed with lead (IV) tetraacetate (2 eq) in the presence of sodium acetate (23 eq) to afford tricyclic **7**, the structure of which was confirmed by X-ray crystallography. (Crystallographic data (excluding structure factors) for the structures of **7**, **8**, **10**, **13**, **14**, and **1** have been deposited with the Cambridge Crystallographic Data Center as supplementary publication numbers CCDC 728664 for **7**, 728665 for **8**, 728666 for **10**, 728667 for **13**, 728668 for **14**, and 728669 for **1**.)

1,2-Reduction of **7** at the C-2 position with DIBAL (in CH_2Cl_2, −78 °C, 30 min) followed by hydrolysis of methyl vinyl ether (addition of THF, 6 N HCl, rt, 2 h) gave enone **8** (the ORTEP drawing is shown in Scheme 1). The hydride reduction of **8** gave 4-*epi*-nidulalin A exclusively.[12] As the methoxycarbonyl group of **8** covered the α-face of C-4 carbon, hydride attacked the C-4 carbonyl group from the β-face to give the α alcohol (4-*epi*-nidulalin A). To invert the face selectivity, we set up *cis*-fused intermediate **10**, which would be submitted to hydride addition from the α-face (the convex face) to give β-alcohol **11**.

The *cis*-fused **9** was derived by 1,4-reduction of the oxidative cyclization product **7**. The subsequent regio-selective reduction of C-2 ketone and hydrolysis gave enone **10** whose structure was determined by X-ray crystallography (the ORTEP drawing is shown in Scheme 1). The α-face of **10** was situated as the convex face as expected. Enone **10** was submitted to regio- and stereoselective reduction to afford β-alcohol **11**. To avoid reduction at the C-9 position of ketone **10**, the reaction mixture was quenched after stirring at −60 °C for 2 h. Dehydrogenation to construct Δ1,9a double bond of nidulalin A was performed in two steps. Treatment of ketone **11** with TMSOTf in the presence of Et_3N provided silyl enol ether **12** concomitant with protection of alcohol. Allylic oxidation of **12** proceeded with SeO_2 at 50 °C, accompanied by de-*O*-silylation at position C-4, to give (±)-nidulalin A [(±)−**1**]. Spectral properties of synthetic (±)−**1** were identical with those of natural products including ^{1}H NMR, ^{13}C NMR, IR and MS.[1]

(±)-Nidulalin A in hand, we next examined resolving the enantiomers with a chiral auxiliary. Esterification of (±)-nidulalin A [(±)−**1**] with (−)-camphanic acid gave diastereomers separable by silica gel column chromatography. The absolute structures of both isomers were determined by X-ray crystallography (the ORTEP drawing of (4*R*, 4a*S*)-nidulalin A ester **13** is shown in Scheme 1). Saponification of camphanic ester of (4*R*, 4a*S*)-nidulalin A (**13**) gave orange crystals of **1**, the solution of which showed the optical rotation $[\alpha]_D^{24}$ –570° (*c* 0.28, $CHCl_3$), levorotatory as the natural nidulalin A[12] (orange needles, $[\alpha]_D^{25}$ −463° (*c* 0.28, $CHCl_3$)). (4*S*, 4a*R*)-nidulalin A (*ent*-**1**) was also obtained from the other diastereomer **14** by the same procedure as above. (4*S*, 4a*R*)-nidulalin A shows the optical rotation $[\alpha]_D^{25}$ +569° (*c* 0.28, $CHCl_3$), being (+)-nidulalin A. Therefore, (−)-nidulalin A was synthesized to confirm the structure of the natural product.

In conclusion, the first total synthesis of nidulalin A has been achieved. Construction of the stereogenic center at the C-4 position was accomplished through *cis*-fused tricyclic intermediate **10** to submit the stereospecific reduction. (−)- and (+)-nidulalin A was obtained from (±)-nidulalin A by derivation to (−)-camphanic esters.

ACKNOWLEDGEMENTS

This work was financially supported by the Consolidated Research Institute for Advanced Science and Medical Care, the Global COE program 'Center for Practical Chemical Wisdom,' and Scientific Research on Priority Area 'Creation of Biologically Functional Molecules' from the Ministry of Education, Culture, Sports, Science and Technology. We also thank the Shorai Foundation For Science and Technology for financial support.

Kuniaki Tatsuta, Shusuke Yoshihara, Nobutaka Hattori, Shinpei Yoshida and Seijiro Hosokawa

Faculty of Science and Engineering, Department of Applied Chemistry, Waseda University, Shinjuku-ku, Tokyo, Japan

1 Kawahara, N., Sekita, S., Satake, M., Udagawa, S. & Kawai, K. Structure of a new dihydroxanthone derivative, nidulalin A, and a new benzophenone derivative, nidulalin B, from *Emericella nidulans*. *Chem. Pharm. Bull.* **42,** 1720–1723 (1994).
2 Sato, S. *et al.* Synthesis of novel antitumor dihydroxanthone derivatives with inhibitory activity against DNA topoisomerase II.. *Bioorg. Med. Chem. Lett.* **9,** 2653–2656 (1999).
3 Fujimoto, H., Asai, T., Kim, Y.-P. & Ishibashi, M. Nine constituents including six xanthone-related compounds isolated from Two ascomycetes, *Gelasinospora santiflorii* and *Emericella quadrilineata*, Found in a screening study focused on immunomodulatory activity. *Chem. Pharm. Bull.* **54,** 550–553 (2006).
4 Tabata, N., Tomoda, H., Matsuzaki, K. & Ômura, S. Structure and biosynthesis of xanthoquinodins, anticoccidial antibiotics. *J. Am. Chem. Soc.* **115,** 8558–8564 (1992).
5 Parish, C. A. *et al.* Isolation and structure elucidation of parnafungins, antifungal natural products that inhibit mRNA polyadenylation. *J. Am. Chem. Soc.* **130,** 7060–7066 (2008).
6 Hussain, H. *et al.* Absolute configuration of globosuxanthone A and secondary metabolites from *Microdiplodia* sp.—a novel solid-state CD / TDDFT approach. *Eur. J. Org. Chem.* 292–295 (2007).
7 Wijeratne, E. M. K., Turbyville, T. J., Fritz, A., Whitesell, L. & Gunatilaka, A. A. L. A new dihydroxanthenone from a plant-associated strain of the fungus *Chaetomium globosum* demonstrates anticancer activity. *Bioorg. Med. Chem.* **14,** 7917–7923 (2006).
8 Zhang, W. *et al.* New mono- and dimerc members of the secalonic acid family, blennolides A-G, isolated from fungus *Blennoria* sp. *Chem. Eur. J.* **14,** 4913–4923 (2008).
9 Nising, C. F., Ohnemüller (née Schmid), U. K. & Bräse, S. The total synthesis of the fungal metabolite diversonol. *Angew. Chem. Int. Ed.* **45,** 307–309 (2006).
10 Nicolaou, K. C. & Li, A. Total syntheses and structural revision of α- and β-diversonolic esters and total syntheses of diversonol and blennolide C. *Angew. Chem. Int. Ed.* **47,** 6579–6582 (2008).
11 Danishefsky, S. *et al.* Derivatives of 1-methoxy-3-trimethylsilyloxy-1,3-butadiene for Diels -Alder reactions. *J. Am. Chem. Soc.* **101,** 7001–7008 (1979).
12 Sato, S. *et al.* F390B and C, new antitumor dihydroxanthone derivatives isolated from *Penicillium* sp. *J. Antibiot.* **50,** 614–616 (1997).

Supplementary Information accompanies the paper on the Journal of Antibiotics website (http://www.nature.com/ja)